CARBONATE FORMATION ON MARS:

EXPERIMENTS AND MODELS

Thesis by

Stuart Keller Stephens

In Partial Fulfillment of the Requirements

for the Degree of

Doctor of Philosophy

California Institute of Technology

Pasadena, California

1995

(Submitted January 31, 1995)

© 1995

Stuart Keller Stephens

All rights reserved

To my parents,

Tom and Ferne Stephens.

Acknowledgments

I am indebted to my thesis advisor, Dave Stevenson, for his theoretical guidance and collaboration, and for his continued support. Dave's invariable willingness to discuss virtually any scientific topic, and the example of his dedicated conceptual thinking, are very much appreciated.

For guidance during the experimental and analytical portions of this thesis, I thank George Rossman at Caltech and Leon Keyser at JPL. George consistently prodded me when needed, and always with good humor. Leon's willingness to provide lab space, his skill in experimental design, and his patience were all essential for the completion of my pressure-drop experiments. Additional analytical support was provided by Paul Carpenter and John Armstrong in the Division analytical labs (SEM and XRD), Iver Lauermann and Alan Rice of the Beckman Institute (XPS), and Kraig Anderson in Chemistry (GC). For the initial funding of experiments at JPL, I am grateful to NASA and Caltech for my 1990 President's Fund grant. I also thank JPL's Earth and Space Sciences Division, for support during an additional two years.

In addition to Dave and George, the other members of my thesis exam committee deserve recognition for their contri-

butions. Bruce Murray was my initial research advisor, and I appreciate the discussions which led me to examine Martian weathering processes. Dewey Muhleman, my academic advisor, has given me many kind words of personal encouragement, for which I am grateful. Andy Ingersoll provided constructive feedback prior to my exam. Also, I appreciate discussions with Roger Burns, Fraser Fanale, Jim Gooding, Bob Haberle, Ralph Kahn, Chris McKay, Jim Pollack, and Aaron Zent.

Although not related to my thesis work, the observational research which I pursued as a graduate student contributed to my professional development. Bruce started me observing Phobos and Mars at Palomar and Table Mountain, and Dave Crisp had me travel to Las Campanas as part of his program of Venus night-side imaging. Besides Dave, I thank Jim Westphal and Jeff Hester for teaching me about photometry, observing with CCDs, and image processing.

I am very grateful to the faculty and staff who have facilitated my teaching interests. I particularly value the experiences of being Teaching Assistant for Lee Silver and Bob Sharp; Bob continues to be a thoughtful friend as well. In 1991, I taught my first summer in Caltech's YESS program (Young Engineering and Science Scholars), and I am grateful to Peter Wyllie and Eddie Grado for their help and administration. In 1994, I was Associate Director for the Summer Science Program in Ojai, and I am looking forward to teaching again with Leo Connolly this summer. Additionally, I

appreciate the opportunity to lead tours of the 200" telescope at Palomar Observatory, courtesy of Caltech.

Numerous administrative departments have helped to make Caltech a welcome place for graduate study. I would like to thank staff in Planetary Science (Kay, Irma, Lorna, Leona, Tammie, Donna, and Rachel) and Arms (Priscilla, Bernice, Donna, and Terry), as well as the Caltech libraries (Jim, Bill, Pat, and Helen), athletic facilities, health center (Marie, Lori, and Flo), and Y. The Honor System and general lack of bureaucracy are greatly appreciated, in addition to Caltech's constant intellectual stimulation. I would also like to thank the other students and members of the Caltech faculty (Peter Goldreich and Kerry Sieh in particular) who have advised or motivated me over the years.

On a personal level, I must thank my parents for their consistent moral and financial support, and Shelley for being my sister (and for her family and Christmas visits). For the past year, Kim Green has been a very good and understanding friend. Also, I've been fortunate to stay in the Vass family's house in Sierra Madre. Officemates Stuart and Janusz have provided welcome company and friendship. Other friends and students have also made my graduate study more enjoyable——Craig, Elizabeth (and family), Mike and Anne (and her family), Eric and Martha (and his family), Ray, Bill, Mark, Rich and Lydia (and friends), the other members of my Planetary Science class (Cathy, Steve, Laszlo, and

Bryan), the Ingersolls, and the players on the volleyball, softball, and soccer teams I've been on. Although I'm not acknowledging them all here, there are many others who have encouraged me, some with as little as a friendly greeting in the hallway.

I think it's important to express my appreciation to all those who have understood or made allowances for the depression I've experienced at many times during the last six years. Those people include Dave and Leon, my family and friends, Kim and Ray, Sue Smith and Dr. Kelly.

Finally, although written using "we," the contents and conclusions presented in this thesis remain the sole responsibility of the author. Any errors are mine.

Abstract

The experiments reported in this thesis were motivated by a desire to explain the small present CO_2 pressure in the Martian atmosphere, given the hypothesis that Mars once possessed a much denser CO_2 atmosphere. We adopted the premise that carbonate production on the surfaces of regolith particles, mediated by small amounts of H_2O, might explain the decline in the surface pressure over geologic timescales.

We exposed powders (~1-20 m^2/g) of basalt glass, and of monomineralic diopside, olivine, plagioclase, and quartz, to conditions simulating the past and present surface of Mars (~7-1000 mb, ~245-300 K, and H_2O contents equivalent to <1 to >5000 monolayers on particle surfaces). A sensitive manometer was used to acquire precise measurements of pressure over periods of 10^{-4} to 10^2 days. Initial pressure drops were attributed to adsorption of CO_2 on particle surfaces and dissolution of CO_2 in H_2O. Continuing uptake of gas in most experiments suggested that CO_2 reacted with powders to form carbonate. Fits to $dP/dt = At^B$ after ~1 day gave $B = -0.85 \pm 0.2$, implying logarithmic reaction kinetics (i.e., reaction rate, $dP/dt \sim 1/t$). Subsequent fits to $P(t) = P_o (1 - e^{-t/\tau}) + D \log_{10}(1 + t/t_o)$, incorporating adsorp-

tion and dissolution, gave rates of D = 0.01-2 monolayers CO_2 per $\log_{10}t$, with t_o << 1 day. Reaction amounts totaled ~0.005-10 monolayers. Parabolic kinetics, arising from diffusion through a product layer, probably did not exceed $P(t) \sim 0.02\ t^{1/2}$.

Rates varied with sample composition (basalt and diopside > olivine > plagioclase and quartz). Basalt glass was *not* more reactive than diopside. Basalt powder pretreated with weak acid displayed rates reduced by over an order of magnitude (although diopside did not), suggesting something removed by acid contributes to CO_2 uptake. Rates increased with H_2O content, temperature, and CO_2 pressure. A fit to data for basalt at 295 K gave $D = 0.55\ H^{0.1}$, where H is H_2O content in monolayers and D is in monolayers CO_2 per $\log_{10}t$; at 248-263 K, the effect of H_2O is stronger: $D = 0.06\ H^{0.7}$. D ~ 0.01-0.2 for "dry" experiments; no lower limit was put on H_2O required for reaction.

Reflectance spectra at mid-infrared wavelengths (2.5-12.5 μm) were obtained for all "dry" and "vapor" experimental powders, and ratioed to starting spectra for maximum sensitivity to added phases. Prominent spectral features near 7 μm in basalt and diopside coincided with CO_3^{-2} absorptions at 6.9 μm for calcite. Additional absorptions near 6.1 μm in basalt and 4.0 μm in diopside were also consistent with the presence of calcite. Absorption ratios near 7 μm ranged from ~0.05 (corresponding to perhaps 3 wt%

added calcite) to as little as ~0.002, below which we were unable to identify added phases. There was a clear positive correlation between absorption ratios and experimental CO_2 uptakes (and hence H_2O content), strengthening the conclusion that carbonate---probably calcite but perhaps magnesite or dolomite---formed in pressure-drop experiments.

Our experiments suggested that this process does occur, but modeling and application to Mars indicated that it may be insufficient to explain the carbonate production required to reduce atmospheric pressure by ~1 bar over geologic time. The principal difficulty lies in the lack of evidence for the reaction proceeding easily beyond one monolayer of product. Although some experiments displayed evidence for the growth of more than a monolayer, they also showed that this arises in a regime of logarithmic reaction kinetics, where CO_2 uptake is limited by declining surface area available for reaction. For a global layer of basalt powder, only high specific surface area (>1 m^2/g), a deep regolith (>100 m), or plentiful H_2O (equivalent to films >5 monolayers thick) allow total CO_2 stored as carbonate to exceed ~10-100 mb. Diffusion-limited kinetics were not ruled out for timescales much longer than experimental durations, and models with thicker carbonate growths show that this could account for storage of an early Martian atmosphere.

Other mechanisms for the loss of CO_2 may also contribute in the transition to the present surface pressure.

Or, Mars may simply never have had a dense CO_2 atmosphere, although this requires explanations other than a CO_2 greenhouse for the morphological features used to support the hypothesis of a warm, wet early Mars. If large amounts of carbonate minerals do represent a sink for atmospheric CO_2, the question of their location on the surface still remains since they have not been confirmed spectroscopically.

Table of Contents

List of Tables

List of Figures

Chapter 1

INTRODUCTION

1.1 DEFINITION OF PROBLEM

The present surface of Mars has a globally averaged temperature of 220 K, is covered with a carbon-dioxide atmosphere with an average pressure of 7 mb, and contains no signs of liquid water. However, the possibility of a dense CO_2 atmosphere and plentiful liquid H_2O on the surface early in the geologic history of Mars motivates many questions, some of which are addressed in this thesis.

If Mars had a substantially warmer, wetter climate 3 to 4 billion years ago than at present, the most likely cause was a CO_2 greenhouse atmosphere. What then has become of the roughly 1 bar of CO_2 required for such a greenhouse? Has a significant portion of that CO_2 been stored in the Martian regolith as chemically bound carbonate?

If the early CO_2 pressure was reduced to 7 mb largely by carbonate reactions with surface rocks, occurring in the presence of liquid water at warm temperatures, then the transition from a greenhouse atmosphere to the present

pressure is not readily explained, since most of the decline from ~1 bar to 7 mb would necessarily occur under non-greenhouse (cold, dry) conditions. Was a mechanism for carbonate formation under colder, drier conditions required to reduce the pressure from ~1 bar to 7 mb? If so, what is the mechanism, and the implications for CO_2 atmospheric history as well as for the present near-surface environment of Mars?

In particular in this thesis, we wish to examine the possibility of significant quantities of carbonate forming over geologic time by reactions between CO_2 and silicates, either under dry conditions or in the presence of small amounts of water.

1.2 REVIEW OF PREVIOUS WORK

The environment at the surface of Mars has been investigated since the 1600s by telescopic observation and more recently by spacecraft reconnaissance and mapping. Following the spectroscopic identification of CO_2 in the Martian atmosphere (Kuiper, 1952), its predominance and the surface pressure of ~7 mb of CO_2 were confirmed by radio occultation with the first Mariner spacecraft to arrive at Mars in the 1960s (Kliore et al., 1965, 1969). Leighton and Murray (1966) proposed that the seasonally variable Martian polar caps are frozen CO_2 in vapor-pressure equilibrium with

the atmosphere. Although this was borne out by Mariner 7 infrared data (Neugebauer et al., 1971), their prediction of a permanent reservoir of CO_2 at both poles was countered for the north pole by Ingersoll's (1974) argument, based on Mariner 9 observations, that there is no excess CO_2 on the surface there, and by later Viking Orbiter findings showing that the north residual cap is composed of H_2O ice (Farmer et al., 1976; Kieffer et al., 1976). Long-term buffering of atmospheric CO_2 pressure by regolith adsorption or depletion of CO_2 by carbonate formation were not ruled out, however.

Water vapor abundances for the Martian atmosphere in the range ~10-100 precipitable microns were first reliably measured by ground-based spectra (e.g., Owen and Mason, 1969). The presence of liquid H_2O was determined to be unlikely at the surface because evaporation of liquid would be exceedingly fast given the very low ambient vapor pressure of H_2O in the atmosphere (Ingersoll, 1970). However, arguments based on diffusion rates of heat and moisture in Martian soil (Smoluchowski, 1968; Farmer, 1976; Flasar and Goody, 1976) led Kahn (1985) to propose that transitory pockets of disequilibrium liquid water were allowable. This would require noontime temperatures to exceed 273 K in at least some locations, a condition met seasonally at equatorial latitudes (Martin, 1981). Globally and seasonally averaged temperatures on Mars are ~220 K, and spatial/temporal lows approach ~130 K (e.g., Kieffer et al., 1977).

Based on observational evidence, it has been speculated that significant quantities of volatiles, including H_2O and CO_2, were outgassed since early in Martian history. Total inventories were estimated to be equivalent to ~100-1000 m of liquid H_2O (e.g., Carr, 1986, 1987; Dreibus and Wanke, 1987; Carr and Wanke, 1992) and ~10 bars of atmospheric CO_2 (e.g., Pollack and Yung, 1980; Pollack and Black, 1982). Fanale (1976) and Carr (1986), in considering prospects for the existence of significant amounts of H_2O on present-day Mars, concluded that most of the outgassed H_2O exists today as ice in a deep megaregolith produced by bombardment early in the planet's history. Hydrologic models for seasonal transport between such a permafrost layer and atmospheric reservoirs of H_2O have been developed (Farmer and Doms, 1979; Jakosky and Farmer, 1982; Jakosky, 1983). Also, the effect of the diffusion of water vapor on the long-term stability of subsurface ice, which is more relevant to this work, has been examined (Clifford and Hillel, 1983; Fanale et al., 1986; Clifford, 1991). Clifford (1993) concluded that the transport of H_2O through the regolith has played an important role in maintaining the long-term cycling of H_2O between regolith, atmosphere, and polar caps.

Measurements at the surface of Mars by two Viking Landers in the 1970s, and continuing telescopic observations from Earth, have added considerably to our understanding of the immediate surface environment. The existence of

iron oxides and clay minerals, inferred from ground-based spectroscopy, has been discussed for many years (e.g., Soderblom, 1992), and a basaltic bedrock composition was concluded (Baird et al., 1976; Toulmin et al., 1977) to be consistent with X-ray fluorescence measurements at Viking Lander sites (Clark et al., 1982). Viking measurements did not rule out the presence of a few weight percent carbonate in surface soils (e.g., Arvidson et al., 1989). The weathering of basalt glass has been suggested by several authors as responsible for the spectroscopic identification of clays and iron-bearing phases (e.g., Gooding and Keil, 1978; Allen et al., 1981). In addition to carbonates, salts such as sulfates and halite have been discussed as soil components (Clark, 1978, 1987, 1993; Clark and van Hart, 1981). Finally, the presence in the Martian soil of oxidants such as H_2O_2 was suggested by Viking Lander biology experiments that detected a very high reactivity for the soil (Klein, 1978). The possible production of these oxidants by photochemical pathways from atmospheric constituents has been discussed by Zent and McKay (1994).

The size of soil particles in the immediate surface environment was estimated from Viking Lander soil mechanics experiments to be in the 10-100 μm range (e.g., Shorthill et al., 1976). The specific surface area determined from adsorption in a Lander gas-exchange experiment (Ballou et al., 1978) gave a model-dependent average particle size of

0.1-1 μm (e.g., Arvidson et al., 1989), consistent with highly porous, but geometrically larger, grains. This is also consistent with the grain size of 0.1-10 μm estimated for drift material covering about 15% of the sample field at the Viking Lander 1 site (Moore and Jakosky, 1989).

The relative contribution of rocks and small soil or dust particles to the regolith has been estimated both from Lander data and by Viking Orbiter visual observations (e.g., Soderblom et al., 1973) and thermal measurements (Christensen, 1982, 1983, 1986b; Jakosky and Christensen, 1986). The transport of surface dust and the total amount that is mobile have also been evaluated (e.g., Christensen, 1986a). Dust depths of ~1-10 m in some regions of Mars were calculated this way, and are consistent with depths inferred from radar images of the "Stealth" feature attributed by Muhleman et al. (1991) to a dust or ash deposit. The regolith below a few meters has not been examined, and the existence of a fractured megaregolith extending to ~100-1000 m remains conjectural (e.g., Fanale et al., 1982).

The diverse geology at the surface of Mars was one of the surprising discoveries of the Mariner and Viking programs. Morphological features suggestive of an earlier warmer climate and possible flowing liquid water on the surface were particularly interesting. In addition to confirmation for the existence of permafrost inferred from lobate crater ejecta patterns and other features (Carr and

Schaber, 1977; Carr et al., 1977; Squyres and Carr, 1986), evidence for subsurface water that may have been mobile in the past included layered deposits in Valles Marineris (Blasius et al., 1977; Nedell et al., 1987; McKay and Nedell, 1988), "outflow" channels (e.g., Lucchitta, 1982), chaotic terrain and other unusual ground patterns (Sharp, 1973; Lucchitta, 1981), and regionally dense systems of small, branching channels in the ancient heavily cratered terrain of Mars (Pieri, 1976, 1980; Carr and Clow, 1981). These channel systems were referred to by Pieri (1980) as valley networks, and their ages from crater-dating arguments suggest that valley formation has not occurred on Mars for billions of years. The speculation that flowing water formed these networks of valleys was apparently supported by the inference, from geomorphic studies of large impact basins, of an episode of erosion early in Martian history (Schultz, 1985; Pollack et al., 1987). However, such a conclusion is still speculative. Finally, the presence of a persistent ocean of liquid water at the time of warmer climate has been proposed to explain morphological features in the northern plains of Mars (Parker et al., 1989, 1993; Baker et al., 1991). The geochemistry of such an ocean has been investigated by Schaefer (1990).

Support for the idea that the early Martian climate was significantly different from today's has come from models of the origin and evolution of its atmosphere. The "greenhouse

effect," resulting in temperatures greater than equilibrium and potential positive feedback to temperature, is due to the radiative properties of gases such as H_2O or CO_2 in planetary atmospheres, and has been recognized for some time as important for Mars as well as the Earth (e.g., Walker, 1978; Pollack and Yung, 1980; Mitchell, 1989). However, a negative feedback has also been proposed (e.g., Walker et al., 1981) to prevent an early greenhouse atmosphere on Mars from running away as it did on Venus; this mechanism involves silicate weathering and carbonate formation, which are more vigorous for higher temperatures yet sequester the CO_2 needed to maintain warm conditions. Additionally, Kahn (1985) proposed a negative feedback mechanism based on carbonate formation in transitory pockets of disequilibrium liquid water.

Kasting (1991) recently pointed out that CO_2 condenses at pressures of <1 bar, and called into question the possibility that a dense atmosphere of CO_2 acting alone could have maintained an early warm environment on Mars. (Two methods Kasting demonstrated for raising temperatures above 273 K were adding greenhouse gases such as CH_4 or NH_3 to the atmosphere, and the modification of standard solar evolution models to allow for a brighter early sun.) Long-term periodic and secular influences on climate have also been proposed, notably the astronomical theory for climate change (Toon et al., 1980) which highlighted the importance

of changes in planetary obliquity and other orbital variables, as well as steadily changing solar luminosity (see also Pollack, 1979; Kasting and Toon, 1989; Kasting, 1991).

The effects of atmospheric interactions with crustal rocks have long been recognized to play an important role in regulating the temperature and CO_2 content of the Earth's atmosphere (e.g., Berner et al., 1983; Lasaga, 1984; Brady, 1991). The chemical weathering of minerals at the surface of Mars has therefore been investigated to determine the importance of such reactions for Martian climate models (Gooding, 1978, 1986; Sidorov and Zolotov, 1986). Gooding (1978) pointed out the importance of liquid water for effecting chemical weathering, including carbonate formation, but primarily discussed the thermodynamics of gas-solid reactions. However, the current terrestrial and hypothetical early Martian situations involving cycling of carbon dioxide may differ from the present environment on Mars where it is possible that depletion continues without significant recycling. Finally, oxidative weathering of iron-bearing minerals has been investigated as the explanation for the presence of abundant clay minerals on the Martian surface (Burns, 1993; Burns and Fisher, 1993).

The only study of the kinetics of carbonate reactions in Mars-like environments has been that of Booth and Kieffer (1978) and Booth (1980), discussed in detail in the next section. Other research has been theoretical, for example

the work of Schaefer (1990, 1993a, 1993b) on equilibrium geochemical models involving aqueous carbonate formation early in Martian history. Also, Huguenin (1976, 1982) proposed photochemically induced weathering as a mechanism for depleting or replenishing atmospheric H_2O and CO_2.

In addition to weathering, other effects have been included in more recent models of climate evolution on Mars. Fanale et al. (1982) considered the interaction of the surface with the atmosphere and CO_2 polar caps to argue for significant storage in a deep regolith. Kahn (1985) used the idea that pockets of liquid water might exist even at low surface pressures and temperatures to argue for carbonate-forming reactions under those conditions. McKay et al. (1985) and McKay and Davis (1991) argued that ice-covered lakes could also permit the existence of a low-temperature environment amenable to carbonate formation. Pollack et al. (1987) included the recycling of CO_2 by thermal decomposition of carbonates following burial, and constructed a scenario in which a balance exists between depletion and addition of atmospheric CO_2 at early times; their model is discussed in the next section. The depleting effect of impact erosion on the early atmosphere of Mars (Melosh and Vickery, 1989) and the possible recharge of CO_2 by impact-induced release of vapor (Carr, 1989) have been proposed more recently.

A number of these effects have been incorporated in recent models for CO_2 evolution (e.g., Haberle et al., 1994; Pepin, 1994), which highlight the importance of atmospheric collapse initiated by polar cap formation early in Martian history, and which also include hydrodynamic and photochemical escape from the atmosphere as well as gas loss by solar-wind induced sputtering (Luhmann et al., 1992; Jakosky et al., 1994). And recent improvements in their earlier work has led Fanale and Salvail (1994) to apparently reduce their estimates of total CO_2 that is exchanged among atmosphere, regolith, and polar caps over geologic time--from as much as ~100-500 mb stored in a deep regolith to ~1-10 mb, all based on laboratory work on the adsorption of CO_2 on Mars-analog rock powders (Fanale and Cannon, 1974, 1978; Zent et al., 1987).

Other experimental work relevant to atmospheric models and this thesis includes studies of the adsorption of H_2O in monomolecular layers onto mineral powders (e.g., Anderson et al., 1978); detailed spectroscopic observations of weathering at mineral surfaces (e.g., Eggleston et al., 1989; Mogk, 1990; Tingle et al., 1990; White and Hochella, 1992); and the kinetics of gas-solid reactions involving SO_2 that may be important for planetary atmospheres (e.g., Fegley, 1988; Fegley and Prinn, 1989). Additionally, calculations to determine rates of formation for carbonates and other minerals through chemical reactions at the surface of Venus

(Fegley and Treiman, 1992; Fegley et al., 1992) can be investigated to compare with the results of such calculations for Mars. Finally, the possible occurrence of carbonates at the surface of Venus has been discussed recently by Kargel et al. (1994), who investigate the consequences of carbonatite magmatism.

Also useful are theoretical models (e.g., Davies and Arvidson, 1981; Stevenson et al., 1983; Schubert et al., 1989; Spohn, 1991) of the internal evolution and volcanic/thermal history of Mars, particularly estimates from those models of the decline in heat flow and rates of lava production following the latest stages of heavy bombardment. Estimates of magma generation and volatile release which incorporate geologic evidence (Greeley and Schneid, 1991; Plescia, 1993), and which follow from these models, are needed for realistic pictures of very early Martian history.

Since the discovery that SNC meteorites contained gases resembling those in the Martian atmosphere (Bogard and Johnson, 1983), SNCs have been investigated as our only samples of the surface of Mars. Evidence in these meteorites of pre-terrestrial aqueous alteration and carbonate minerals (e.g., Gooding et al., 1988, 1991; Treiman et al., 1993; Mittlefehldt, 1994) have recently turned attention to the possibility that hydrothermal circulation or other mechanisms involving more water than presently available operated in the Martian crust in the past (e.g., Karlsson et al.,

1992; McSween and Harvey, 1993; Romanek et al., 1994; Watson et al., 1994).

Finally, it is important to point out the other remote constraints on the existence of carbonates at the surface of Mars. Blaney and McCord (1989), in ground-based infrared spectra of Mars, saw a hint of surface carbonate absorption near 4 μm that allowed them to limit weight abundances to 5% or less. Pollack et al. (1990) attributed absorptions in mid-infrared observations of Mars near 7 μm from the Kuiper Airborne Observatory to airborne carbonate-bearing dust, also limited to a few weight percent. Other than such limited observational evidence, and the speculation that carbonates formed in ancient liquid-water environments, there are no clues for precise locations to search for carbonates on Mars.

1.3 BASIS FOR EXPERIMENTAL APPROACH

Our work was initially motivated by the model of Pollack et al. (1987), in which CO_2 loss on Mars, estimated from scaling the terrestrial silicate weathering rate, was balanced by juvenile outgassing and volcanically driven recycling of carbonates. The cycling between these competing processes, both with timescales of $\sim 10^7$ years during the first $\sim 10^9$ years following heavy bombardment, was considered

in terms of the long-term maintenance of a dense CO_2 atmosphere. However, they only briefly addressed the transition from a dense atmosphere, with liquid water causing carbonate formation and high heat flow causing recycling, to the present-day atmosphere with no liquid water and a much smaller heat flow. There is a problem, because there would have come a point where the pressure and thus the temperature dipped low enough to prevent liquid water and hence carbonate formation. This pressure is far greater than the present globally-averaged surface pressure of 7 mb. Although they explained the subsequent drop in pressure to its present value in terms of spatial and temporal localization of carbonate formation during the transition, a better description is desired of a mechanism which permits carbonate formation in colder, drier environments than the Earth.

Although initially we examined the transition from conditions favorable to aqueous carbonate formation in terms of diffusion-limited growth of carbonate in non-aqueous environments (Stephens and Stevenson, 1990, 1992), we soon turned our attention to the experimental investigation of carbonate formation, with water and without (Stephens et al., 1993, 1994). These experiments followed previous laboratory work by Booth and Kieffer (1978) and Booth (1980), upon which we elaborate below.

Booth used a vacuum chamber to expose basalt and mineral powders to a range of conditions meant to simulate

Martian temperatures (180-297 K), CO_2 pressure (20-150 mb), H_2O abundances (10-50 precipitable microns), and ultraviolet illumination. Additionally, temperature and illumination were cycled every 6-24 hours. Following experiments run for a total of 18-138 hours, powders were treated with acid to evolve carbon dioxide from newly formed carbonate. This was measured and correlated with experimental parameters.

Carbonate formation in Booth's experiments appeared to be influenced by soil temperature and composition, soil temperature cycling frequency, CO_2 pressure, and H_2O content. The direct proportionality of carbonate growth to specific surface area of powders suggested heterogeneous reaction of CO_2 with silicate surfaces. The mechanism was speculated to involve the presence of approximately one adsorbed monolayer of H_2O, and the hydration of silicate surfaces by unsaturated valences of exposed surface atoms. CO_2 molecules were considered to collide with hydroxyl-coated silicate soils, with the rejuvenation of the hydroxyl film by periodic lowering of temperature possibly crucial to the carbonate reaction. Involvement of carbonate ions (CO_3^{-2}) rather than bicarbonate (HCO_3^-) was favored.

Booth's rates of carbonate formation, for powders with surface areas of ~1-10 m^2/g, were equivalent to ~1 μmole of CO_2 per gram of silicate in tens of hours. In all experiments, much less than the equivalent of one monolayer of carbonate was formed. However, experiments of different

durations indicated that rates were linear with time; upon extrapolation, these rates were more than adequate to explain hypothetical large inventories of CO_2 on early Mars.

Booth's results are questionable or lacking for several reasons:

- The inference of carbonate formation was made by the production of CO_2 from powder with acid. This leaves open the possibility that the evolved CO_2 was from something other than a chemically bound phase. He took care to get rid of any weakly adsorbed gas by exposing the powder to vacuum before testing with acid; however, CO_2 may have been more strongly adsorbed or stored in small pores within or between powder grains.
- There is the possibility that mercury contamination in the gas evolution apparatus may have resulted in spurious signal.
- Most importantly, Booth's results are difficult to extrapolate because his experiments did not proceed beyond a monolayer. A linear extrapolation to geologic timescales on Mars is thus not justified. Also, the limiting effect of the formation of a non-porous rind was not examined.

We intended in experiments presented here to (a) attempt to verify the reaction rates observed by Booth, and (b) carry his experiments further by:

- Proceeding beyond a monolayer of carbonate formed, thus determining how rates changed with time, and allowing us to examine any effect due to a non-porous rind.
- Characterizing the products of carbonate-forming reactions with infrared spectroscopy and other analytical techniques, to better understand reaction mechanisms and the textures, compositions, and physical arrangements of reacted phases.
- Performing experiments under various conditions of $P(CO_2)$, T, and H_2O content, to be better able to extrapolate results to a range of past and present Martian conditions.

In proceeding with an experimental investigation of carbonate formation on Mars, we made several assumptions about surface and near-surface conditions. For our experiments, we maximized powder surface area and used adsorption-determined grain sizes near 1 μm, consistent with results from Viking experiments (Arvidson et al., 1989). Also, in calculating the total amount of Martian atmospheric CO_2 involved in carbonate formation, we used a planet-wide

regolith depth of 100 m, consistent with other models (e.g., Fanale and Salvail, 1994).

Since our primary interest was carbonate formation under relatively cold and dry conditions, we investigated T in the range 245 to 300 K, $P(CO_2)$ from 7 mb to 1 bar, and H_2O abundances anywhere from nominally dry to small amounts of vapor to completely wet, i.e., 0 to 10^{-3} to 1 g of H_2O per g of silicate. In making calculations regarding monolayer coverage, storage of the Martian atmosphere, and regolith involvement, we assumed planet-wide applicability of these conditions, as with regolith depth above.

1.4 PREVIEW OF THESIS

Chapter 2 of this thesis contains a description of the apparatus which, unlike Booth (1980), was designed to carefully *monitor* for days and weeks the reaction of CO_2 with powdered basalt and other minerals thought to exist on Mars, under conditions of temperature and H_2O content similar to those at the past and present Martian surface. Following an account of experiments performed, samples used, and procedures followed, we present the unprocessed results of these experiments, in terms of a drop in experimental pressure as a linear function of time. These pressure drops lead us to hypothesize that reaction has occurred in our experiments.

Consideration of the time-dependent pressure signal leads us to consider a logarithmic behavior for reaction kinetics, and we attempt a preliminary discussion of resulting reaction rates and their relation to experimental conditions.

In Chapter 3, we present our analysis of experimental powders with infrared reflectance spectroscopy. The ratio of absorptions in experimental versus starting samples permits the sensitive determination of added phases, and we use this to test the hypothesis that signals produced in pressure-drop experiments were due to reaction to form carbonate. The generally positive results, and correlations with experimental rates and amounts of pressure drop, strengthen our conclusion that carbonates formed from our powders.

Chapter 4 contains our interpretation of experimental and analytical results. Logarithmic kinetics for extended reaction are modeled by the depletion at particle surfaces of available sites for reaction, due to the deposition of reaction product. Adsorption, which occurs at early times in our experiments, is considered as well. Model fits to data which incorporate expressions for both processes give slightly revised rates, and they are discussed in relation to experimental variables. The possible effect of rind buildup, leading to diffusion-limited kinetics, is modeled separately, and we consider the implications for this behavior, which, although it was not observed in our experiments,

may be important at longer timescales. We then apply our results to Mars.

Finally, Chapter 5 continues our discussion of the application of our results to Martian CO_2 history, and, although carbonate formation is concluded to be potentially important under past and present Martian conditions, we give arguments for and against its power to explain the transition from an early dense atmosphere to the present low pressure.

Chapter 2

PRESSURE-DROP EXPERIMENTS

2.1 CONCEPT AND DESIGN

2.1.1 Purpose

The goal of our experiments was to determine the kinetics and mechanism of any carbonate-forming reaction that occurs on Mars——past or present.

If a silicate powder with high specific surface area is brought into contact with a fixed volume of carbon dioxide gas, then any reaction between the two causes a reduction in gas mass and hence gas pressure. We call such an experiment a **pressure-drop experiment**, and use a sensitive manometer in a system of constant total carbon. (The investigations reported here were conducted in Leon Keyser's lab at JPL.)

Since Martian surface rocks are probably basaltic in composition (e.g., Baird et al., 1976), and since the pyroxene, olivine, and plagioclase minerals contained in basalt are thought to be thermodynamically *un*stable under past and present surface conditions on Mars (Gooding, 1978), experi-

mental powders consisted of either basalt glass or mono-minerallic crystals of pyroxene, olivine, or plagioclase.

It was assumed that timescales for diffusion of heat and gas through ~10 g of powdered sample were short compared to reaction timescales. Heat diffusion through a layer of powder $\ell \sim 1$ cm thick would require an interval on the order of $\tau \sim \ell^2/\kappa = \ell^2 \rho c/k$, where κ is thermal diffusivity and k is thermal conductivity. Using conservative numbers for basalt powder from Wechsler and Glaser (1965) for conductivity in powders near room temperature——$k \sim 10^{-2}$ W/m/K (~7 mb gas pressure) to 10^{-1} W/m/K (~1 bar)——with density $\rho \sim 2$ g/cm^3 and heat capacity c ~ 0.2 cal/g/K, gives $\kappa \sim 6 \times 10^{-5}$ cm^2/s to 6×10^{-4} cm^2/s, and $\tau \sim 25$ minutes to 4 hours. Thus, the initial thermal equilibration of our samples should not have interfered with the detection of long-term signals recorded after many hours or days.

For gas transport, we also took a conservative approach and looked at Knudsen diffusion through small pores in a powdered sample. The Knudsen diffusion coefficient in the case of a straight cylindrical pore of radius r (Clifford and Hillel, 1986) is given by $D = 2r/3 \times (8RT/\pi M)^{1/2}$, where R is the gas constant, T is temperature, and M is molecular weight. Using $r \sim 10^{-2}$ μm, $R = 8.3 \times 10^7$ ergs/mole/K, $T \sim 250$ K, and M = 44 g/mole (CO_2), we get $D \sim 0.02$ cm^2/s. For a layer of powder $\ell \sim 1$ cm thick, the timescale for gas transport would have been $\tau \sim \ell^2/D \sim 1$ minute, even less

than the thermal diffusion timescale. We were not concerned a priori with solid-state diffusion into powders, since one experimental goal was to empirically look for the limiting effect of this process on rates of carbonate formation.

Initial experiments were conducted at greater than room temperature, to enhance the *rate* of reaction (while staying within the bounds of thermodynamic stability for carbonate). The partial pressure of CO_2 was 1 bar. Surface areas were also greater than anticipated for typical regolith grains on Mars, to enhance the *detectability* of the reaction. For experiments involving water vapor or thin films of water, we attempted to ensure against water in bulk liquid form, and for dry experiments, we tried to minimize water content by pretreating samples with heat and exposing them to vacuum.

2.1.2 Expected pressure behavior

By monitoring pressure over an interval of hours or days, we anticipated (Figure 2-1) that the partial pressure of CO_2 would drop due to: (1) adsorption in pores and on grain surfaces, a measurable and reversible (by desorption) pressure drop whose rate should decrease until there is no more adsorption; and (2) chemical reaction to form carbonate, probably a smaller reduction in pressure, but still measurable---whose rate should be constant provided it proceeds beyond a monolayer (until diffusion plays a role),

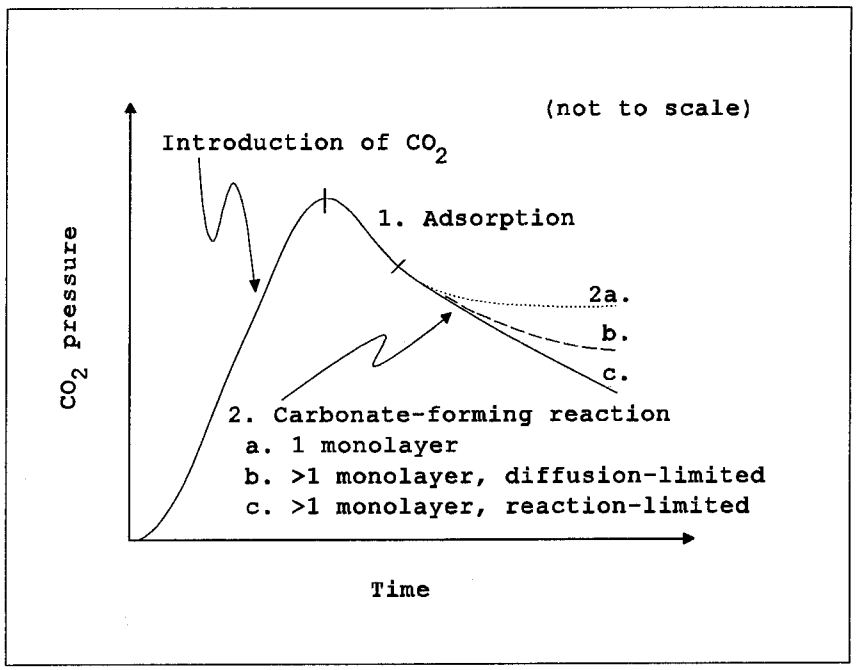

Figure 2-1 Rough drawing of expected pressure-drop behavior

or which should tail off if it is just a surface reaction that stops when a monolayer is formed.

The amount of reaction product was anticipated as follows. An experimental volume of 200 ml consists of 10^{-2} moles of CO_2 at STP:

$$(10^6 \text{ dynes/cm}^2 \times 200 \text{ cm}^3) \\ / (8\times10^7 \text{ ergs/mole/K} \times 300 \text{ K}) \\ \sim 10^{-2} \text{ moles} \qquad [2\text{-}1]$$

If one monolayer of sample reacts, then 10 g of silicate, finely powdered, is sufficient to destroy 10^{-4} moles of CO_2:

$$(10\ g \times 1\ m^2/g/monolayer) / (20\ Å^2/molecule \times 6\times10^{23}\ molecules/mole) \sim 10^{-4}\ moles/monolayer \quad [2\text{-}2]$$

(a specific surface area of 1 m^2/g is used for purposes of this example, and the area occupied by a CO_2 molecule is taken from McClellan and Harnsberger, 1967). This gives $\Delta P/P \sim 1\%$, easily detectable with a sensitive manometer.

The rate of the reaction was also anticipated, using Booth's (1980) results as a guide. Extrapolating linearly from his rates (~1 µmole of CO_2 per g of silicate, in tens of hours), the time taken to destroy 10^{-4} moles of CO_2 should be on the order of 10 days:

$$(10^{-4}\ moles) / (1\ \mu mole/g/day \times 10\ g) \sim 10\ days \quad [2\text{-}3]$$

The higher temperatures of initial experiments were expected to increase the rate of the reaction, as well as the likelihood of proceeding beyond a monolayer. However, we had no guarantee that we would proceed that far, nor that Booth and Kieffer's results were a reliable guide for what to expect.

2.1.3 Schematic and specifications (see Table 2-1)

Initial experiments (numbered EX1-4) utilized an apparatus that monitored changes in pressure using a simple

Table 2-1 Conditions and results of experiments

EX #	Date started	Δt_{tot} [days]	Δt_{eff} [days]	Sample	Mass [g]	True density [g/cm^3]	A_{s2} [m^2/g]
GROUP 0 [control experiments]							
5C	9-16-91	21	[1.0h]	Di0	26.95	3.2	~3
7C	10-14	8	[4.4h]	*none*	-	-	-
9C	11-25	8	8	*none*	-	-	-
10C	12-3	35	5	*none*	-	-	-
11C	1-7-92	6	6	*none*	-	-	-
14C	9-21	57	4	*none*	-	-	-
17C	12-18	4	4	*none*	-	-	-
18C	12-22	17	17	*none*	-	-	-
GROUP 1 [Di0,Di1]							
6	10-7-91	7	[5.4h]	Di0	26.95	3.2	~3
8	10-23	31	26(5)	Di1	5.03	3.2	2.7
12	1-13-92	21	9(12)	Di1	5.03	3.2	2.7
13	2-5	229	10(25)	Di1	5.02	3.2	2.7
15	11-17	24	24	Di1	5.02	3.2	2.7
16	12-11	7	5	Di1	5.03	3.2	2.7
25	8-9-93	4	4	Di1	5.02	3.2	2.7
29	8-30	4	4	Di1	10.02	3.2	2.7
30	9-3	4	4	Di1	10.01	3.2	2.7
32	9-10	10	10	Di1	10.01	3.2	2.7
GROUP 2 [Di2,Ol1,Qtz,Plag,Ol2,Calc]							
19	1-8-93	63	63	Di2	5.02	3.2	10
20	3-12	20	20	Ol1	5.02	3.2	21
21	4-1	11	11	Qtz	5.02	2.65	2.3
22	4-12	17	13	Qtz	5.02	2.65	2.3
23	4-29	95	95	Plag	5.02	2.72	6.1
24	8-2	7	7	Ol2	4.30	3.1	21
39	11-24	5	5	Calc	5.01	2.7	1.5
GROUP 3 [Bas/warm]							
26	8-13-93	4	4	Bas1	5.02	2.9	0.65
27	8-17	6	6	Bas1	15.09	2.9	0.65
28	8-23	7	7	Bas2	4.00	2.9	1.5
31	9-7	3	3	Bas3	5.01	2.9	1.0
33	9-20	4	4	Bas3	5.01	2.9	1.0
34	9-24	3	3	Bas3	1.00	2.9	1.0
35	9-27	4	4	Bas4	5.02	2.9	0.66
36	10-1	7	7	Bas3	5.01	2.9	1.0
37	10-8	7	7	Bas3	5.01	2.9	1.0
38	10-15	40	17	Bas3	4.62	2.9	1.0

EX #	T [°C]	$P_o(CO_2)$ [mb]	H_2O content [ml]	[monolayers]		Results B	D
GROUP 0							
5C	-10	-	-	-	dry		
7C	-29	957	0.000041	-	vapor		
9C	-25	964	0.0015	-	vapor		
10C	-25	-	-	-	dry		
11C	-25	-	-	-	dry		
14C	22	-	-	-	dry		
17C	22	949	5.00	-	wet		
18C	20	949	-	-	dry		
GROUP 1							
6	-30	1033	0.000041	~0.002	vapor		
8	-25	965	0.00080	0.20	vapor	-1.0	0.11
12	-25	964	-	-	dry	-0.7	0.09
13	-25	948	0.0060	1.5	vapor	-0.6	0.25
15	25	957	1.00	250	damp	-0.9	0.63
16	23	947	5.00	1200	wet	-1.6	1.05
25	25	957	1.00	250	damp	-0.5	0.55
29	22	951	-	-	dry	-0.5	0.02
30	22	949	0.0038	0.47	vapor	-0.4	0.37
32	22	949	0.00081	0.10	vapor	-0.6	0.42
GROUP 2							
19	22	952	1.00	67	damp	-0.4	0.45
20	20	932	1.00	32	damp	-0.5	0.18
21	20	963	1.00	290	damp	0.3	0.03
22	21	963	-	-	dry	0.0	0.04
23	21	975	1.00	110	damp	-0.4	0.02
24	25	955	0.86	32	damp	-0.3	0.08
39	23	967	5.0	2200	wet	0.5	0.03
GROUP 3							
26	23	944	1.00	1000	damp	-1.0	1.38
27	22	950	0.00060	0.20	vapor	-1.0	0.59
28	22	954	0.20	110	damp	-0.8	0.58
31	22	952	-	-	dry	-0.8	0.06
33	22	947	5.00	3300	wet	-1.0	1.15
34	22	954	5.00	17000	wet	0.1	1.18
35	22	952	5.00	5000	wet	-1.4	1.36
36	22	101	1.01	670	damp	-0.9	0.51
37	22	34	1.00	670	damp	-0.1	0.03
38	21	101	0.0014	1.2	vapor	-1.0	0.65

(continued, with legend, on next page)

Table 2-1 Conditions and results of experiments (continued)

EX #	Date started	Δt_{tot} [days]	Δt_{eff} [days]	Sample	Mass [g]	True density [g/cm^3]	A_{s2} [m^2/g]
GROUP 4 [Bas/cold]							
40	11-29-93	16	16	Bas5	5.00	2.9	2.0
41	12-15	20	20	Bas5	5.00	2.9	2.0
42	1-4-94	71	13(58)	Bas5	5.00	2.9	2.0
43	3-16	23	23	Bas6	5.01	2.9	12
44	4-8	14	14	Bas7	5.01	2.9	0.79
45	4-22	7	7	Bas7	5.01	2.9	0.79
46	4-29	6	6	Bas7	5.01	2.9	0.79
47	5-5	5	5	Bas7	5.00	2.9	0.79
48	5-10	7	7	Bas7	5.01	2.9	0.79
49	5-17	2	2	Bas7	5.00	2.9	0.79
50	5-19	4	4	Bas7	5.01	2.9	0.79
51	5-24	3	3	Bas7	5.01	2.9	0.79
52	6-7	6	6	Bas7	5.01	2.9	0.79
53	6-13	56	8	Bas9	5.01	2.9	3.9

EX #: "C" refers to control experiments

Δt_{tot}: Total run time of experiment (including temperature changes and desorption legs)

Δt_{eff}: Run time of experiment at initial temperature and CO_2 partial pressure (desorption leg in parentheses) [in hours for EX5-7]

A_s: BET-determined specific surface area (using inert-gas adsorption——see Appendix A.4)

T: Temperature of circulating bath (or mean room temperature, if > 0°C) at t = 0

$P_o(CO_2)$: CO_2 partial pressure at t = 0, not corrected for pressure drop or for dissolution in H_2O

H_2O content: **[ml]** = volume of H_2O, measured by pipette for liquid, estimated from ΔP for vapor (see section 2.3.2)

[monolayers] = surface depth of H_2O (at ~10 Å^2/molecule), assuming all of it was deposited uniformly on particle surfaces

EX #	T [°C]	$P_o(CO_2)$ [mb]	H_2O content [ml]	[monolayers]		Results B	Results D
GROUP 4							
40	-25	100	0.0098	3.3	vapor	-1.1	0.15
41	-25	100	0.0013	0.42	vapor	-0.8	0.06
42	-25	101	-	-	dry	0.5	-0.04
43	-20	100	0.010	0.56	vapor	-1.0	0.01
44	-15	33	0.0060	5.1	vapor	-1.1	0.24
45	-15	6.6	0.0060	5.1	vapor	-0.8	0.10
46	-15	100	0.00075	0.64	vapor	-0.8	0.04
47	-15	33	0.00065	0.55	vapor	-0.8	0.03
48	-15	6.6	0.00065	0.55	vapor	-1.3	0.01
49	-15	100	0.00050	0.43	vapor	-0.6	0.03
50	-15	995	0.00065	0.55	vapor	-0.1	0.06
51	-15	995	0.0044	3.7	vapor	-0.5	0.41
52	-24	100	0.00040	0.34	vapor	-0.8	0.02
53	-23	100	0.021	3.6	vapor	-0.9	0.00

Results: (see section 2.4)

B = exponent in modeled power-law fit to dP/dt, the rate of CO_2 uptake

D = slope of modeled linear fit to $P(t) \sim \log_{10}t$—i.e., $dP/d\log_{10}t$, in equivalent monolayers of CO_2 per 10-folding time

capacitance manometer. This setup is described in Appendix A.1, since the bulk of our experiments were performed with a differential-manometer setup. The latter arrangement proved desirable for more precisely measuring pressure changes.

Experiments numbered EX5 through EX53 utilized the apparatus shown in Figure 2-2. A manifold for gas and vacuum was connected to an air-cooled diffusion pump (with a liquid-nitrogen-cooled trap), which was in turn connected to a mechanical roughing pump. The diffusion pump was routinely capable of achieving pressures below 10^{-2} torr (1 torr = 1.33 mb), as measured with a thermocouple gauge. Carbon dioxide gas (commercially available dry CO_2 from Matheson Company) was available through the manifold using a connection made of copper tubing and stainless-steel Swagelok™ fittings. Other connections (shown as thin lines in the schematic) were similarly constructed using copper and stainless-steel tubing, flexible-metal bellows tubing (near glass connections), and Swagelok™ fittings and valves.

Pressures in various portions of the apparatus were measured using a general-purpose absolute manometer, designated PA. Valves and discrete volumes of the apparatus are labeled in Figure 2-3. Once the experimental and reference volumes were closed off from the rest of the system (by closing valve *f* between the two and valve *e* leading to the rest of the system), PA was no longer able to monitor experimental total pressure. Rather, differential pressure was

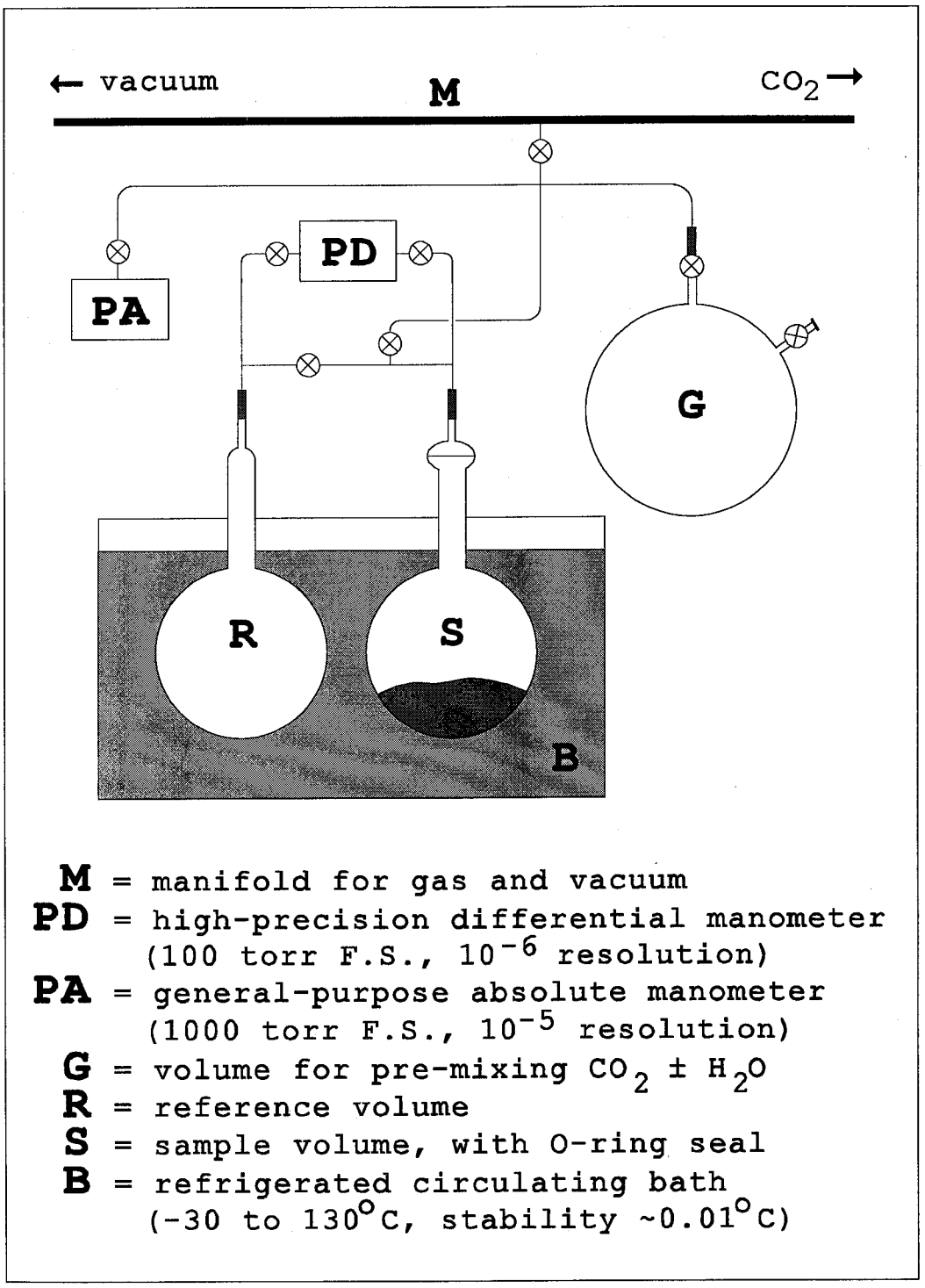

M = manifold for gas and vacuum
PD = high-precision differential manometer (100 torr F.S., 10^{-6} resolution)
PA = general-purpose absolute manometer (1000 torr F.S., 10^{-5} resolution)
G = volume for pre-mixing CO_2 ± H_2O
R = reference volume
S = sample volume, with O-ring seal
B = refrigerated circulating bath (-30 to 130°C, stability ~0.01°C)

Figure 2-2 Schematic of differential pressure-drop apparatus

monitored by leaving open valves *g* and *h* on either side of a high-precision differential manometer, designated PD.

Manometers were purchased from MKS Instruments in 1991; both consisted of a capacitance-based pressure transducer, along with a combined power-supply/readout with DC output for automatic data acquisition. The PA transducer was Baratron™ type 127A, temperature-controlled (heated at 45°C), with a range of 1000 torr full-scale (F.S.), a resolution of 1×10^{-5} of F.S., and an accuracy of 0.15% of reading. Its power-supply/readout was type PDR-C-1C, single-channel, with a digital 4-1/2 place LED display (pressure was displayed to 0.1 torr, but could be monitored by DC output to 1000 torr $\times 10^{-5}$ = 0.01 torr). The PD transducer was Baratron™ type 398H, also heated at 45°C, with a range of 100 torr F.S. (reliably read to ±125 torr), a resolution of 1×10^{-6} of F.S., and an accuracy of 0.05% of reading. Its power-supply /readout was type 270-5, also single-channel, with a digital 5-1/2 place LED display (pressure was displayed to 0.001 torr, but could be monitored by DC output to 0.0001 torr).

Separate sample and reference volumes, S and R, were designed, so that the effects of temperature fluctuations in a circulating bath were minimized (point-to-point variations were less than temporal fluctuations in the spatially averaged temperature of the bath——see section 2.1.4). **PD was connected so that *positive* differential pressure corresponded to S having *less* pressure than R.**

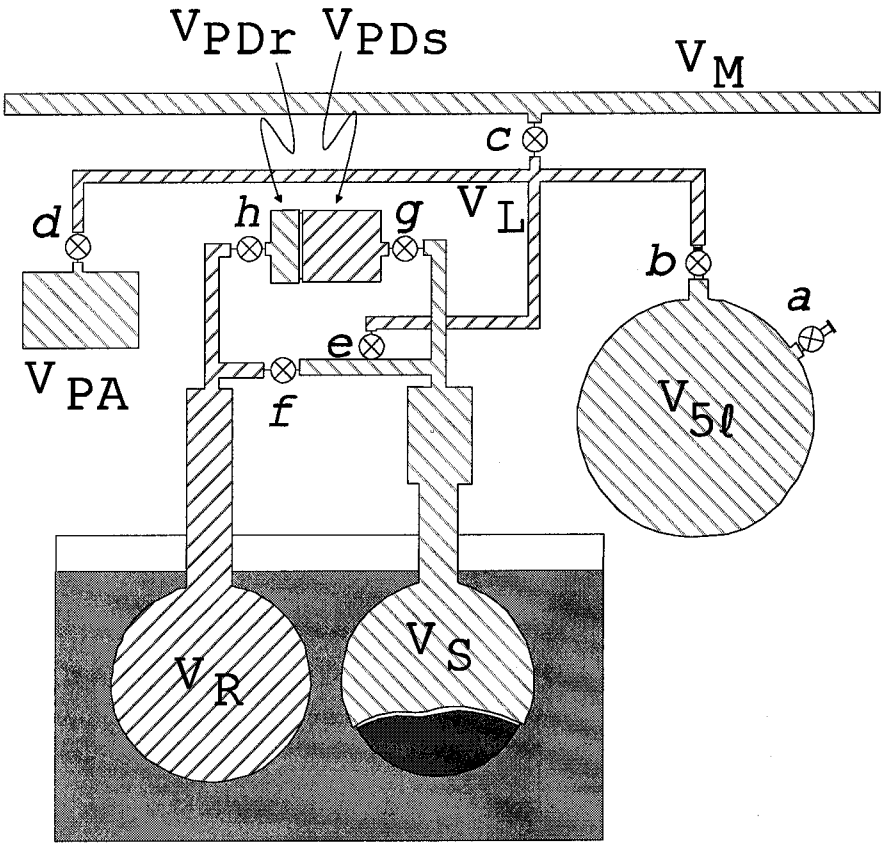

Volumes in cm^3 (±0.5%):

$V_{5\ell}$	= 5105	V_R	= 65.3
V_L	= 27.25	V_S	= 64.5
V_{PA}	= 8.95	V_{PDr}	= 5.17
V_M	= 214.0	V_{PDs}	= 13.10

Figure 2-3 Schematic of apparatus, illustrating valves and volumes

The bath, designated B, was purchased from Neslab Instruments in 1991, and was type RTE-110D, with an operating temperature range of -30 to 130°C, temperature stability of ±0.01°C (achieved in practice, although excursions were observed——see section 2.1.4), cool-down time of 55 minutes (from 20 to -30°C), and bath volume of 5 liters. We used the bath without external circulation, and arranged for the necks of sample and reference volumes to fit through a removable sealed lid. Reagent-grade methanol was used as the bath fluid for experiments at room temperature and below. The circulator was a bench-top unit and came with a digital readout (of actual bath temperature, displayed to 0.1°C, although set temperature could be displayed to the same precision at the press of a button); the DC signal output (both set temperature and actual bath temperature) could be monitored to 0.01°C.

The 5-liter pre-mixing volume, G, as well as the sample and reference volumes, were adapted by glass-blowing existing spherical volumes, and were capable of holding total pressures of up to roughly 1.3 bars. G had a Kontes 4-mm bent-neck stopcock fitted at one port, and was connected via Swagelok™ fittings to copper tubing and hence the rest of the system. The other port of the 5-liter volume consisted of a straight-through 4-mm Teflon stopcock, with enough 8-mm O.D. glass tubing at the outer end to allow for securing a rubber septum, through which a needle could be inserted to

introduce small amounts of liquid water to the 5-liter volume (so that a 2-inch needle could make it all the way through the Teflon stopcock). The schematics in Figures 2-2 and 2-3 are not to scale (e.g., tubing lengths are not representative, and G is much bigger than R and S). We generally used deionized water from a spigot in the lab (we occasionally used CO_2-free distilled water).

The sample and reference containers, R and S, were both modified from 2-inch O.D. spherical volumes, and so were each roughly 60 ml in volume. Although slightly different in shape at the end that was connected to the rest of the system, they were designed with nearly the same volume, and rested at approximately the same vertical level in the bath fluid. S had a neck wide enough to allow powder to be poured in and out easily (and the neck fit through an opening in the bath lid that was by necessity slightly larger than that for R), and had an O-ring seal (clamped during experiments) next to a Swagelok™ connection between glass and metal tubing segments. R had a neck the same width as but longer than S, extending to the same height as the O-ring seal in S, and had a similar connection between glass and metal tubing. The stainless-steel lid was custom-made, and was fitted underneath with a flat rubber gasket.

All tubing which was active during experiments (i.e., below valve *e*) was covered with black foamed insulation, as were the parts of R and S protruding above the lid of the

circulator. R and S sat in the methanol bath so that the entire spherical portions of the volumes were below the top of the fluid.

Finally, temperatures in the lab near and on several parts of the apparatus were monitored using thermocouples, which were connected to an automatic data acquisition unit. The thermocouples were E-type cromel-constastan, readable to 0.1°C and accurate to 0.5°C.

Prior to 11-8-91, data were recorded manually by the author, and recording sessions typically were limited to a few hours at a time. Frequency was anywhere from less than once per minute to once per hour or more, and precision was limited to the displayed values of parameters.

Automatic acquisition of data began 11-8-91, using a Fluke™ data acquisition unit capable of reading voltages from PD, PA, and B, as well as temperatures from thermocouples. In all, ten parameters (differential and absolute pressures, bath and set temperatures, and six environmental temperatures recorded with thermocouples) were read at regular intervals, and recorded via computer onto diskette for later data reduction. Full use was made of the precision of each device that was read, so that differential pressure was recorded to 0.0001 torr, absolute pressure to 0.01 torr, bath and set temperatures to 0.01°C, and environmental temperatures to 0.1°C. Beginning with EX8 and continuing until EX38 (11-91 through 10-93), data were generally

recorded every 60 seconds, although at times the frequency was greater (up to every 10 seconds). Starting during EX38 (11-93), the frequency was reduced to every 5 minutes, and then to every 20 minutes (parts of EX53 were recorded every 1 hour). The beginning of each experiment——at least the first 5-10 minutes——was always recorded manually with a frequency of at least every 60 seconds.

Vapor pressure tables for H_2O (over water and over ice) and for CO_2 are included in Appendix A.2.

2.1.4 Testing and leaks

Once the apparatus was constructed, testing consisted of determining: (i) discrete volumes in different parts of the system, (ii) leak rates in R, S, and PD, and (iii) the effect of temperature changes (lab and bath) on differential pressure between R and S.

We designated the discrete volumetric capacities in the system as $V_{5\ell}$, V_L, V_{PA}, V_M, V_R, V_S, V_{PDr}, and V_{PDs} (see Figure 2-3). $V_{5\ell}$, V_R, and V_S were the volumes between glass apparatuses G, R, and S and their respective valves; V_L was the total line volume of copper and stainless-steel tubing segments; V_{PA}, V_{PDr}, and V_{PDs} were the internal volumes of manometers between their pressure diaphragms and corresponding nearby valves; and V_M was the manifold volume between valve G and other valves connecting it to vacuum and

CO_2. Introducing gas to one part of the system, and letting it expand into other parts of the system (all at room temperature), and doing this two or more different ways so that there existed sufficient equations of the form $P_1V_1 = P_2V_2$ to allow determination of the eight discrete volumes, allowed us to measure the volumes to within 0.5% accuracy. The resulting capacities are shown in Figure 2-3.

Leaks in all parts of the system, for timescales of experimental *preparation* (minutes to hours), were determined to be less than errors introduced by the above uncertainties in experimental volumes. The more crucial leak rates were for two parts of the system exposed to sample or reference atmospheres *during* experiments——i.e., the two combined volumes, $V_R + V_{PDr}$ (the "combined reference volume," which totaled 70.5 ml) and $V_S + V_{PDs}$ (the "combined sample volume," 77.6 ml), which are created when valves *e* and *f* are closed. (For calculations involving $V_S + V_{PDs}$ during experiments, it was necessary to take into account the volume of sample as determined from its mass and true density.)

Leak rates——during experimental runs and for durations of weeks and longer——were estimated in a number of ways (usually involving air leaking *into* the volumes): (a) from direct monitoring of pressures, using PA, in one or both of the combined volumes; (b) by recording the differential pressure, using PD, between the combined volumes (or between the combined reference volume and the rest of the system);

and (c) in later experiments, using absolute pressure along with differential pressure to determine the final total pressure in the combined reference volume and comparing it to the starting total pressure in both volumes.

- Method (a) allowed us to determine that, prior to the start of experiments with this apparatus (9-16-91), leak rates in the two combined volumes were each less than ~0.1 torr/day (~0.13 mb/day).
- Monitoring differential pressure in control experiment EX7C (starting 10-14-91), using method (b), gave us a slightly better differential leak rate of less than ~0.09 mb/day. Control experiments EX10C (starting 12-3-91) and EX11C revealed that any leak in the combined reference volume was less than ~0.08 mb/day, and the differential leak rate was less than ~0.03 mb/day.
- Finally, using method (c) with more recent experiments conducted at 100 mb total pressure or less (EX40 through EX49, plus EX52, all performed from 11-93 through 6-94), we determined that any leak in the combined reference volume was less than ~0.03 mb/day.

This latter result, for more recent **GROUP 4** experiments, allowed us to say that (since any pressure changes in the combined reference volume or the combined sample volume must each have positive signs for CO_2 partial pressure less than

1 bar) the maximum absolute value of a differential leak rate was ~0.03 mb/day. (Negative differential leak rates concerned us less, since they would have constituted a less severe constraint on experimental pressure-drop curves, which generally had positive slopes.)

The effect of temperature differences on the differential pressure was assessed by monitoring lab and apparatus temperatures with thermocouples, and bath temperature with DC signal output from the circulator, and correlating both with differential pressure. We determined the following (for CO_2 partial pressure of 1 bar and bath temperature of $-25^{o}C$):

- A change in *lab* temperature of $1^{o}C$ (for *both* volumes) gave a change in differential pressure of 0.2 mb. Fluctuations in lab temperature were observed to occur on diurnal timescales, and--since adequate interpretation of results could be obtained with these results (and since removal of this diurnal effect was not straightforward)--data were not "cleaned up" by removing this effect (although see section 2.4.2).
- A change in *bath* temperature of $0.1^{o}C$ (again for *both* volumes) gave a change in differential pressure of 0.03 mb. We found that bath temperature only fluctuated as much as $0.1^{o}C$ (or, on occasion, greater than $1^{o}C$) when there were large excursions in lab tempera-

ture. Results were generally sufficiently interpretable that removal of this effect was not necessary.

- Finally, if the *bath* temperature were to change for, say, *only* the reference volume (i.e., if we were to have temperature differences *within* the bath), then we calculated a larger change in differential pressure, 0.4 mb for 0.1°C. Using thermocouples allowed us to determine that temperature variability within the bath was less than ~0.1°C. However, observed measurements of differential pressure changes showed that fluctuations of differential pressure on timescales of a few minutes were less than about 0.02 mb, so this was determined not to be a problem.

2.1.5 Sources of uncertainty

Typical continued pressure drops (after ~3-10 days) were greater than ~0.03 mb/day. We compared these to uncertainties in raw pressure-drop results (differential pressure versus time), which were due to several factors: (a) leaks, (b) the known accuracy of the PD manometer, (c) diurnal lab temperature fluctuations and bath temperature fluctuations on various timescales, and (d) repeatability of experiments.

(a) (See previous section.) Differential leak rates were less than ±0.03 mb/day (for **GROUP 4** experiments).

(b) A calibration (performed by MKS Instruments on 8-5-91) of PD yielded less than ±0.04 mb error at 100 mb, and better than ±0.04% accuracy (0.05% accuracy was claimed) for the full range of 0 to 100 mb.

(c) The effect of lab and bath temperature fluctuations on differential pressure was usually less than ±0.2 mb. However, there were occasions——when lab temperature fluctuated several degrees, or when bath temperature fluctuated a few degrees (e.g., in response to lab temperature excursions)——when differential pressure was made to change ±1-2 mb (typically diurnally). These effects were most noticeable with a total pressure of 1 bar in the system. Again, these effects were generally separable from the longer-term trend without difficulty.

(d) Repeatability of experiments yielded the most reliable, and entirely empirical, estimate of uncertainty in pressure-drop results. Sources of uncertainty included systematic procedural errors. An example was the way experiments were begun——manually closing valves *e* and *f* immediately after introducing gas(es) by simultaneously opening *e* and *f*, typically resulting in initial negative differential pressure offsets of several mb, especially with larger total pressures (typically with 1 bar). Presumably, this meant that more gas was introduced into the combined sample volume than into

the combined reference volume, in such a way that some variation occurred from experiment to experiment. Although this particular effect was accounted for in later interpretations of results by estimating the initial differential pressure offset, some variability between experiments was likely to remain.

Ultimately, two experiments were performed as deliberate repeats of previous runs (EX25 was a repeat of EX15; EX32 was a repeat of EX30, albeit with less H_2O), allowing us to estimate an uncertainty. In terms of differential pressure, EX25 deviated less than 5% from EX15, and EX32 deviated about 10-15% from EX30. Table 2-1 shows that, for both pairs of experiments, the variability was on the order of 12-15% for the crucial slope of a linear fit to $P(t) \sim \log_{10} t$ behavior (see section 2.4.3). (For further evidence of the consistency of results for experiments with similar starting conditions, see section 2.4.4 and Chapter 4.)

2.2 SAMPLES

2.2.1 Selection

Samples used in pressure-drop experiments are shown in Table 2-2. Initial experiments focused on monominerallic

Table 2-2 Samples used in pressure-drop experiments: (a) Bulk samples

Sample	Approximate composition	Sample description	Locale
Diopside 0-1 [Di0-1]	$CaMgSi_2O_6$	bulk, broken crystals, ~5% impurities	Dog Lake, Quebec
Diopside 2 [Di2]	$CaMgSi_2O_6$	green, euhedral crystals, <2% impurities	Rajasthan, India
Olivine 1 [Ol1]	$(Mg_{.98}Fe_{.02})_2SiO_4$ [Forsterite 98%]	bulk, broken crystals, ~5% impurities	Gabbs, Nevada
Olivine 2 [Ol2]	$(Mg_{.88}Fe_{.12})_2SiO_4$	translucent green pebbles (crystals), <2% impurities	San Carlos, Arizona
Quartz [Qtz]	SiO_2	clear, euhedral crystal, <1% impurities	Mt. Ida, Arkansas
Plagioclase [Plag]	$Ab_{.3}An_{.7}$ [Ab = $NaAlSi_3O_8$, An = $CaAl_2Si_2O_8$]	clear, euhedral crystal, <1% impurities	Ponderosa Mine, Oregon
Calcite [Calc]	$CaCO_3$	reagent grade powder	Fisher Scientific
Basalt 1-6 [Bas1-6]	tholeiite [50 wt% SiO_2, 13% Al_2O_3, 12% FeO, 9% MgO, 11% CaO]	~98 wt% black glass, ~0.3 wt% dissolved H_2O, ~1 wt% crystals, 1991 lava flow, quenched in air	Kilauea, Hawaii
Basalt 7-9 [Bas7-9]	tholeiite, similar to Bas1-6	mostly glass, very similar to Bas1-6, 1994 lava flow, quenched in air	Kilauea, Hawaii

Table 2-2 (b) Powder preparation

Sample	Final preparation date	Shatterbox ground?*	Acid-treated?	Heat-treated?	Briefly mortar-ground?
Di0	2-16-91	✓	✓		
Di1	10-21	✓			
Di2	1-8-93	✓	✓		
Ol1	3-9	✓	✓	✓	✓
Ol2	8-13	✓	✓	✓	✓
Qtz	4-13	✓	✓	✓	
Plag	4-29	✓	✓	✓	
Calc	11-23				
Bas1	8-12	✓		✓	✓
Bas2**	8-23	✓		✓	✓
Bas3	9-6	✓		✓	✓
Bas4	9-6	✓ (1)		✓	✓
Bas5	11-21	✓ (60)		✓	✓
Bas6**	3-15-94	✓ (60)	✓	✓	✓
Bas7	4-5	✓ (20)		✓	✓
Bas8**	5-26	✓ (20)		✓	✓
Bas9**	6-9	✓ (20)	✓	✓	✓

*Duration, in minutes, of shatterbox grinding (parentheses), 5 minutes if not shown

**Some Basalt powders were modified from previously-prepared powders:

Bas2 = Bas1 + briefly mortar-ground a second time
Bas6 = Bas5 + further acid-treated, heat-treated, and briefly mortar-ground
Bas8 = Bas7 + 4 hours automatic grinding, plus further heat-treated and briefly mortar-ground (ultimately not used)
Bas9 = Bas7 + further acid-treated, heat-treated, and briefly mortar-ground

components of basalt, since we wanted to minimize the number of possible reaction products. We began with a clinopyroxene, diopside ($CaMgSi_2O_6$). Diopside, forsteritic olivine (i.e., near-endmember Mg_2SiO_4), and calcic plagioclase feldspar (i.e., near-endmember $CaAl_2Si_2O_8$) were determined from thermodynamic arguments (Gooding, 1978) to be *un*stable with respect to gas-solid reaction at past and present Martian near-surface conditions of temperature and CO_2 partial pressure. (See Appendix A.3 for an adaptation of Gooding's P-T stability diagram for diopside and a comparison with our experimental conditions.) These minerals can react with CO_2 to form carbonate minerals, by reactions such as:

$$CaMgSi_2O_6 + 2\ CO_2 \rightleftharpoons CaMg(CO_3)_2 + 2\ SiO_2\ , \quad \text{or} \qquad [2\text{-}4]$$

$$CaMgSi_2O_6 + 2\ CO_2 \rightleftharpoons CaCO_3 + MgCO_3 + 2\ SiO_2 \qquad [2\text{-}5]$$

The first reaction yields dolomite, $CaMg(CO_3)_2$, from diopside, and the second gives calcite, $CaCO_3$, and magnesite, $MgCO_3$. Any carbonate-forming reaction was expected to also yield silicates (such as silica, SiO_2) as reaction by-products. Pure diopside, forsterite, and plagioclase do not contain iron, so that oxidizing reactions were minimized.

If reactions involving iron did take place in our experiments, the following would have to be true: (i) any such reaction taking CO_2 out of the experimental atmosphere must have led to the formation of iron-bearing carbonates

(see Gooding, 1978), since that is the only logical place to put carbon; and (ii) reactions of iron-bearing minerals with H_2O (or leaked O_2) may have resulted in the formation of iron oxides or hydroxides, but they would not have contributed significantly to observed pressure-drop signals.

After initially using bulk diopside crystals with visually obvious impurities, we considered that pressure-drop signals might be adversely affected by reaction with impurities instead of with the main constituent, so we attempted to perform experiments with purer crystalline samples. Diopside 2 and Olivine 2 were purer samples than their Diopside 1 (or Diopside 0) and Olivine 1 counterparts. Quartz and Plagioclase were similarly pure crystalline samples. All of the samples mentioned so far (Di0, Di1, Di2, Ol1, Ol2, Qtz, Plag) were either purchased from Ward's Geology or from local mineral dealers, or were obtained from Caltech collections maintained by George Rossman. At one point, we desired to examine the effect of exposing calcite (Calc, $CaCO_3$) to our experimental atmosphere, and the sample used was reagent-grade powder with minimal impurities.

In order to more closely mimic what is likely to exist at the surface of Mars, it was our goal to use samples of whole-rock basalt, preferably glass. Basaltic glass was considered to be at least as reactive in our experiments as individual crystalline minerals, and is an expected constituent in the near-surface environment of Mars, where

volcanism has played a major role. We initially obtained basaltic glass courtesy of Laszlo Keszthelyi, who collected air-quenched lava (cooled in air within 1 cm of the metal of a geology hammer) from a 1991 East-Rift flow of Kilauea volcano in Hawaii. Starting with EX44, basaltic glass was from samples collected by the author (in 3-94) in a similar manner from another active flow of Kilauea. Basaltic glass samples were designated Bas1 through Bas9 to distinguish different powder preparations (but very similar starting compositions).

See Table 2-2, part (a), for more detailed sample compositions, descriptions, and locales.

2.2.2 Powder preparation

Summaries of sample preparation are given in Table 2-2, part (b). After 1-2 cm pebbles were crushed in a metal jaw-crusher to 1-2 mm pieces, all of the powders (with the exception of Calc) were prepared by grinding the smaller pieces in a tungsten-carbide shatterbox. Unless otherwise indicated, shatterbox grinding lasted 5 minutes. Contamination of samples during grinding was minimized by pretreating the shatterbox (grinding a small amount of sample first), and by only taking powder that was not near the O-ring seal of the shatterbox following grinding. With the exception of Di0 and Di1, all of the powders were heated in an oven at

120°C for at least 12 hours (sometimes left for as long as a few days).

The acid-treatment can be summarized as follows: Di0, Di2, Ol1, Ol2, Qtz, Plag, Bas6, and Bas9 *were* acid-treated; Di1, Bas1-5, and Bas7-8 were *not* acid-treated. The acid-treatment procedure for Di0, Di2, Ol1, Ol2, Qtz, and Plag involved putting powder in weak acetic acid (~15% glacial acetic acid, ~85% deionized water), and then washing with deionized water before drying and heating. In some cases these procedures were done more than once before going to the next step. In one case (Di2) a gravity-separation technique (centrifuge) was used to carefully retain as much powder as possible; otherwise, powder fractions that took longer to settle were lost in washing. In the case of Bas6 ultrasound (putting the beaker with stirred powder into an ultrasonic cleaner for an hour at a time) was added to the acid- and water-washing steps, and in the case of Bas9 this was done in a more scrupulous fashion, keeping the liquids poured off after acid-washes. (After the first acid-wash the liquid was colored orange, suggesting the presence of oxidized Fe, or iron rust, but it was grey after the second and third washes. Iron was present in all of our Basalt samples, and for the most part would not have been removed by treatment with acid. It was argued in section 2.2.1 that the presence of iron in experimental samples is not particularly troubling.) Powders typically caked a bit when dried

(in sunlight or in the oven) after acid- and water-washing, so mortar-grinding was used mainly to re-powder samples (although it took very little grinding).

Differences in powder preparation probably affected the resulting distributions of particle sizes. In addition, acid-treated powders seemed to give weaker differential pressure results. This may have been very significant, given our speculation that something removed by the acid-treatment was responsible for at least part of the pressure-drop results (see discussion in section 2.4.3).

To measure specific surface areas of powders used in experiments, an inert-gas adsorption technique pioneered by Brunauer, Emmett, and Teller (hence BET) in the 1930s, and based on a criterion for monolayer coverage, was used (Brunauer et al., 1938). Introducing N_2, Ar, or Kr in stages, so that adsorption isotherms could be determined for pressures up to one half of the vapor pressures of these gases at liquid nitrogen temperature, allowed us to empirically determine the specific surface areas of powders (see Orr, 1977b).

A discussion of the BET technique, our measurement setup, results, and uncertainties is given in Appendix A.4. Specific surface areas are tabulated for individual experimental powders in Table 2-1.

2.2.3 SEM images

We used direct imaging of powders with scanning electron microscopy (SEM) in an attempt to investigate changes on particle surfaces due to exposure to experimental atmospheres. In so doing, we obtained pictures of particle surfaces (see Figure 2-4) which reveal them to have a wide distribution of grain sizes, although generally most of the surface area was contained in a multitude of smaller particles. Fracturing and cleavage of larger grains was also clear from these images (obvious cleavage surfaces for Diopside 1 and Plagioclase, and conchoidal fracture for Basalt 1), and was consistent with expected patterns based on mineralogy. In general, grain sizes were on the order of 1 μm in diameter, similar to what could be inferred from specific surface area measurements (Appendix A.4) and from rough estimates using optical microscopy. No changes between experimental samples and original powders were apparent at resolutions of 10-100 nm (see, for example, Diopside 1 in Figure 2-5, parts (a) and (b)), although a detailed attempt to investigate the formation of reaction products was not attempted.

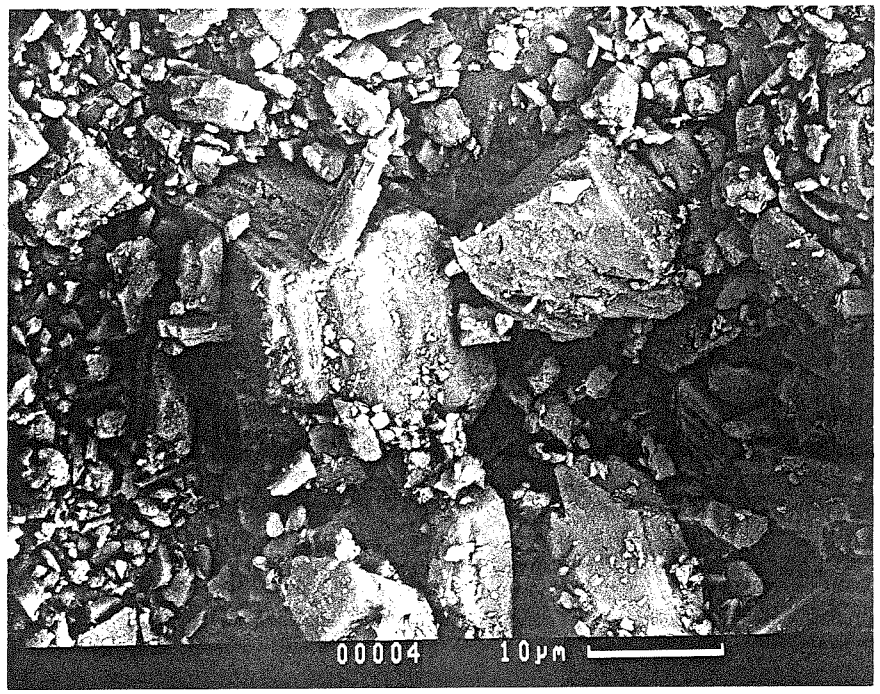

Figure 2-4 SEM images of experimental powders
(a) Diopside 1 (before experiments)

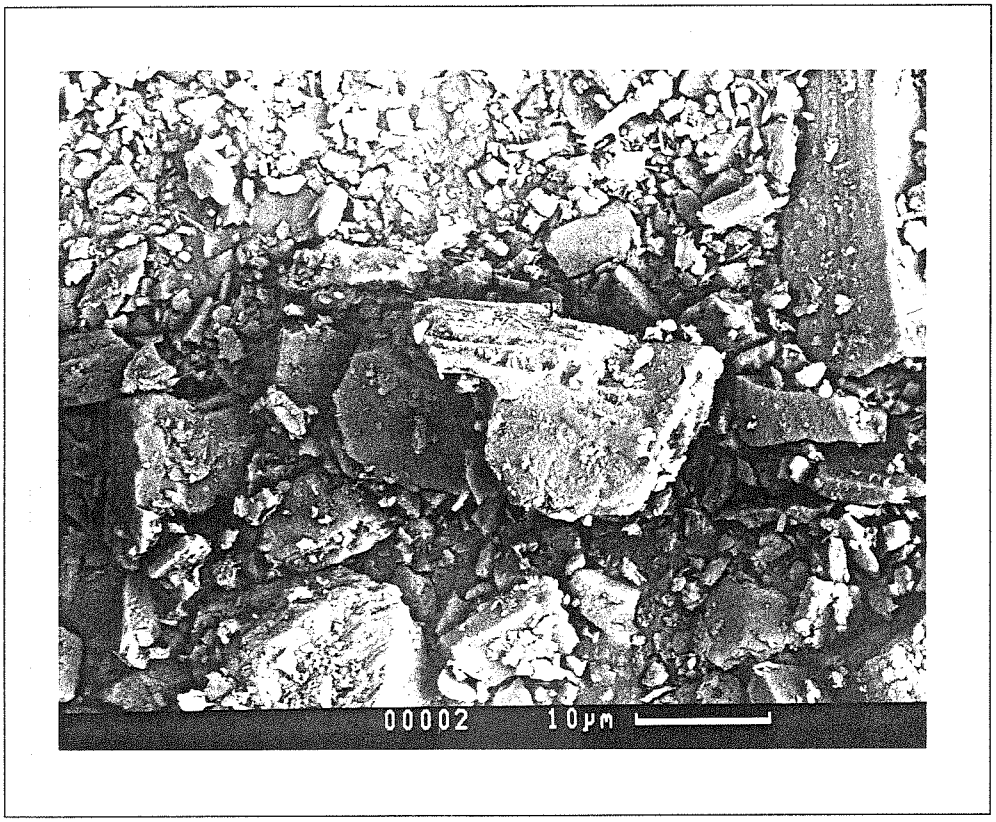

Figure 2-4 (b) Diopside 1 (after EX25)

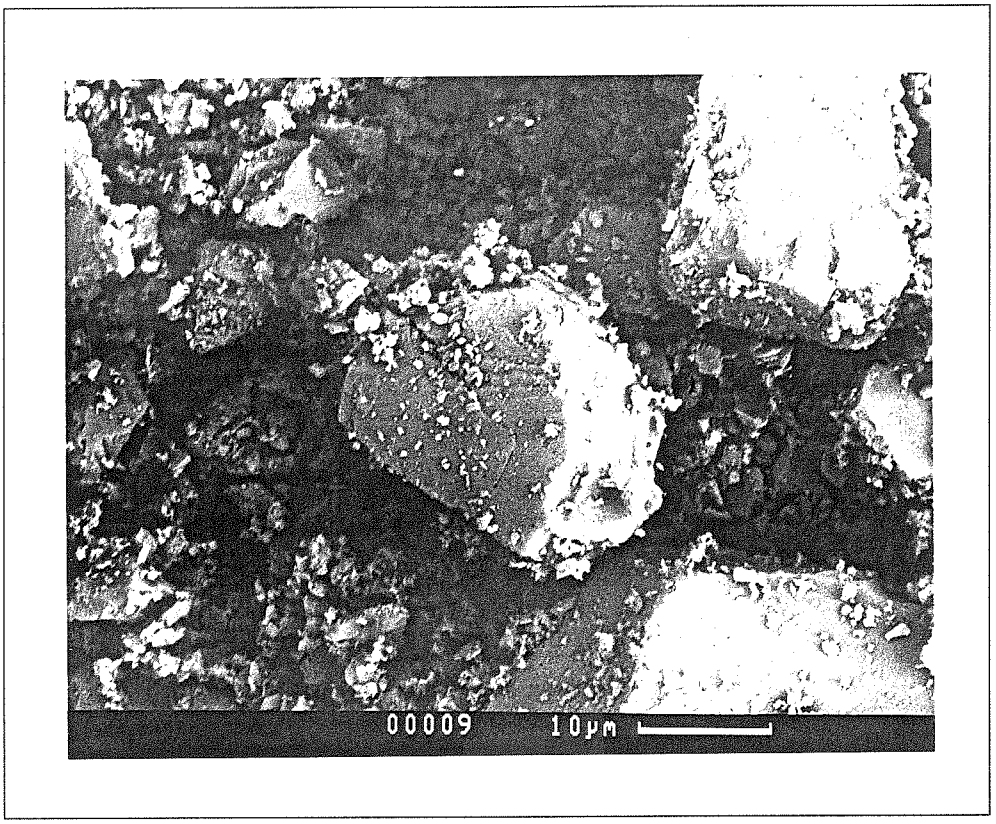

Figure 2-4 (c) Plagioclase (before experiments)

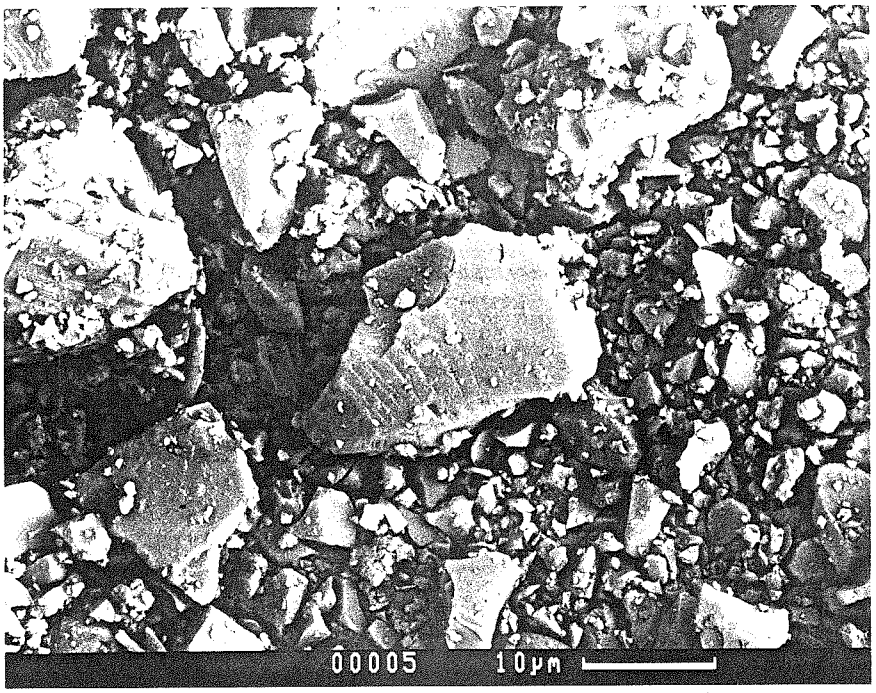

Figure 2-4 (d) Basalt 1 (before experiments)

2.3 PROCEDURE

2.3.1 Typical protocol (refer to Figure 2-3)

Below is a description of the preparation and startup of a typical experiment at cold temperature and with water vapor. The circulator is assumed to have been running continuously and already at experimental temperature. For room-temperature experiments, the circulator was simply left off. Consequently, data on bath and set temperature were not automatically collected but were instead occasionally checked by turning the unit on briefly. Estimation of H_2O content for experiments conducted under "vapor" conditions is discussed in the next section.

Dry powder (from a clear glass vial) was weighed on a sensitive pan balance accurate to 0.5 mg. Typically, 5 g of sample was used. No precautions were taken to avoid contact of powder with air (vials with screw-tops were not air-tight), and after weighing, the powder typically was set aside on weighing paper (covered by another piece of weighing paper) for about an hour. Before and during weighing, all parts of the pressure-drop apparatus——including $V_{5\ell}$ (typically left filled with CO_2 from a previous experiment)——were evacuated with the diffusion pump (through a liquid-nitrogen-cooled trap), and the CO_2 line was prepared. The absolute manometer, PA, was generally re-zeroed at this

point (it was sometimes off by 0.1 torr or more, but tended to be good to ±0.1 torr).

Next, S was unclamped (care was usually taken to prevent powder from getting into PD by temporarily closing valve *g* connecting it to S), and the O-ring removed after taped pieces of insulation were taken off. The metal lid of the circulator, with a rubber gasket between it and the top of the bath, was untaped from the rest of the circulator, so that S could be carefully removed through the underside of the lid and out of the bath. A piece of insulation at the neck of S was removed at this point, and the "after" sample from the previous experiment was saved in a labeled glass vial. If methanol in the bath of the circulator needed refilling, that was done as well.

While S was being cleaned, and with PA open to lab atmosphere, the difference between differential and absolute pressure was used (with the combined reference volume, $V_R + V_{PDr}$, still isolated at its experimental total pressure) to determine the total pressure remaining in the combined reference volume. If low CO_2 partial pressure had been used, care was taken to partially evacuate all parts of the system except the combined reference volume (using a finger to temporarily seal the O-ring connection so that pressures as measured with PD and PA were nearly stable after closing the pump), since otherwise differential pressure would have been off-scale. After cleaning with

deionized water and acetone, S was refilled with the new experimental powder, and reattached with neck insulation through the lid of the circulator at its O-ring connection, which was then clamped. When this was done, one of the thermocouples, which would have been detached in taking the previous experiment apart, was reinserted between S and its neck insulation to provide a (rough) record of temperature just below the lid of the circulator. Remaining insulation was reattached, and the lid was taped to the circulator.

Once S was reattached, S and R were evacuated, usually for a 20-minute period at $< 10^{-2}$ torr, before being closed at *e* and *f* so that preparation of water vapor could begin. It was verified that the pre-mixing volume, G, was evacuated, and then with valves *a*, *b*, and *d* open (valves *c* and *e* closed), deionized water was injected through the clamped rubber septum on G using a Hamilton 100-µl gas-tight syringe. Usually the pressure in $V_{5\ell} + V_L + V_{PA}$ rose without the plunger of the syringe being depressed, since water was immediately drawn by capillary action into the larger, evacuated volume. Typically, care was taken to insert into G an amount of water less than the vapor pressure of water at room temperature, and if too much was added or if condensation was observed to take place (e.g., if droplets of water remained after a minute or two), this was followed by some initial sustained pumping. In any case, it was usually necessary to briefly pump on G after

adding water, to reduce the pressure to that calculated to condense in S in roughly the amount desired. After this was done, valve *a* was closed and pressure stabilized within about 10 minutes. Then $V_{5\ell} + V_L + V_{PA}$ was opened at valve *e* to volume S, and both differential and absolute pressure were monitored while most of the water condensed in S. After 20 minutes, pressure was nearly stabilized, and the difference between this pressure and what it was before opening valve *e* was used to infer the water content (condensed, adsorbed, and vapor) of experimental runs.

When this period was over, valve *e* was closed, lines were evacuated, and CO_2 gas was introduced into G, carefully monitoring with PA, until an amount calculated to equilibrate in S to roughly experimental partial pressure was prepared. With *c* and *e* closed, and *b* and *d* open, the experiment was ready to begin. Time t = 0 occurred when valves *e* and *f* were simultaneously opened by hand (usually 5 turns, quickly) and then, within about 3 seconds, simultaneously closed in the same way. Differential pressure, as measured at PD, sometimes took a few seconds to respond, but usually after that there was a rapid rise in the first few minutes, often starting at negative differential pressure (in which case a differential pressure offset was taken into account in data reduction). After manually recording readings for a minute or two, the system above valve *e* was evacuated (except G, which was isolated with its

remaining CO_2——it would have taken longer to pump down), including the CO_2 line. With vacuum and CO_2 isolated, and valve *c* open, the manifold was finally left open to lab air so that lab atmospheric pressure could be monitored with PA (fluctuations in atmospheric pressure were later observed to have minimal effect on differential pressure). The data acquisition unit subsequently recorded data every 20 minutes (more often in earlier experiments).

2.3.2 Introduction of water

The principal way in which this typical experimental protocol varied involved the water-introduction procedure. Except for "damp" and "wet" cases, the amount of water actually contained in experimental volumes wasn't directly measured. "Dry" experiments were very similar to the typical "vapor" experiment described above, except that the water-introduction step was eliminated. "Damp" (1 ml of water) and "wet" (5 ml) experiments involved directly pipetting a carefully measured amount of deionized water onto powders after samples had been added to the cleaned sample volume, S. After attaching and sealing S, only very brief pumping occurred before CO_2-introduction (more would have been futile given the bulk liquid water and its vapor pressure).

Initially (up to EX9, inclusive), "vapor" experiments were genuine "pre-mixing" experiments in that a known amount

of CO_2 had already been introduced into G before water was carefully injected in the desired quantity. At t = 0, the gases were introduced together, and experimental amounts of each were calculated using simple PV = nRT relations and assuming that the water was carried along with the CO_2.

For EX40 through EX47, water was introduced as described for the typical experiment, except that, after preparation in G, valves *e* and *f* to both S *and* R were opened, and pressure was monitored for 20 minutes using PA only, before valve *e* was closed. Valve *f* was thus kept open until t = 0, when *e* was opened to allow introduction of CO_2, and then *e* and *f* were simultaneously closed. The procedure for EX48 onward returned to the simplified protocol described in section 2.3.1 above.

The calculation of water content——[ml] and [monolayers]——was performed as follows:

$$n_1 = \text{"pre-mixed" \# moles of } H_2O = \Delta P_1 V/RT_r \qquad [2\text{-}6]$$

where ΔP_1 = observed pressure change (absolute pressure, measured with PA) when H_2O was initially injected, $V = V_{5\ell} + V_L + V_{PA}$, R is the ideal gas constant, and T_r = room temperature (i.e., the temperature of volume V).

For EX6-9, the amount n_2 of H_2O vapor transferred along with CO_2 was assumed to be proportional to n_1 but weighted by temperature in addition to volume:

$$n_2 = n_1 \times V_S'/T \;/\; [\; (V_S' + V_R')/T + V/T_r \;] \qquad [2\text{-}7]$$

where $V_S' = V_S + V_{PDs} - m/\rho$ (i.e., "combined sample volume," corrected for powder volume), $V_R' = V_R + V_{PDr}$, T = experimental temperature, and V and T_r were as above. This gave a lower bound on n_2 since it assumed that the gases were transferred in proportion to the volumes (but the gases were less likely to make it into V_R' due to the longer distance), and that no H_2O was preferentially adsorbed or condensed in V_S' in the time that valves were open at t = 0.

In the case of the "typical" procedure for "vapor" experiments, n_1 remained the same, but a second pressure, P_2, was recorded when H_2O was added to V_S'. For cold experiments, assuming the H_2O was efficiently adsorbed or possibly condensed, and that there was insufficient time when valves were open at t = 0 to transfer much H_2O into V_R' (the vapor that would have been carried along would have been much less than the H_2O adsorbed or condensed in V_S'):

$$n_2 = n_1 - P_2V/RT_r \qquad [2\text{-}8]$$

This gave an upper bound on n_2 since it assumed that all the vapor remained in V_S' when valves were open. For warm experiments, assuming the H_2O was *not* substantially adsorbed, i.e., that it was redistributed in proportion to the volumes:

$$n_2 = (n_1 - P_2V/RT_r) \times [\ V_S' / (V_S' + V_R')\ ] \qquad [2\text{-}9]$$

As before when H_2O was assumed transferred in proportion to volumes, this gave a lower bound on n_2.

For EX40-47, when H_2O was added to V_S' and V_R', the calculations (all for cold experiments) were the same as those described in the previous paragraph. In this case we could assume the H_2O vapor was preferentially adsorbed or condensed in V_S' because of the much greater surface area available than in V_R', and that it would have stayed there in the brief time valves were open at t = 0.

(The effect of the partial pressure of water vapor—— for warm experiments where no condensed water was present, and hence no guarantee that a secular drop in pressure was not due to water vapor being removed from the system by reaction——is discussed at the end of section 2.4.1.)

Therefore, to calculate experimental water content:

$$H_2O \text{ content [ml]} = n_2 \times (18 \text{ g/mole}) / (1 \text{ g/ml}) \qquad [2\text{-}10]$$

$$H_2O \text{ content [monolayers]} = n_2 \times (6\times10^{23} \text{ molecules/mole}) \times (10^{-19} \text{ m}^2\text{/molecule}) / [(\text{surface area in m}^2\text{/g/monolayer}) \times (\text{mass in g})] \qquad [2\text{-}11]$$

where 10^{-19} m^2/molecule = 10 $Å^2$/molecule is the surface area of an H_2O molecule (McClellan and Harnsberger, 1967).

2.3.3 Rationale for individual experiments

In general, early experiments with this apparatus—EX5C through EX14C—consisted of either control experiments, typically to test for leaks in the apparatus, or "dry" or "vapor" experiments with Diopside 1 (EX6,8,12,13), to test the performance of the system.

Beginning during EX13, experiments were performed at room temperature (and generally 1 bar) to maximize CO_2 uptake. Emphasis then shifted to obtaining sufficient signal to investigate and constrain the role of water. EX15 through EX39 were thus generally "damp" or "wet" experiments, and the complete range of desired sample compositions was studied. Sufficient experiments were performed with Diopside 1 and Basalt to characterize the dependence of pressure-drop results on water—both compositions were studied under "dry," "vapor," "damp," and "wet" conditions. The other samples—Diopside 2, Olivines 1 and 2, Quartz, and Plagioclase—were only subjected to "damp" conditions, for comparison with Diopside 1 and Basalt. And, one experiment with Calcite was performed under "wet" conditions to investigate the possible effect of reactions between CO_2 and H_2O and preexisting carbonate in samples. Late in this period, the first experiments with lower CO_2 partial pressures were run, on Basalt at 100 mb and 33 mb.

Finally, beginning with EX40, experiments focused on Basalt at lower temperatures and CO_2 partial pressures, and under "vapor" conditions, so that experimental conditions more closely resembled the proposed analog, the past and present surface of Mars (see Appendix A.3).

2.4 RESULTS

2.4.1 Raw data

See Table 2-1 (section 2.1.3) for a summary of experimental conditions and results. Raw data for all non-control experiments, and for times t = 0 to t = Δt_{eff}, are shown in Figure 2-5 (pages 67-87). The interval Δt_{eff} in Table 2-1 refers to the total time that experiments were run while initial temperature and CO_2 partial pressure were maintained (e.g., until temperature was changed, or a desorption leg was begun).

The plots in Figure 2-5 are for automatically-acquired differential pressure, with slight corrections made for reproducible systematic offsets due to the data acquisition unit, and uniformly degraded to 20-minute resolution (i.e., sampled only every 20 minutes for those experiments where data were actually acquired more frequently), with the exception of the manually-recorded data——shown as dots for

EX6 and EX8——before automatic acquisition began. A few data gaps occurred (EX12,19,23,24), and experiments with higher CO_2 partial pressures and/or greater water contents showed more pronounced diurnal fluctuations due primarily to fluctuations in room and bath temperature (see section 2.1.4). We have converted differential manometer readings from torr to mb, and have left in any offsets in pressure at t = 0 (corrected for in later plots), so many plots begin with negative differential pressure.

All plots are individually scaled, in both time and differential pressure, so care must be taken in interpreting differences among experiments. They are also grouped (as are plots in subsequent sections): **GROUP 1**, Diopside 1 (and Diopside 0); **GROUP 2**, Diopside 2, Olivines 1 and 2, Quartz, Plagioclase, and Calcite; **GROUP 3**, warm Basalts; and **GROUP 4**, cold Basalts. Results for control experiments (**GROUP 0**), and results for times after t = Δt_{eff} (i.e., including those portions with a temperature change or a desorption leg) are grouped separately in Appendix A.5.

The following preliminary observations can be made:

(a) Initial rapid adsorption: Almost all experiments began with a very short period (usually roughly 15-20 minutes) of rapid pressure drop (remember that a rise in differential pressure indicated that the total pressure had dropped in the sample volume relative to the

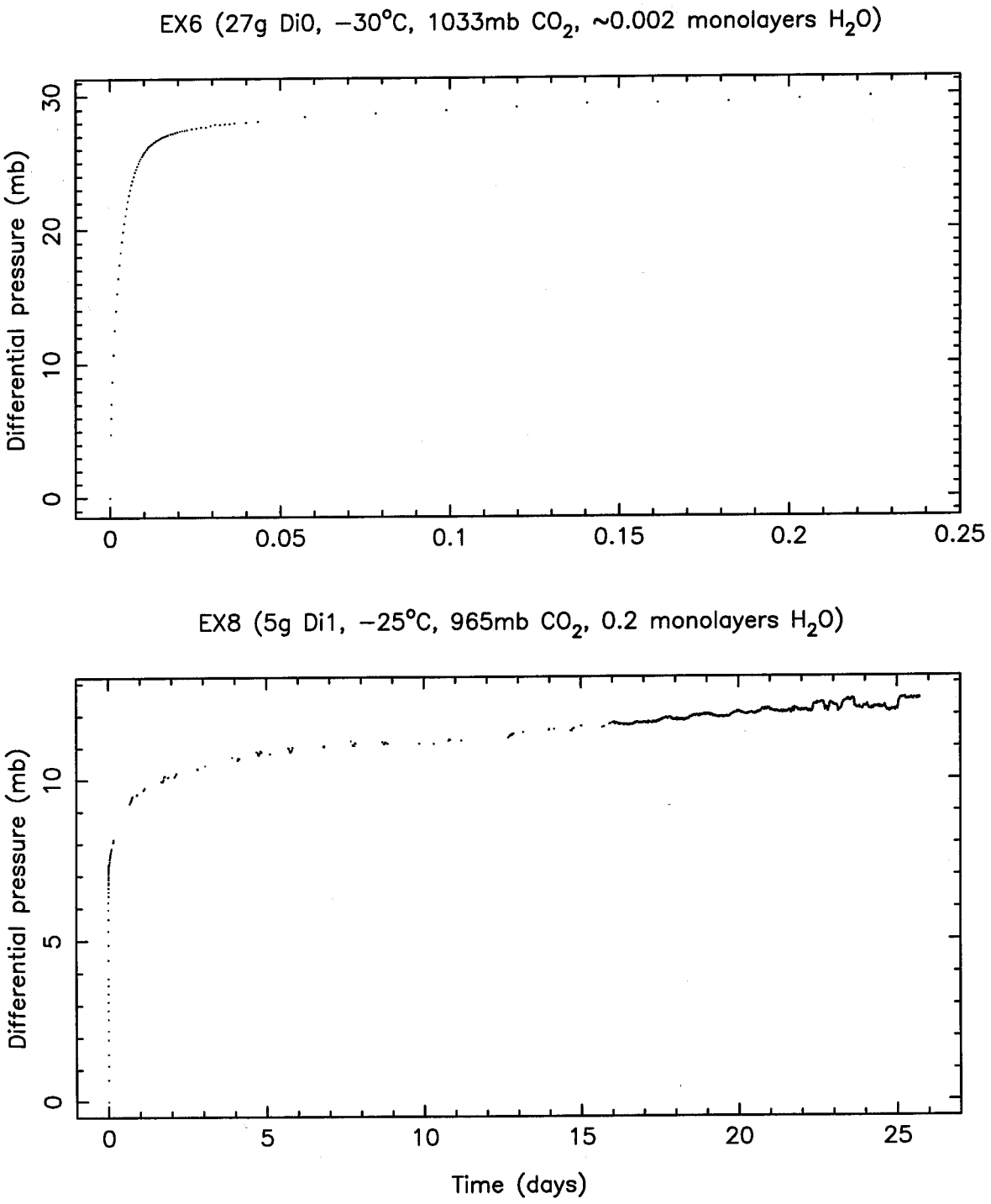

Figure 2-5 Plots of raw P(t) data
(a) **GROUP 1** [Di0,Di1]

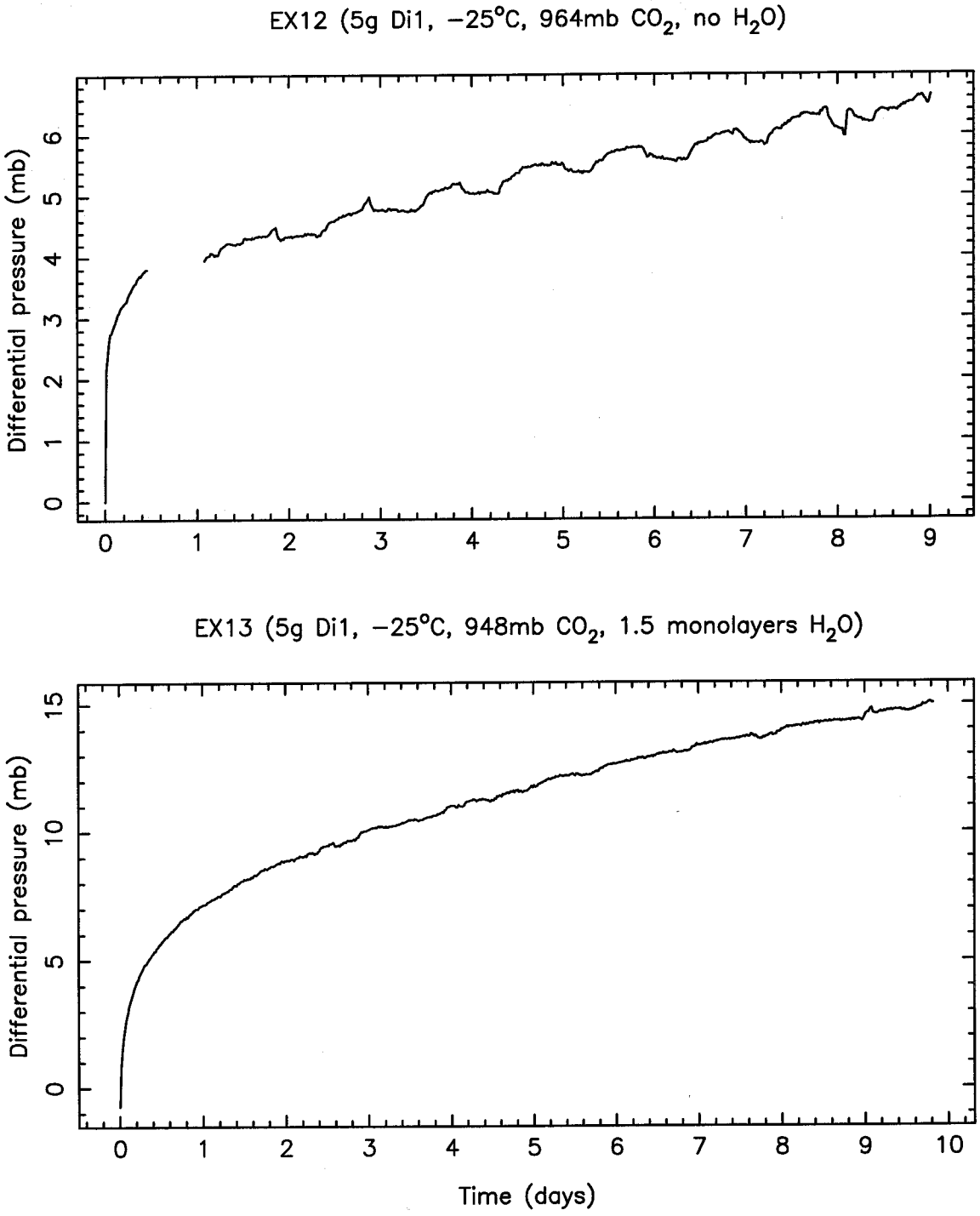

Figure 2-5 Plots of raw P(t) data (continued)
(a) **GROUP 1** [Di0,Di1]

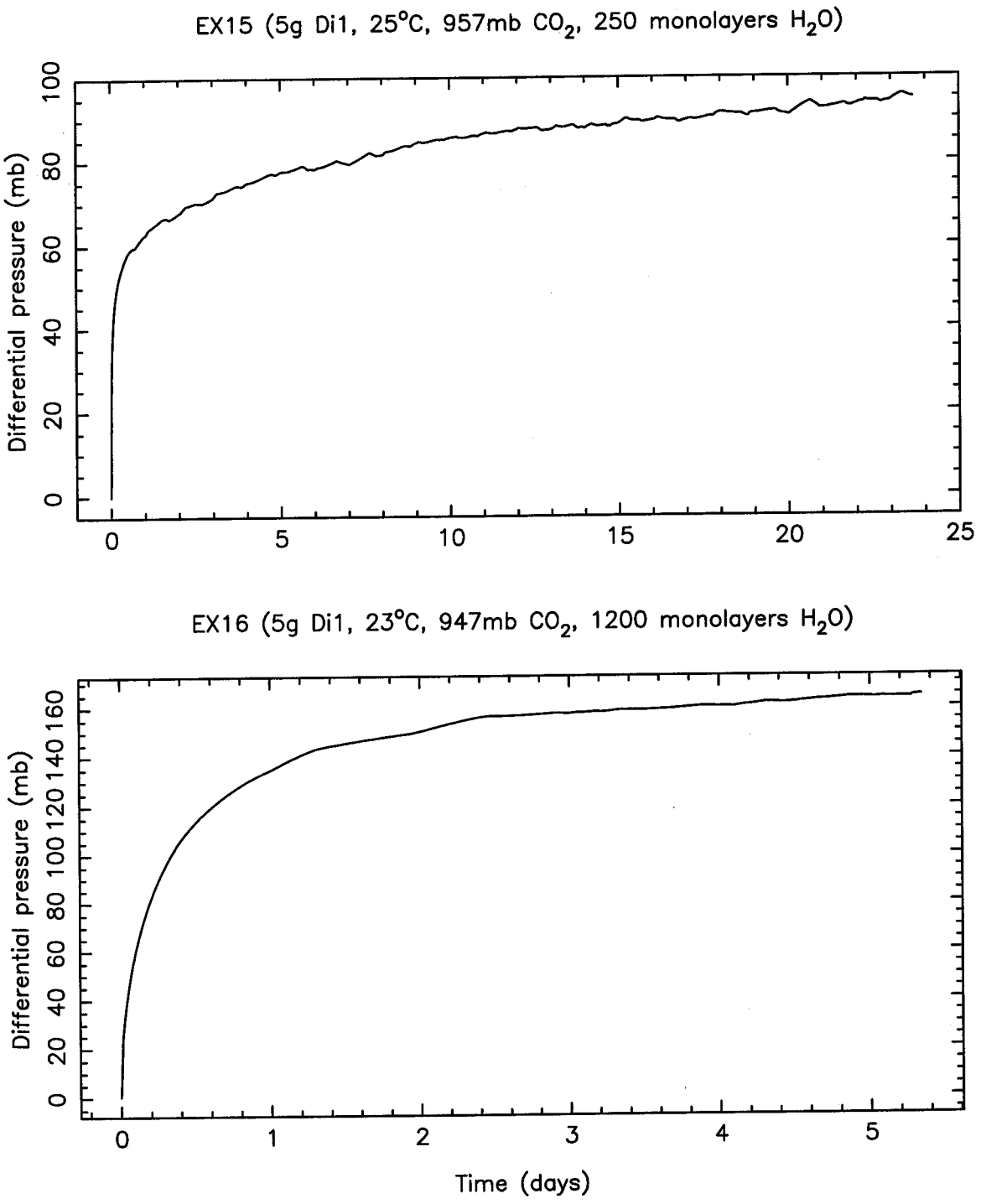

Figure 2-5 Plots of raw P(t) data (continued)
(a) **GROUP 1** [Di0,Di1]

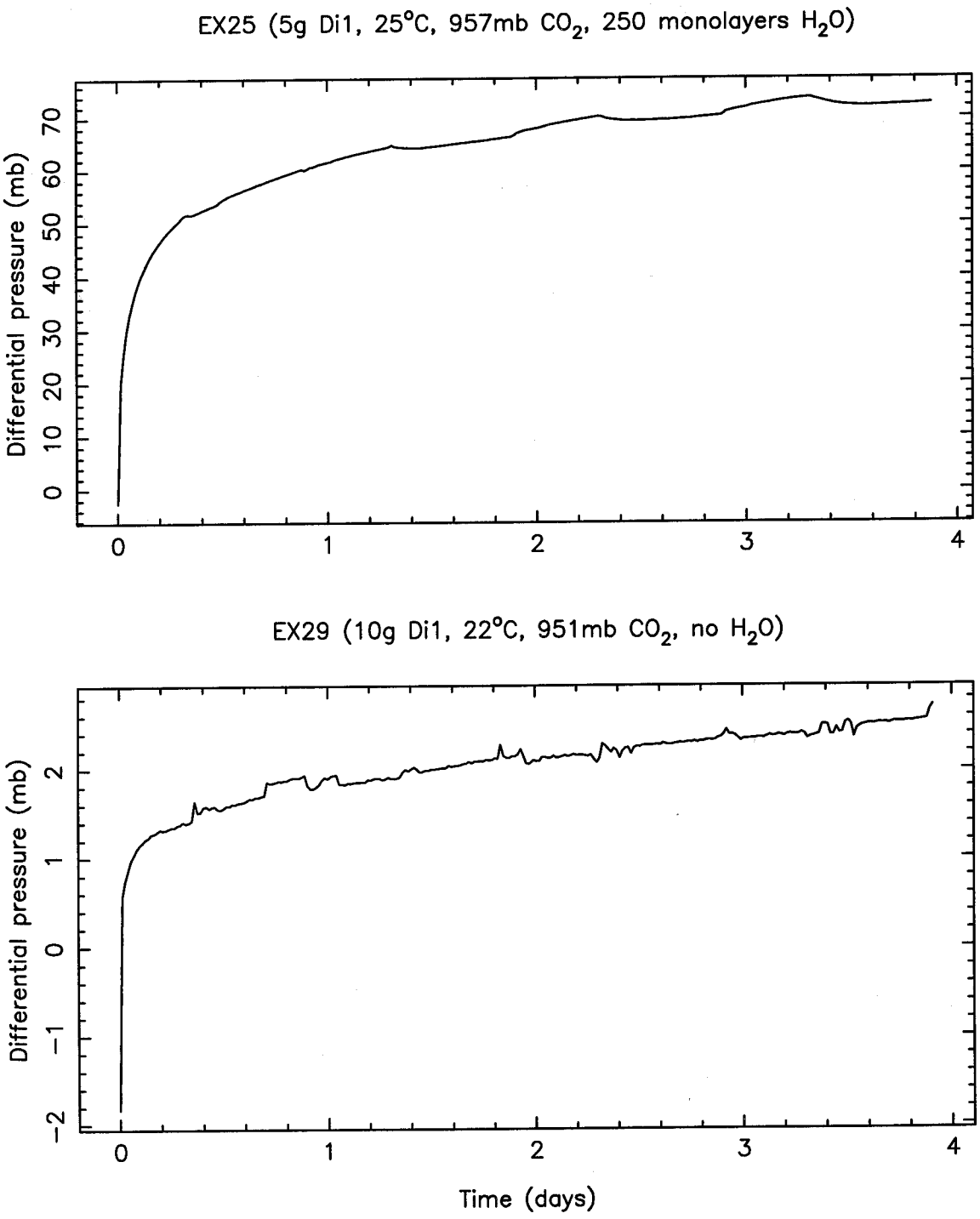

Figure 2-5 Plots of raw P(t) data (continued)
(a) **GROUP 1** [Di0,Di1]

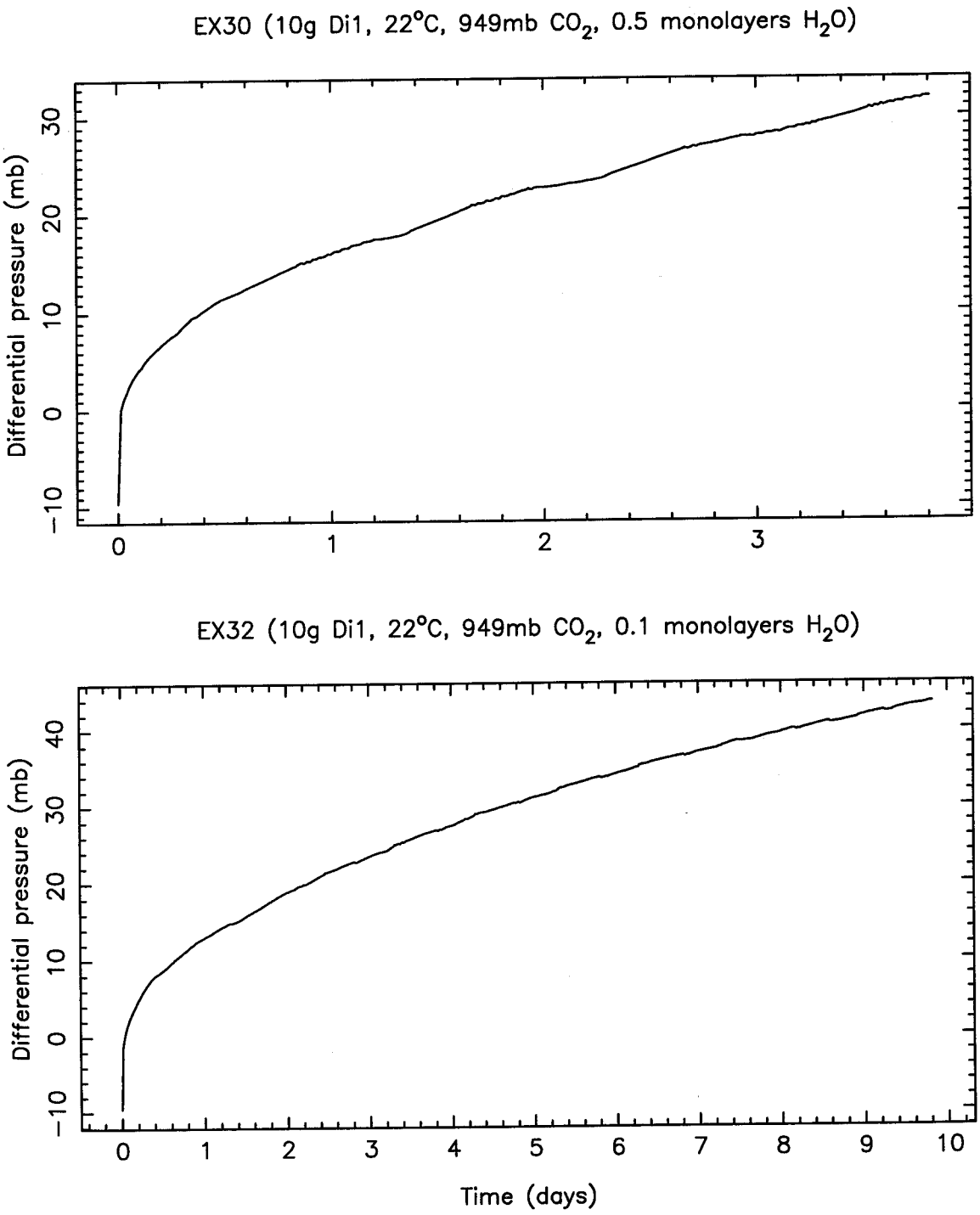

Figure 2-5 Plots of raw P(t) data (continued)
(a) **GROUP 1** [Di0,Di1]

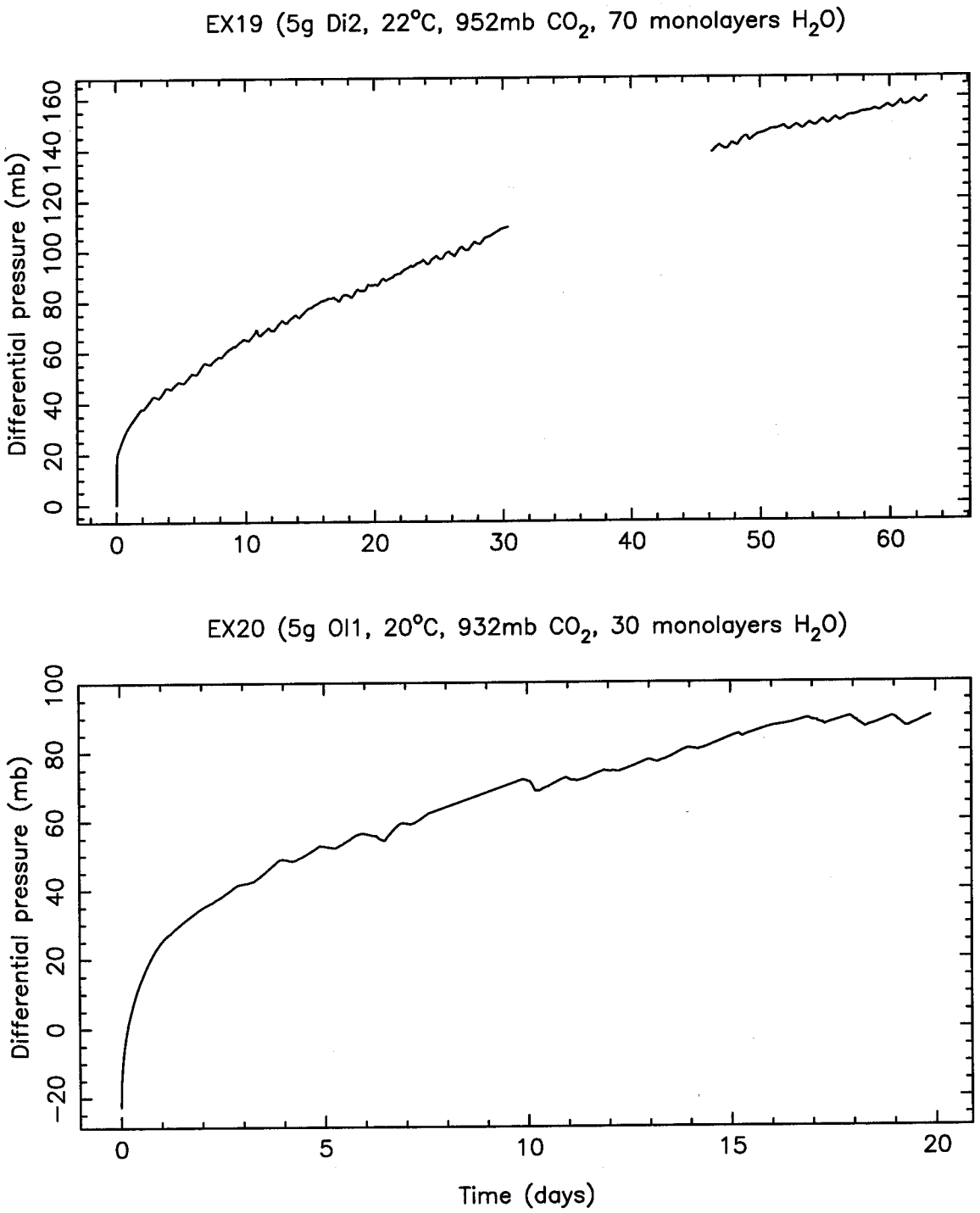

Figure 2-5 Plots of raw P(t) data
(b) **GROUP 2** [Di2,Ol1,Qtz,Plag,Ol2,Calc]

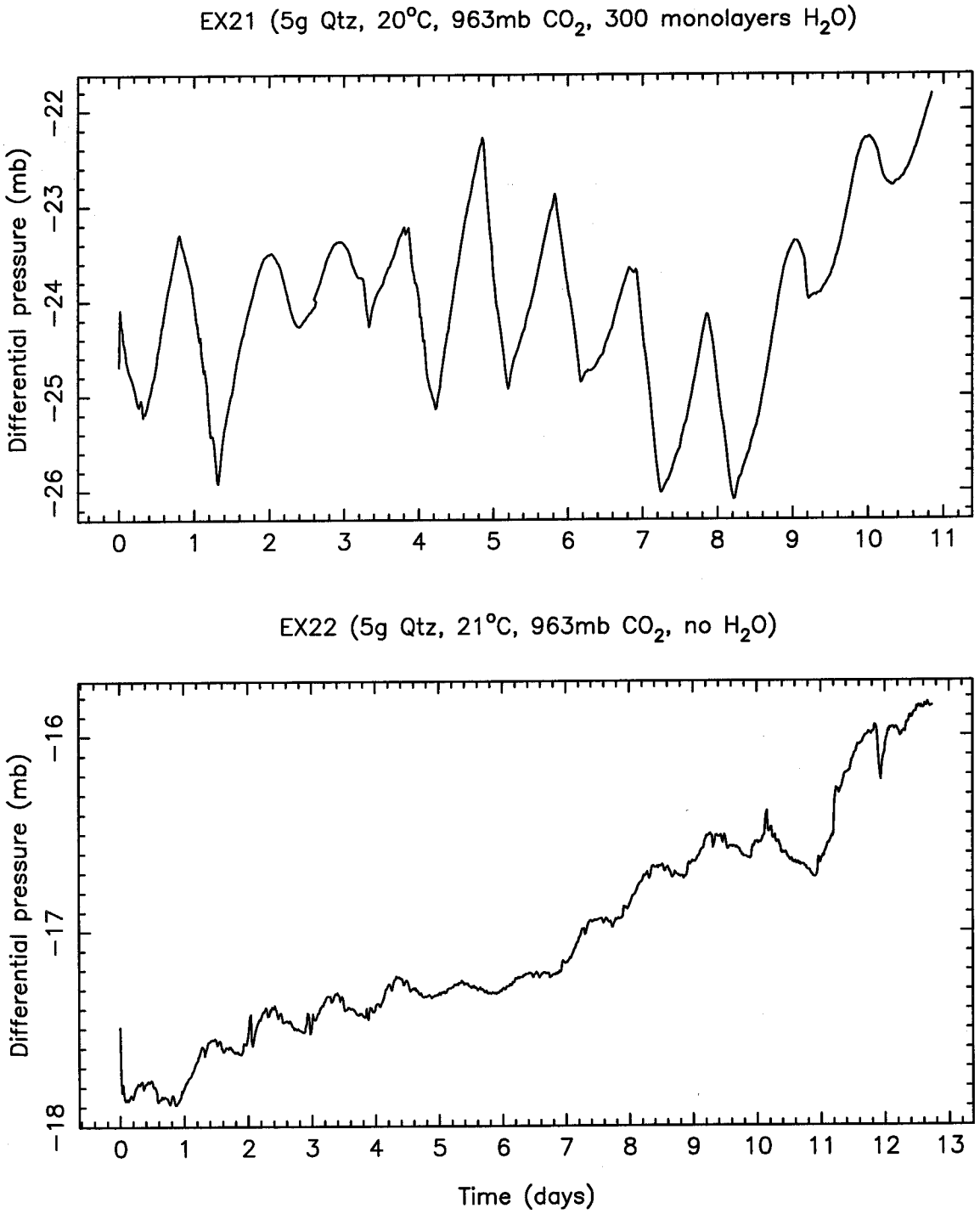

Figure 2-5 Plots of raw P(t) data (continued)
(b) **GROUP 2** [Di2,Ol1,Qtz,Plag,Ol2,Calc]

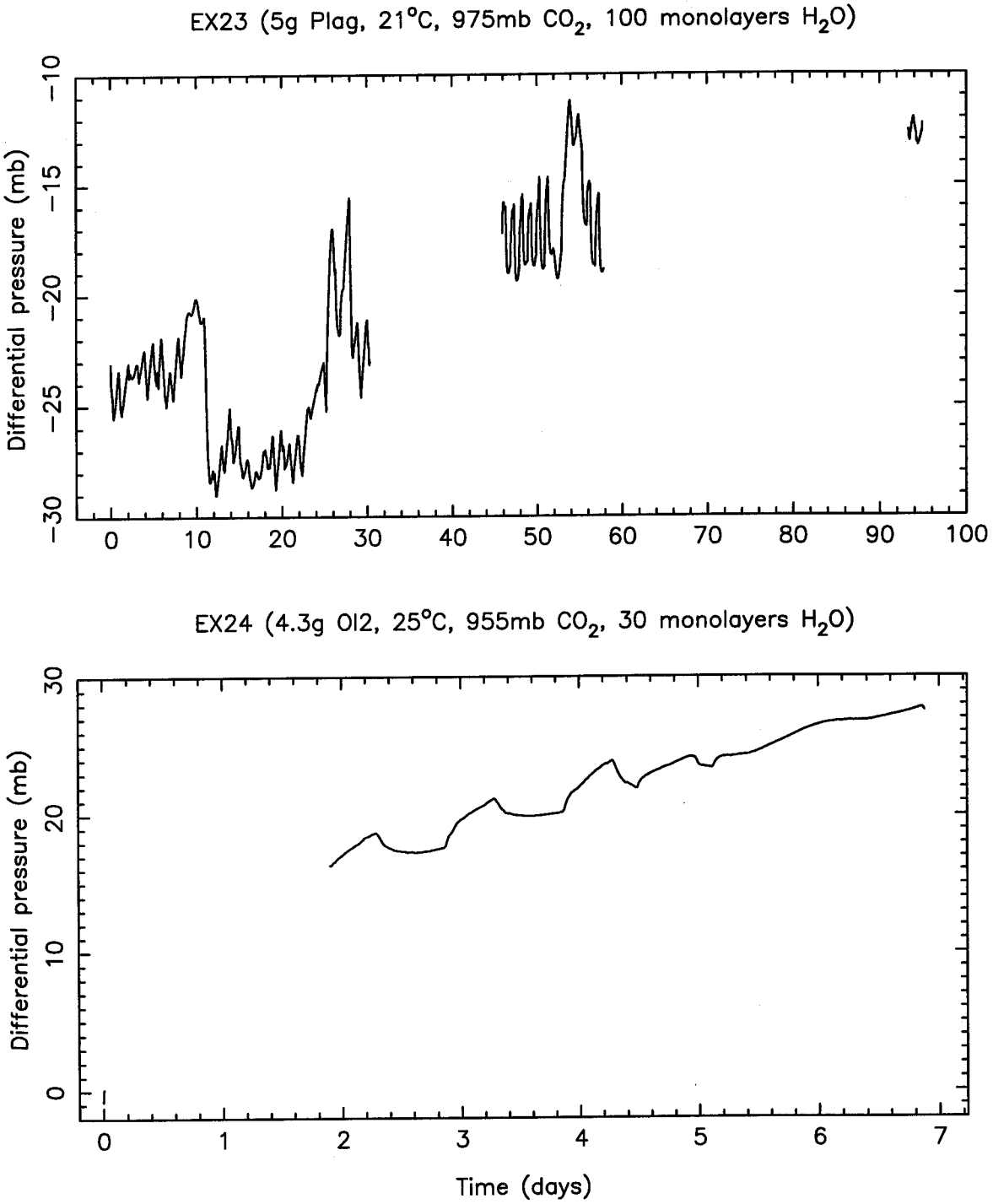

Figure 2-5 Plots of raw P(t) data (continued)
(b) **GROUP 2** [Di2,Ol1,Qtz,Plag,Ol2,Calc]

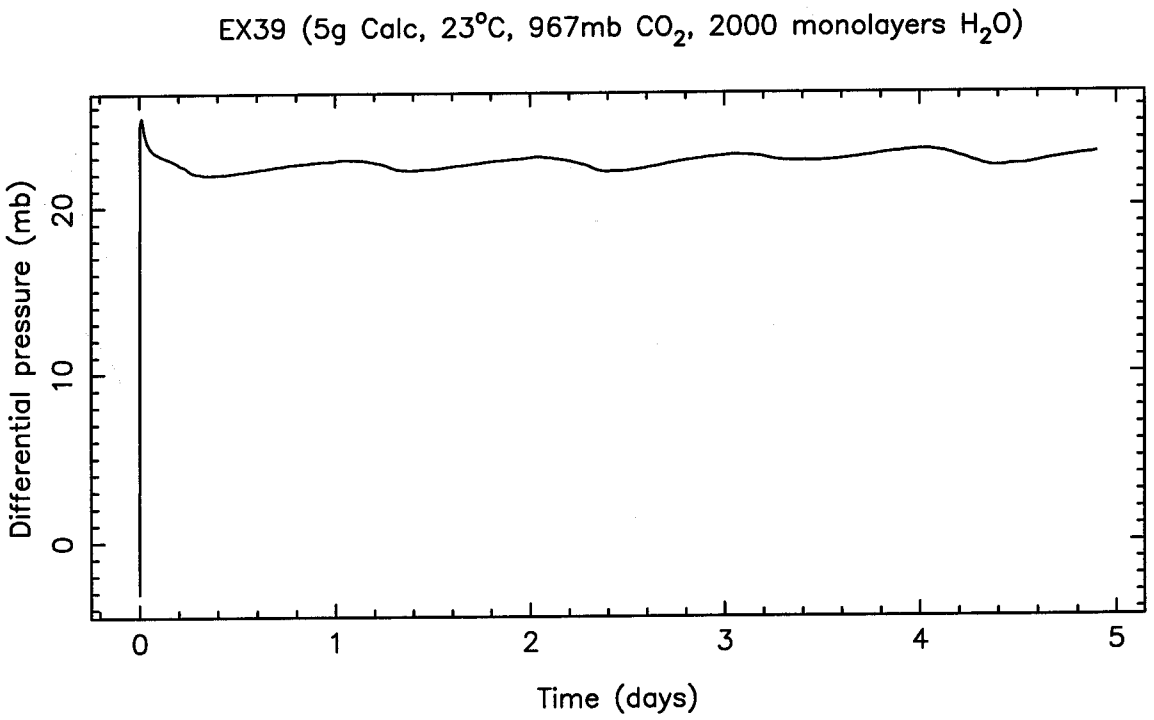

Figure 2-5 Plots of raw P(t) data (continued)
(b) **GROUP 2** [Di2,Ol1,Qtz,Plag,Ol2,Calc]

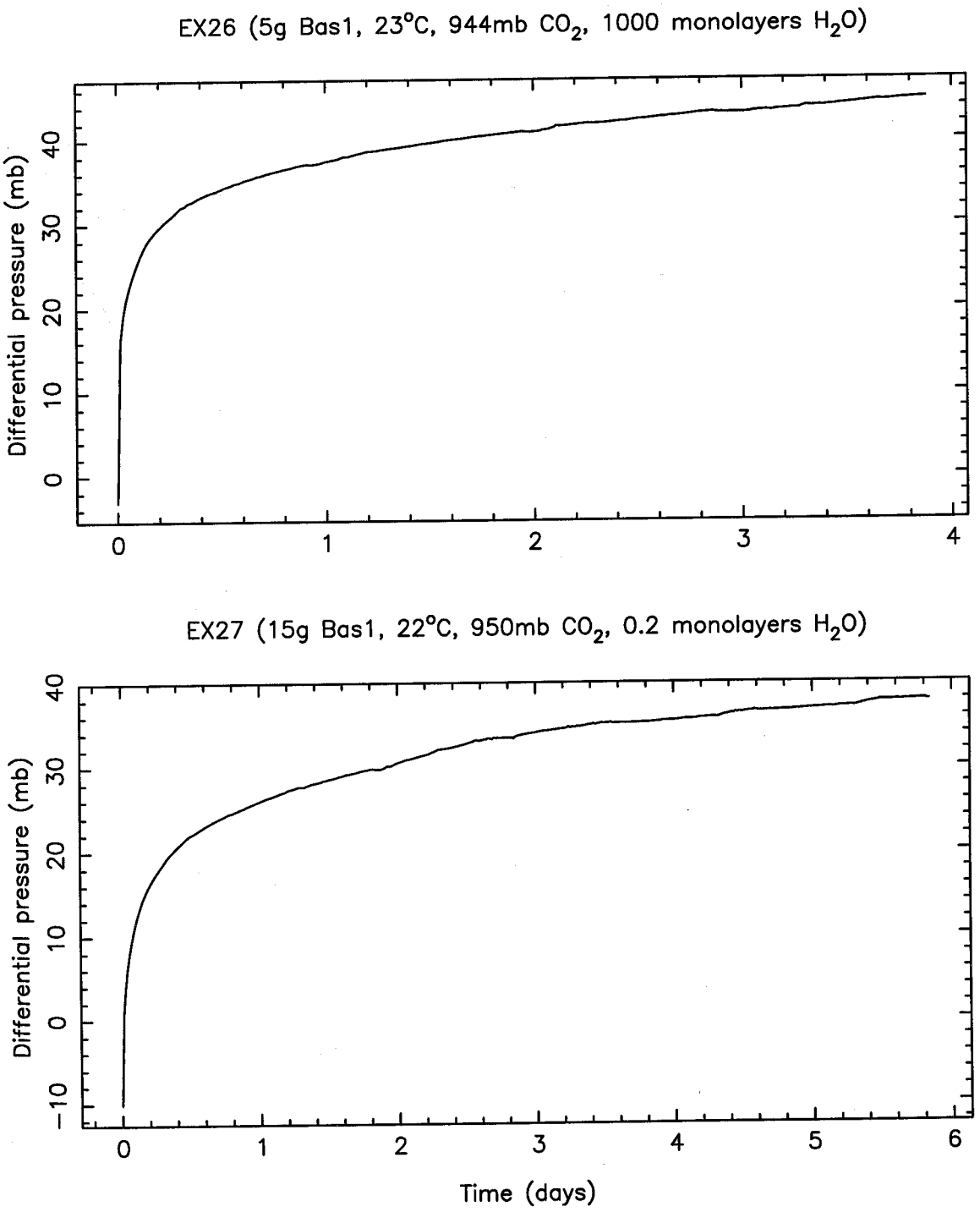

Figure 2-5 Plots of raw P(t) data
(c) **GROUP 3** [Bas/warm]

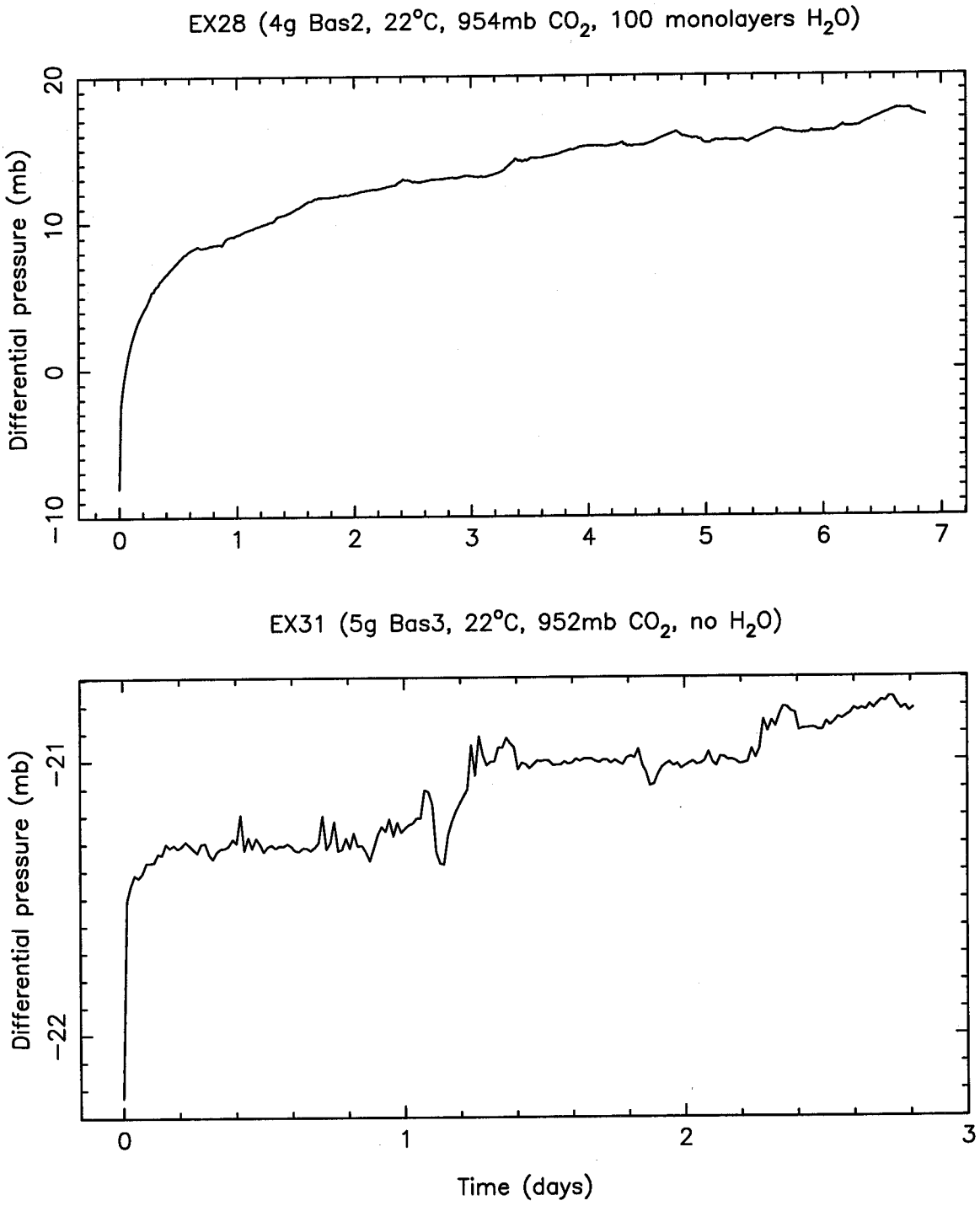

Figure 2-5 Plots of raw P(t) data (continued)
(c) **GROUP 3** [Bas/warm]

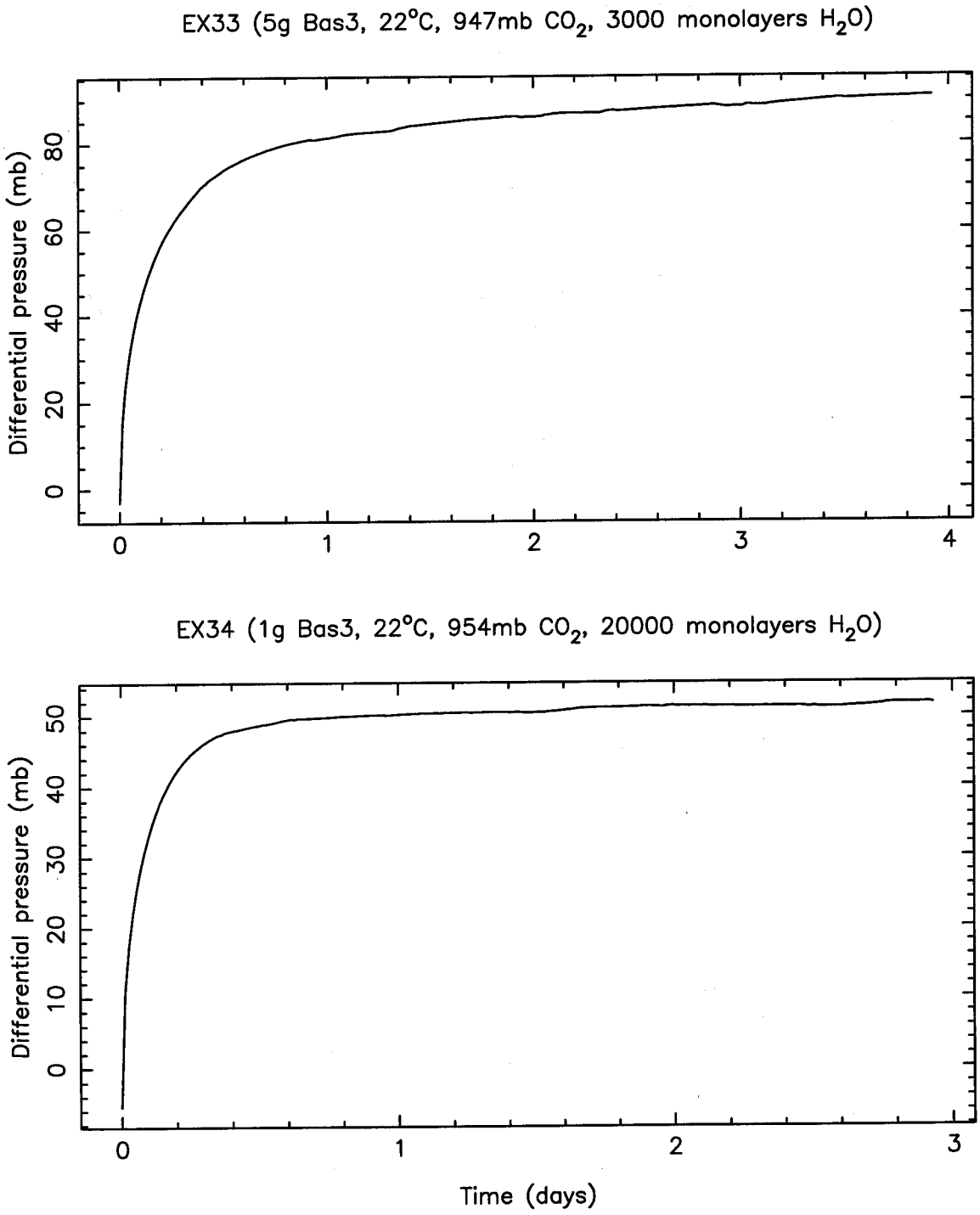

Figure 2-5 Plots of raw P(t) data (continued)
(c) **GROUP 3** [Bas/warm]

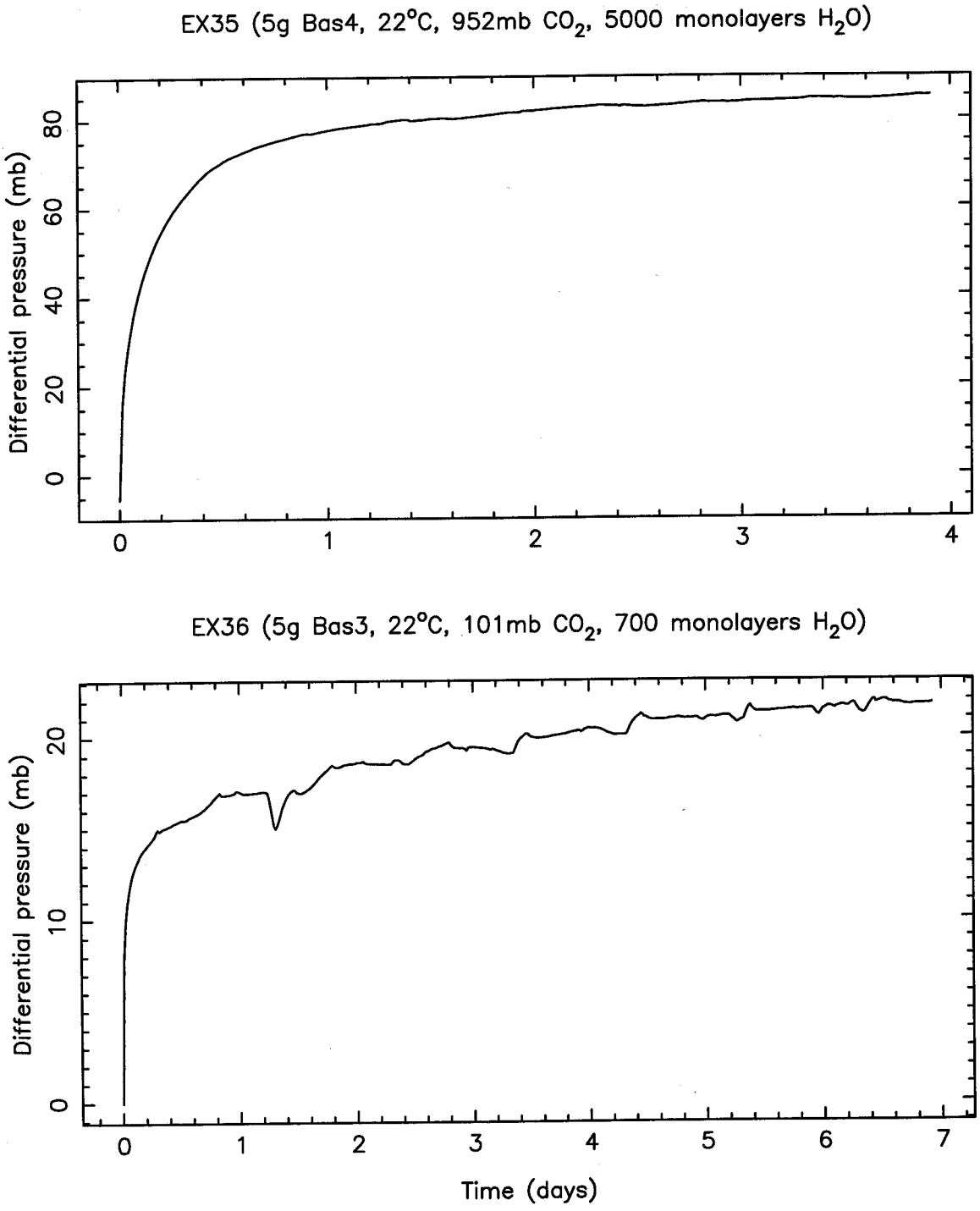

Figure 2-5 Plots of raw P(t) data (continued)
(c) **GROUP 3** [Bas/warm]

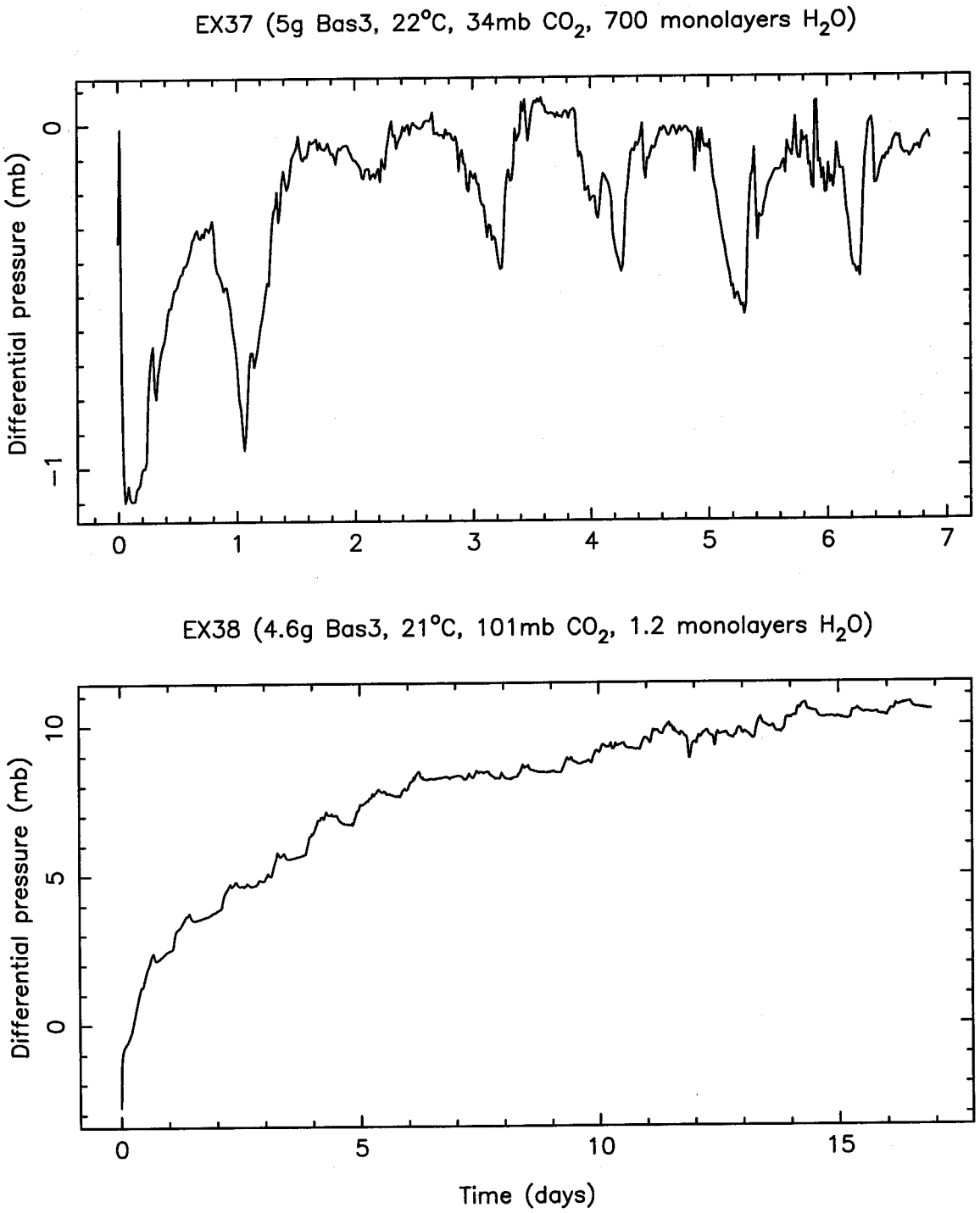

Figure 2-5 Plots of raw P(t) data (continued)
(c) **GROUP 3** [Bas/warm]

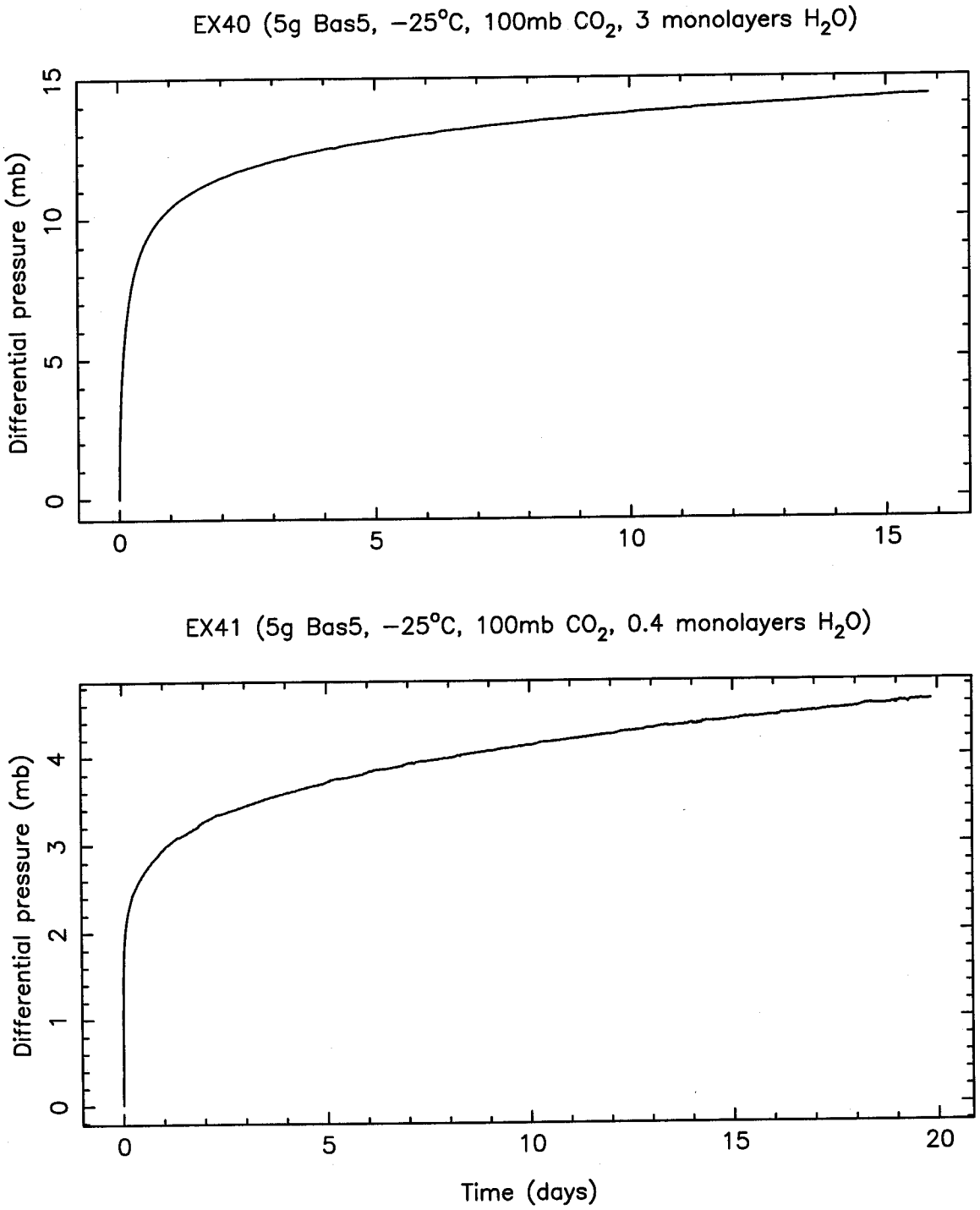

Figure 2-5 Plots of raw P(t) data
(d) **GROUP 4** [Bas/cold]

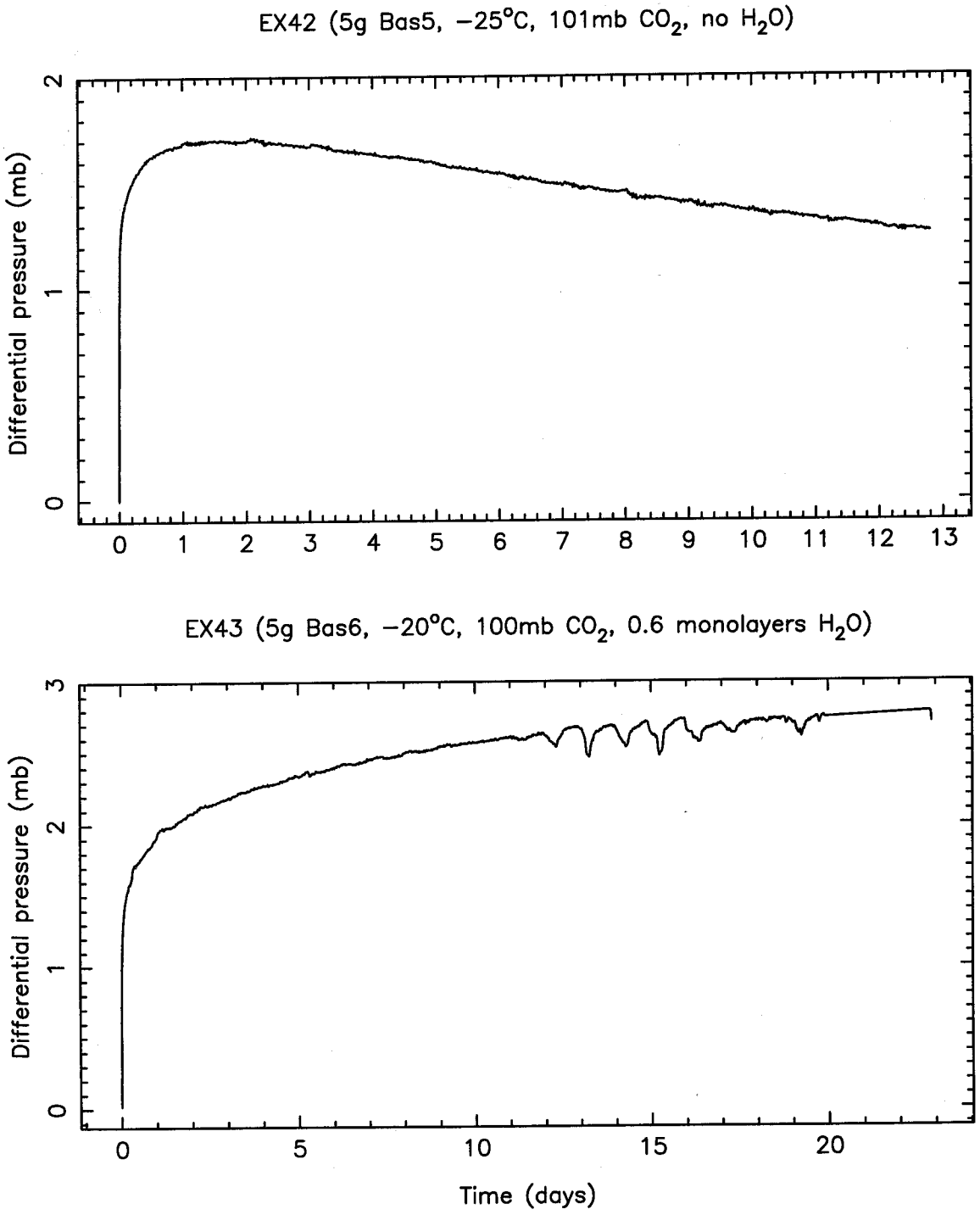

Figure 2-5 Plots of raw P(t) data (continued)
(d) **GROUP 4** [Bas/cold]

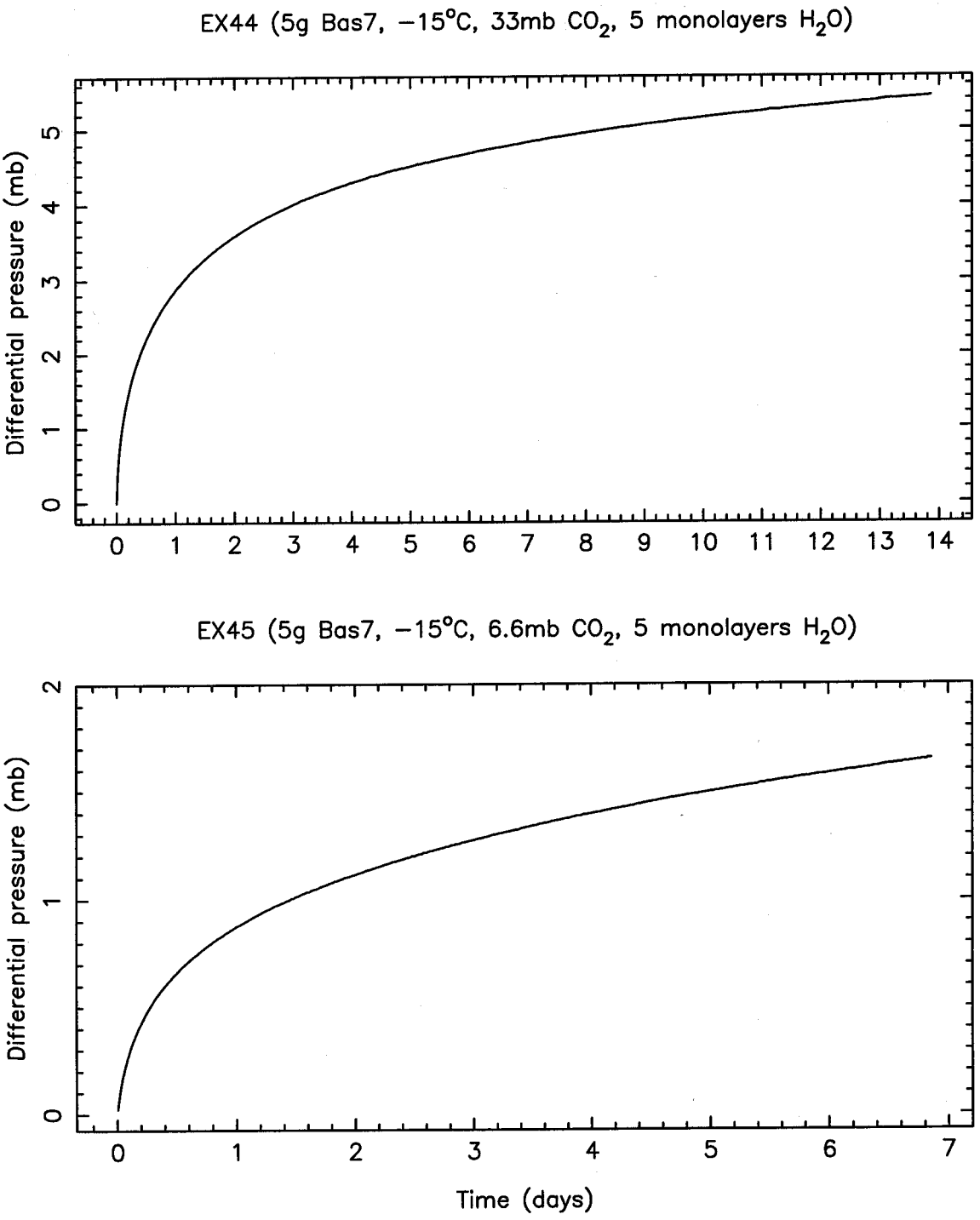

Figure 2-5 Plots of raw P(t) data (continued)
(d) **GROUP 4** [Bas/cold]

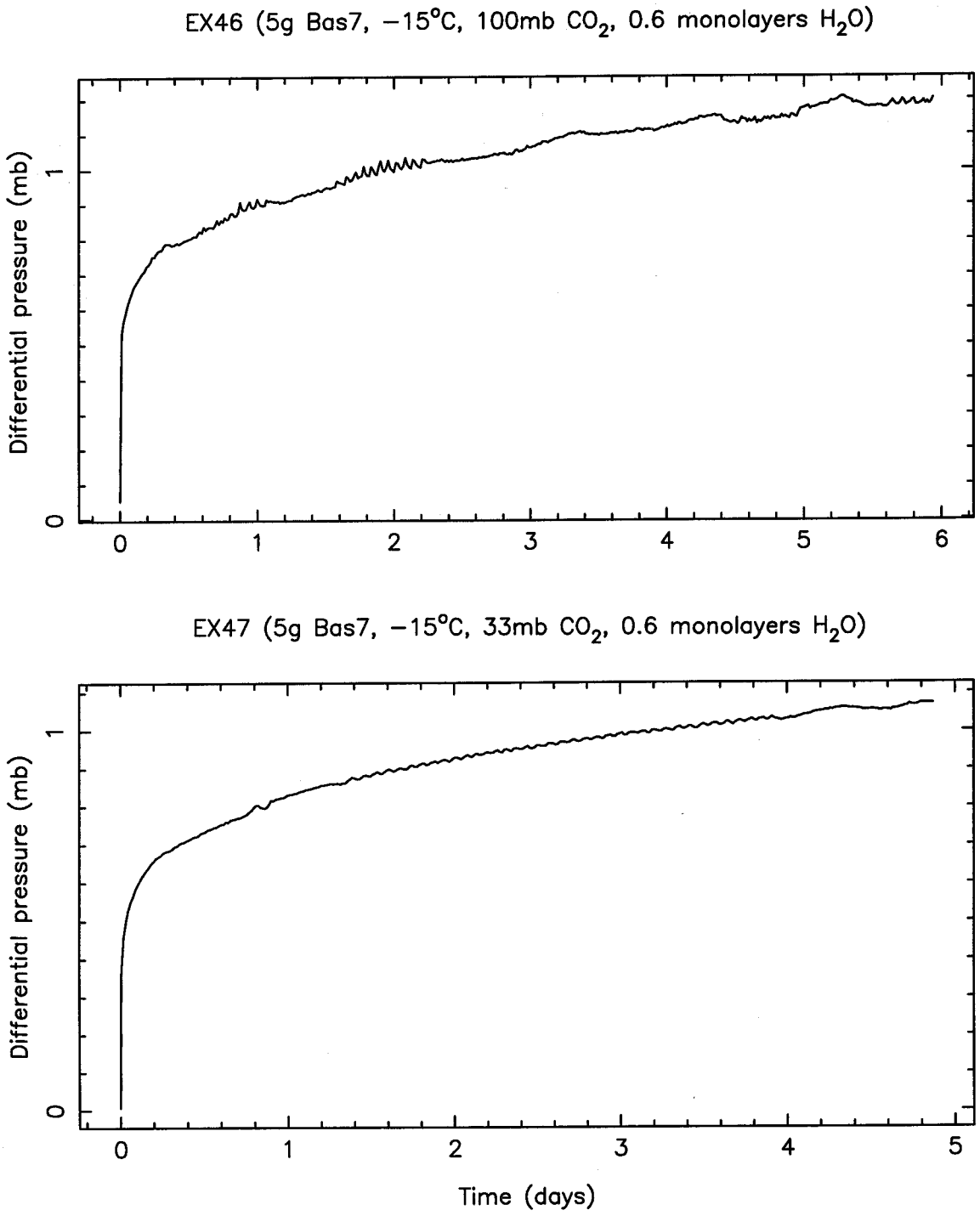

Figure 2-5 Plots of raw P(t) data (continued)
(d) **GROUP 4** [Bas/cold]

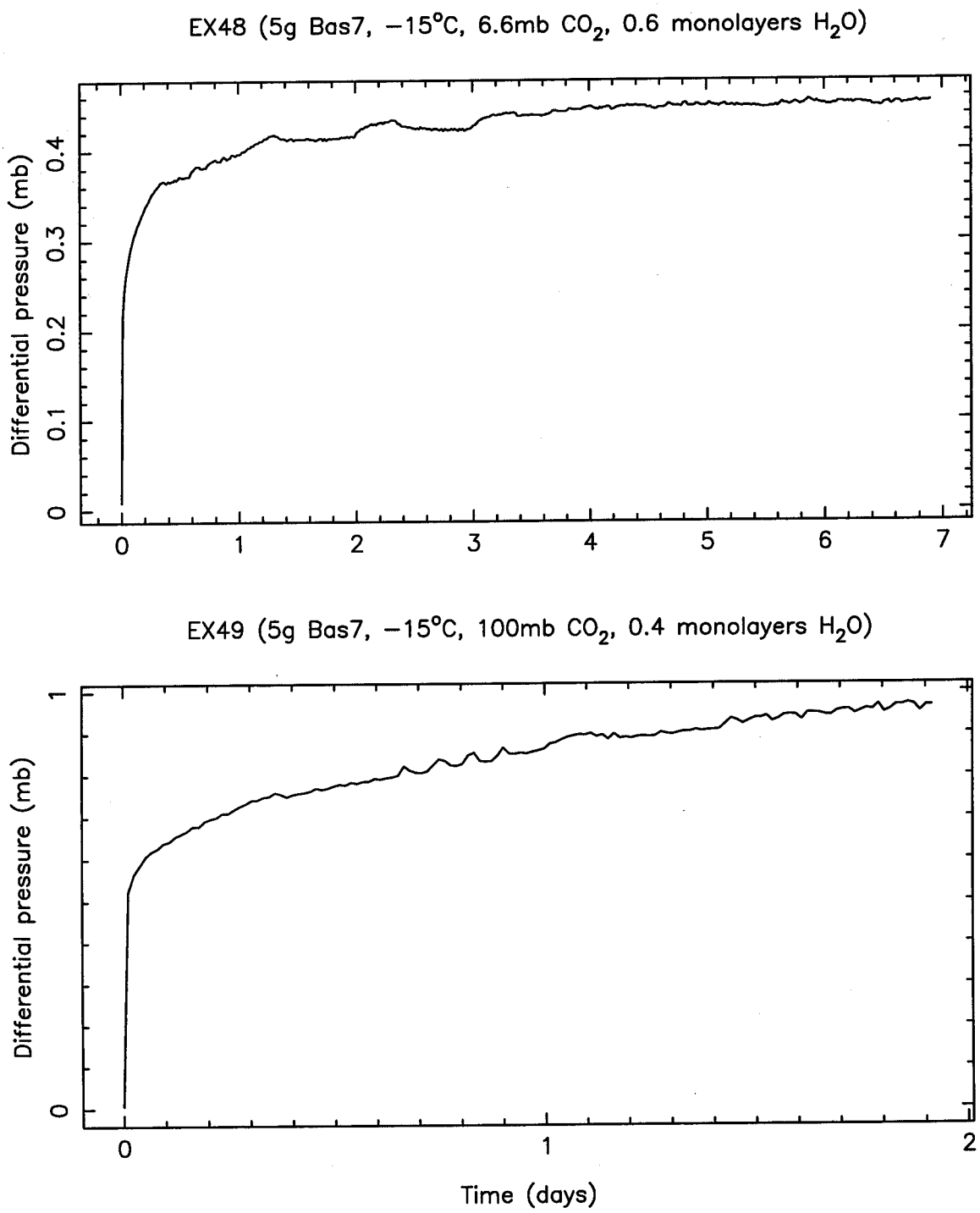

Figure 2-5 Plots of raw P(t) data (continued)
(d) **GROUP 4** [Bas/cold]

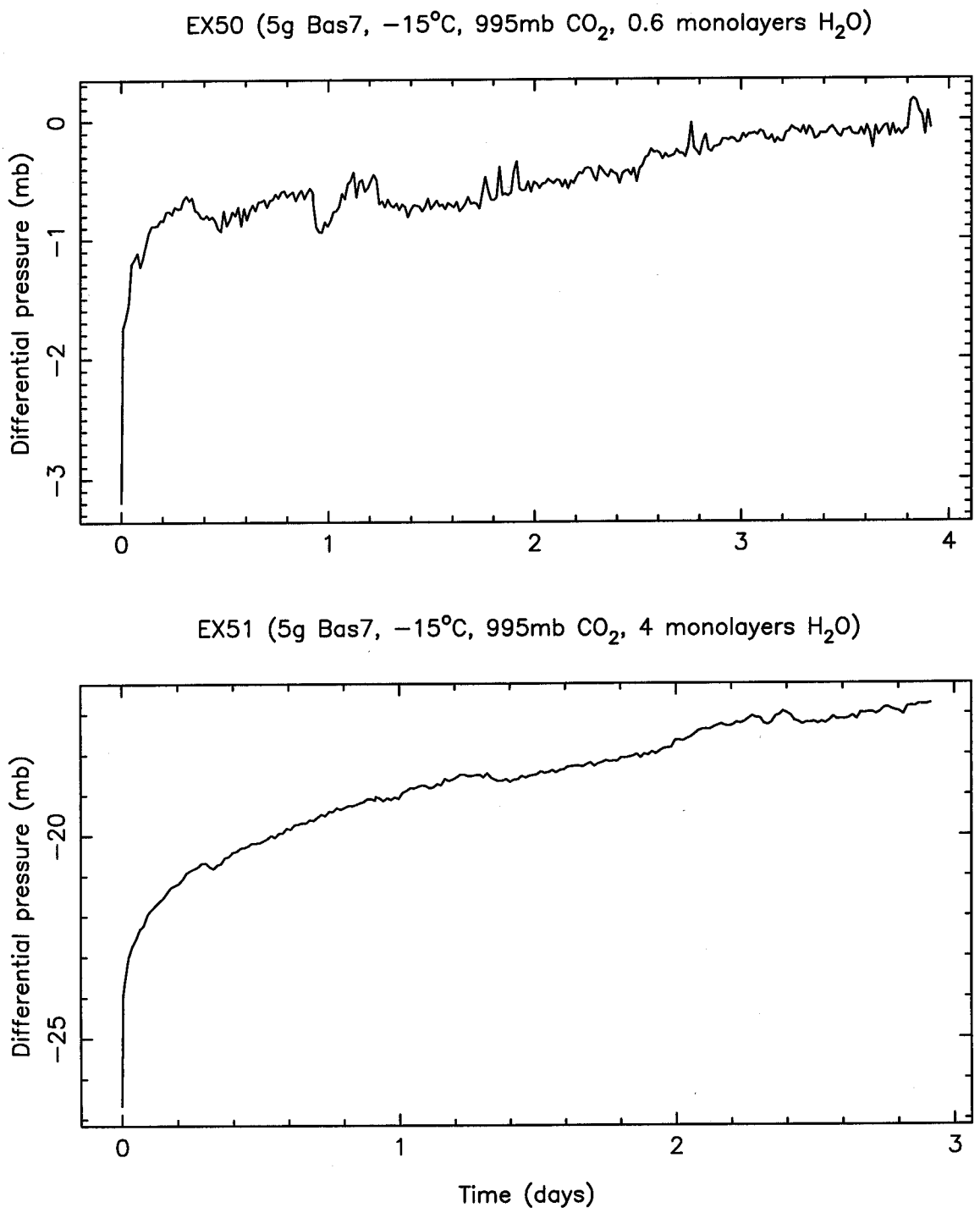

Figure 2-5 Plots of raw P(t) data (continued)
(d) **GROUP 4** [Bas/cold]

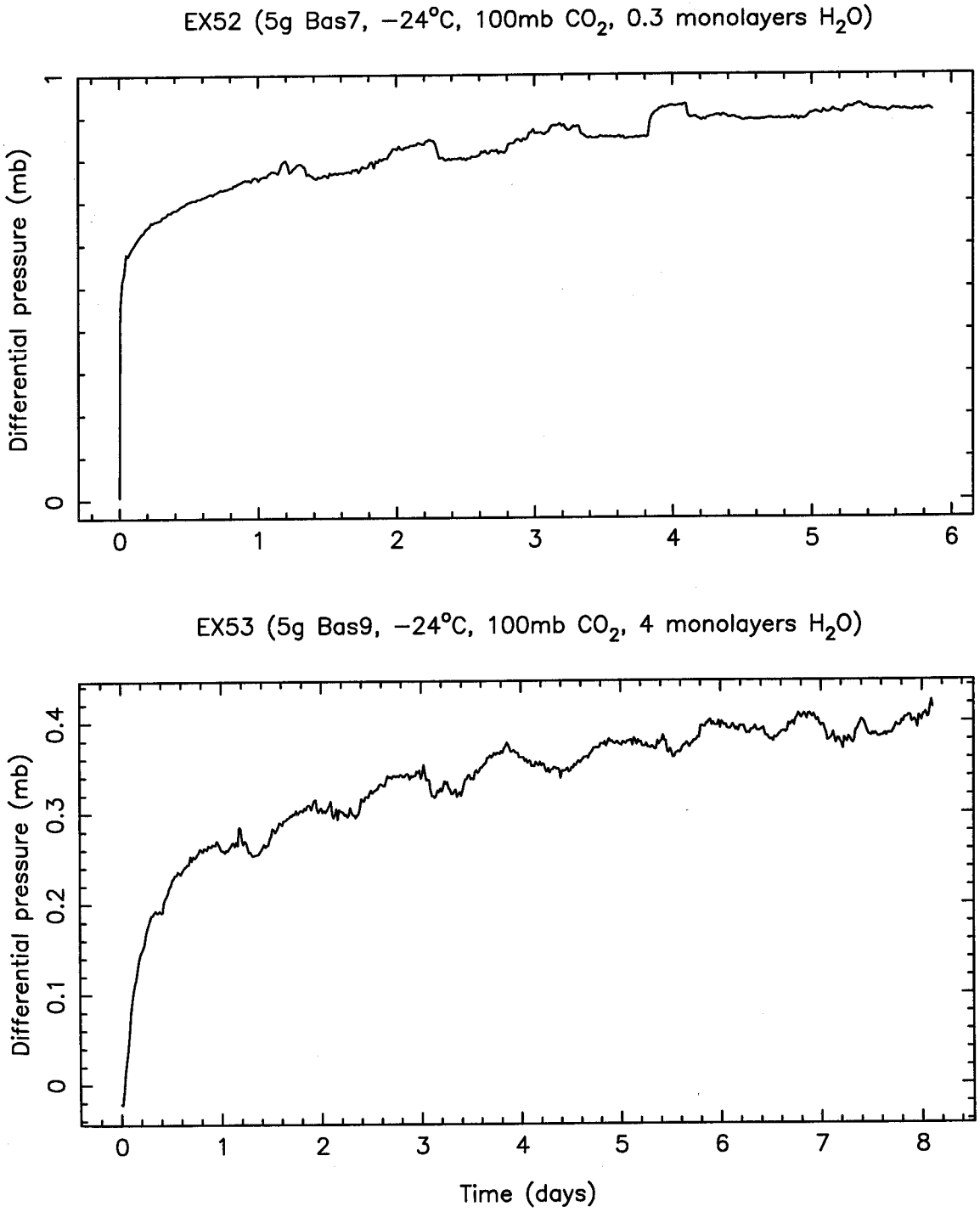

Figure 2-5 Plots of raw P(t) data (continued)
(d) **GROUP 4** [Bas/cold]

reference volume). See, for example, EX6, where this occurred in ~0.01 days. This initial, rapid uptake of CO_2 is attributed---for "dry" and "vapor" experiments---to the physical adsorption of CO_2, which is known to take place very quickly for our experimental pressures (e.g., Gregg and Sing, 1982, and Adamson, 1990; see discussion in Chapter 4). Adsorption also accounts for initial signals in some "damp" experiments (see below).

Gas diffusion through small pores in powder particles is unlikely to have continued beyond this time (see discussion in section 2.1.1). Thus, any further drop in pressure would not have been due to adsorption on pore surfaces. (The possibility of solid-state diffusion through a rind is addressed in Chapter 4.)

There were four experiments for which an initial rapid drop in pressure was *not* apparent (although see Chapter 4, in which logarithmic plots of data at early times *do* show signals consistent with CO_2 adsorption or dissolution in H_2O). EX21-23 contained Quartz and Plagioclase, and were run partly as controls. Presumably SiO_2 was not reactive with CO_2, but according to Gooding (1978), anorthitic (Ca-rich) plagioclase should have been unstable under our experimental conditions. It was somewhat surprising, therefore, that our Plagioclase sample showed no strong continued pressure drop. An explanation for this may involve the nature of the

tectosilicate framework structure of feldspar (like quartz in this respect), or perhaps plagioclase is simply less thermodynamically favored to react.

EX37 involved 34 mb of CO_2 and "damp" basalt; the result was not trustworthy because we realized afterward that 34 mb is close to the vapor pressure of water at room temperature (hence the CO_2-introduction, which follows H_2O introduction, may have been unreliable).

(b) CO_2 dissolution in H_2O: For "wet" and most "damp" experiments, initial CO_2 uptake is attributed to the solubility of CO_2 in H_2O. Empirically, EX17C (see Appendix A.5), a warm experiment similar to EX16, but with no sample, and with 949 mb of CO_2 over 5 ml of liquid H_2O, recorded ~40 mb of CO_2 uptake in ~0.01 days, consistent with the volume of CO_2 expected to be soluble in H_2O, as calculated from solubility coefficients in *Lange's Handbook of Chemistry*, 13th edition (Dean, 1985). If this is compared with results from "wet" experiments with 5 g of sample at 1 bar CO_2 pressure and room temperature in 5 ml of H_2O, dissolution of H_2O in CO_2 represented from a quarter (EX16) to a half (EX33,35) of the signal observed. It was also observed that initial large drops in CO_2 pressure for "wet" experiments were spread out over ~1 day, probably related to the interaction of carbonate and silicate ions in solution (for more discussion, see Chapter 4).

In "damp" experiments, pressure drops due to dissolution would have been less. Not only was there less H_2O, but powders were generally able to soak up the available water so that a pool of bulk liquid was no longer available for dissolution. For "vapor" experiments, dissolution would have been negligible.

Finally, since results for long-term CO_2 *rates*, representing carbonate formation, were not dependent on CO_2 dissolution, results presented in later plots (next section) were not significantly affected.

(c) Subsequent gradual pressure drop (reaction?): This occurred for virtually all experiments; only for a few (EX43,48,52-53) did it approach the upper limit on leak rate of ~0.03 mb/day (and even then it was not likely that leaks would all be in the direction of positive differential pressure). (Rates are more clearly depicted in the plots of the next section.)

One "dry" experiment, EX42, displayed a decrease in differential pressure after about 2 days, which was interpreted to be due to desorption of H_2O vapor that was not removed in the 20-minute evacuation prior to the start of the experiment. Calcite, in EX39, showed a decrease in differential pressure, following an initial large increase, and before a subsequent very gradual increase. Rather than being something like a "rebound" in gas dissolution, it was more likely, since

it was a "wet" experiment, that it was related to $CaCO_3$ dissolution chemistry.

It was (c)--subsequent gradual pressure drop--that this experiment was designed to investigate (a signal whose amount and rate separate it from adsorption or dissolution). We needed to demonstrate that this was due to a carbonate-forming reaction, using infrared spectroscopy or other analytical techniques (or, conversely, to prove that something else was responsible).

The possibility that observed continued experimental pressure drops in "vapor" experiments were due to changes in the partial pressure of water vapor could generally be discounted, because--at least for cold-temperature experiments--any water in the sample volume was mainly condensed (as opposed to vapor), and so the H_2O partial pressure should have been controlled by the vapor pressure, which shouldn't have changed except diurnally (due to fluctuations in lab temperature). Also, for "damp" and "wet" experiments conducted at warm temperatures, there was no reason to expect the vapor pressure of liquid water to change except diurnally. However, for four "vapor" experiments at warm temperatures--EX30,32 (**GROUP 1**) and EX27,38 (**GROUP 3**)--it is possible that part of the observed long-term pressure drop was due to water vapor being removed from the system by reaction or adsorption. This complicating

effect entered because there was no guarantee that condensed water was present to control the partial pressure of vapor.

2.4.2 Model dP/dt behavior

The long-term continued pressure drop observed in most experiments made us suspect that a reaction occurred between the gas and the mineral surface, leading to the formation of carbonate. This reaction could have had several possible time dependences. Rates commonly noted in the corrosion literature (e.g., Landsberg, 1955; Kubaschewski and Hopkins, 1962; Evans, 1982) include: (1) logarithmic, where a reaction occurs with $dP/dt \sim 1/t$ if it is limited by decreasing availability of surface area (i.e., reaction sites); and (2) parabolic, where $dP/dt \sim t^{-1/2}$ if it is limited by diffusion (e.g., through a product layer). In Chapter 4, we discuss possible physical mechanisms of carbonate growth as explanations for logarithmic behavior in our experiments.

In both of these cases, dP/dt varies as some inverse power of time. To test this, and determine the best-fitting power law in our case, we found the exponent in:

$$dP/dt = At^B \quad (t \text{ in days}) \qquad [2\text{-}12]$$

For logarithmic CO_2 uptake, B would be -1 and $P(t) \sim \log t$. In practice, we used a linear least-squares fit to:

$$\ln dP/dt = \ln A + B \ln t \qquad [2\text{-}13]$$

Clearly, A = dP/dt at t = 1.

If the data were noisy (due to diurnal lab signals), we first smoothed P(t) with a simple averaging filter in linear time (EX8,12,25,29,19,21-24,39,31,34,36-38,48,50-53). Any bias that smoothing would have introduced into the determination of dP/dt would have been minimal, and uncertainties in the results for those experiments were estimated from analysis of unfiltered data. Next, data were sampled over intervals equally spaced in ln t, as was appropriate for testing the existence of a power-law relationship through linearity of dP/dt in a log-log plot. This was also appropriate for fitting a slope to the derivative dP/dt in the first place. We only fit dP/dt for times greater than 1 day (except for EX8, 16 days; EX42, 5 days; EX46-48,50-52, 0.2 days; and EX49, 0.1 days), in order to avoid as much as possible the complicating effects of adsorption and dissolution signals (although using data to t = 0 would not have significantly changed the results). Finally, it was necessary to eliminate points with dP/dt < 0 (actually only dP/dt > 0.001 were used), but this was observed to introduce little bias to the result (comparing with manual fits to dP/dt).

Results for A and B are tabulated in Table 2-3, along with standard errors (results for noise in P(t), σ_P, are explained below; the logarithmic fit to P(t) is discussed in

the next section). Numbers for B are also summarized in Table 2-1 (section 2.1.3). Log-log plots of dP/dt are shown in Figure 2-6 (pages 96-107). The times at which fits were begun (typically t = 1 day) are shown with a vertical dotted line, and upper bounds on differential leak rates (dP/dt = 0.03 mb/day, determined for **GROUP 4** experiments, but displayed for all experiments) are shown with a horizontal dotted line. Also, for reference, diagonal dashed lines representing slopes of B = -1 are shown. Least-squares fits appear as fine dotted lines (dots represent fitted points, evenly spaced in logarithmic time). Data for EX6, which were manually sampled, were fitted without first evenly spacing them in log t.

In our fitting routine, standard deviations for dP/dt were supplied by the routine which took the derivative. The derivative routine also used a least-squares fit (to points 0.05 $\log_{10}t$ on either side of the point to be fitted) to P(t) versus t. The fitting routine was performed twice: (1) assuming zero standard deviation of the data ($\sigma_P = 0$) to first take a derivative, then run the power-law fitting routine once, and finally calculate the standard deviation of $P(t) - P_{fit}(t)$, where $P_{fit}(t)$ was determined from the resulting fit to dP/dt; and (2) using this artificial, non-zero σ_P to run the fitting routine again and calculate a second standard deviation of $P(t) - P_{fit}(t)$. Thus, σ_P is

Table 2-3 Preliminary model results

	Power-law fit to dP/dt			Logarithmic fit to P(t)		
EX #	A (t=1) [mb/day]	B	σ_P [mb]	C (t=1) [monolayers]	D [monolayers/log$_{10}$t]	σ_P [mb]
GROUP 1 [Di0,Di1]						
8	1.7(1.4)	-1.0(0.3)	0.04	0.25(0.01)	0.11(0.01)	0.06
12	1.0(0.1)	-0.7(0.1)	0.12	0.12(0.00)	0.09(0.00)	0.17
13	2.1(0.1)	-0.6(0.0)	0.07	0.25(0.00)	0.25(0.00)	0.30
15	10.0(0.8)	-0.9(0.0)	0.97	1.67(0.00)	0.63(0.00)	0.73
16	31.1(1.0)	-1.6(0.1)	0.75	3.88(0.01)	1.05(0.02)	1.43
25	9.2(1.0)	-0.5(0.1)	0.89	1.74(0.01)	0.55(0.02)	0.68
29	0.4(0.1)	-0.5(0.1)	0.04	0.08(0.00)	0.02(0.00)	0.04
30	8.2(0.3)	-0.4(0.0)	0.30	0.33(0.00)	0.37(0.01)	0.55
32	7.8(0.2)	-0.6(0.0)	0.33	0.27(0.00)	0.42(0.01)	1.22
GROUP 2 [Di2,Ol1,Qtz,Plag,Ol2,Calc]						
19	7.8(0.8)	-0.4(0.0)	2.09	0.11(0.01)	0.45(0.01)	11.69
20	12.2(0.9)	-0.5(0.0)	1.78	0.15(0.00)	0.18(0.00)	3.03
21	0.5(2.2)	0.3(0.4)	2.36	0.01(0.01)	0.03(0.01)	0.78
22	0.2(0.1)	0.0(0.1)	0.14	0.00(0.00)	0.04(0.00)	0.20
23	3.5(3.3)	-0.4(0.3)	5.32	-0.01(0.01)	0.02(0.01)	2.82
24	3.7(3.0)	-0.3(0.2)	0.85	0.05(0.00)	0.08(0.00)	0.87
39	0.2(0.9)	0.5(0.6)	0.50	1.26(0.00)	0.03(0.01)	0.28
GROUP 3 [Bas/warm]						
26	5.3(0.1)	-1.0(0.0)	0.09	4.61(0.00)	1.38(0.01)	0.09
27	7.6(0.5)	-1.0(0.1)	0.39	1.34(0.00)	0.59(0.01)	0.30
28	4.1(0.3)	-0.8(0.1)	0.31	1.10(0.00)	0.58(0.01)	0.26
31	0.3(0.2)	-0.8(0.3)	0.08	0.10(0.00)	0.06(0.01)	0.07
33	7.4(0.3)	-1.0(0.1)	0.22	6.47(0.00)	1.15(0.01)	0.23
34	1.1(0.4)	0.1(0.5)	0.18	21.47(0.02)	1.18(0.06)	0.15
35	7.6(0.3)	-1.4(0.1)	0.24	9.36(0.01)	1.36(0.02)	0.24
36	2.7(1.2)	-0.9(0.1)	0.51	1.23(0.01)	0.51(0.01)	0.43
37	0.4(0.5)	-0.1(0.5)	0.28	-0.03(0.00)	0.03(0.01)	0.20
38	4.0(0.8)	-1.0(0.1)	0.71	0.46(0.01)	0.65(0.01)	0.33
GROUP 4 [Bas/cold]						
40	1.6(0.0)	-1.1(0.0)	0.01	0.46(0.00)	0.15(0.00)	0.03
41	0.4(0.0)	-0.8(0.0)	0.01	0.13(0.00)	0.06(0.00)	0.04
42	-0.1(0.0)	0.5(0.0)	0.00	0.10(0.00)	-0.04(0.00)	0.01
43	0.3(0.0)	-1.0(0.1)	0.04	0.01(0.00)	0.01(0.00)	0.02
44	1.1(0.0)	-1.1(0.0)	0.01	0.31(0.00)	0.24(0.00)	0.02
45	0.3(0.0)	-0.8(0.0)	0.00	0.09(0.00)	0.10(0.00)	0.01
46	0.2(0.0)	-0.8(0.1)	0.02	0.10(0.00)	0.04(0.00)	0.02
47	0.1(0.0)	-0.8(0.0)	0.01	0.09(0.00)	0.03(0.00)	0.01
48	0.1(0.0)	-1.3(0.1)	0.01	0.04(0.00)	0.01(0.00)	0.00
49	0.2(0.0)	-0.6(0.1)	0.01	0.09(0.00)	0.03(0.00)	0.01
50	0.4(0.2)	-0.1(0.3)	0.23	0.28(0.00)	0.06(0.00)	0.15
51	2.1(0.1)	-0.5(0.1)	0.21	0.84(0.00)	0.41(0.01)	0.19
52	0.1(0.0)	-0.8(0.1)	0.02	0.08(0.00)	0.02(0.00)	0.02
53	0.1(0.0)	-0.9(0.1)	0.01	0.01(0.00)	0.00(0.00)	0.01

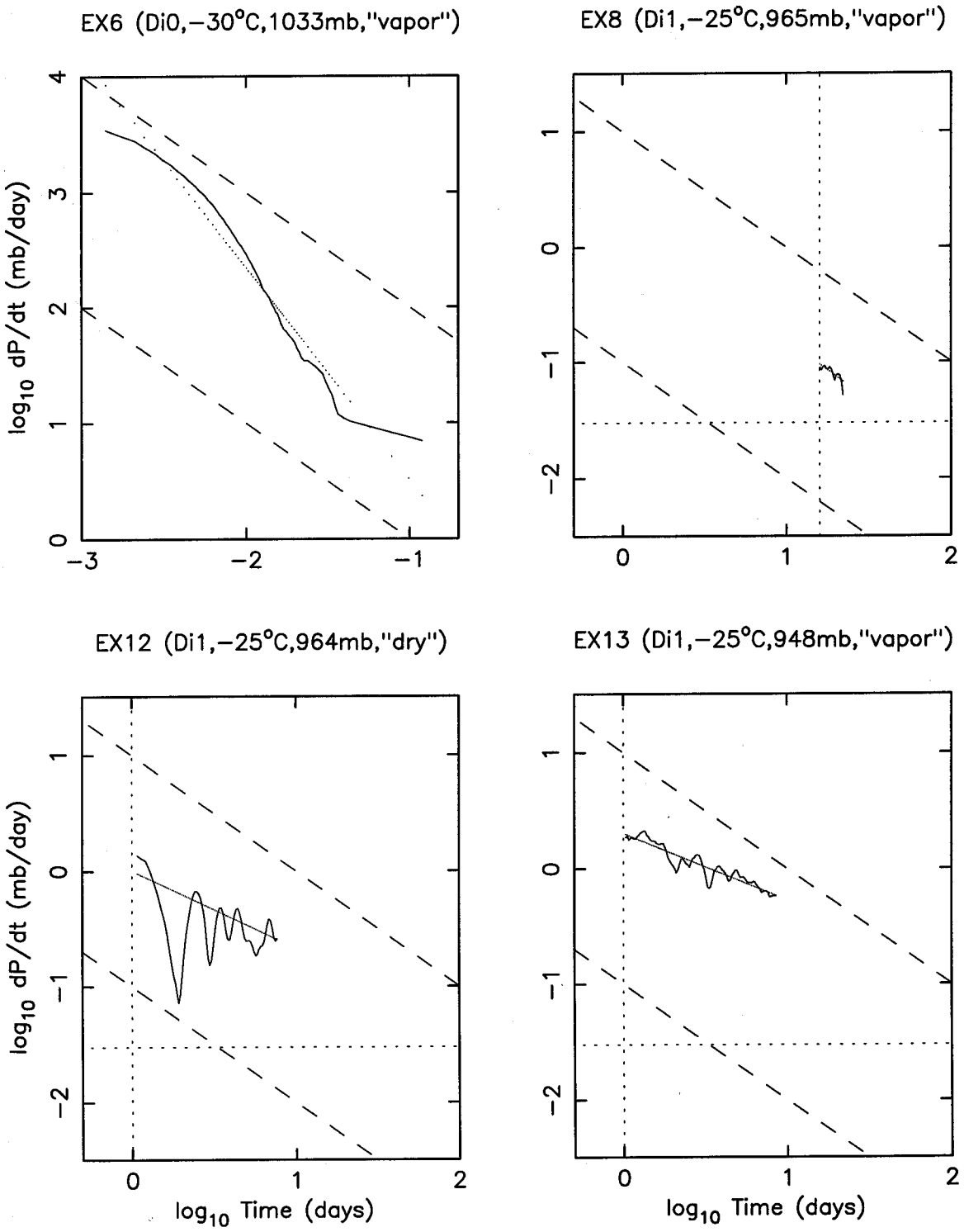

Figure 2-6 Model power-law fits to dP/dt
(a) **GROUP 1** [Di0,Di1]

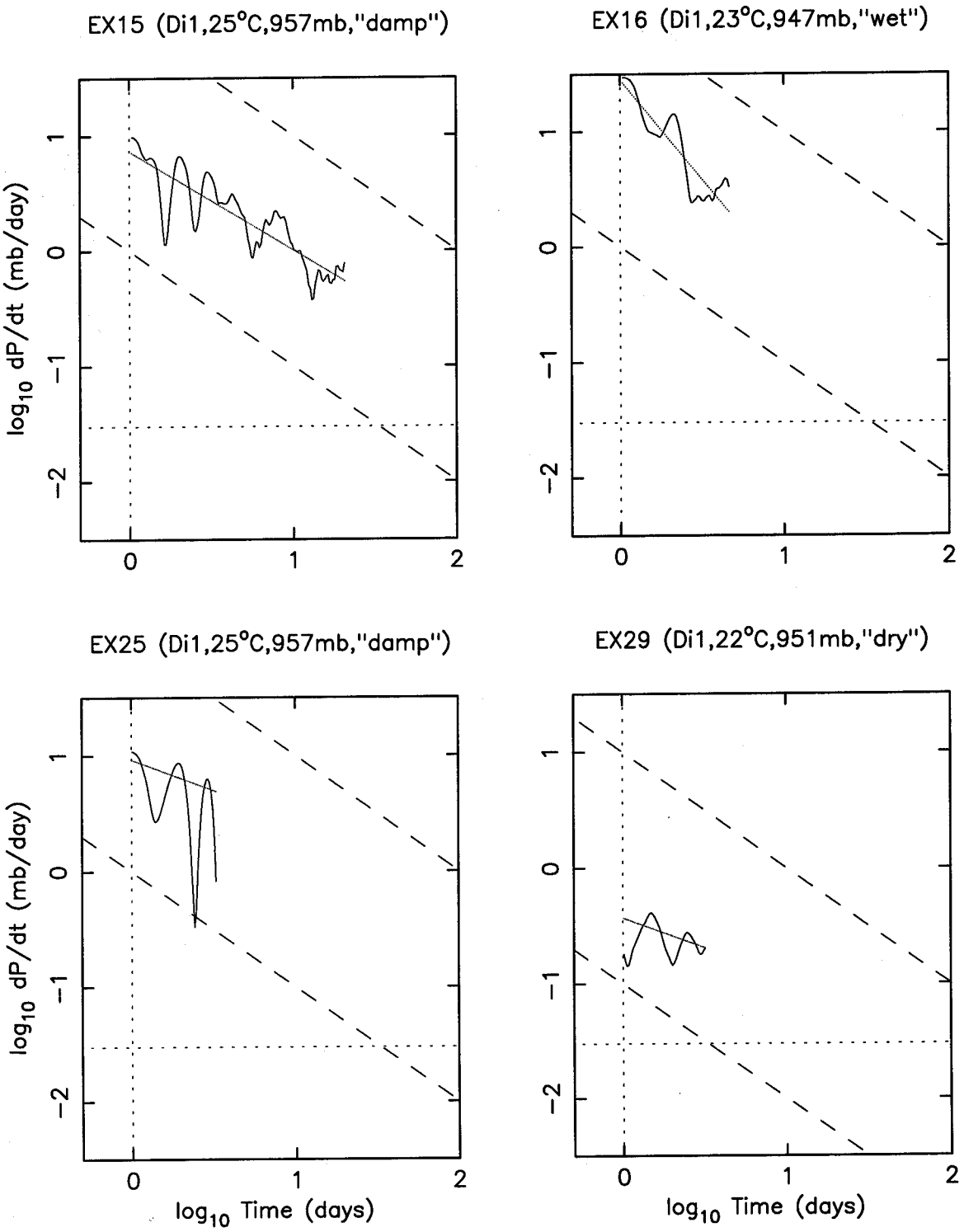

Figure 2-6 Model power-law fits to dP/dt (continued)
(a) **GROUP 1** [Di0,Di1]

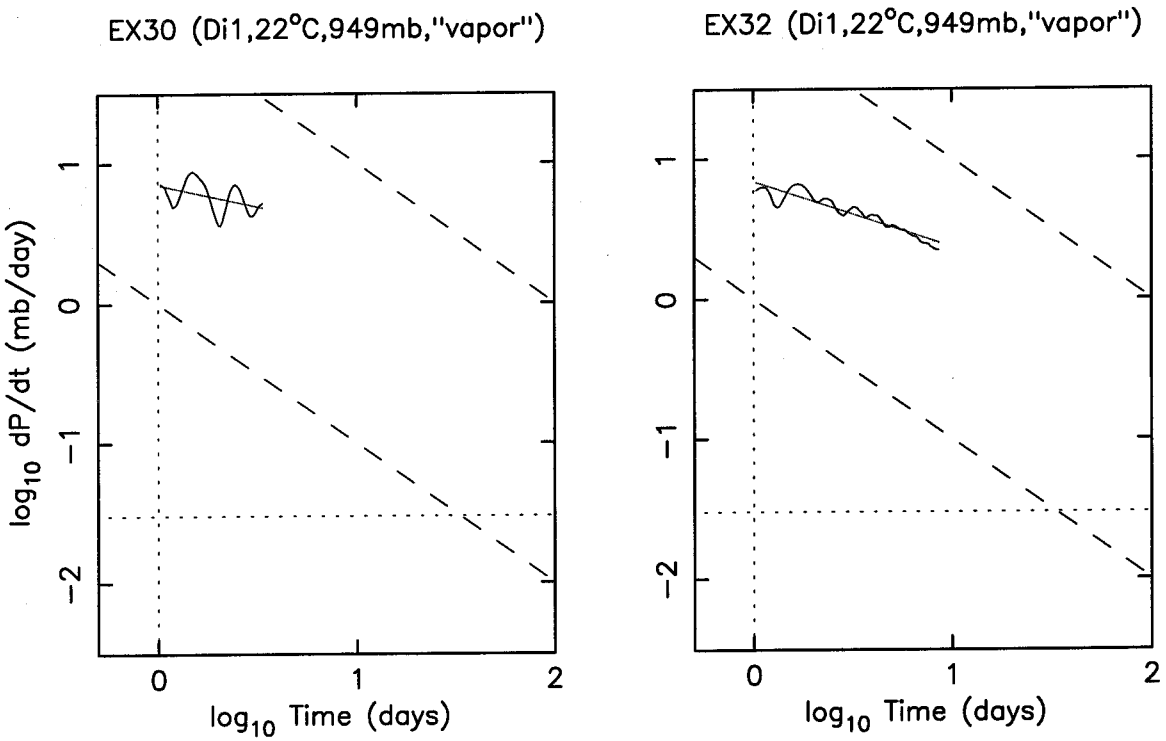

Figure 2-6 Model power-law fits to dP/dt (continued)
(a) **GROUP 1** [Di0,Di1]

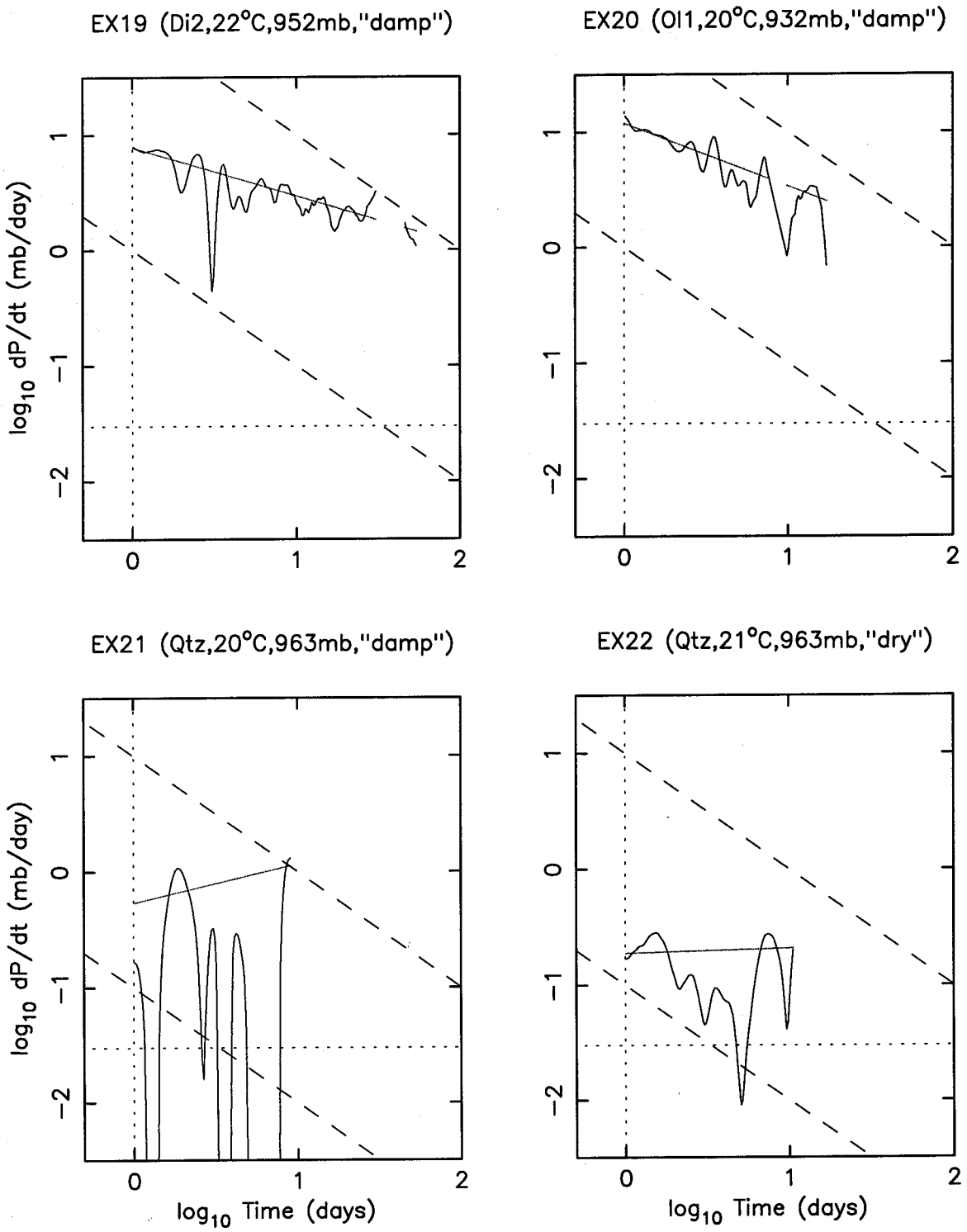

Figure 2-6 Model power-law fits to dP/dt
(b) **GROUP 2** [Di2,Ol1,Qtz,Plag,Ol2,Calc]

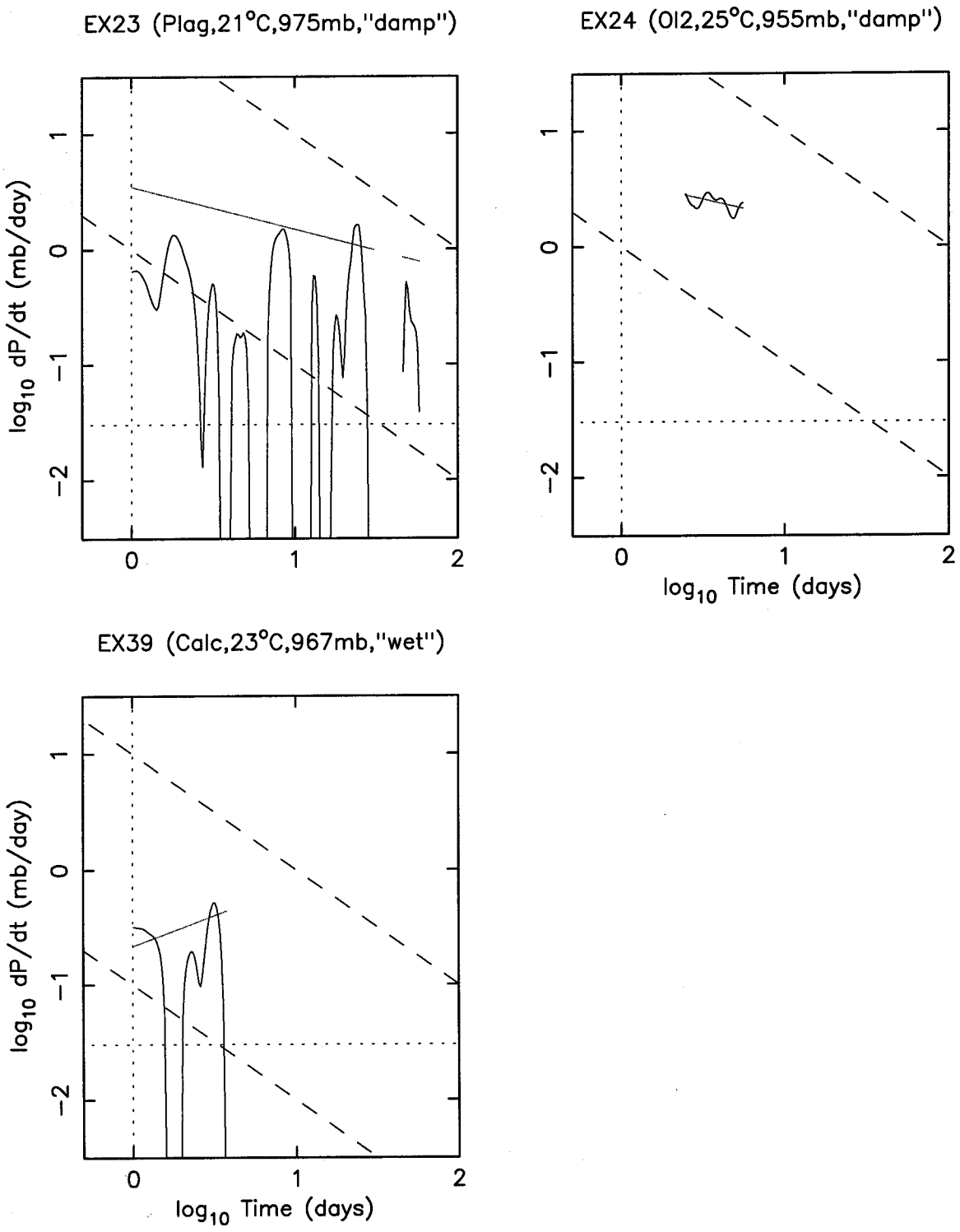

Figure 2-6 Model power-law fits to dP/dt (continued)
(b) **GROUP 2** [Di2,Ol1,Qtz,Plag,Ol2,Calc]

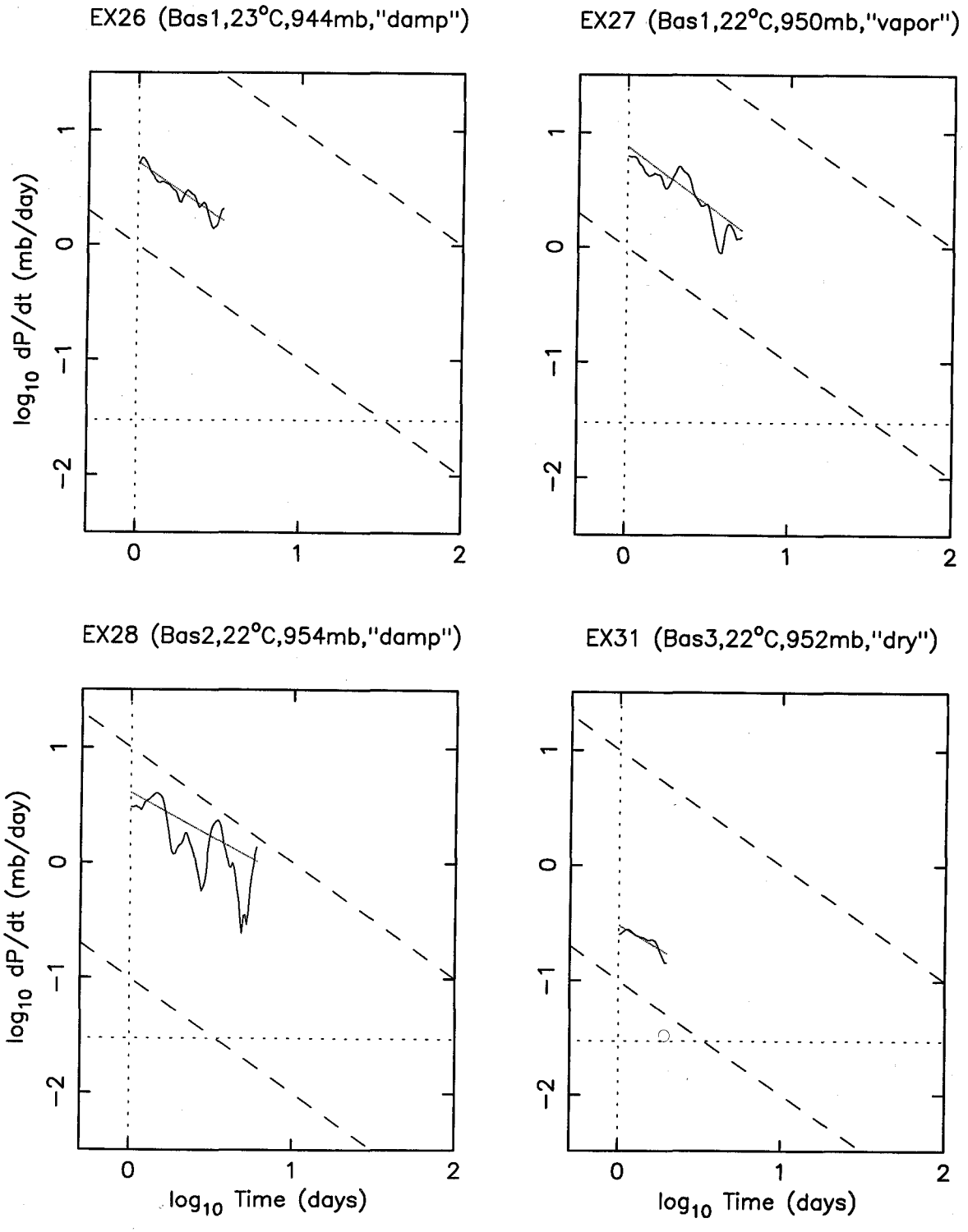

Figure 2-6 Model power-law fits to dP/dt
(c) **GROUP 3** [Bas/warm]

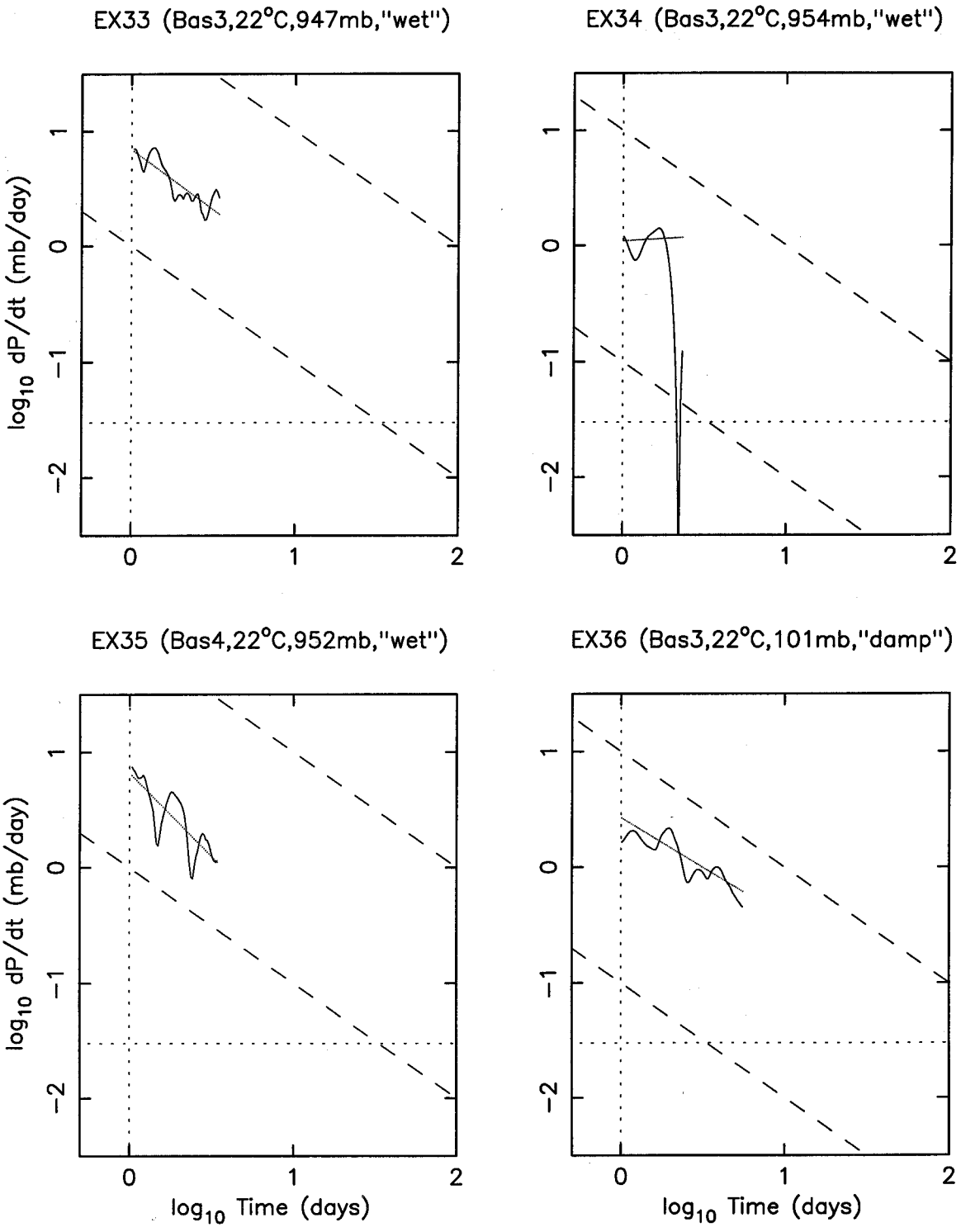

Figure 2-6 Model power-law fits to dP/dt (continued)
(c) **GROUP 3** [Bas/warm]

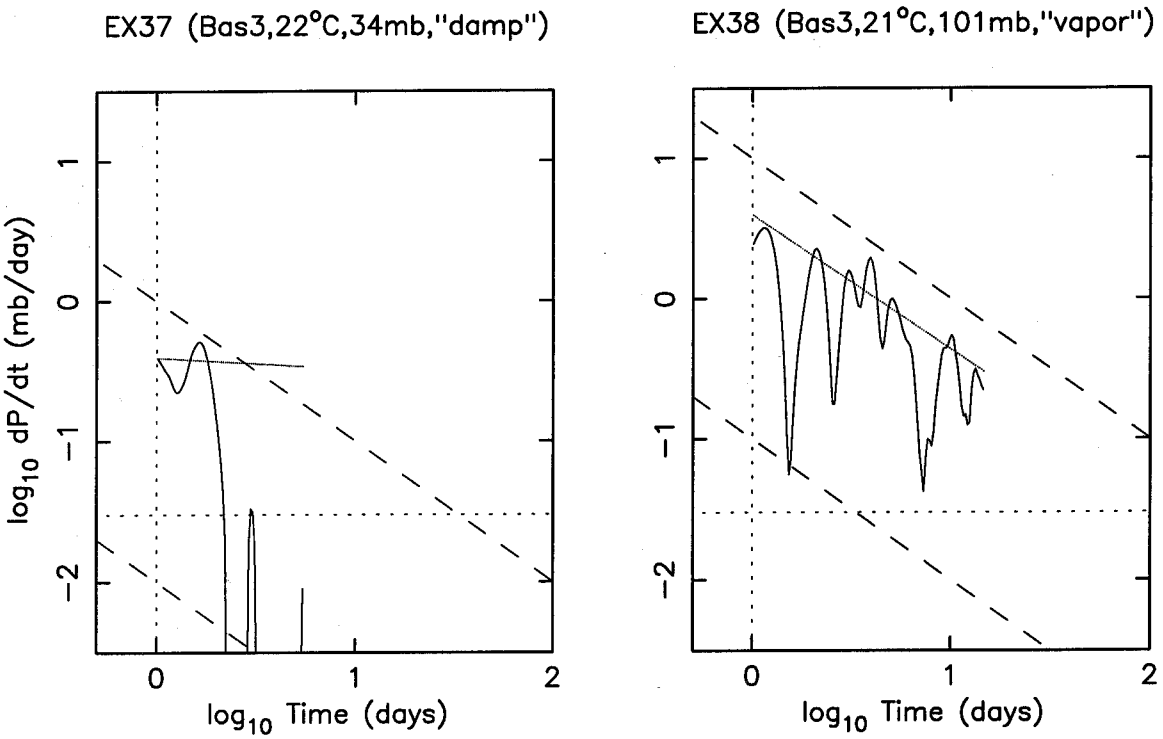

Figure 2-6 Model power-law fits to dP/dt (continued)
(c) **GROUP 3** [Bas/warm]

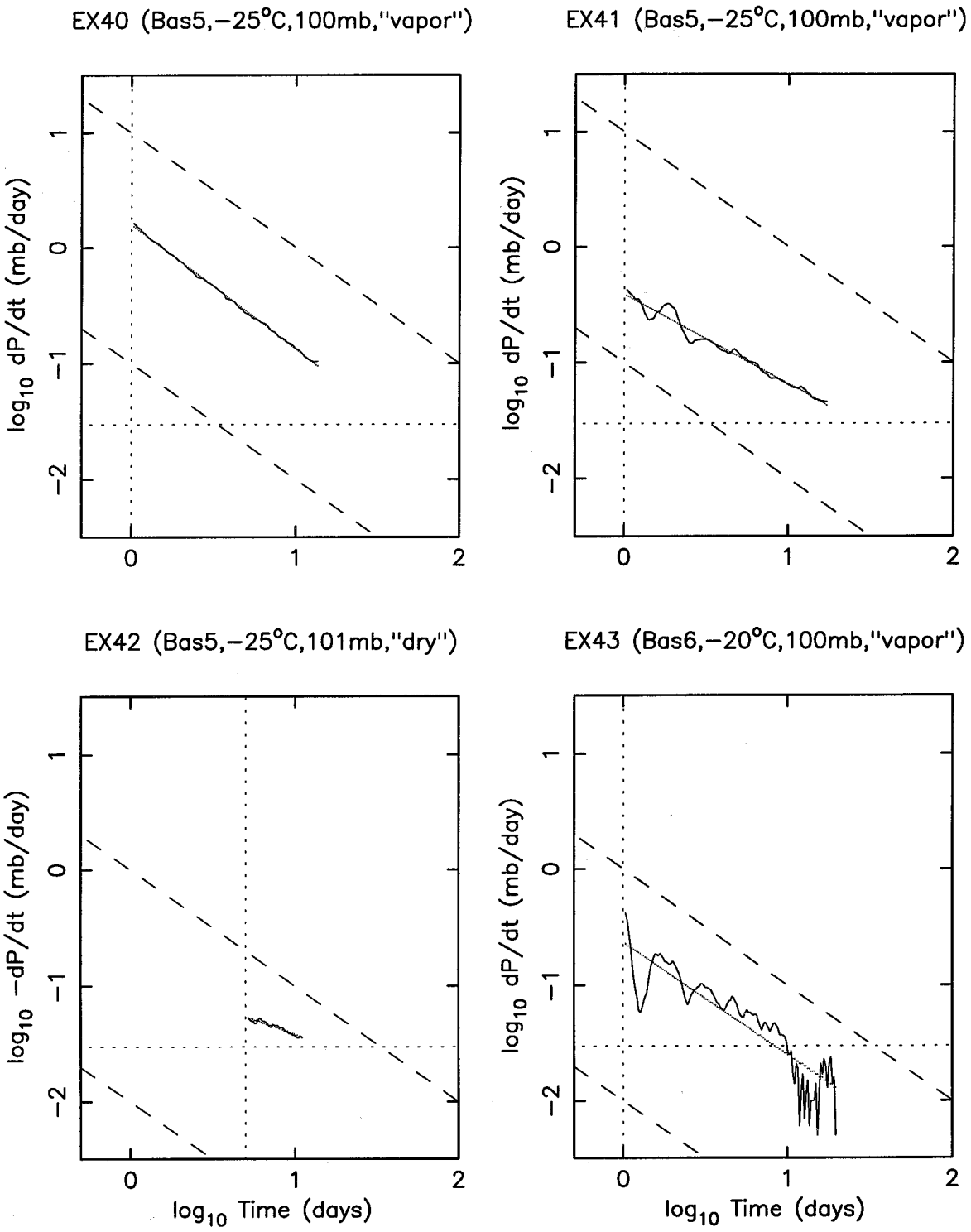

Figure 2-6 Model power-law fits to dP/dt
(d) **GROUP 4** [Bas/cold]

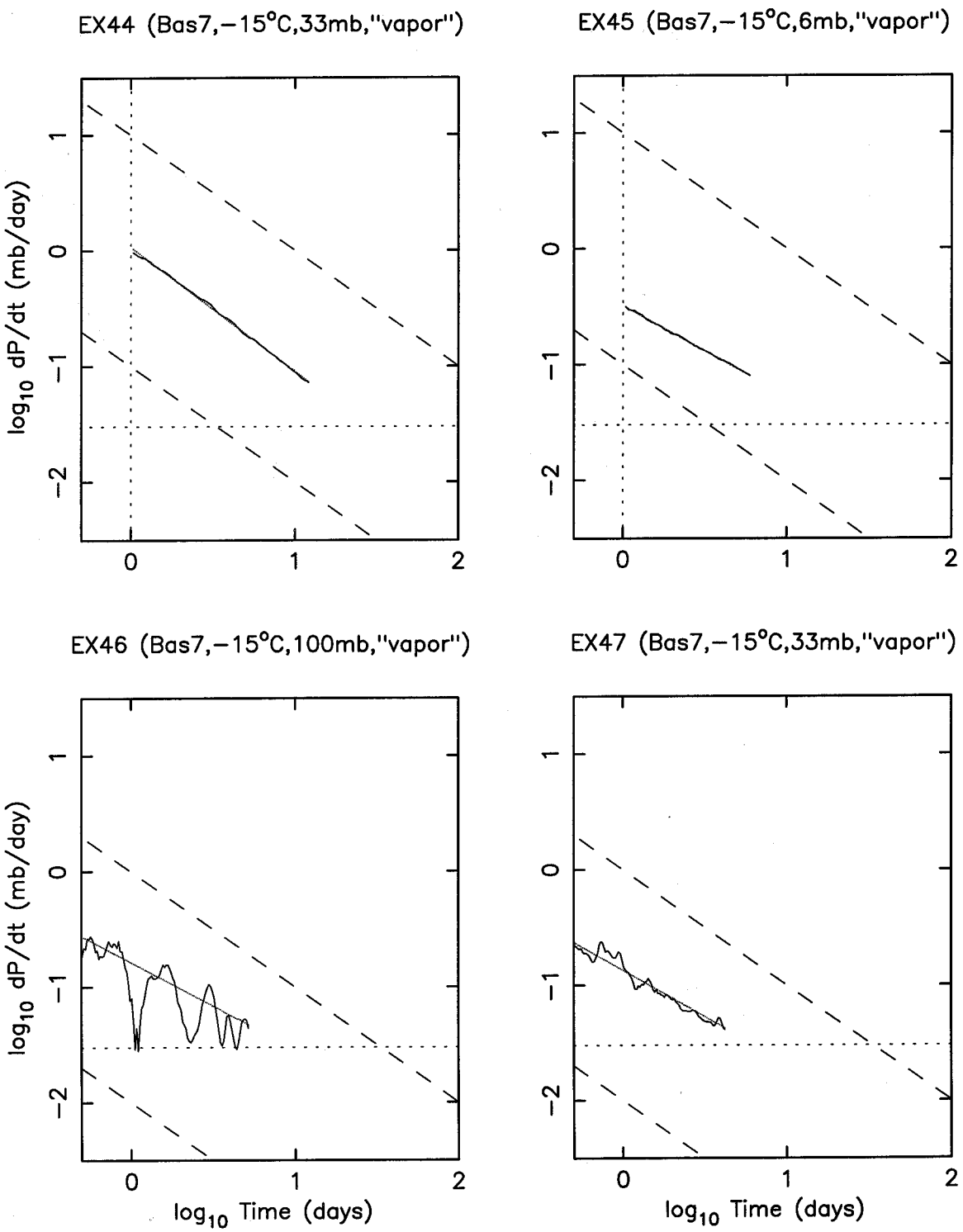

Figure 2-6 Model power-law fits to dP/dt (continued)
(d) **GROUP 4** [Bas/cold]

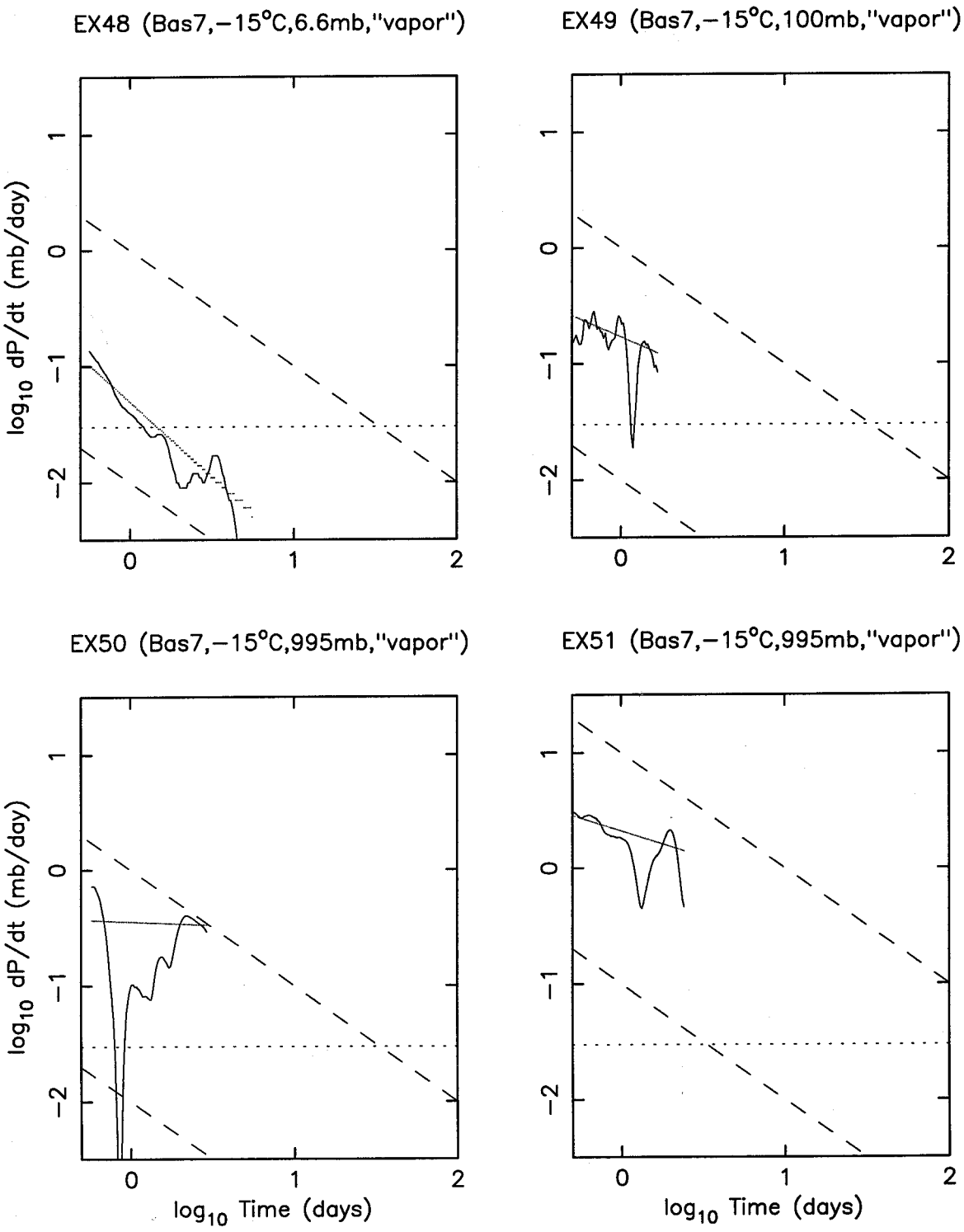

Figure 2-6 Model power-law fits to dP/dt (continued)
(d) **GROUP 4** [Bas/cold]

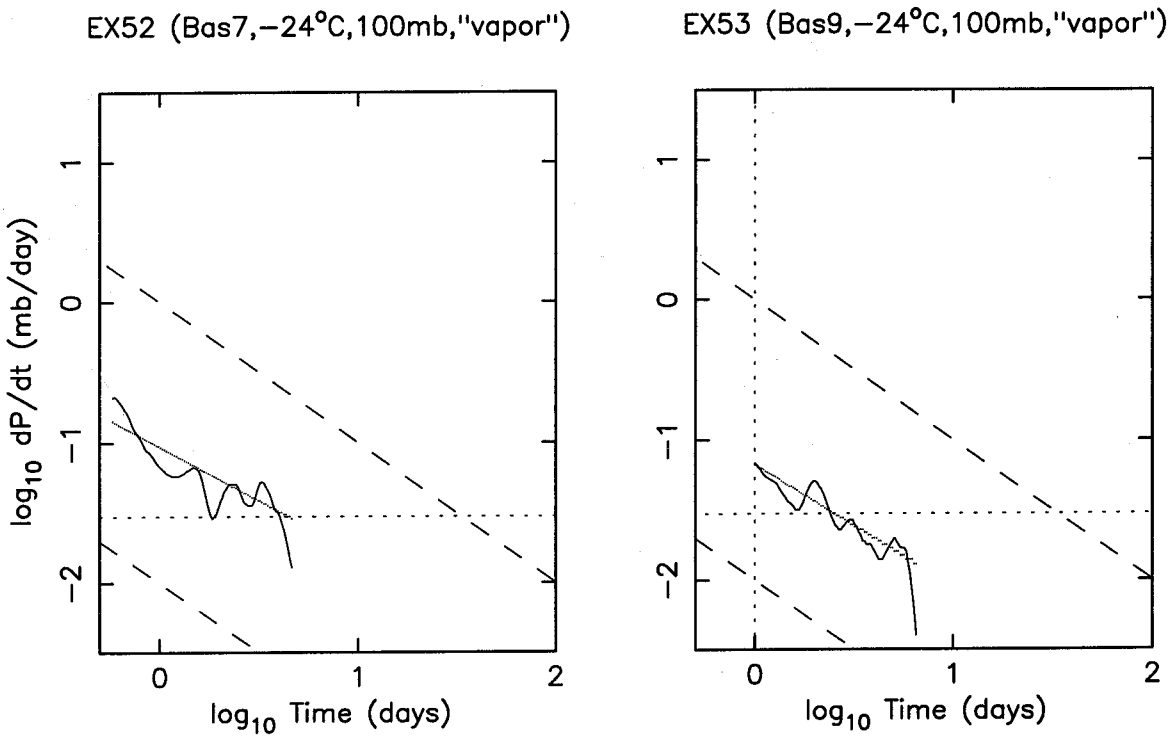

Figure 2-6 Model power-law fits to dP/dt (continued)
(d) **GROUP 4** [Bas/cold]

a measure of noise in the data. (The numbers for σ_P listed in Table 2-3 were obtained from fits to unsmoothed data.)

Fits for experiments with a lot of noise (often first reduced by smoothing P(t)) favor higher values of dP/dt over lower values. The bias results from very large standard deviations for small values of dP/dt, and is a real result of the fitting process.

Results are discussed further in section 2.4.3, but for now it is possible to observe that, in general, dP/dt is better fit with an exponent B closer to -1.0 (logarithmic behavior) than to -0.5 (parabolic). In fact, taking all **GROUP 4** [Bas/cold] "vapor" experiments (except EX50, which has an unusual curve for P(t) versus t, and which gives B = -0.1, an outlier), we obtain B = -0.85 ± 0.2, where the standard error indicates that B = -1.0 is much more likely to be a fit to the data than B = -0.5. (EX42, a "dry" experiment, with a decrease in pressure that we inferred to be due to water vapor desorption, is plotted with log(-dP/dt).)

2.4.3 Logarithmic behavior

Once fits to dP/dt were obtained, it was possible to assign meaning to logarithmic fits for P(t). This was done as above, but with a linear least-squares fit to:

$$P(t) = C + D \log_{10} t \qquad [2\text{-}14]$$

Again, points were evenly spaced in ln t. Results are tabulated in Table 2-1 (section 2.1.3) and Table 2-3 (section 2.4.2). Results for the noise in P(t), σ_P, are generally consistent with those obtained from dP/dt fits (Table 2-3).

The parameters C and D have physical meaning. C is the amount of CO_2 taken up at t = 1 day, and D is equivalent to $dP/d\log_{10}t$, a measure of the rate of CO_2 uptake (per 10-folding time). To further interpret these results, we converted differential pressure to equivalent monolayers of CO_2, in a manner similar to that carried out for calculating equivalent monolayers of H_2O in experiments (section 2.3.2):

$$CO_2 \text{ uptake [monolayers]} = (\Delta P \, V_S' / RT) \times (6\times10^{23} \text{ molecules/mole}) \times (2\times10^{-19} \text{ m}^2\text{/molecule}) / [(\text{surface area in m}^2\text{/g/monolayer}) \times (\text{mass in g})] \quad [2\text{-}15]$$

where ΔP is pressure drop in dynes/cm^2 (= 10^{-3} mb), V_S' is the "combined sample volume" corrected for powder volume, T is experimental temperature, and 20 Å^2/molecule is the area of a CO_2 molecule (McClellan and Harnsberger, 1967).

These logarithmic plots permit more reliable comparison among experiments than those for raw pressure data, since they are scaled for experimental conditions (especially specific surface area and mass). Results are presented in Figure 2-7 (pages 110-121). The horizontal dotted line is

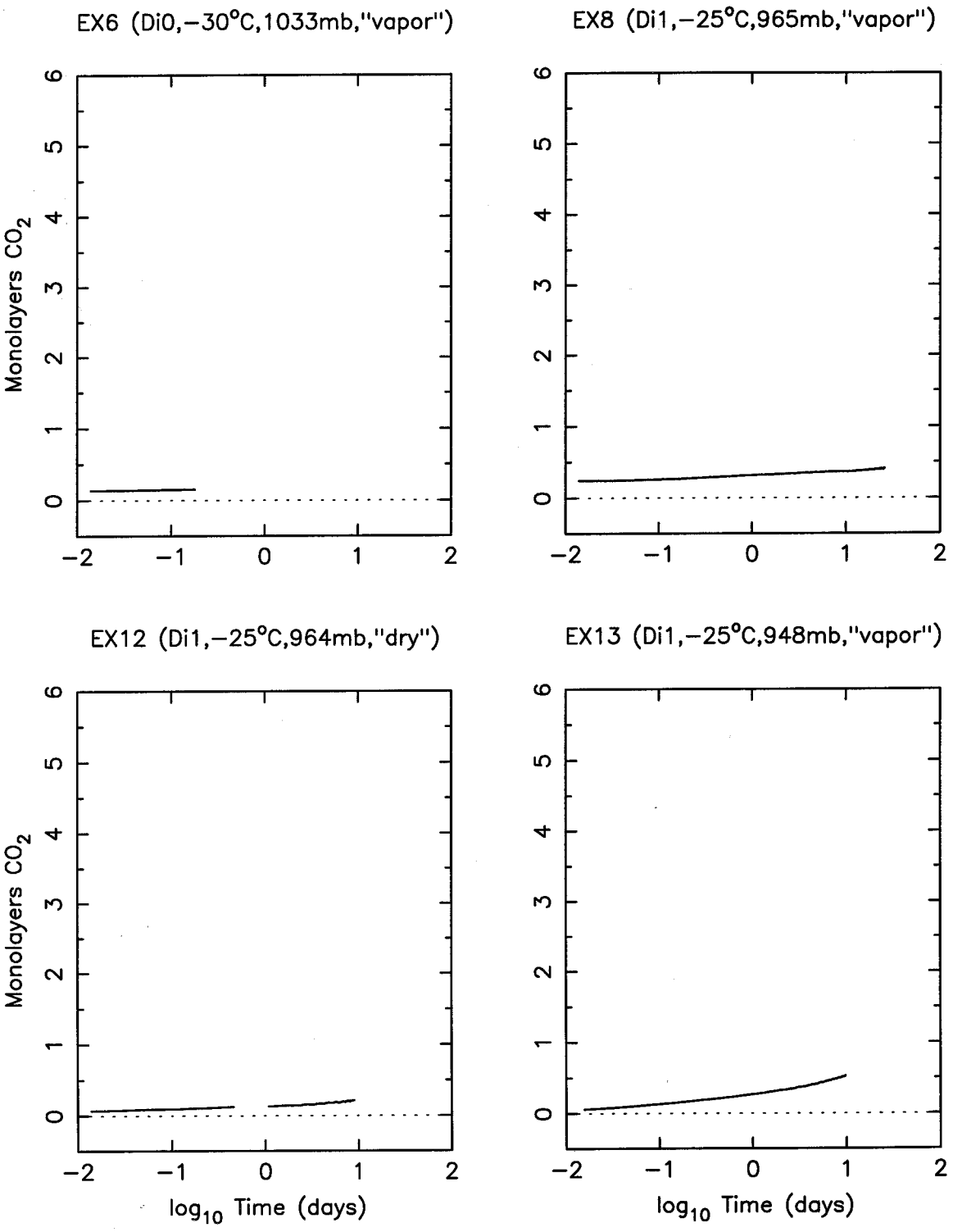

Figure 2-7 Logarithmic plots of data
(a) **GROUP 1** [Di0,Di1]

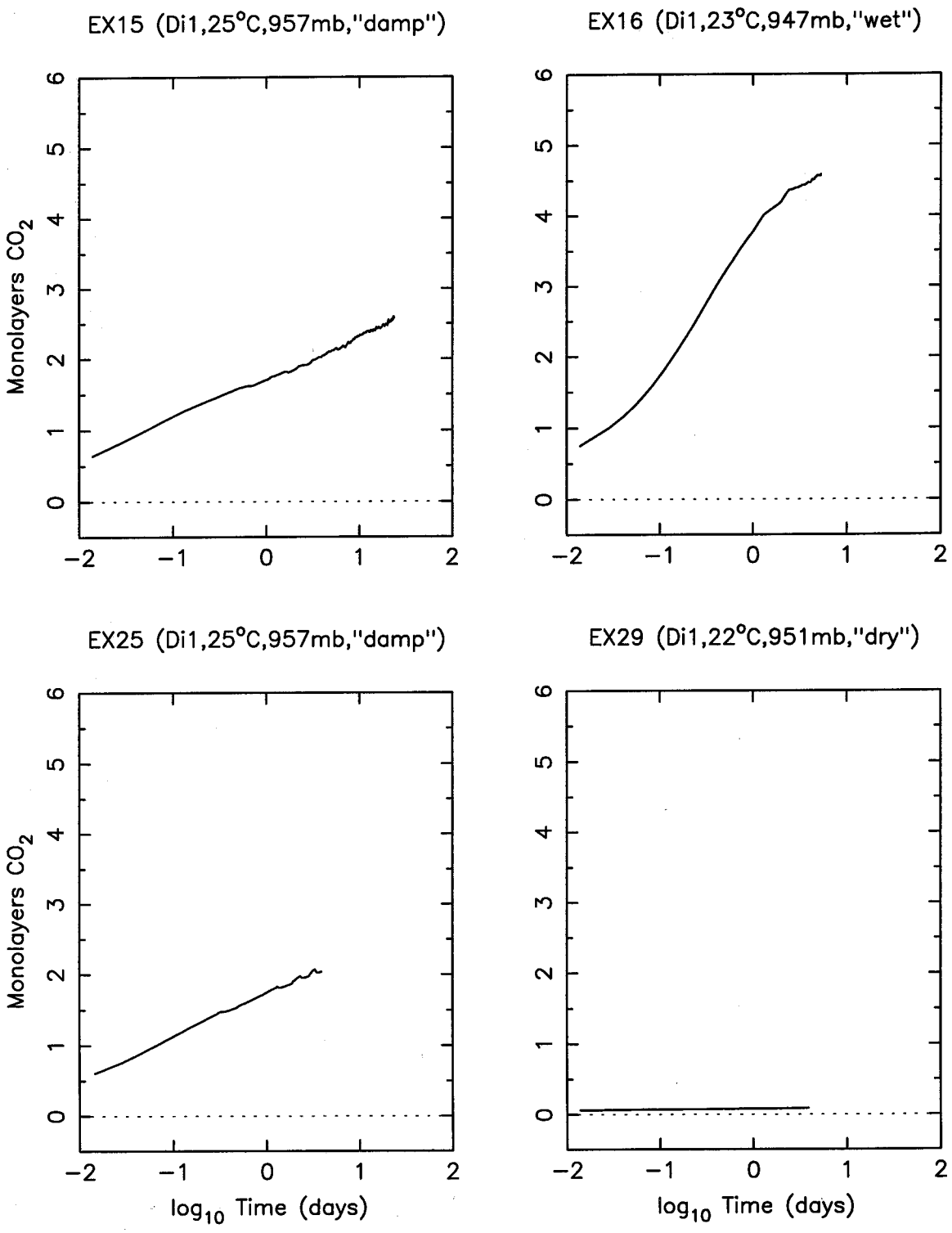

Figure 2-7 Logarithmic plots of data (continued)
(a) **GROUP 1** [Di0,Di1]

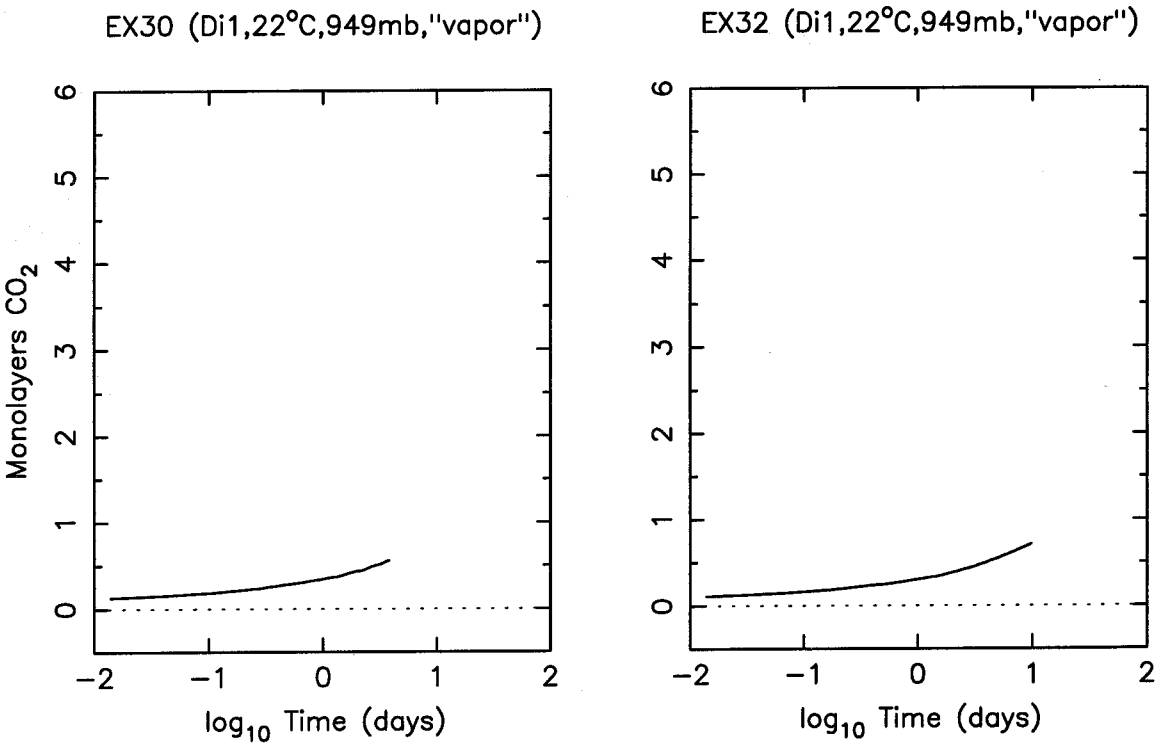

Figure 2-7 Logarithmic plots of data (continued)
(a) **GROUP 1** [Di0,Di1]

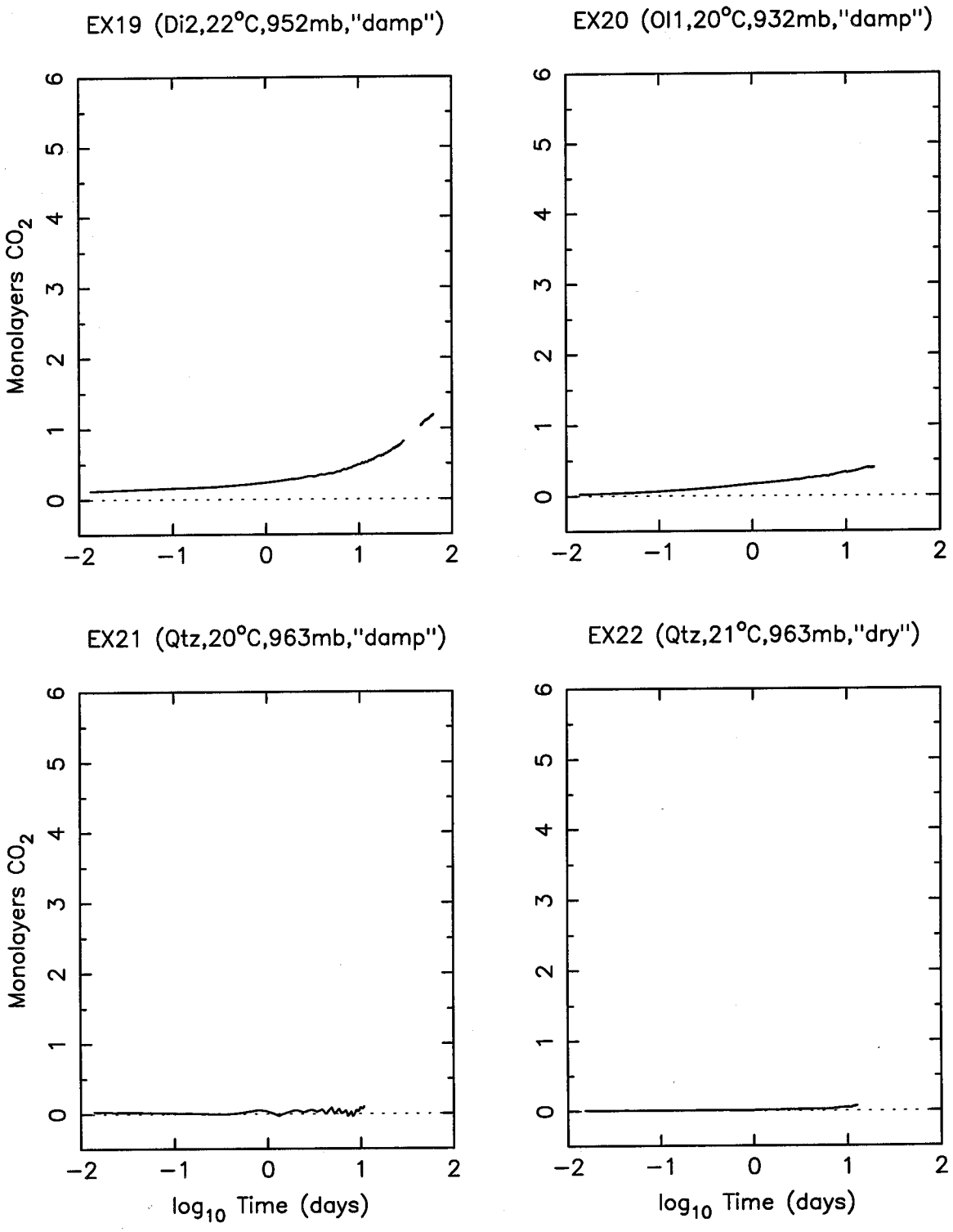

Figure 2-7 Logarithmic plots of data
(b) **GROUP 2** [Di2,Ol1,Qtz,Plag,Ol2,Calc]

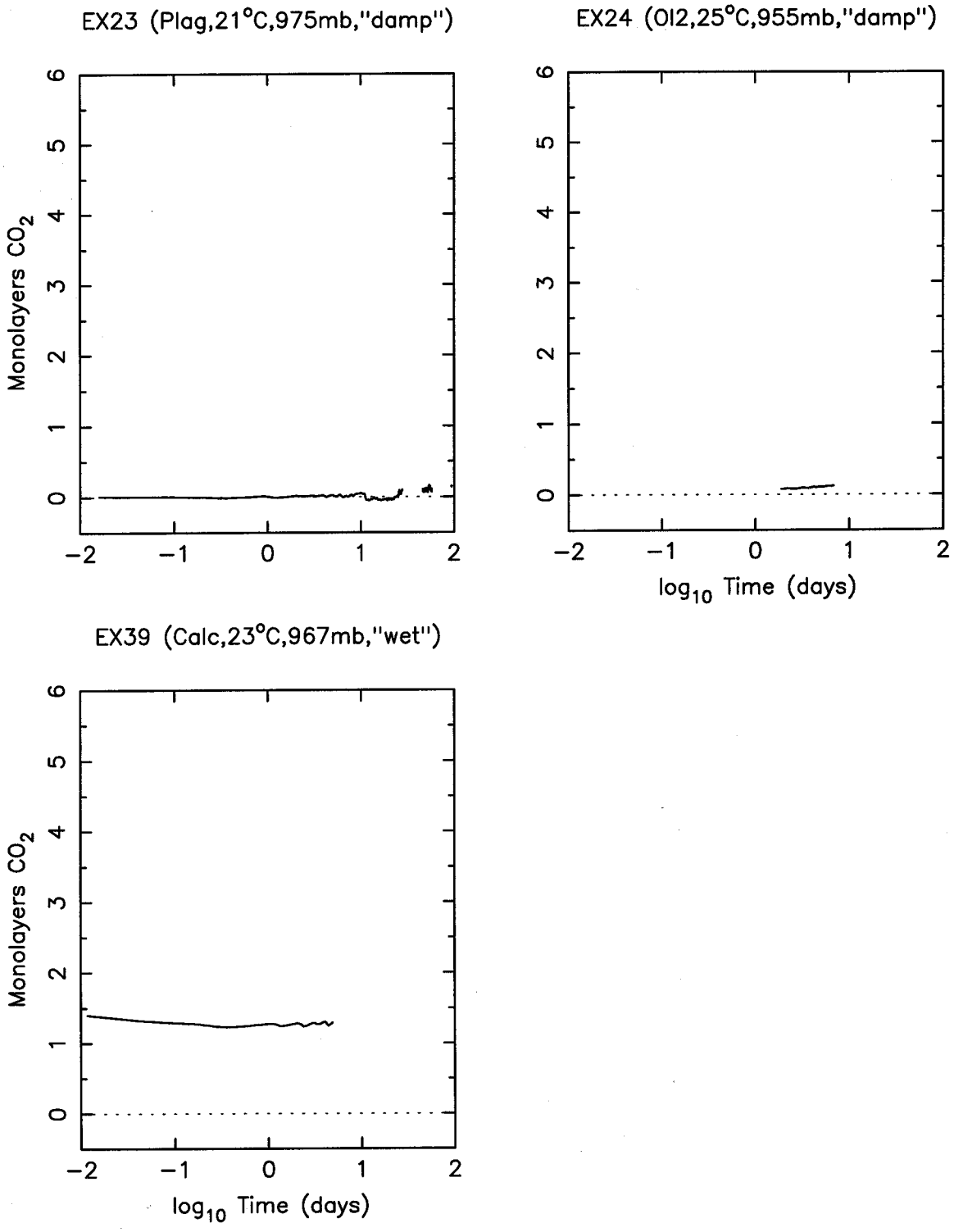

Figure 2-7 Logarithmic plots of data (continued)
(b) **GROUP 2** [Di2,Ol1,Qtz,Plag,Ol2,Calc]

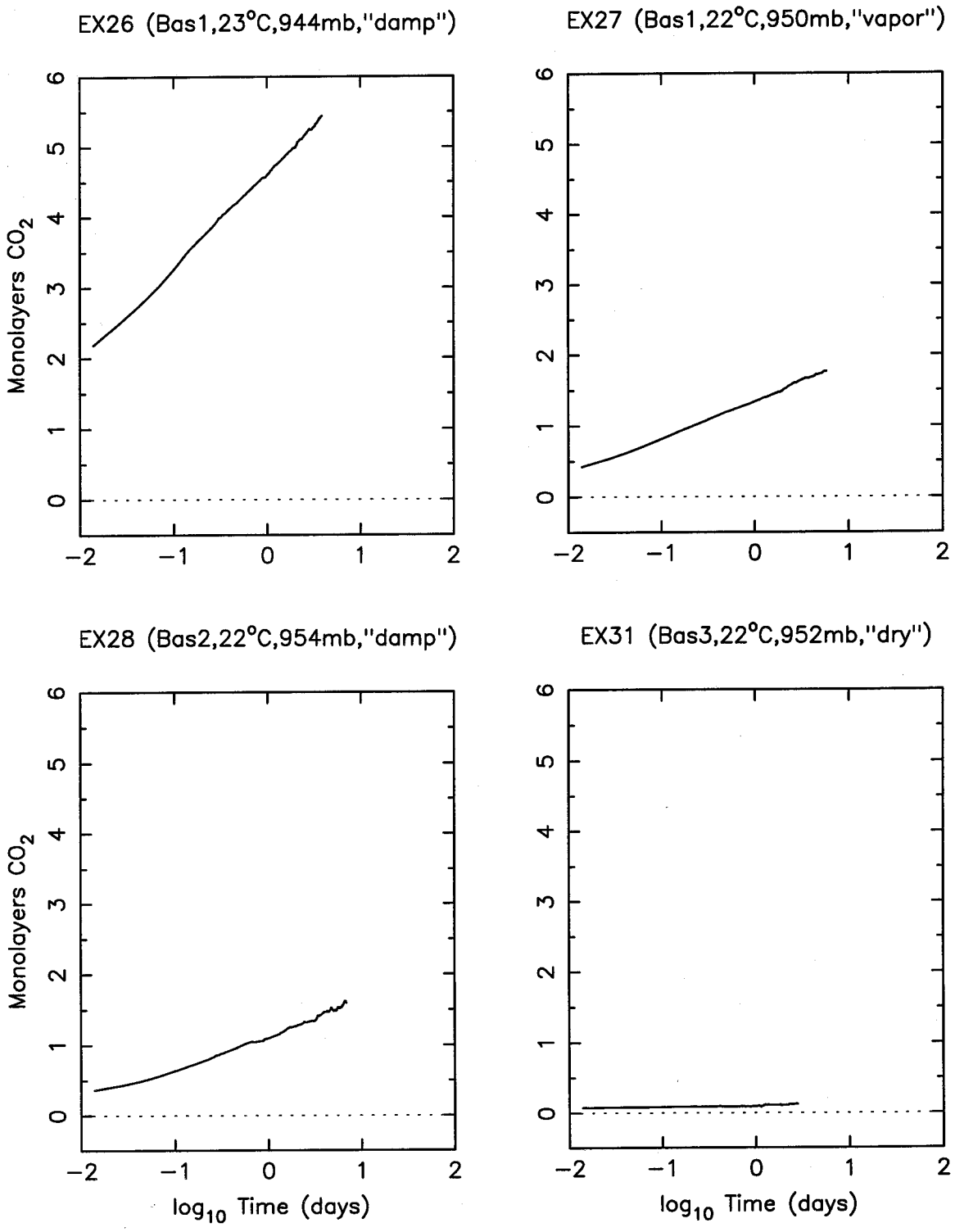

Figure 2-7 Logarithmic plots of data
(c) **GROUP 3** [Bas/warm]

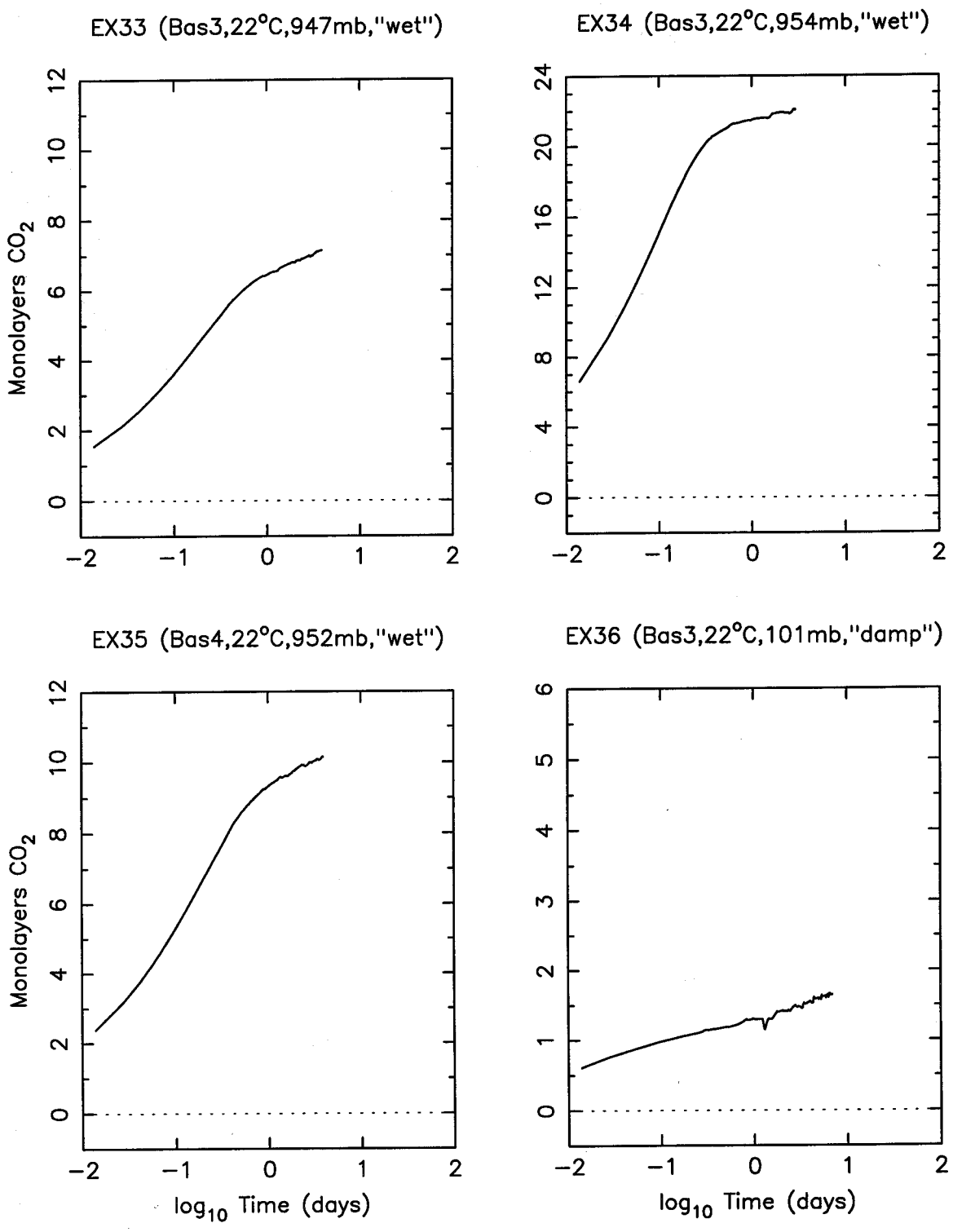

Figure 2-7 Logarithmic plots of data (continued)
(c) **GROUP 3** [Bas/warm]

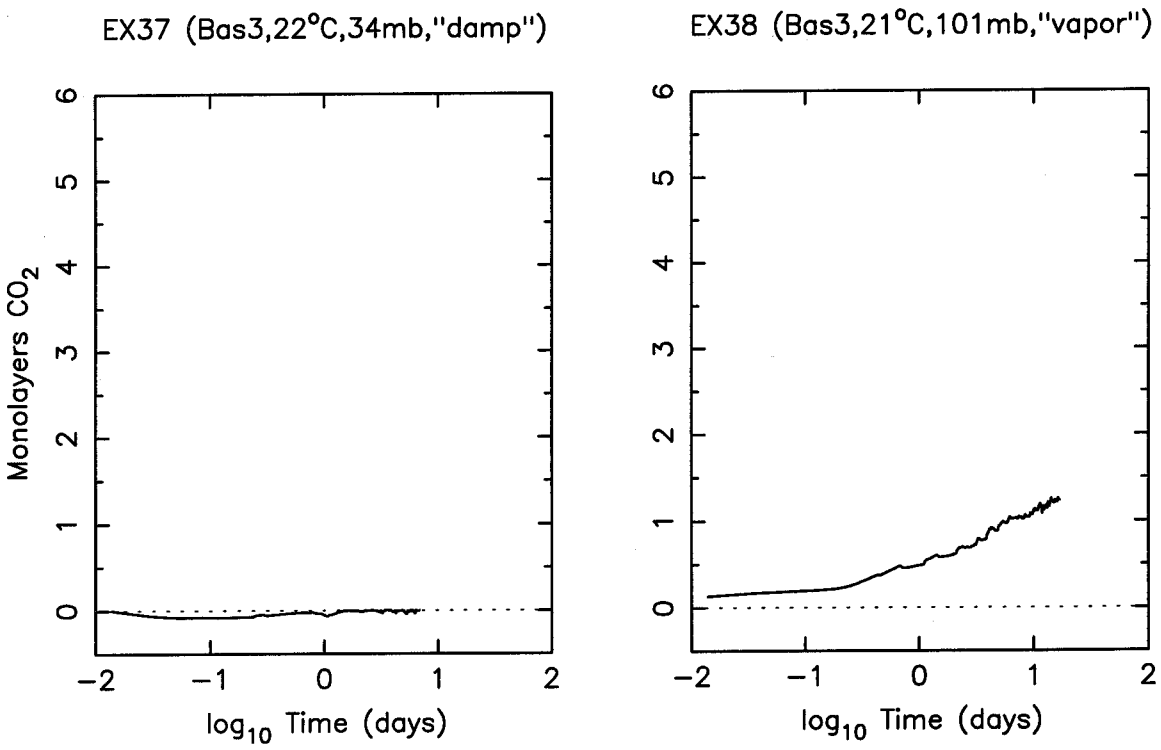

Figure 2-7 Logarithmic plots of data (continued)
(c) **GROUP 3** [Bas/warm]

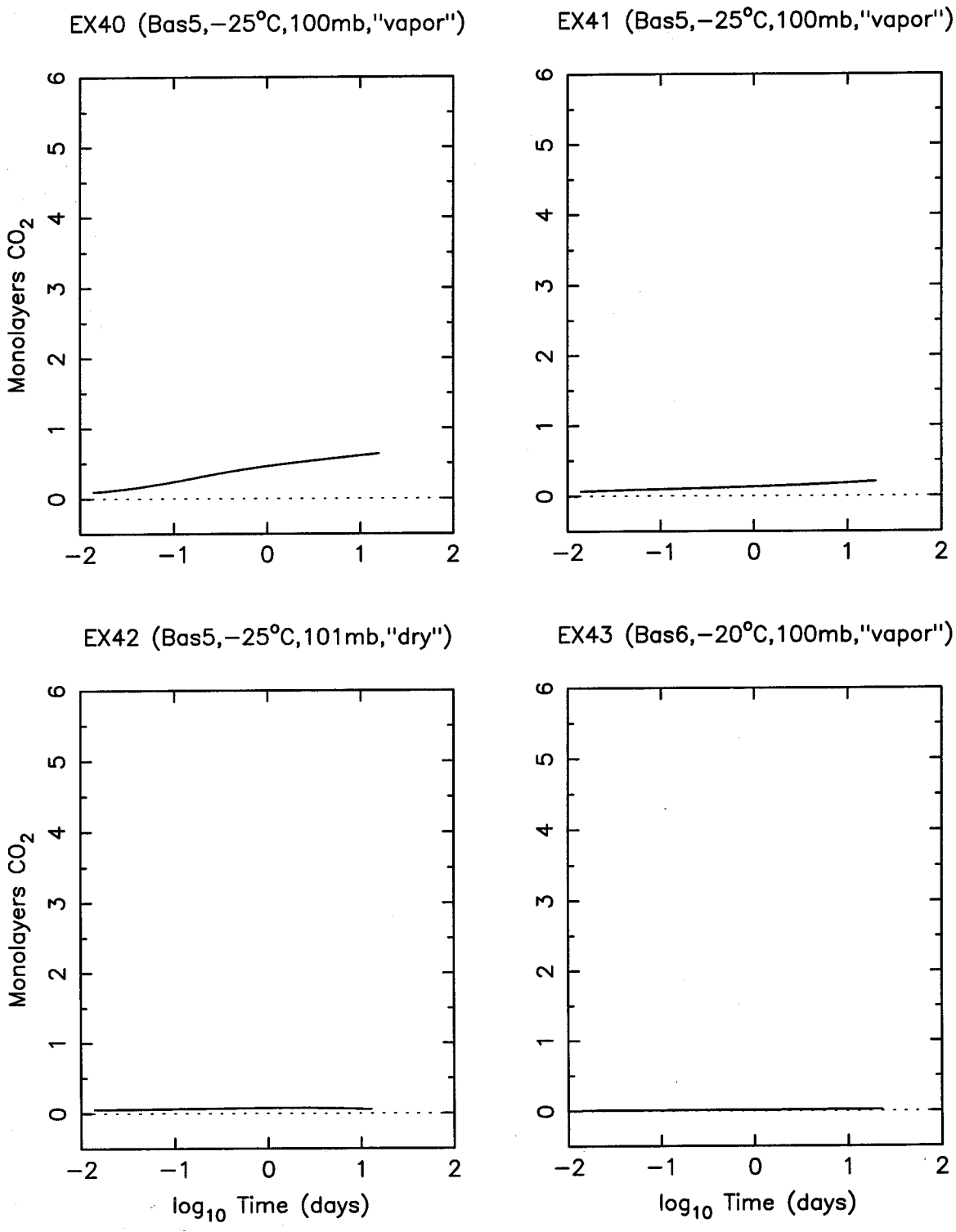

Figure 2-7 Logarithmic plots of data
(d) **GROUP 4** [Bas/cold]

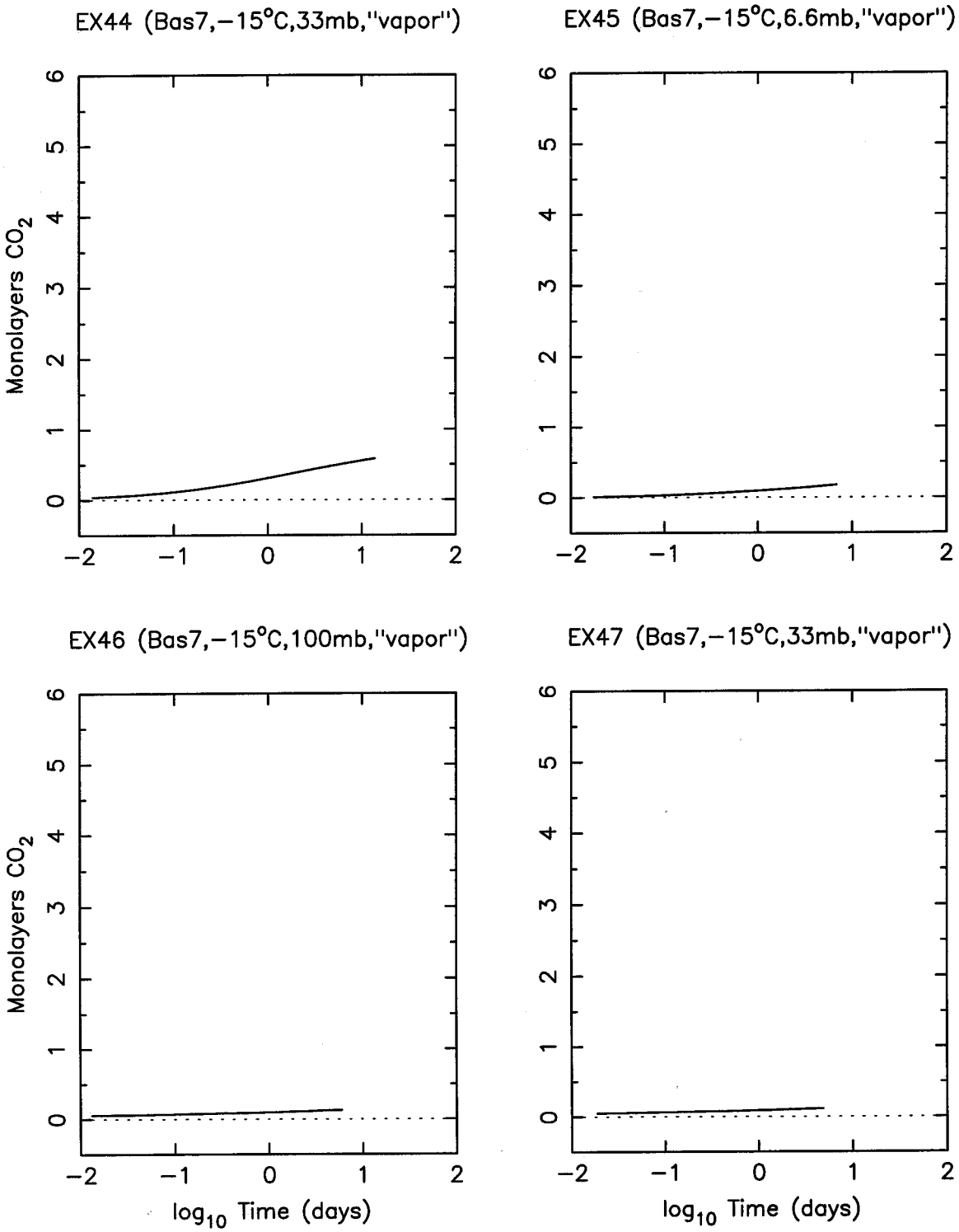

Figure 2-7 Logarithmic plots of data (continued)
(d) **GROUP 4** [Bas/cold]

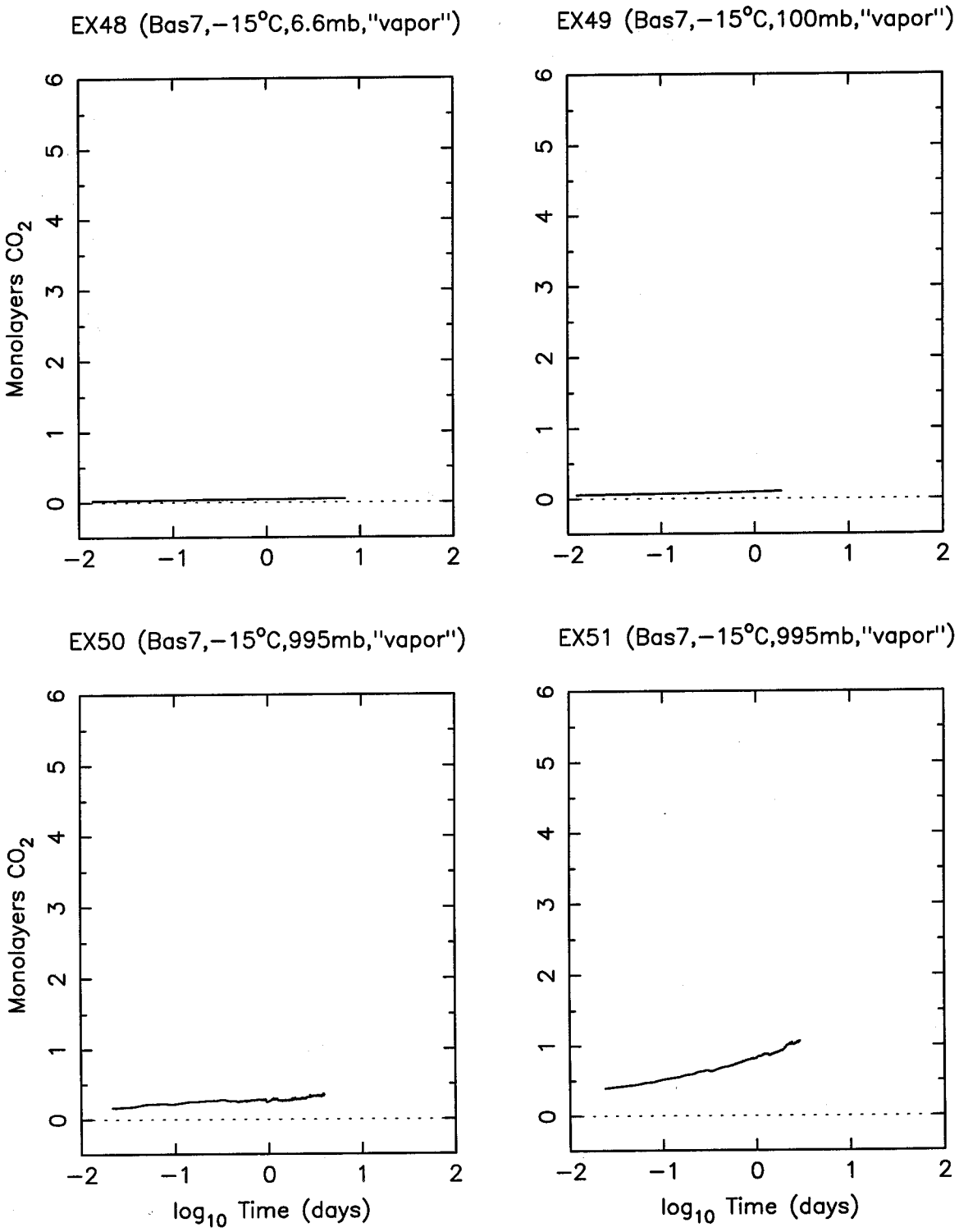

Figure 2-7 Logarithmic plots of data (continued)
(d) **GROUP 4** [Bas/cold]

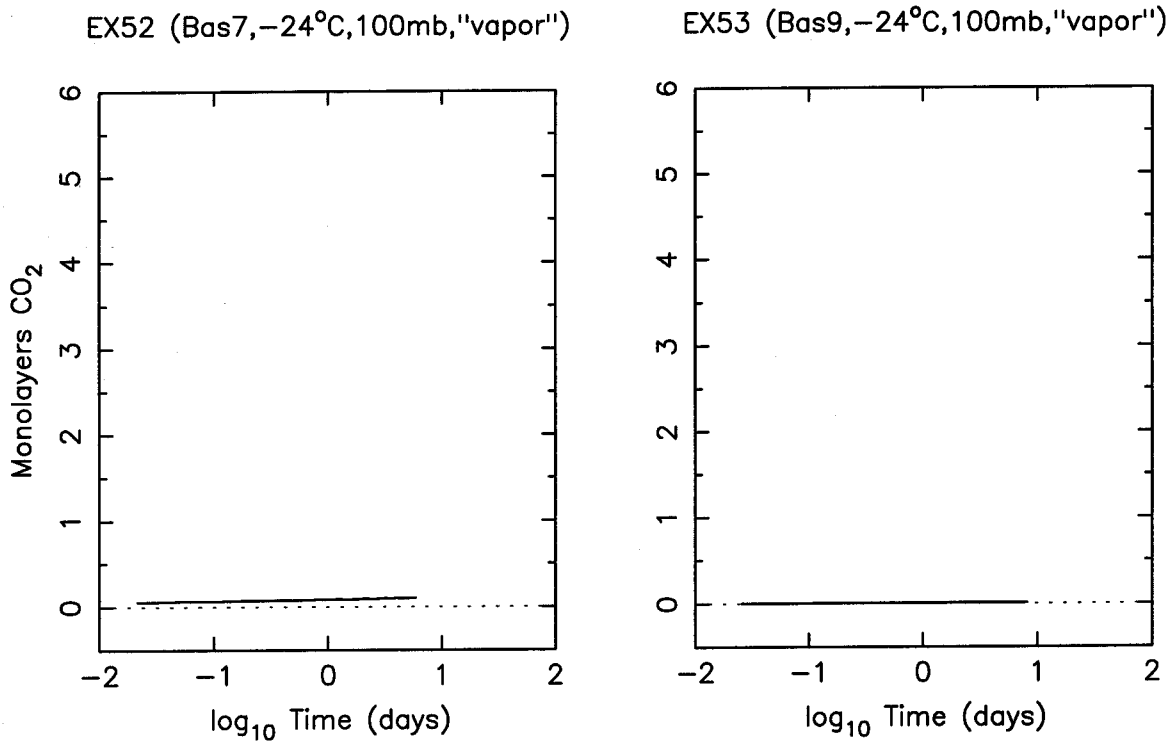

Figure 2-7 Logarithmic plots of data (continued)
(d) **GROUP 4** [Bas/cold]

for reference and represents zero uptake. For the times displayed, most experiments show nearly linear growth as a function of log t, consistent with our hypothesis that any reaction that we were observing was obeying a logarithmic rate law. All experiments are to the same scale except EX33-35; the difference between behaviors at early and late times for these and for the other "wet" experiment, EX16, is most likely due to dissolution, along with changing solution chemistry (see discussion in Chapter 4).

As a *logarithmic* rate, the parameter D obtained from fits to $P(t) = C + D \log_{10} t$ is very useful, because it allows us to extrapolate conclusions about reaction rates occurring over days in the laboratory to geologic timescales for carbonate formation on the surface of Mars, resulting in physically reasonable amounts of CO_2 destroyed (see Chapter 4).

2.4.4 Preliminary conclusions

Reaction rates obtained here can be compared to those obtained by Booth and Kieffer (1978) and Booth (1980) (see section 2.1.2). From Table 2-3, we see that long-term CO_2 uptake in our experiments lies in the range ~0.01-1 monolayer of CO_2 per interval of $\log_{10} t$. For a specific surface area of 1 m^2/g, this is equivalent to ~0.1-10 μmoles of CO_2 per g of silicate per unit $\log_{10} t$. Although not a *linear*

rate, it can be compared to Booth's rate of ~1 µmole/g/day. If Booth did in fact measure total CO_2 that reacted with silicate, our results are somewhat consistent with his, since the duration of his experiments was typically tens of hours (although our extrapolation differs from his).

Before correlating reaction rates with experimental conditions, we examined the ranges of temperatures, initial CO_2 pressures, and H_2O contents used. For EX8 onward:

T:	248-298 K
$P_o(CO_2)$:	7-1000 mb
H_2O content:	0-0.1-17000 monolayers (including "dry")

There was a greater range in observed reaction rate for experiments in which H_2O content was varied, but that is because the range of H_2O contents examined was much greater than that for temperature or CO_2 pressure. Temperature varied only about 20%, while $P_o(CO_2)$ was examined over a range of three orders of magnitude, and H_2O content over five (not including "dry" experiments).

All three of these parameters had an influence on resulting kinetics, as did the composition of powders (and whether they were pretreated with acid). A qualitative comparison among results for varying experimental conditions is presented below, in Figure 2-8, where we plot results for model fits against H_2O content (linear plots, so that "dry"

results may be included). Additional quantitative analysis of results occurs in Chapter 4.

In Figure 2-8, part (a), the exponent B in our dP/dt fits is plotted, with a vertical dotted line representing "dry" conditions, and two horizontal lines representing ±1 σ confidence limits on B for **GROUP 4** [Bas/cold] experiments (see section 2.4.2). "Dry" and "vapor" results are plotted separately from "damp" and "wet" results because of vastly different H_2O contents. In Figure 2-8, part (b), the rate $D = dP/d\log_{10}t$ in our P(t) fits is plotted, with the horizontal line this time representing zero rate of growth. Again, there are two plots for different H_2O contents. Additionally, in Figure 2-8, part (c), results for **GROUP 4** [Bas/cold] "vapor" experiments are presented in more detail, to better illustrate the dependence on CO_2 pressure (there are three different vertical scales in parts (b) and (c)).

We have not included several experiments (see section 2.4.1). EX6 was not included because it was not run for a sufficiently long time; EX21-23 and EX37, because they gave very unusual or suspicious results; EX39, because it is affected by carbonate dissolution chemistry; EX42, because it involved probable gas desorption and a negative signal; and EX31 and EX50, due to their odd pressure-drop curves. Also, although they are included, warm "vapor" experiments---EX30,32,27,38---are suspect (section 2.4.1) due to

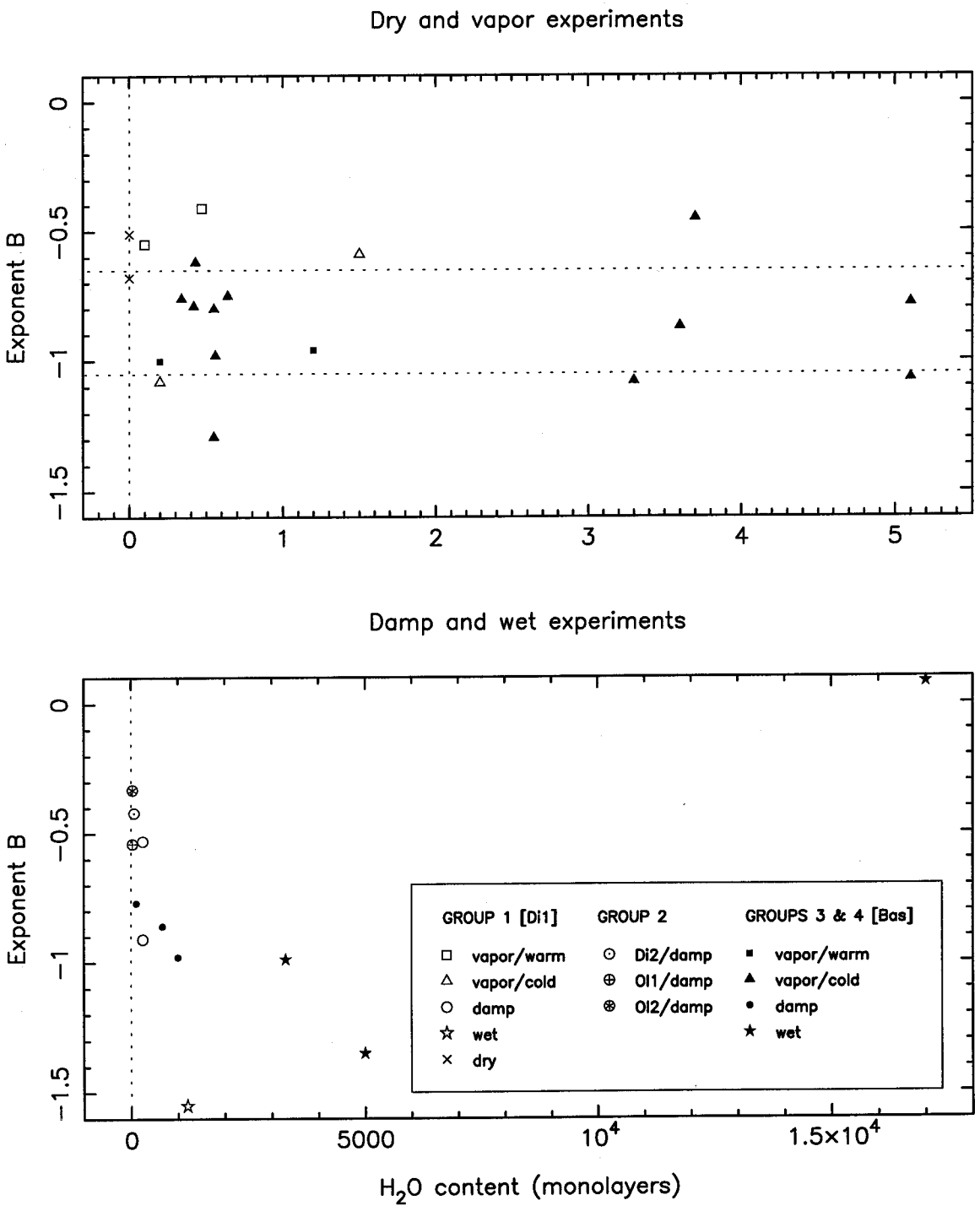

Figure 2-8 Correlations with experimental conditions (a) Exponent B

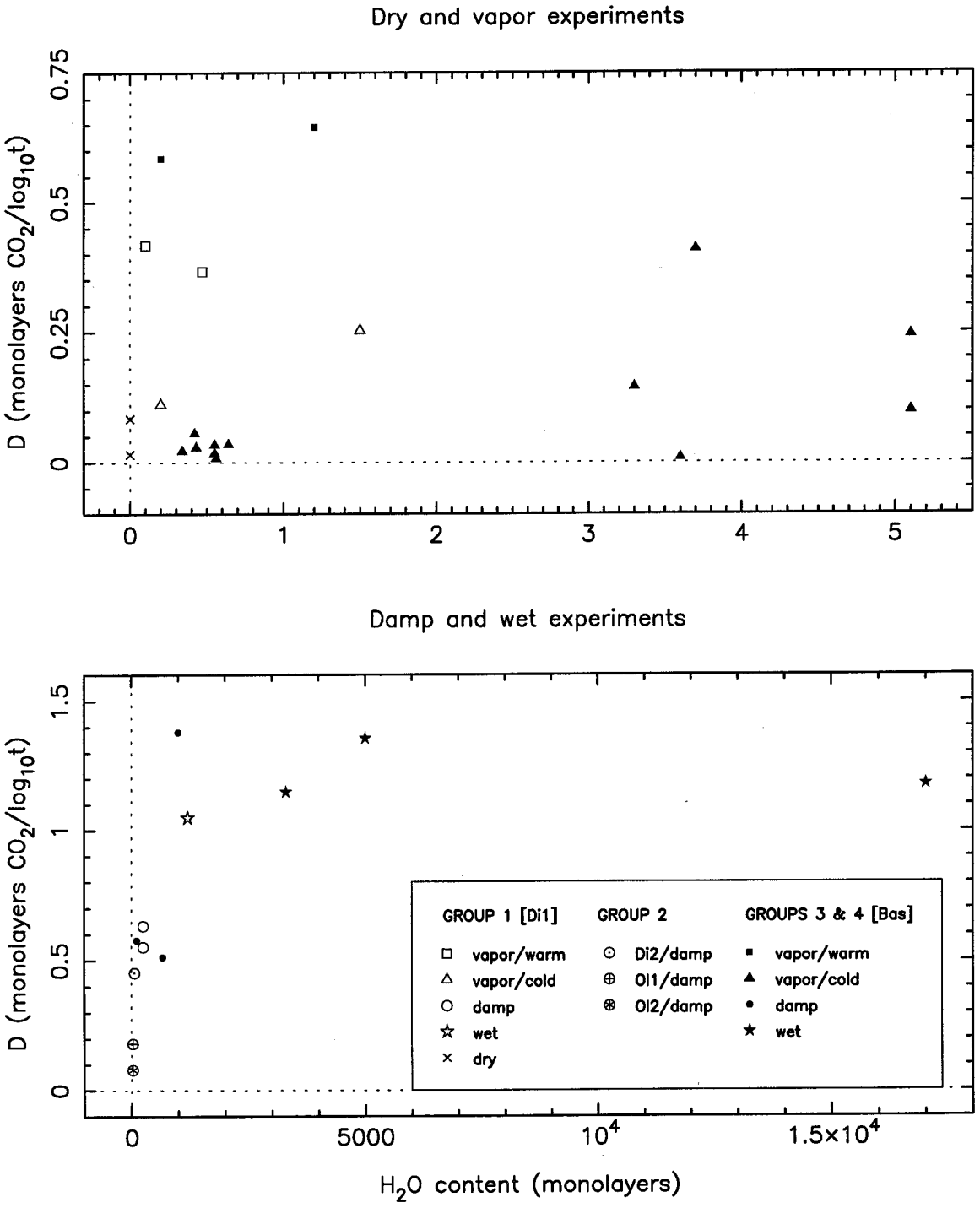

Figure 2-8 Correlations with experimental conditions (b) Rate D = $dP/dlog_{10}t$

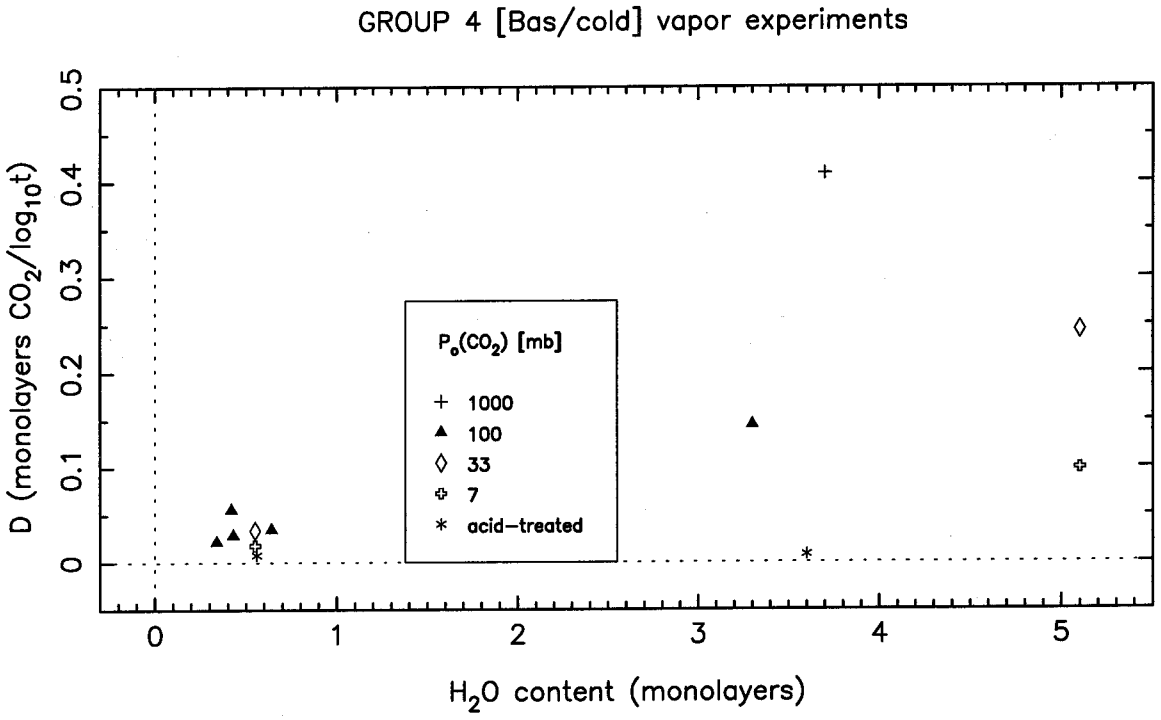

Figure 2-8 Correlations with experimental conditions (c) Rate D = $dP/dlog_{10}t$, and CO_2 pressure

the uncertain contribution to observed pressure drop of H_2O vapor pressure.

We can make the following preliminary observations:

- It is difficult to find any clear correlation of B with experimental conditions. It is possible that there is a dependence on CO_2 pressure for **GROUP 4** [Bas/cold] "vapor" experiments——the high outlying solid triangle in Figure 2-8, part (a), is for $P_o(CO_2)$ = 995 mb, and the low outlier is for 6.6 mb. All of the data seem to

be reasonably well fit by the B = -0.85 ± 0.2 result for **GROUP 4** experiments.

- The rate D, as plotted in Figure 2-8, parts (b) and (c), is more interesting. A clear dependence on H_2O content is observed, CO_2 pressure as well as temperature are also very important, and there are minor (although not as clear-cut) differences due to sample composition. Acid-treated Basalt (Figure 2-8, part (c)) shows a very small rate compared to untreated Basalt, implying that something removed by acid treatment contributes to observed uptake of CO_2 in other experiments.

These results, their correlation with spectroscopic results, and their application to Mars, will be discussed in more detail in Chapter 4.

Chapter 3

ANALYSIS USING INFRARED SPECTROSCOPY

3.1 PURPOSE

After hypothesizing (Chapter 2) that carbonate was formed in pressure-drop experiments, we sought to determine: (a) the chemical identity of the product (i.e., whether, and what kind of, carbonate formed); and (b) quantitative bounds on the amount of product produced in experimental samples.

Near- and mid-infrared reflectance spectroscopy has been used to examine carbonates in rock powders——both in characterizing nearly pure laboratory minerals (e.g., Salisbury et al., 1991), and in telescopic searches for carbonates on Mars (Blaney and McCord, 1989; Pollack et al., 1990). After performing sensitivity tests (section 3.2.3) which demonstrated that the amount of carbonate potentially added in pressure-drop experiments was detectable by reflectance spectroscopy in the 4000-800 cm^{-1} (2.5-12.5 μm) spectral region, we decided to use the Fourier transform

infrared spectrometer (FTIR, described below) in George Rossman's lab at Caltech as our principal analytical tool.

Infrared spectroscopy of carbonates is sensitive to vibrations within the carbonate (CO_3^{-2}) and bicarbonate (HCO_3^-) ions (White, 1974), and is capable of distinguishing the resulting absorptions from those due to CO_2 which is adsorbed or in the gas phase. It can also identify differences among individual carbonates (such as hydrous versus anhydrous carbonates, and calcite versus aragonite structures; e.g., Jones and Jackson, 1993). Also, because of the way that light at these wavelengths scatters among powder grains, the signal from sub-monolayer amounts of added carbonate (assuming it is added on the surfaces of grains) may be detectable with this technique. (The FTIR wavelengths are much greater than the thickness of one monolayer of product, but are the same order of magnitude as powder grain sizes.)

3.2 PROCEDURE

3.2.1 Raw spectra

Reflectance spectra for wavenumbers 4000-800 cm^{-1} (wavelengths 2.5-12.5 μm, near- to mid-infrared) were collected on a Nicolet™ 60SX FTIR spectrometer, using an

Analect™ biconical diffuse reflectance attachment. Each spectrum was obtained by integrating 1024 interferograms, with a resolution of 2 cm^{-1} (or 0.01 μm at 7 μm). The spectrometer was purged with dry air. We used the silicon-carbide Globar™ as a source, a KBr beamsplitter, and a liquid-nitrogen-cooled HgCdTe detector.

The sample holder in the biconical reflectance attachment held two machined aluminum cups, 3.5 mm deep and with 12 mm inside diameter. Sample loading consisted of using a thin spatula to scoop powder from screw-top vials, avoiding unnecessary compaction, after first overturning and shaking vials to promote particle-size homogeneity. Powders were deposited by pouring from the spatula just above the level of the cup. After the cup was filled, the straight edge of the spatula was moved horizontally along the lip of the cup to remove excess powder. Thus, a fairly flat powder surface usually resulted. (In the case of Qtz, there was not enough powder to fill a cup, so a slight tap of the cup on a table top resulted in a similar surface. EX22 (Qtz) powder was treated similarly, even though there was sufficient sample.)

Two cups (on one holder) were typically loaded simultaneously onto the biconical reflectance attachment in the standard compartment of the spectrometer. One cup was carefully placed under the reflected beam, and a chamber purge was begun. This involved closing the entrance door to the chamber, then opening shutters leading to the source and de-

tector. Following an interval of 5-15 minutes, the spectrum of the first sample was taken. After 1024 scans (taking about 5 minutes), the shutters were closed, the chamber door was opened, the sample holder was manually shifted to put the second powder under the beam, and a second purge was begun before taking the next spectrum. Following every two samples, the routine was repeated, powders were carefully returned to their vials, and the next set of powders was loaded.

3.2.2 Ratioed spectra

By experimenting, we determined that the ratio of two very similar spectra would give us the capability to detect small amounts of new phases. Thus, we ratioed spectra for experimental powders to spectra for starting (background) powders. The ratio obtained by the Nicolet™ software is the intensity of sample signal divided by the intensity of background signal, minus unity, computed at each wavenumber. We expected any deviations (aside from noise and atmospheric signal) from flat ratioed spectra to be due to added phases in experimental powders. This technique was far more sensitive than ratioing separate spectra for experimental and starting powders to the same background spectrum (e.g., NaCl), and then attempting to compare slight differences in the two ratioed spectra. (No Bas3 remained to ratio against

after pressure-drop experiments, so for EX31 we ratioed to Bas1, and for EX38 we ratioed to EX31.)

3.2.3 Controls and reference spectra

A number of control runs were conducted to test the sensitivity of our spectral results to slight variations in procedure. We tested the effects of chamber purging, powder handling, and number of interferometer scans. Purging the sample chamber for intervals of 5 minutes or longer had the effect of reducing atmospheric signals (CO_2 and H_2O), which was helpful in reducing noise near absorptions due to added phases, but otherwise had minimal effect on detectability of signal. We also varied the way we smoothed powder surfaces prior to collecting spectra. Only a minimal effect was observed——for (a) no smoothing, (b) disturbing the surface by tapping the holder on a table or the spectrometer, and (c) packing powder in the holder with a spatula. Finally, 1024 scans with the spectrometer were deemed to be sufficient, since subsequent integrations of 12,288 scans (taking 1 hour) without moving the sample gave very little noticeable improvement in noise level. This suggested that most of the noise either was due to environmental conditions or was from inherent instrument noise.

We were also able to constrain the repeatability of spectral results. Ratioing the spectrum for an experimental

sample against two different backgrounds (obtained using different portions of the same starting powder) confirmed the repeatability of our method for taking ratioed spectra. Ratioing two spectra taken from the same powder (but different portions) to each other also gave us what we predicted, namely, a fairly flat signal containing only atmospheric signal and noise. Additionally, we verified that ratios of spectra did not change over time, by taking (effectively random) portions of the same powders on different dates and then ratioing. No change was noticed——for the few powders that were tested in this way——even over intervals of more than two years. This also had the effect of reassuring us that we were not contaminating samples by repeatedly taking (and returning to vials) portions for spectral analysis.

For reference, we obtained spectra for four carbonate powders (calcite, $CaCO_3$; dolomite, $CaMg(CO_3)_2$; magnesite, $MgCO_3$; and siderite, $FeCO_3$) and talc ($Mg_3Si_4O_{10}(OH)_2$). Ratioing these to background spectra obtained from our starting powders helped us to determine the minerals responsible for absorptions that appeared in experimental ratioed spectra.

Finally, we calibrated our ability to detect carbonate by examining physical mixtures of experimental starting samples with calcite. Using weight percentages of calcite in the range 0.1-10% allowed us to show that calcite added to diopside (Di1), for example, was easily noticed at the 0.3% level in resulting ratioed spectra (i.e., $CaCO_3$ + Di1

mixture versus Di1 alone). Results for this and the other FTIR runs discussed above are shown in the next section.

3.3 RESULTS

3.3.1 Interpretation

An example of a ratioed spectrum (EX52 versus Bas7) for the full range of wavenumbers examined appears in Figure 3-1, and has characteristics common to most of our spectra. The prominent (doublet) feature at 2350 cm^{-1} was due to varying absorption by atmospheric CO_2 in the spectrometer, and can safely be ignored. Noise near 1800-1400 cm^{-1} was

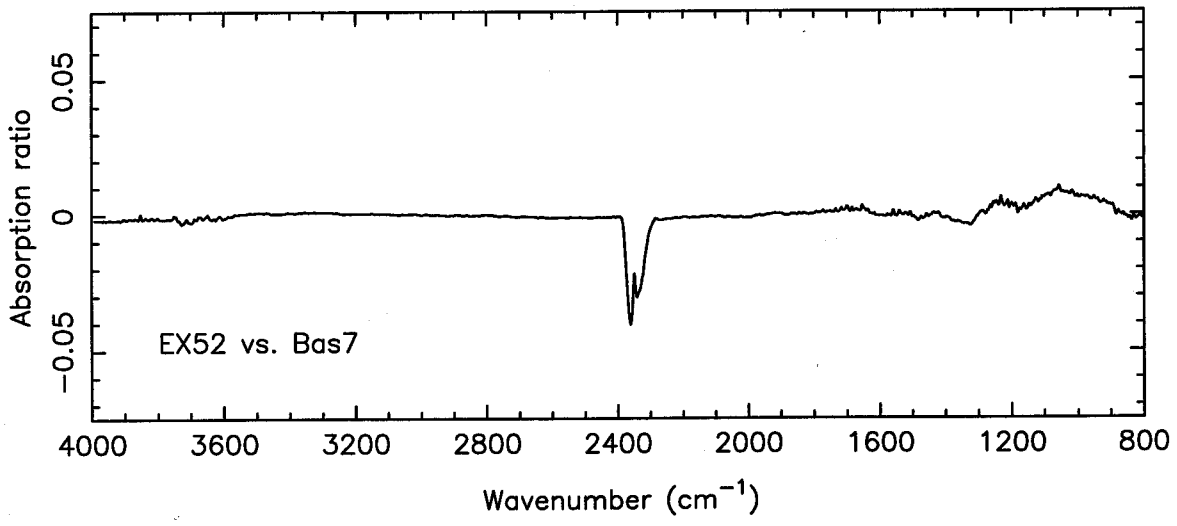

Figure 3-1 Example of full range of ratioed FTIR spectrum (4000-800 cm^{-1})

from atmospheric H_2O absorption (Salisbury et al., 1991), but it was not responsible for conspicuous features observed in some ratioed spectra. Absorption by H_2O also contributed at wavenumbers greater than about 2800 cm^{-1}. For wavenumbers lower than about 1300 cm^{-1}, there was often a lot of noise because we were ratioing spectra for silicates which absorb strongly in this region. Therefore, we did not interpret features beyond about 1300 cm^{-1} (although silicates, such as SiO_2, that are byproducts of carbonate-forming reactions may have contributed to those signals).

From controls and reference spectra, we established that the absorption ratios seen in Figure 3-1 in the range 2000-1300 cm^{-1}——about ±0.002 with respect to continuum——represented the limit of our ability to detect added phases.

Due to the spectrometer's sensitivity to unbound water, we have not analyzed spectra from "damp" and "wet" experiments, although, for reference, a ratioed spectrum from a "damp" experiment (EX28 versus Bas2) is shown in Figure 3-2. Samples exposed to less H_2O, such as this one, show absorptions that are consistent with the conclusions reached below. However, wetter samples give spectra that are difficult to interpret because of absorption by water.

Ratioed experimental spectra are shown in Figure 3-3, (pages 138-144) for the wavenumber range 2800-1200 cm^{-1} (3.6-8.3 μm), for all "dry" and "vapor" experimental samples (except EX53, for which a spectrum had not been measured at

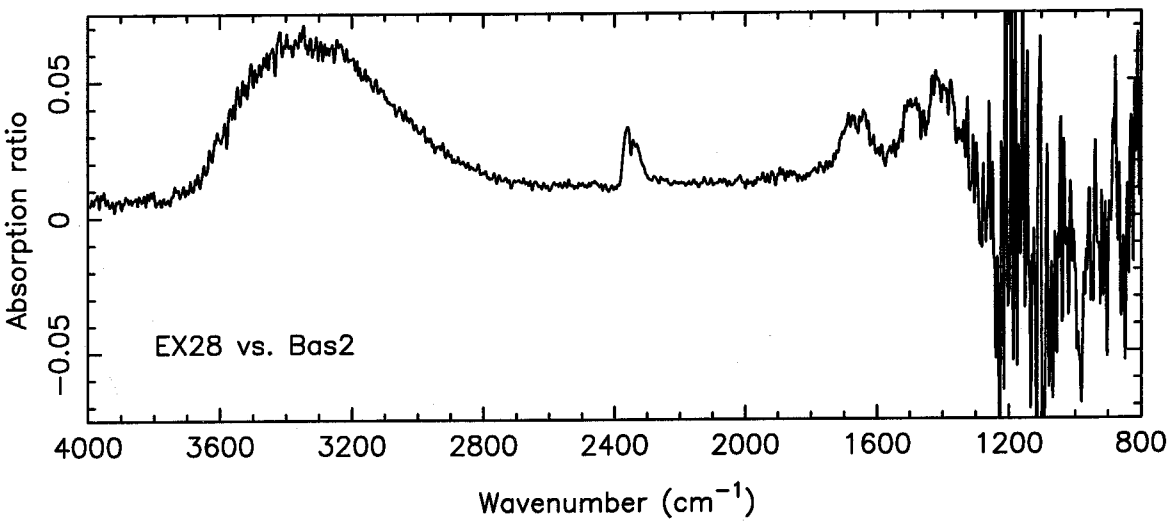

Figure 3-2 Example of ratioed spectrum from "damp" experiment

the time of writing). Spectra are grouped in the same manner as pressure-drop results. Continuum levels in ratioed spectra are often displaced from zero because of varying angles of reflection of infrared light from powder surfaces.

Ignoring absorptions in Figure 3-3 due to atmospheric CO_2 and H_2O, what remains are features in the range 2000-1300 cm^{-1} for Di1 (and Qtz), and 1800-1300 cm^{-1} for Bas. For Di1, there was sometimes an additional absorption near 2550-2500 cm^{-1}. These results, along with measured feature heights, are summarized in Table 3-1 (page 145).

Features that are negative with respect to continuum ratioed spectra (e.g., EX8/Di1 and EX43/Bas6) also correspond to absorption differences between experimental and starting samples, but in these cases there are probably

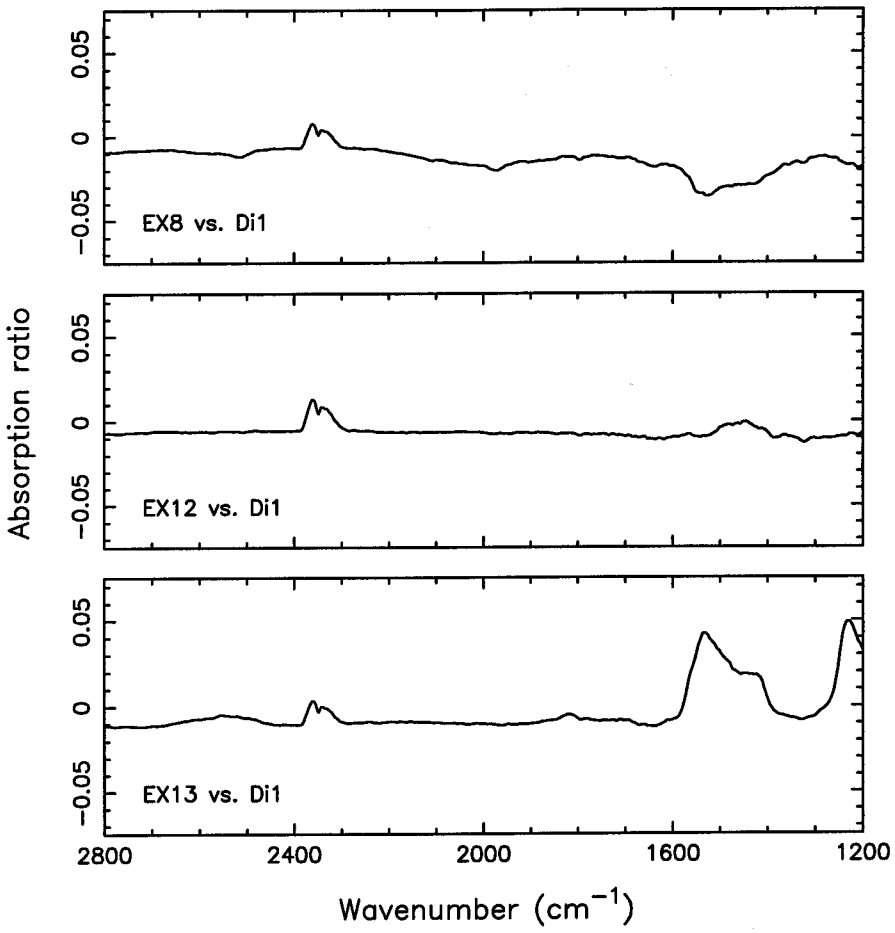

Figure 3-3 Ratioed FTIR spectra (2800-1200 cm^{-1}) of powders from "dry" and "vapor" experiments (a) **GROUP 1** [Di1]

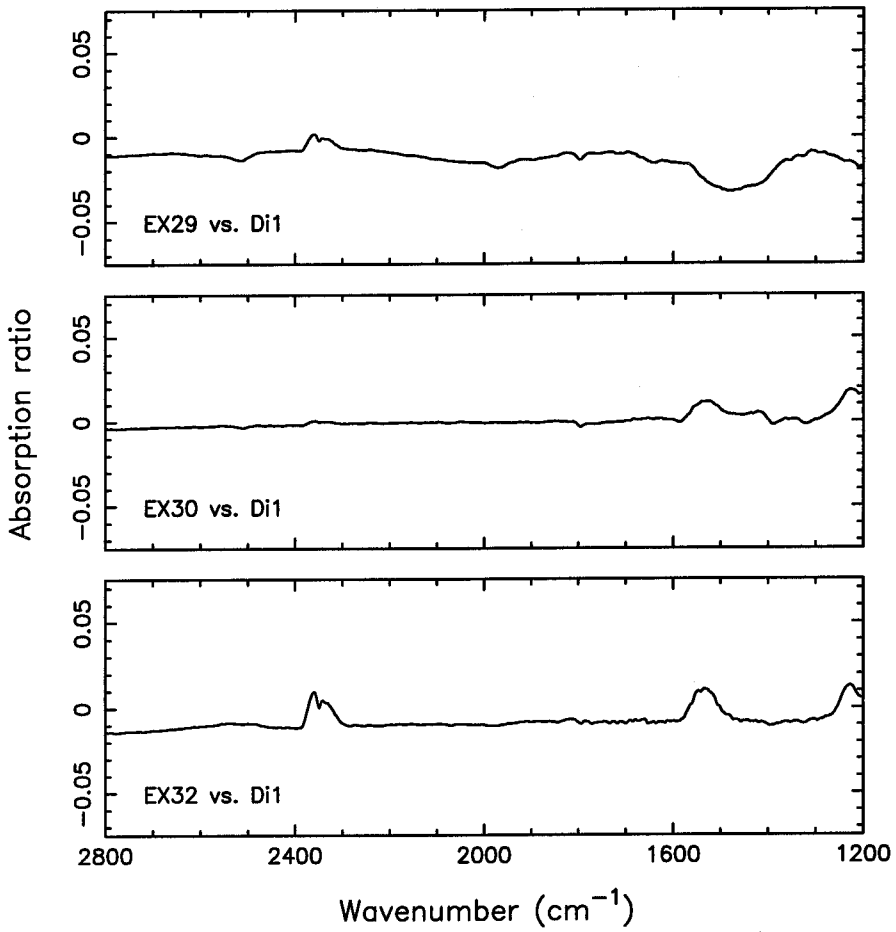

Figure 3-3 Ratioed FTIR spectra (2800-1200 cm^{-1}) of powders from "dry" and "vapor" experiments (a) **GROUP 1** [Di1] (continued)

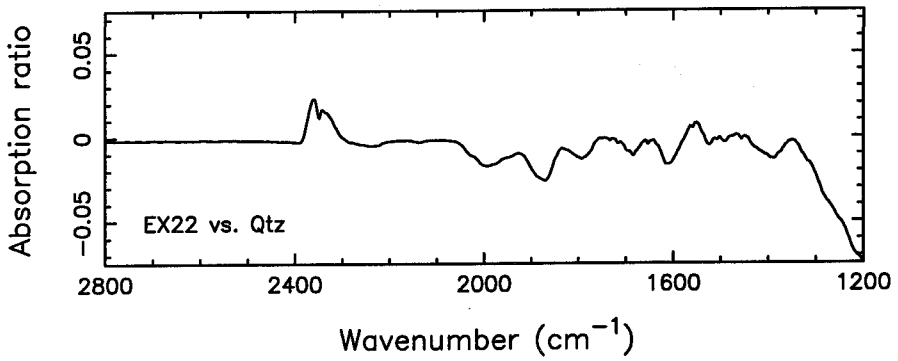

Figure 3-3 Ratioed FTIR spectra (2800-1200 cm^{-1}) of powders from "dry" and "vapor" experiments (b) **GROUP 2** [Qtz]

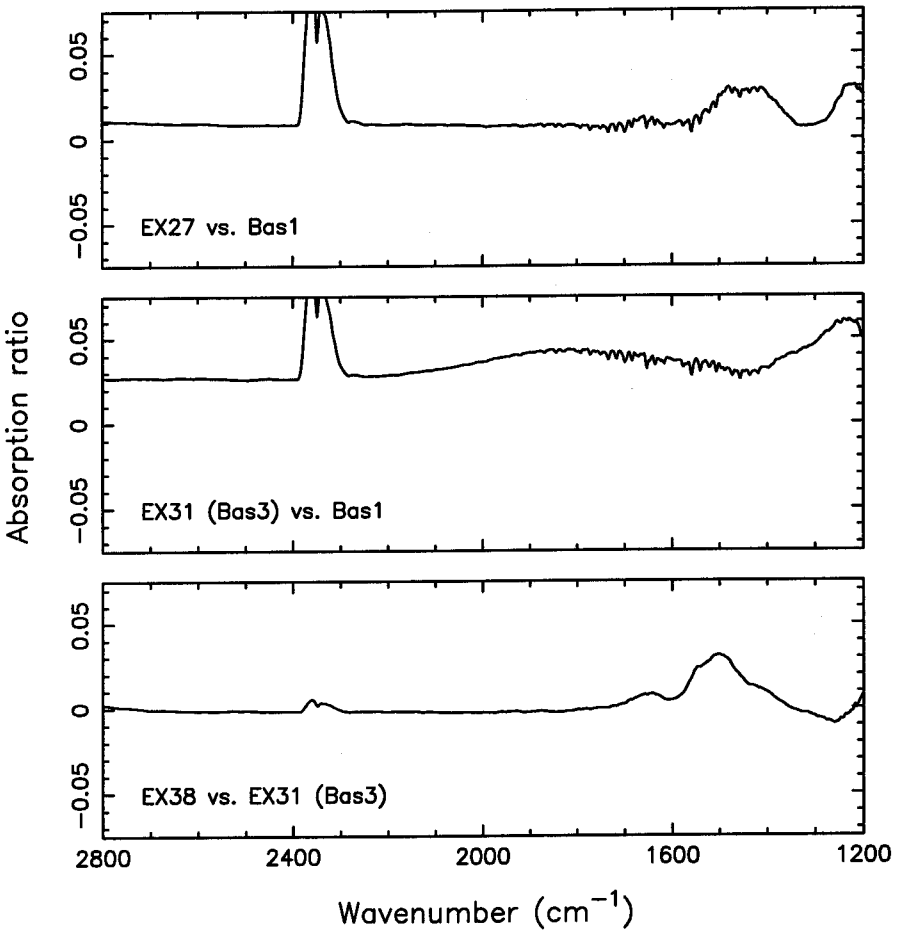

Figure 3-3 Ratioed FTIR spectra (2800-1200 cm^{-1}) of powders from "dry" and "vapor" experiments (c) **GROUP 3** [Bas/warm]

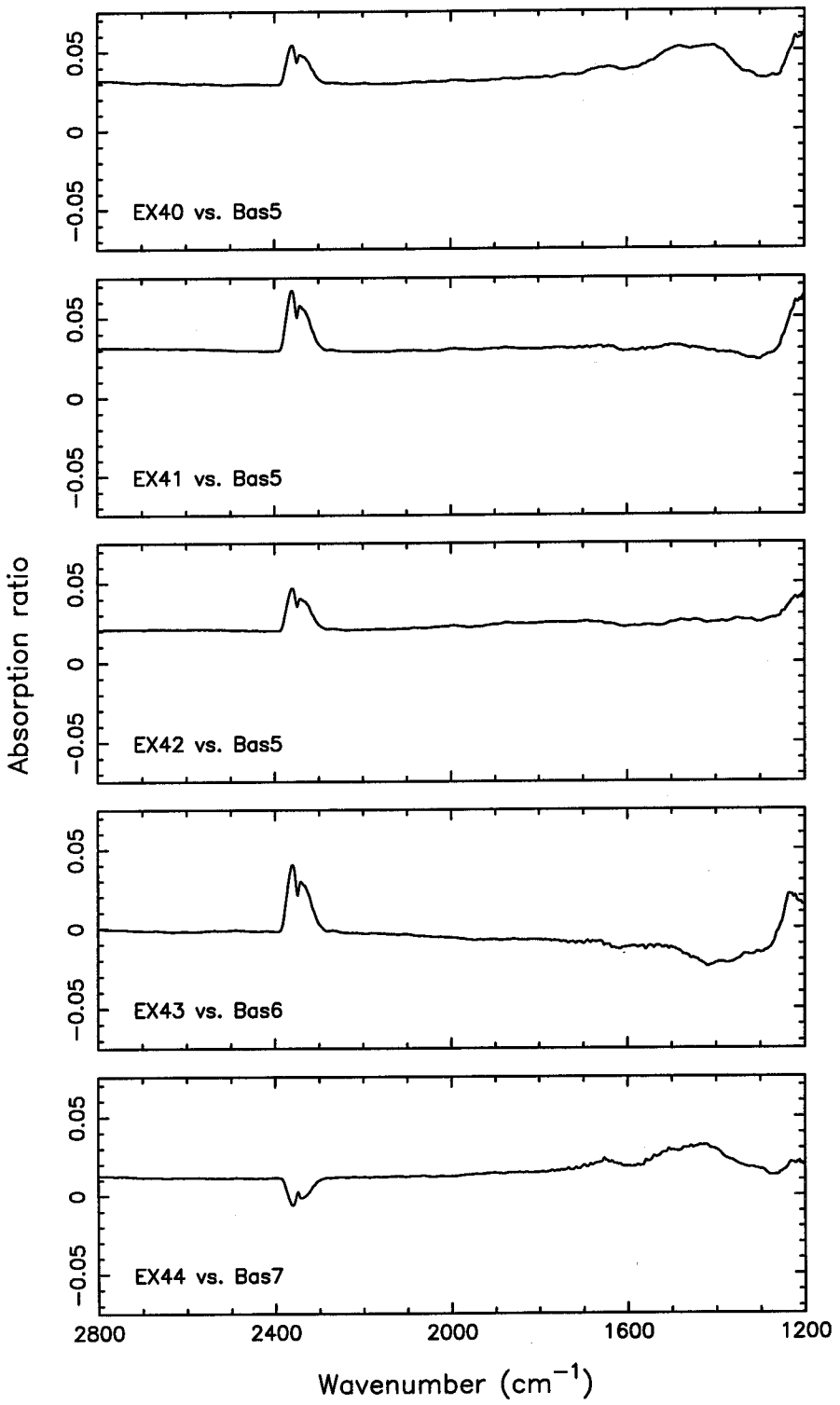

Figure 3-3 Ratioed FTIR spectra (2800-1200 cm^{-1}) of powders from "dry" and "vapor" experiments (d) **GROUP 4** [Bas/cold]

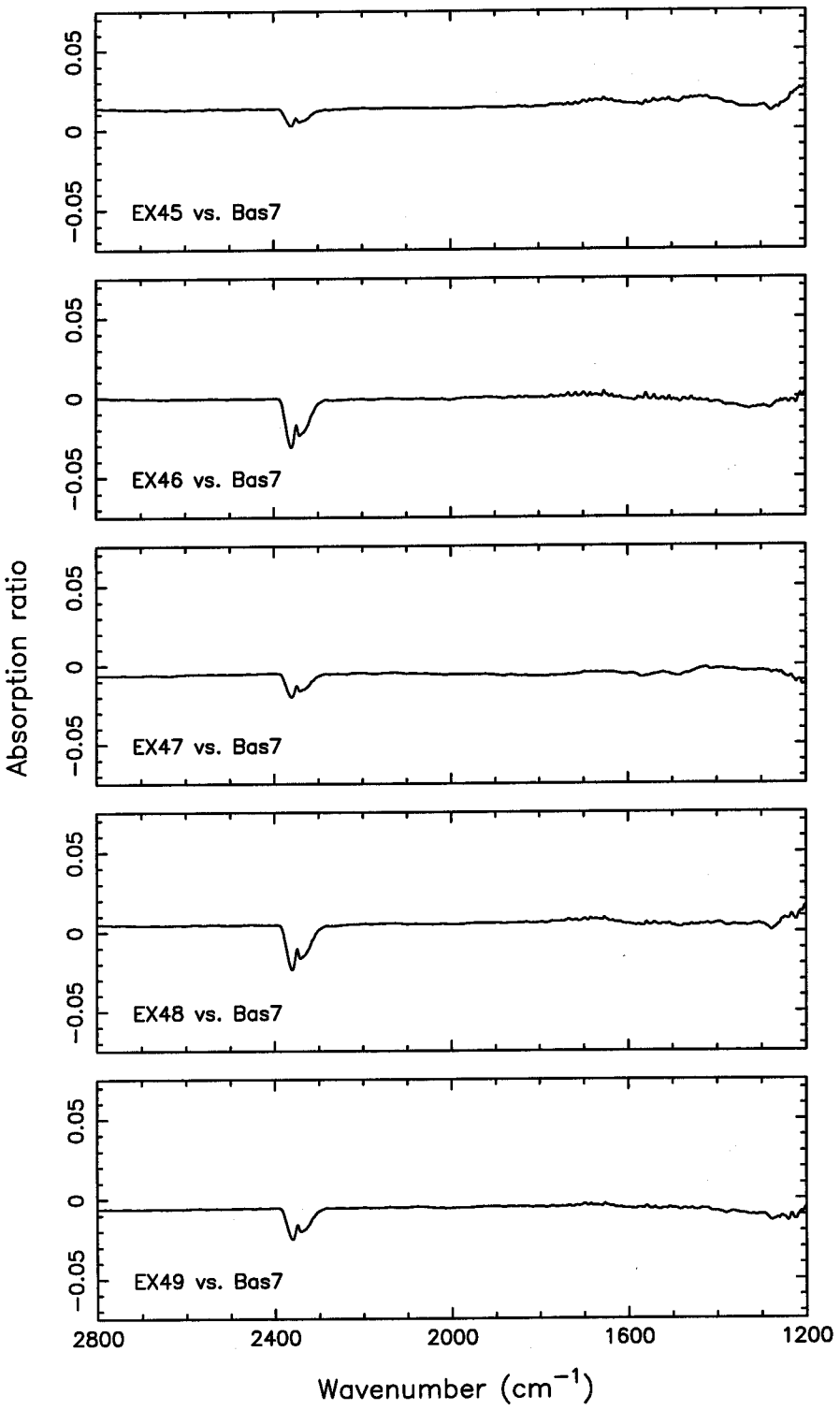

Figure 3-3 Ratioed FTIR spectra (2800-1200 cm^{-1}) of powders from "dry" and "vapor" experiments (d) **GROUP 4** [Bas/cold] (continued)

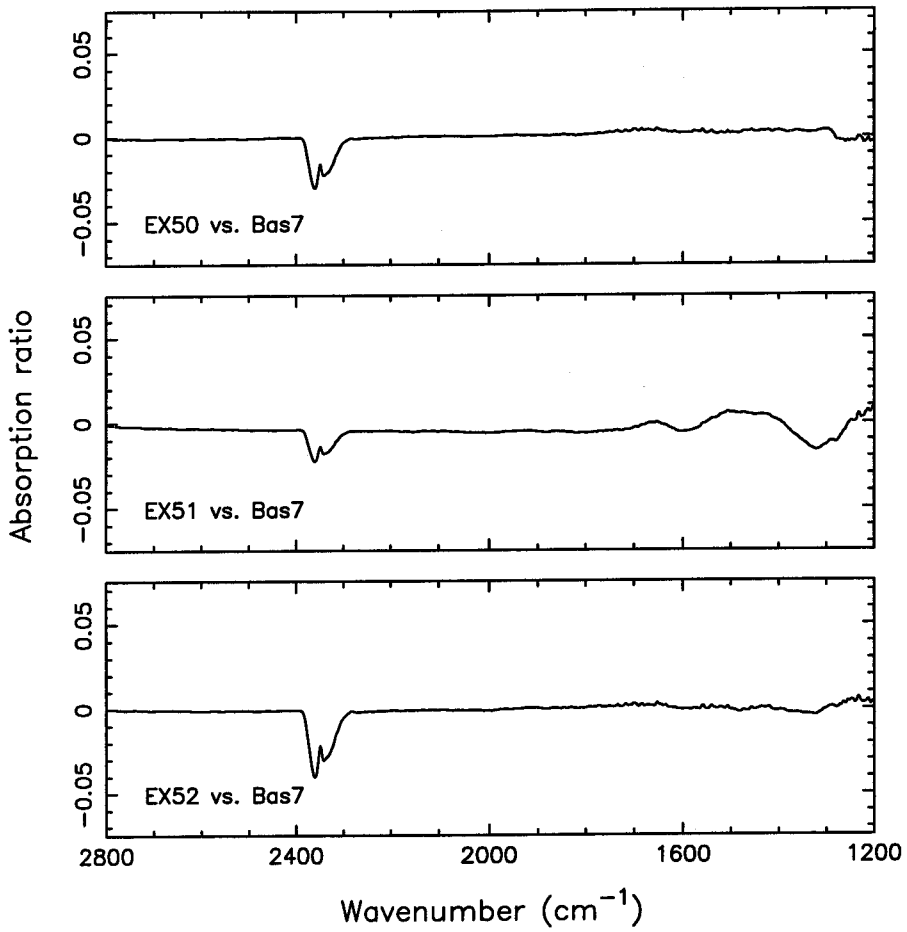

Figure 3-3 Ratioed FTIR spectra (2800-1200 cm^{-1}) of powders from "dry" and "vapor" experiments (d) **GROUP 4** [Bas/cold] (continued)

Table 3-1 Summary of FTIR results: Ratioed spectra for experimental powders versus starting powders

Ratioed spectra	Approximate center positions (cm^{-1}) of features (with selected heights* in italics)						
GROUP 1							
EX8/Di1	~2510		~1530				*0.022*
EX12/Di1				1447			*0.010*
EX13/Di1	~2530	1819	1534		1419		*0.054*
EX29/Di1	~2510			1475		1308	*0.022*
EX30/Di1	~2510		~1529		1419		*0.012*
EX32/Di1	~2530		1531				*0.020*
GROUP 2							
EX22/Qtz	?						
GROUP 3							
EX27/Bas1	1646		1478	~1419			*0.018*
EX31/Bas1							
EX38/Bas3	~1641	1544?	1501				*0.032*
GROUP 4							
EX40/Bas5	~1641		1480	1407			*0.020*
EX41/Bas5	~1661		~1490				*0.002*
EX42/Bas5							
EX43/Bas6				1417	1335		*0.014*
EX44/Bas7	1652		1505	~1426			*0.016*
EX45/Bas7	1652			~1423			*0.004*
EX46/Bas7							
EX47/Bas7				1426			*0.002*
EX48/Bas7	1652						
EX49/Bas7	1652						
EX50/Bas7	1652						
EX51/Bas7	1655		1505	~1423			*0.010*
EX52/Bas7	1652			1429?			
EX53/Bas7							

*Heights are ratios of beam intensities, and are for the largest observed peak in the 1550-1350 cm^{-1} region. Sometimes magnitudes of negative peaks (see text) are used.

particle size effects which cause peaks to appear as negative rather than positive features (e.g., see discussion, as well as spectra for different particle sizes, in Salisbury et al., 1991).

As preliminary observations, several (but not all) spectra had absorption ratios exceeding our detection limit, and the strongest results occurred for experiments that recorded the most prominent pressure drops. (The features in the ratioed spectrum for EX22, which contains Qtz, are probably due to the fact that absorption by SiO_2 is strong at wavenumbers less than 2000 cm^{-1}.)

3.3.2 Identification of carbonate

Ratioed spectra for mixtures of calcite and Di1 (versus Di1) are shown in Figure 3-4; spectra for our reference minerals versus Di1 and Bas7 are shown in Figure 3-5 (bad ratios result in some gaps). From these figures, we see that all of our reference minerals have absorptions in the 2000-1300 cm^{-1} region. A closer look, focusing near 1500-1400 cm^{-1}, confirms that carbonates (in addition to talc and quartz) constitute the most likely possibilities for added phases in our experiments. This is corroborated by an examination of reflectance spectra in Salisbury et al. (1991).

Figure 3-5, with ratios of calcite to our experimental starting powders (Di1 and Bas7), is particularly revealing.

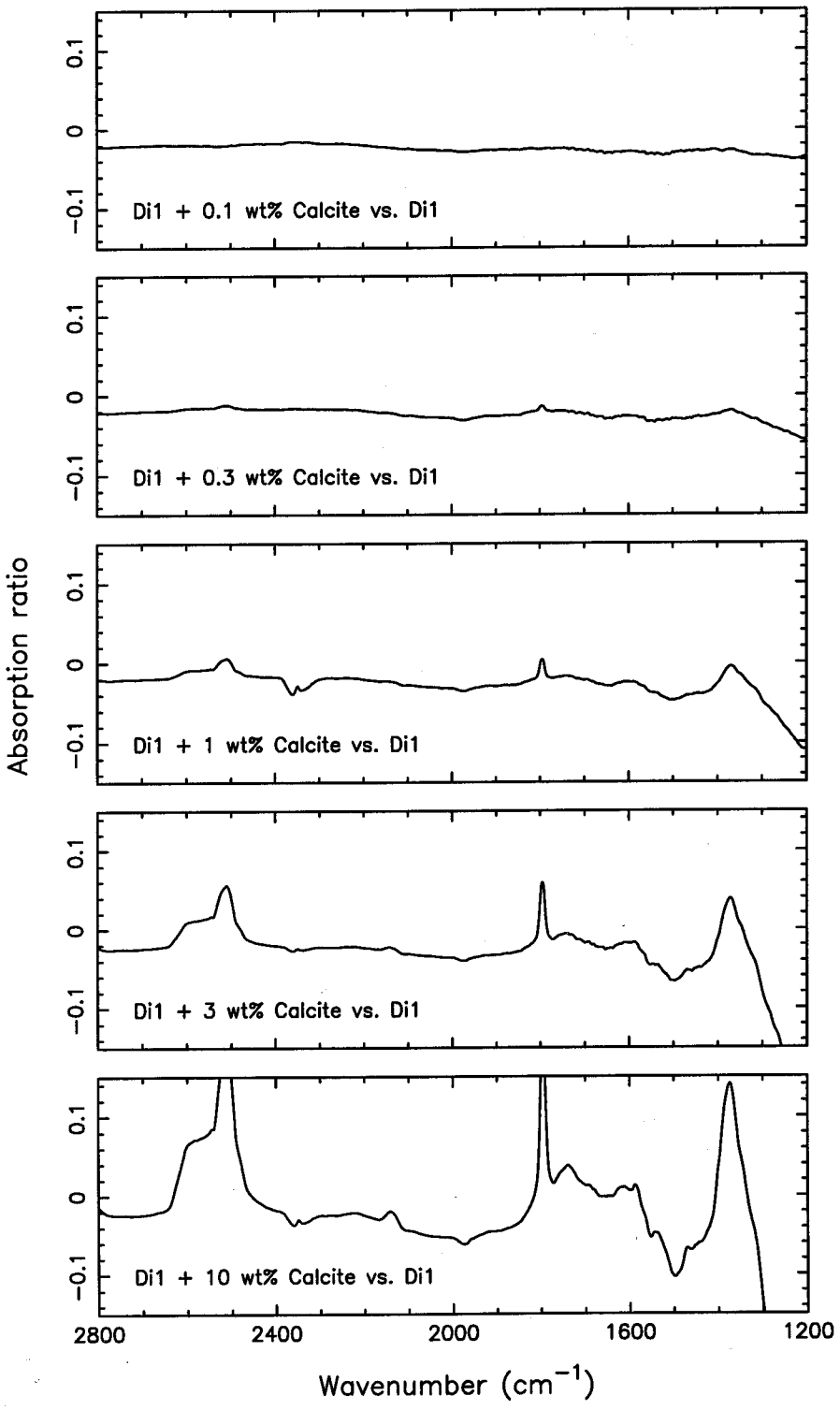

Figure 3-4 Ratioed spectra for mixtures of calcite and Diopside 1

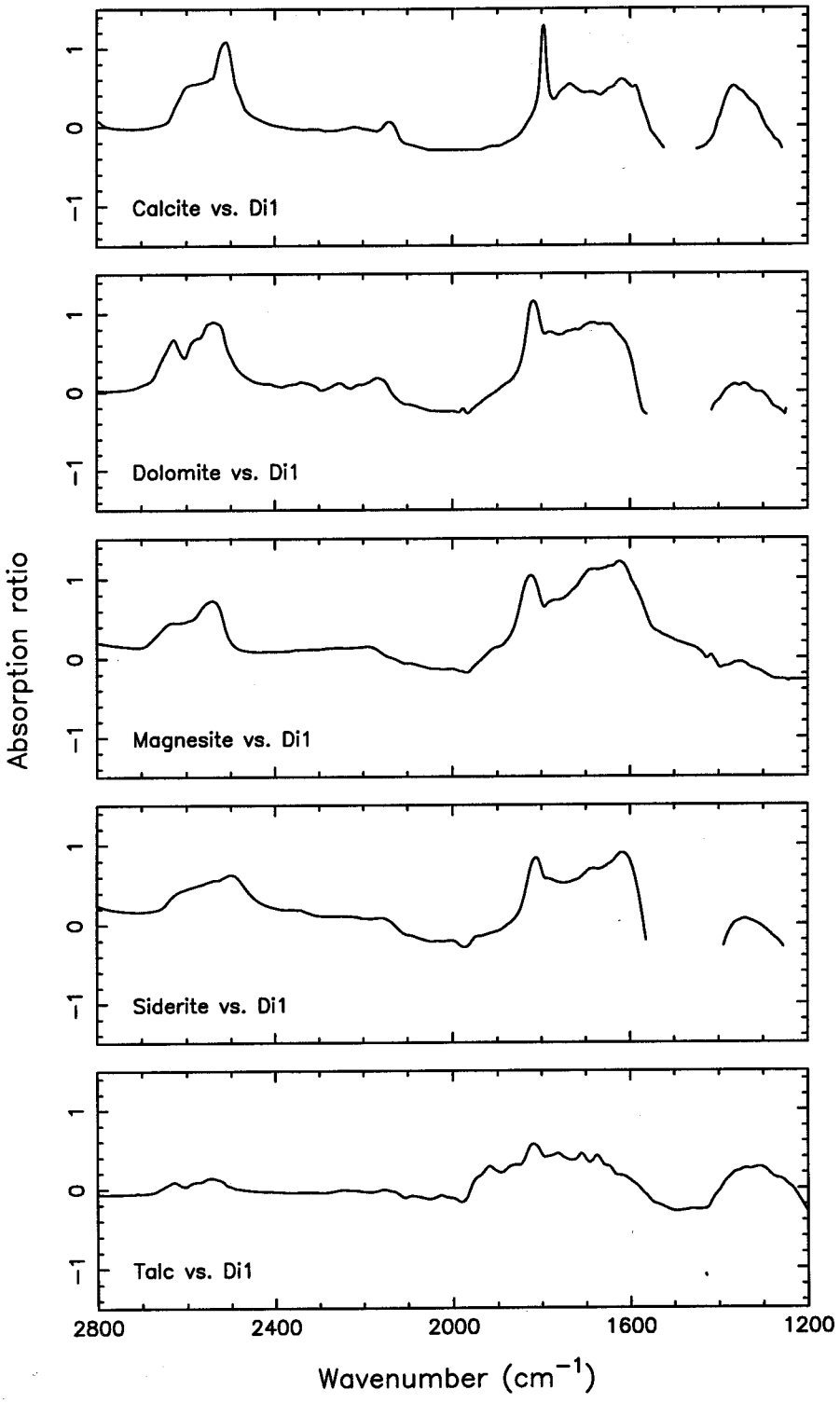

Figure 3-5 Ratioed spectra of reference minerals
(a) Minerals ratioed to Diopside 1

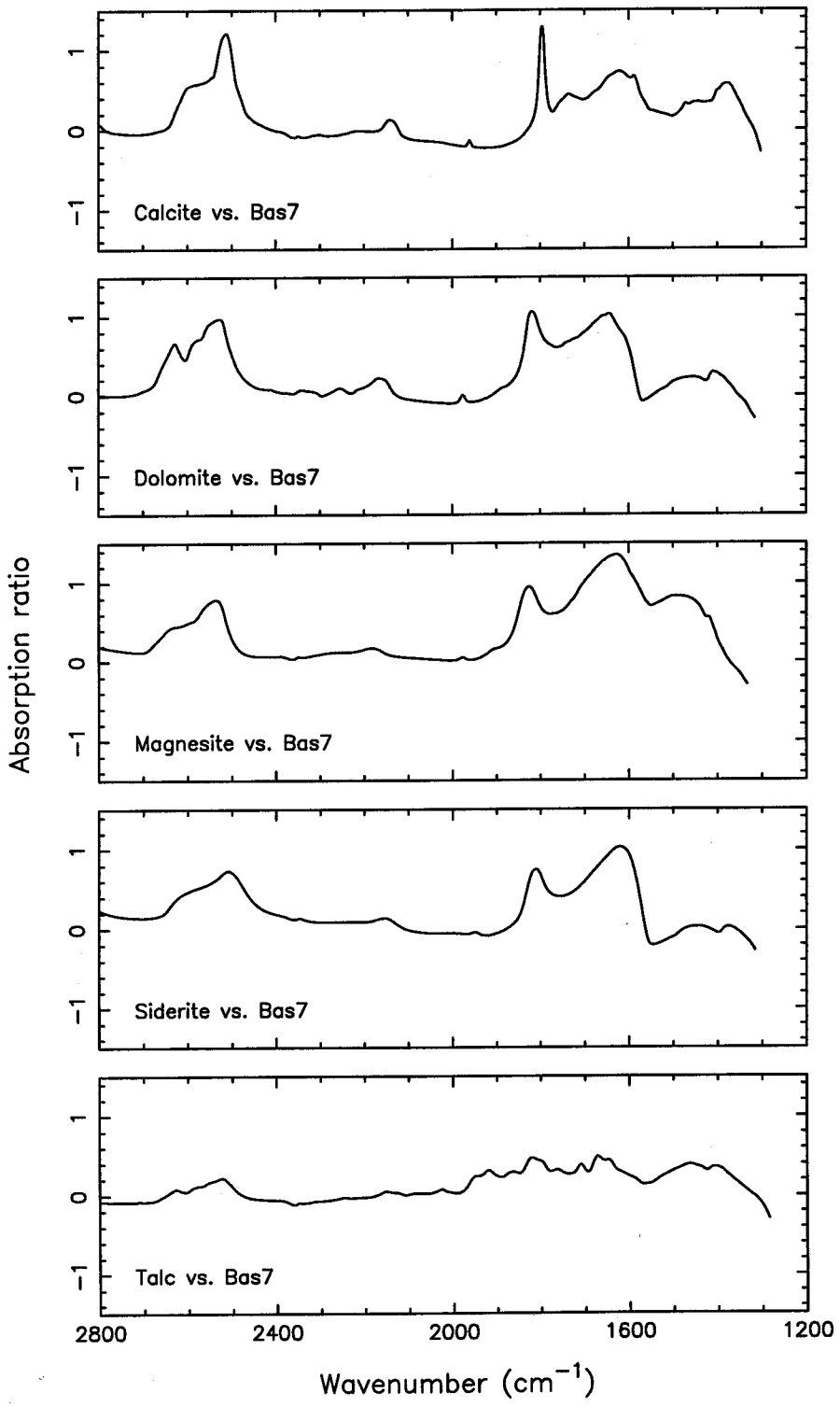

Figure 3-5 Ratioed spectra of reference minerals (b) Minerals ratioed to Basalt 7

Absorptions are prominent around 1400-1300 cm^{-1} for Di1, and in the 1500-1300 cm^{-1} range for Bas7. This is consistent with the strong absorption near 1450 cm^{-1} for calcite that occurs with transmitted light (Jones and Jackson, 1993).

Strong calcite absorptions around 1800-1600 cm^{-1} do not appear prominent in spectra for our experimental powders, although a small feature around 1650 cm^{-1} does occur for powders containing Bas, and a small feature near 1820 cm^{-1} is evident in the EX13 spectrum. Also, although it was not present in Bas spectra, there was a small peak around 2550-2500 cm^{-1} in Di1 spectra, possibly corresponding to another strong calcite absorption (see Figure 3-5). Since calcite that formed on the surfaces (or in the pores) of experimental powder grains may give spectroscopic signatures different from a spectrum of calcite taken when light is reflected from individual grains, the peaks we are seeing in ratioed spectra are consistent with calcite absorption.

From trials with mixtures (Figure 3-4), we saw that it was at about the 0.3 wt% level that calcite became evident in Di1 when the two powders were physically mixed. A comparison of peak heights (e.g., to results from EX13 versus Di1) suggests that as much as about 3 wt% calcite formed in experimental powders. This exceeds the amount of calcite present to begin with in Di1 (which was not acid-treated).

Figure 3-6 shows a summary of our spectroscopic results, showing representative comparisons between

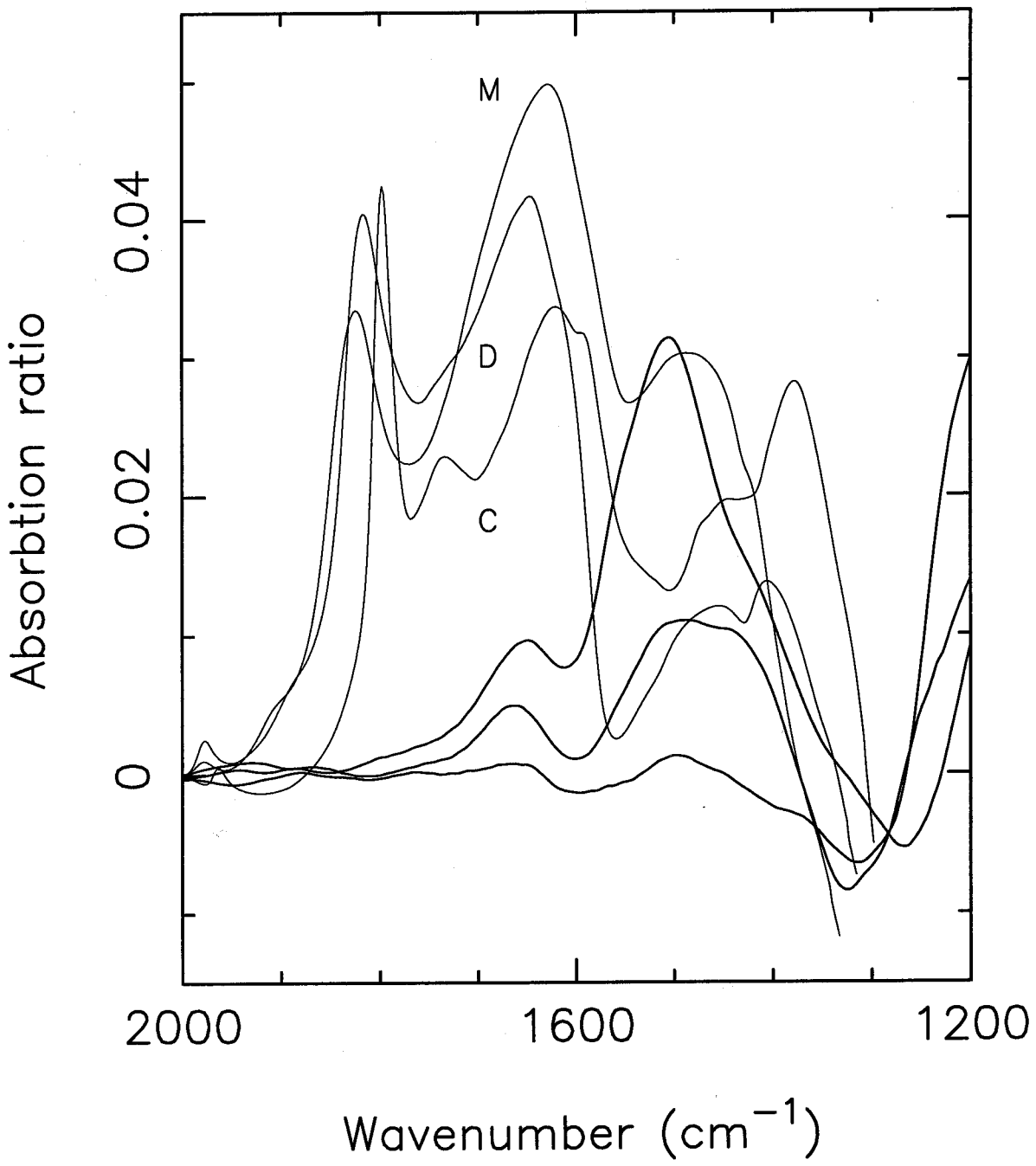

Figure 3-6 Comparison between experimental and reference spectra (typical experimental results shown with thick lines; M = magnesite, D = dolomite, C = calcite, all three scaled for comparison)

experimental and reference spectra. Spectra for experiments EX38,51,41 (in decreasing order of peak absorption ratio) are shown with thick lines. Carbonate powders (M = magnesite, D = dolomite, and C = calcite) ratioed to starting basalt powders are shown with thin lines; these spectra are scaled for comparison to experimental results. All ratioed spectra are set to zero at 2000 cm^{-1} to facilitate comparison. The presence of absorptions noted previously---near 1500-1400 cm^{-1} and near 1650 cm^{-1}---in both carbonate and experimental spectra supports the conclusion that added carbonate is present in experimental powders.

3.3.3 Comparison with experimental results

We plotted FTIR absorption ratios against results from pressure-drop experiments to see if observed pressure drops and infrared features are correlated. Peak heights were obtained from Table 3-1, and total experimental CO_2 uptake due to reaction was estimated from:

$$\#\ \text{estimated monolayers of } CO_2 = D\ (\text{monolayers } CO_2/\log_{10}t) \times \log_{10}\Delta t_{eff} \qquad [3\text{-}1]$$

Results for experiments with Basalt conducted under "vapor" conditions are shown in Figure 3-7. There is a clear positive correlation between pressure drop and FTIR

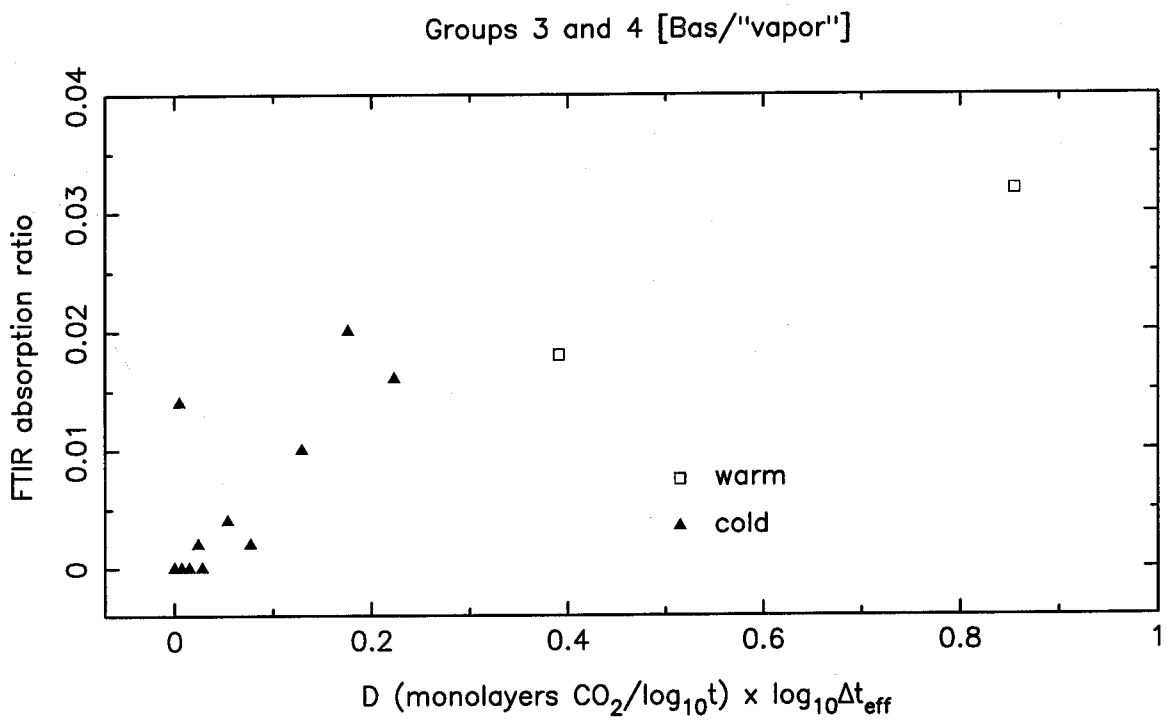

Figure 3-7 Correlation with pressure-drop results

absorption ratio, consistent with the formation of carbonate in our experiments. Also supporting this conclusion is the observation that powders with greater H_2O contents (giving larger rates of CO_2 uptake) demonstrated stronger infrared absorptions. The point with ratio 0.014 is for an experiment on acid-treated Basalt (see Chapter 4).

3.4 OTHER ANALYTICAL METHODS

In addition to using FTIR, we conducted studies of the detectability of added phases with two other spectroscopic techniques. X-ray fluorescence (XRF) was unable to detect any added carbonate in experimental sample from EX13, but calcite would only have been detectable above a threshold of 1-5 wt%.

We also used X-ray photoelectron spectroscopy (XPS), in which electrons generated by incident X-rays allow quantitative identification of surface elements and chemical states from binding energy spectra. With an instrument at Caltech's Beckman Institute, we analyzed both crystals of diopside (the Di2 described in Chapter 2) and chips of the same basalt glass used as powders in pressure-drop experiments. Both were exposed at room temperature for 2 to 4 weeks to a 1-bar CO_2 atmosphere saturated with H_2O vapor, and then compared with controls exposed to N_2.

Oxidized carbon, representing carbonate, would have been seen under XPS as a carbon signature shifted to higher binding energy relative to, e.g., organic carbon. None was detected on either diopside or basalt, suggesting that any carbonate formation in pressure-drop experiments may be related to the surface or subsurface texture of crushed powders, or alternatively it may occur deep enough that XPS cannot see it at the surface of bulk samples. However, more

work could be done, since it was very difficult to obtain carbon signatures sufficiently different in binding energy from organic carbon to allow unambiguous identification of carbonates. This was true as well for the experimental and starting *powders* which we examined with XPS.

Chapter 4

MODELING AND APPLICATION TO MARS

4.1 INTRODUCTION

We have made the following observations from pressure-drop experiments and subsequent analysis:

- Initial rapid pressure drops in experimental powders were attributed to adsorption of CO_2 or dissolution of CO_2 in H_2O. In general, for times after ~10^{-2} days, declining rates of CO_2 uptake were consistent with a power-law expression for the rate of pressure drop: $dP/dt = At^B$, with $B = -0.85 \pm 0.2$ for cold experiments on Basalt exposed to H_2O vapor. This is consistent with P varying as log t, henceforth referred to as *logarithmic reaction kinetics*.
- The rate of carbonate growth inferred from $P(t) = C + D \log_{10} t$ was in the range D ~ 0.01-1 monolayer of CO_2 per unit $\log_{10} t$, somewhat consistent with the kinetics reported by Booth (1980). Aside from varying over

a large range of H_2O content, D also showed a direct relationship to temperature and CO_2 pressure. Powders pretreated with acid gave considerably reduced rates.

- Reflectance spectroscopy of experimental powders identified absorptions near 7 μm due to vibrations within the carbonate (CO_3^{-2}) ion. Spectra of carbonate reference powders, greater absorptions for powders exposed to more H_2O, and positive correlations with modeled logarithmic CO_2 uptakes all supported the conclusion that carbonates formed in experimental samples.

In this chapter, we will identify candidate physical or chemical processes responsible for observed behavior, and then model those processes. Specifically, we will attempt to answer:

- Are rates and amounts of CO_2 uptake at early times (<1 day, but especially $<10^{-2}$ days) consistent with physical adsorption of CO_2 in "dry" and "vapor" experiments and with dissolution of CO_2 in H_2O for "damp" and "wet" conditions?
- What processes explain the hypothesized logarithmic reaction kinetics for later times, and how are these related to earlier behavior? Can parabolic kinetics ($dP/dt \sim t^{-1/2}$), resulting from CO_2 diffusion through a rind, explain any of the observed pressure drops?

- What conclusions can be made from correlating reaction rates with experimental conditions? Is the resulting model behavior consistent with carbonate formation?

Finally, we will address the implications of models for Martian climate history.

4.2 PHYSICAL PROCESSES

4.2.1 Behavior at early times

There are a number of physical/chemical processes that may be involved in reaction to form carbonates in our experiments. (a) CO_2 may dissolve in a thin layer of aqueous H_2O that coats or partially coats the particles. (b) In regions of incomplete or no H_2O coverage, CO_2 may adsorb directly onto particle surfaces. (c) In either case, gas may diffuse into the particle interiors through cracks and pores. (d) Reactions may take place in the thin H_2O layer, leading to the deposition of carbonate. (e) In regions of a carbonate rind, reaction might conceivably occur at the interface between the rind and underlying unreacted solid, because of diffusion of CO_2 through the rind.

In section 4.3.1 we will discuss expected rates and amounts for the first three of these processes; section

4.3.2 contains a mathematical treatment of (d), while models are fitted to data in 4.4.1; and (e) is discussed in section 4.4.3. First we present a qualitative discussion of how adsorption and dissolution can be inferred from our data (below), and hypothetical processes for logarithmic growth (section 4.2.2), in order to motivate the physical models discussed later.

We expect physical adsorption of H_2O and CO_2 onto powder surfaces to occur very quickly (e.g., Gregg and Sing, 1982; Adamson, 1990), especially since we are operating at moderate gas pressures. However, because CO_2 pressure is well below its vapor pressure (see Appendix A.2), the total amount of CO_2 adsorbed should be limited to a fraction of a monolayer (Brunauer et al., 1938; Orr, 1977b). Thus, we anticipate that the most rapid adsorption should be followed by substantially decreased rates as adsorption sites are used up, and a resulting convex-upward inflection in P(t).

Dissolution of CO_2 into liquid H_2O also occurs fairly quickly, as seen in a control experiment with no sample, EX17C (Appendix A.5), and in "wet" experiments with powders, EX16,39,33-35 (Chapter 2). In the former, this took place in $\sim 10^{-2}$ days; in the latter it was spread out over ~1 day (although the longer time for experiments with powders is probably the result of pH balance involving silicate cations, perhaps as reaction is initiated). In addition, observations were consistent with calculated *amounts* of CO_2

uptake by dissolution (Chapter 2, or see Stumm and Morgan, 1981), and with a *limit* for this signal (although aqueous reactions involving silicate cations may delay its approach). A convex-upward shape also follows.

Figure 4-1 displays examples of logarithmic plots (modified from Figure 2-7) of data from experiments EX8 (cold/"vapor") and EX16 (warm/"wet"), which show the full range of experimental behavior. CO_2 uptake (see Chapter 2) is plotted as equivalent monolayers deposited on powder surfaces, while $\log_{10}t$ is extended to 10^{-4} days, so that all recorded data are shown. Notice the different vertical scales used for the two experiments.

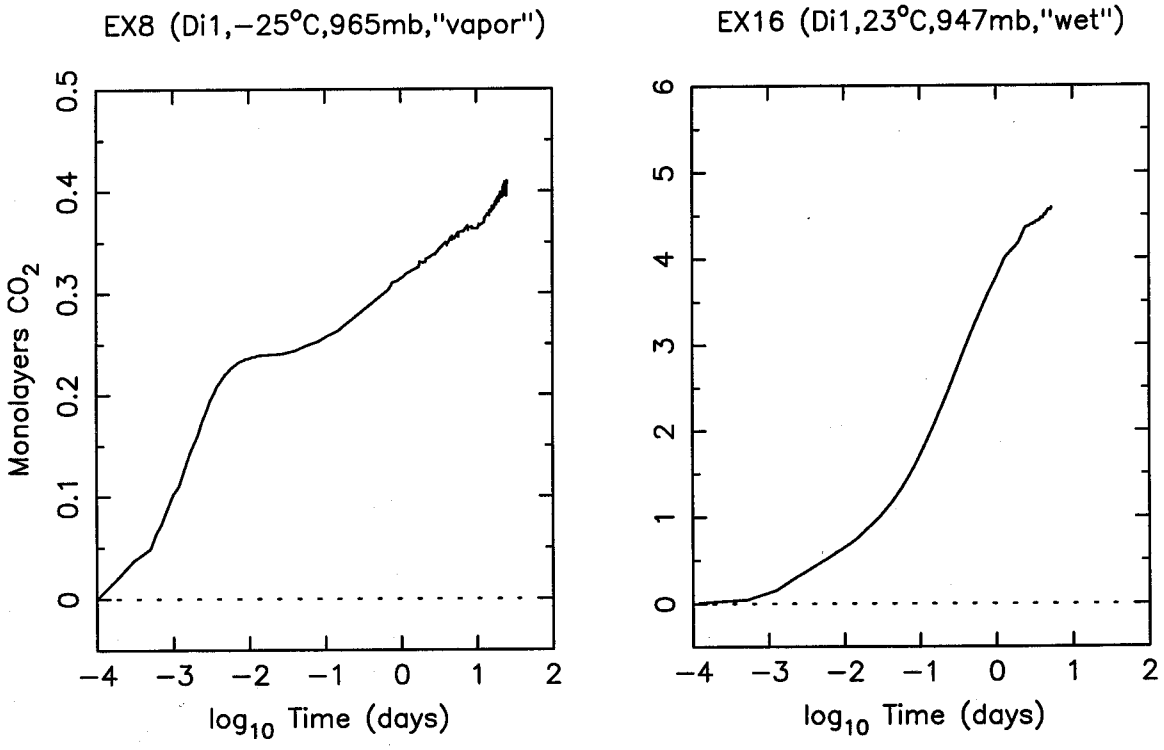

Figure 4-1 Examples of full range of experimental behavior

Aside from showing the longer-term signal attributed to reaction in Chapter 2, these examples make it clear that something else is occurring at earlier times——before ~10^{-2} days for EX8 and ~1 day for EX16. The conditions of the two experiments, along with timescales and amounts of CO_2 uptake, suggest that adsorption (in EX8) and dissolution (in EX16) contribute to the S-shaped portions of the pressure-drop curves. We elaborate further and apply these arguments to the rest of our data in sections 4.3 and 4.4.

4.2.2 Extended reaction

Processes in which reaction is the rate-limiting step (i.e., reactants are immediately available and in unlimited supply, and there is no limiting effect due to product formation) ought to result in constant rates and hence $P(t) \sim t$. Mechanisms involving diffusion (e.g., through a rind; see section 4.4.3) as the step which limits the amount of product formed, and of CO_2 used, should give $dP/dt \sim t^{-1/2}$ and $P(t) \sim t^{1/2}$. However, neither of these rates was observed.

Results of pressure-drop experiments (Chapter 2) point to a mechanism for long-term CO_2 uptake involving a logarithmic process. Thus, what model can be constructed, with the fewest ad hoc assumptions, that will give $dP/dt \sim 1/t$, and thus $P(t) \sim \log t$?

Suppose we examine the surface area that is available for reaction, and assume that it decreases with time as newly formed product on particle surfaces prevents that surface from being available for further reaction. In both aqueous and non-aqueous cases, the fraction of active surface *not* covered with reaction product would be available for providing additional cations (such as Mg^{+2} or Ca^{+2}) to react with carbonate or bicarbonate ions—at adsorption sites in the non-aqueous case, or in solution in the aqueous case.

If reaction rate is proportional to the fraction of active surface not covered with reaction product, then we have two possible situations for placement of newly formed product: (i) it remains where it forms (e.g., at surface adsorption sites); or (ii) reaction and hence product placement are not physically coincident with the source of cations (e.g., diffusion in solution occurs). In case (i), a single product layer is built up, and the dynamics of active surface loss are identical to those for adsorption. In case (ii), carbonate deposits *uniformly* onto particle surfaces (i.e., onto product *and* onto active surface), resulting in a more gradual decrease of active surface area and hence prolonged reaction. A fuller treatment of these mechanisms is presented in section 4.3.2.

4.3 MATHEMATICAL INTERPRETATION

4.3.1 Adsorption and dissolution

A simple model in which CO_2 molecules are adsorbed at decreasingly available surface sites, in a single layer and without interfering with one another, can be described by an equation in which the *rate* of depletion of surface area (for adsorption) varies directly with the *amount* of surface area (adsorption sites) left:

$$df/dt \sim -f \qquad [4\text{-}1]$$

where f is the fraction of surface area available for adsorption, and the component of total experimental pressure drop due to adsorption, $P_{ads}(t)$, is proportional to 1 - f. The resulting behavior is exponential:

$$P_{ads}(t) = P_o\ (1 - f) = P_o\ (1 - e^{-t/\tau}) \qquad [4\text{-}2]$$

Here, P_o is the total amount of CO_2 adsorbed for $t >> \tau$, and τ is a characteristic timescale for gas adsorption.

Real adsorption physics (e.g., adsorption at one site affects what happens at another, or simultaneous adsorption at two sites is necessary) probably causes actual behavior to differ slightly from this simple model (e.g., Adamson,

1990). Nevertheless, we will use this equation later to adequately fit our data.

Dissolution is driven by a chemical potential difference between CO_2 in an ideal gas and CO_2 dissolved in H_2O, and involves diffusion across the interface between these phases. Since the difference falls to zero as equilibrium approaches, we expect that dissolution will obey an equation of the form $dP/dt \sim P_{eq} - P$, where P_{eq} is the thermodynamic equilibrium pressure drop. This leads to an equation for P(t) that has the same form as that for adsorption.

In Figure 4-2, we show data from EX17C, in which 45 mb of a CO_2 atmosphere initially at 949 mb dissolved in

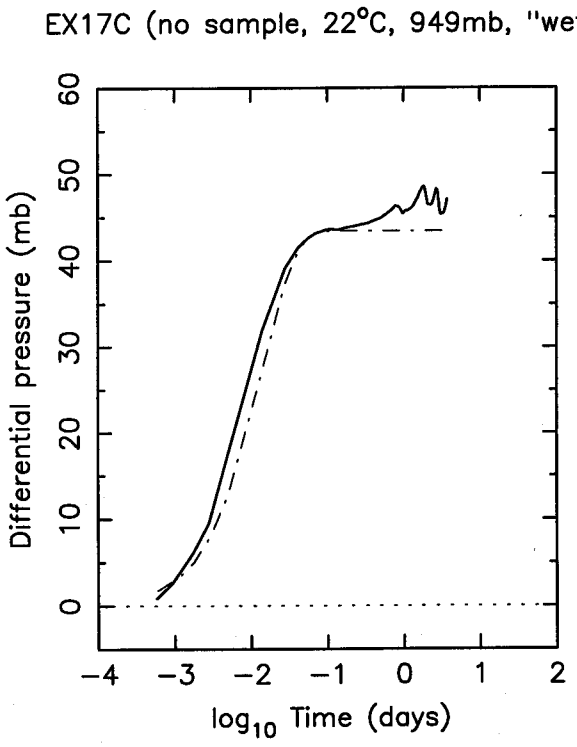

Figure 4-2 Experiment showing dissolution of CO_2 in H_2O, and model fit to dissolution signal

5 ml of H_2O. (Differential pressure has been corrected for the offset at t = 0.) The dashed-dotted line is [4-2] plotted for P_o = 43.4 mb and τ = 20 minutes. Additional fits for adsorption and dissolution are given in section 4.4.1.

It is also useful to compare timescales for adsorption (and dissolution) with estimates of the time for gas to diffuse through particle pores. We can estimate a timescale, τ_{diff}, for transport through pores using $\tau_{diff} \sim \ell^2/D$, where D is the Knudsen diffusion coefficient, calculated (Chapter 2) to be ~0.02 cm^2/s (for CO_2, pores with a radius of ~100 Å, and T ~ 250 K). The diffusion length, ℓ, should not exceed the grain size of ~1 μm. Gas diffusion should thus be very rapid, with τ_{diff} less than $\sim 10^{-11}$ days. Diffusion times approaching experimental timescales for CO_2 uptake would require diffusion lengths $\sim 10^3$ times greater than particle sizes, an unlikely situation.

4.3.2 Mechanisms for logarithmic growth

We return now to the two hypothetical cases in section 4.2.2, in which reaction product encroaches on an active silicate surface (the source of cations) exposed to a gas or a liquid (the source of carbonate ions). In case (i), carbonate that forms remains at surface adsorption sites, and in case (ii) (illustrated in Figure 4-3) reaction and deposition occur following transport in solution or along

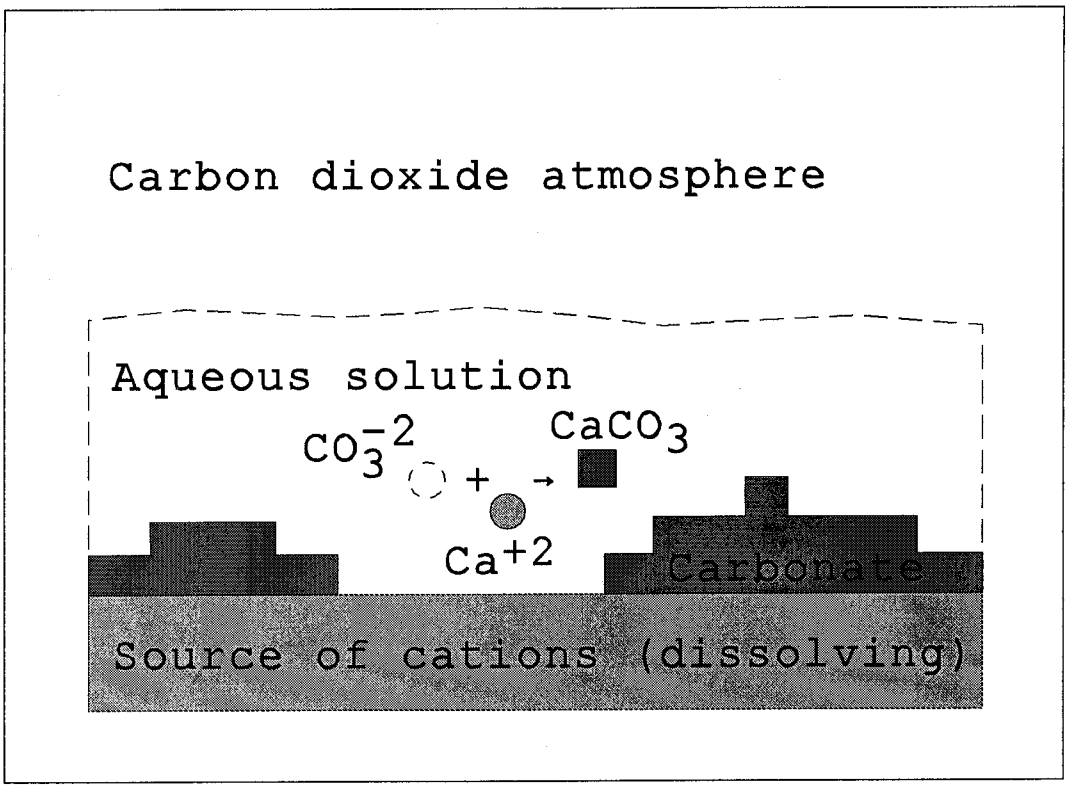

Figure 4-3 Model illustrating logarithmic growth of carbonate rind

particle surfaces (e.g., through a thin film of water). Case (i) can be dismissed as an explanation for logarithmic kinetics, because it results in the same time dependence as our simple model for adsorption (see previous section): reaction product builds up in only one layer and must exponentially approach a limiting amount.

However, in case (ii), since carbonate deposits *uniformly* onto particle surfaces, i.e., onto product *and* onto active surface, only a fraction f (portion of active surface not covered with product) of the newly formed product deposits onto the active surface. The rate of depletion of

active surface is given by df/dt. Since it is proportional to both the fraction f and to the reaction rate (which also varies with f), we have:

$$df/dt = f \times -kf = -kf^2 \qquad [4\text{-}3]$$

$$\int_1^f \frac{df}{f^2} = -k \int_0^t dt \qquad [4\text{-}4]$$

$$1/f - 1 = kt \qquad [4\text{-}5]$$

$$f = \frac{1}{1 + kt} \qquad [4\text{-}6]$$

Reaction rate, $dP/dt \sim 1/t$ for large t, which is the desired result. The amount of product is no longer measured by 1 - f, since it is free of the constraint to be one layer thick, and so $P(t) \sim \log t$, more gradual than $1 - e^{-kt}$, and without bound (assuming a continuing supply of reactants).

Models in which carbonate deposition is non-uniform will yield the same long-term behavior, provided a finite deposition rate exists for regions already possessing carbonate (i.e., provided the carbonate is not strictly limited to a monolayer). Logarithmic kinetics is a natural outcome of any situation in which the source of a crucial reactant is a dissolving surface that can be encroached upon by deposition of the product.

In general, $P(t) \sim \log(1 + t/t_o)$, where t_o is a time-scale corresponding to the transition from an early linear regime, when $\log(1 + t/t_o) \sim t/t_o$ for $t << t_o$. Physically, t_o represents the time when enough product has formed to affect the availability of surface cations, i.e., when the amount of product formed becomes comparable to 1 monolayer.

The corrosion literature contains references to logarithmic kinetics which involve similar explanations for underlying physical behavior. See, for example, Landsberg (1955), Kubaschewski and Hopkins (1962), and Evans (1982); Cabrera and Mott (1949) provide a discussion of parabolic kinetics in metal oxidation.

4.4 MODEL FITS TO DATA

4.4.1 Effect of combining mechanisms

We considered a fitting function for logarithmic reaction which includes the transition time, t_o, and is otherwise identical to the model behavior analyzed in Chapter 2:

$$P_{reac}(t) = D \log_{10}(1 + t/t_o) \qquad [4\text{-}7]$$

In addition, we incorporated a simple fit to the rapid adsorption of less than a monolayer of CO_2 molecules:

$$P_{ads}(t) = P_o\ (1 - e^{-t/\tau}) \qquad [4\text{-}8]$$

$P_{ads}(t)$ also can be considered to represent the signal due to dissolution (see section 4.3.1). $P_{reac}(t)$ and $P_{ads}(t)$ are components of the total pressure drop, P(t), due to reaction and adsorption (or dissolution) of CO_2.

Strictly speaking, it is not legitimate to add the two mechanisms, since either adsorption or dissolution must occur before reaction. For example, some adsorption sites may become reaction sites; they are not necessarily independent populations. However, assuming any adsorbed or dissolved CO_2 used up by reaction is replaced by gas from experimental atmosphere, we combined the two expressions to give:

$$P(t) = P_o\ (1 - e^{-t/\tau}) + D\ \log_{10}(1 + t/t_o) \qquad [4\text{-}9]$$

Two timescales result, representing different physical processes. New fits to data were performed using this equation, resulting in values of τ and t_o which minimize residuals from a least-squares fit to $P/(1-e^{-t/\tau})$ versus $\log_{10}(1+t/t_o)/(1-e^{-t/\tau})$, for data evenly spaced in log t. Although this fitting technique is potentially unstable for small values of t ($<< \tau$), and requires that data fit smoothly with the requirement that P(0) = 0, it was found to give numbers and curves which were best fits to data upon visual inspection.

Figure 4-4 (pages 172-183, modified from logarithmic plots in Chapter 2) presents results of pressure-drop experiments, now including manually recorded data for very early times, and with plots individually scaled to display their full range of behavior. Model fits are shown with thin dashed lines; adsorption (or dissolution) and reaction components are plotted with dashed-dotted lines. We can now more clearly discern details of rapid gas adsorption and dissolution, and the transition to logarithmic reaction kinetics for $t >> t_o$.

Results are tabulated in Table 4-1 (page 184), and are comparable to earlier results (fits to $P(t) = C + D \log_{10} t$) in Table 2-3. There are some experiments for which data do not permit a best fit for $\log_{10} t_o \leq 1$; results are shown for $\log_{10} t_o = 1$. Standard errors from least-squares fits are not shown but are very small, as in Table 2-3. Negative P_o obtained for two sets of data is not physically realistic (see below).

These new fits to experimental data demonstrate a range of modeled adsorption, dissolution, and reaction behaviors:

- Adsorption occurs rapidly, with e-folding times of seconds to minutes (typically 10^{-4} to 10^{-2} days). Table 4-1 includes results for "wet" and "damp" experiments; in most of these cases, the large numbers for τ are

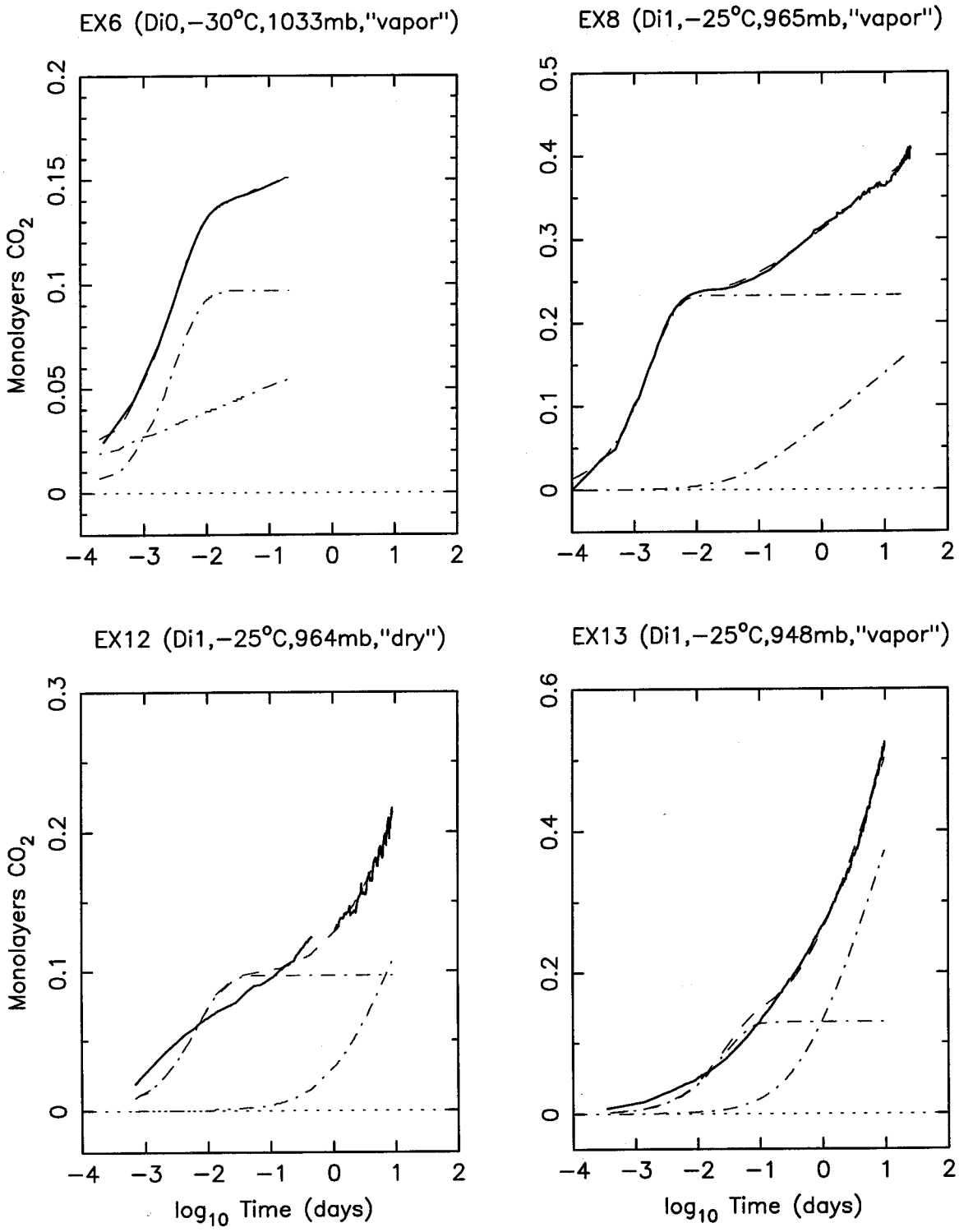

Figure 4-4 Model fits to data, with early times
(a) **GROUP 1** [Di0,Di1]

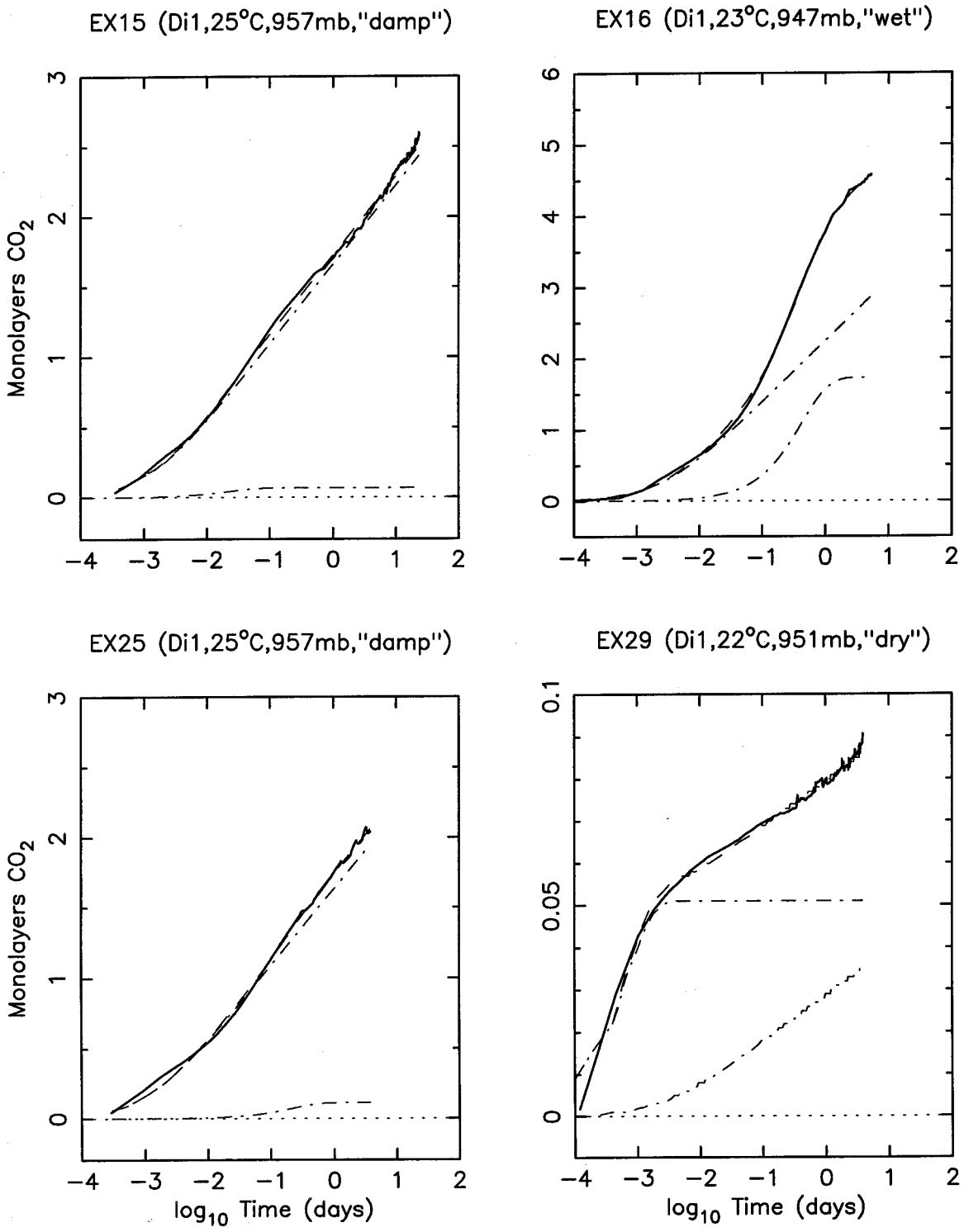

Figure 4-4 Model fits to data, with early times (continued)
(a) **GROUP 1** [Di0,Di1]

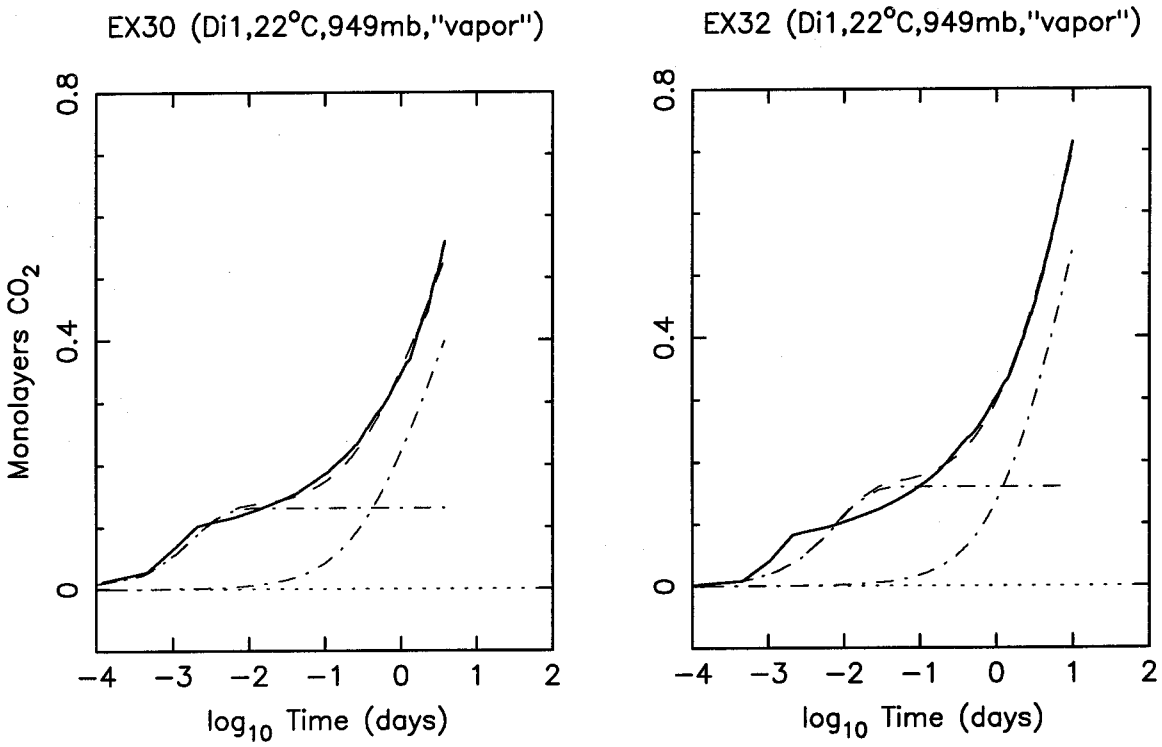

Figure 4-4 Model fits to data, with early times (continued)
(a) **GROUP 1** [Di0,Di1]

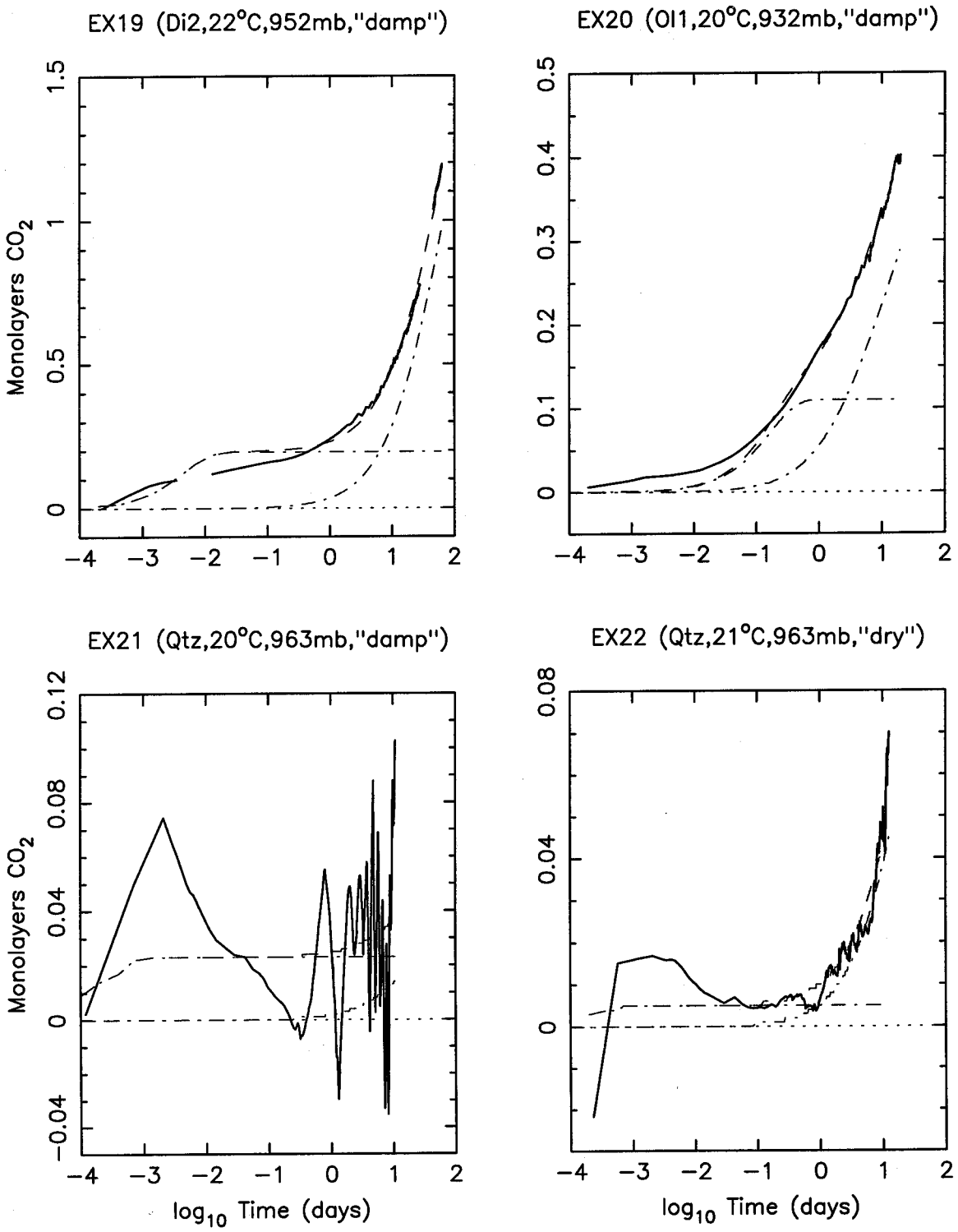

Figure 4-4 Model fits to data, with early times
(b) **GROUP 2** [Di2,Ol1,Qtz,Plag,Ol2,Calc]

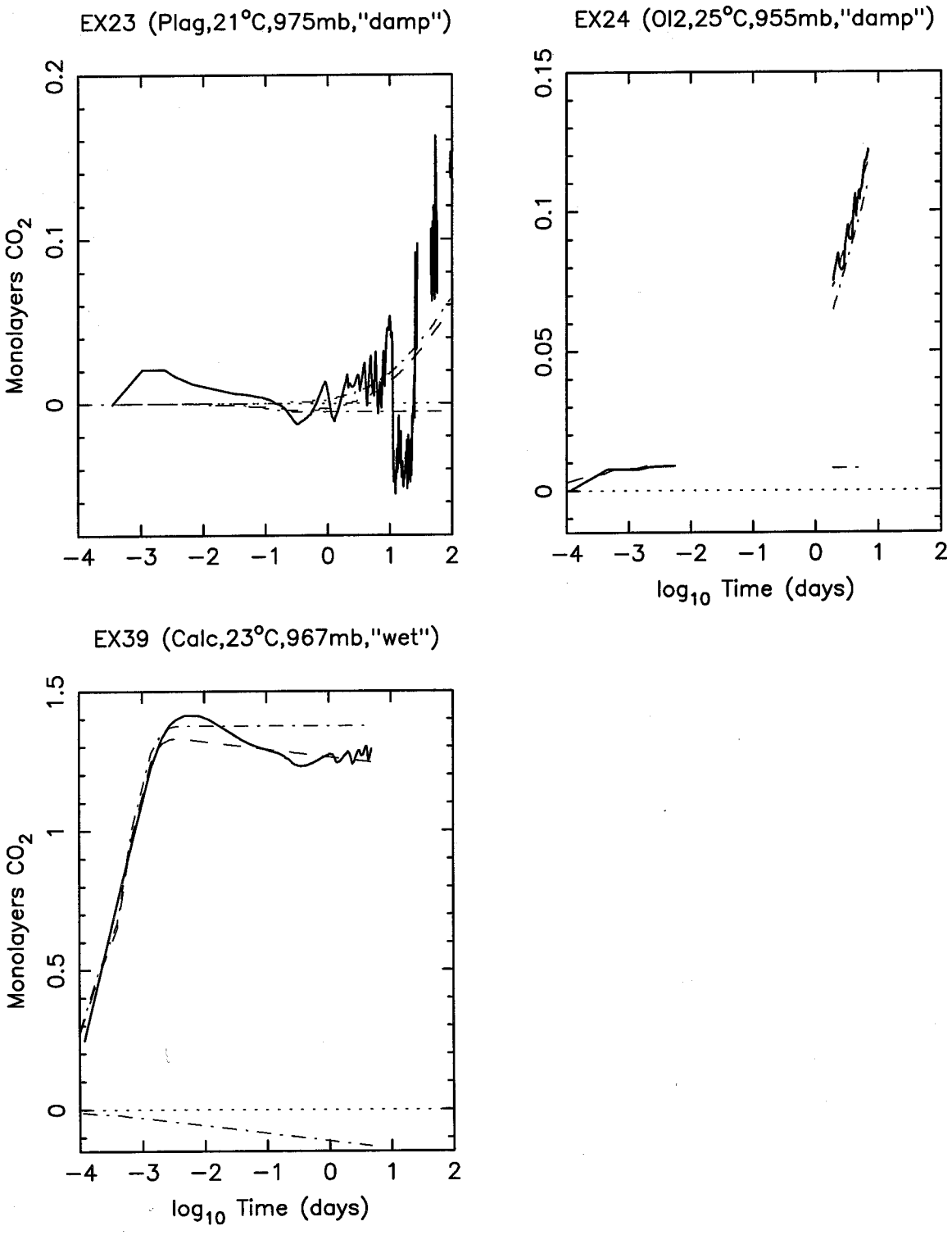

Figure 4-4 Model fits to data, with early times (continued)
(b) **GROUP 2** [Di2,Ol1,Qtz,Plag,Ol2,Calc]

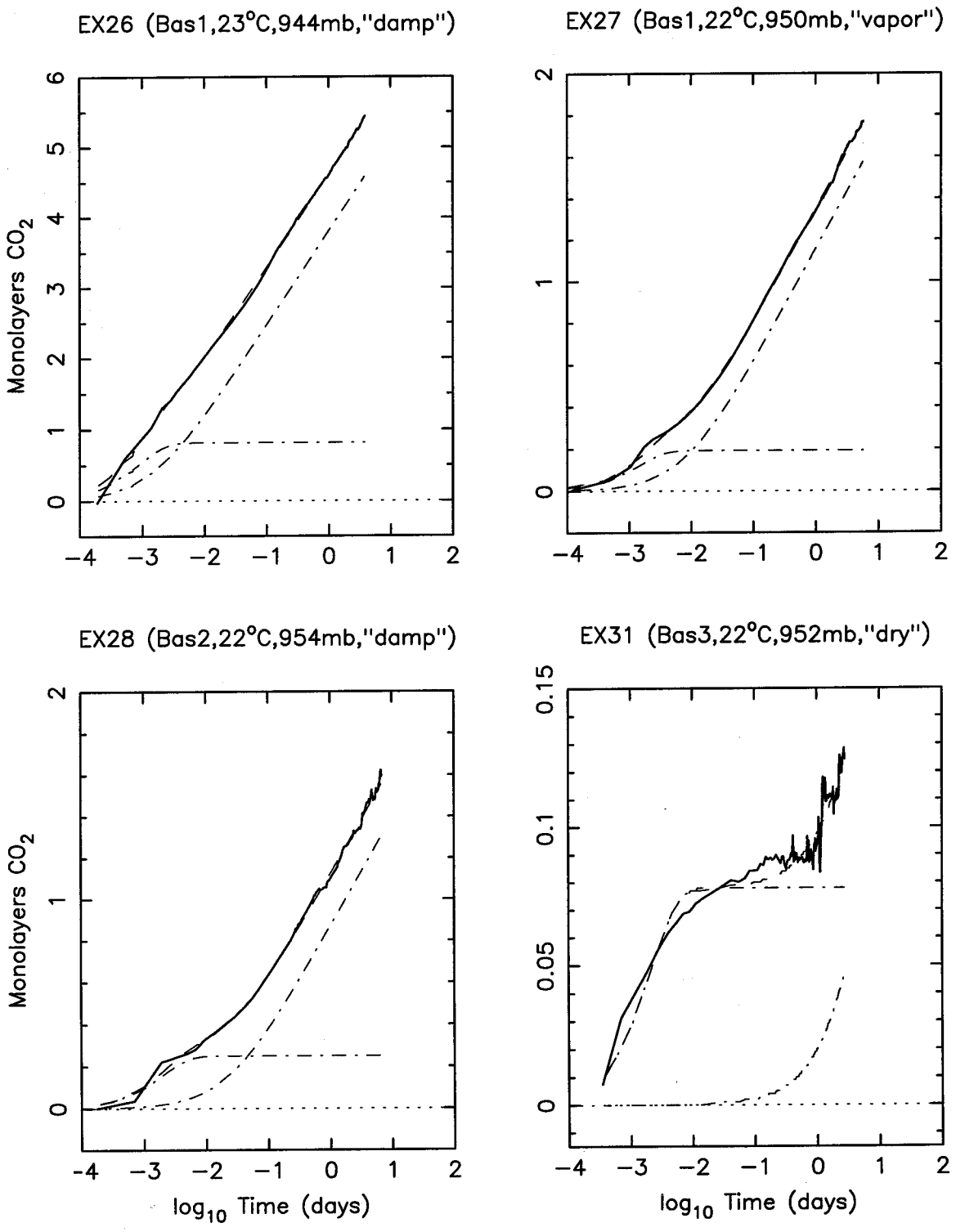

Figure 4-4 Model fits to data, with early times (c) **GROUP 3** [Bas/warm]

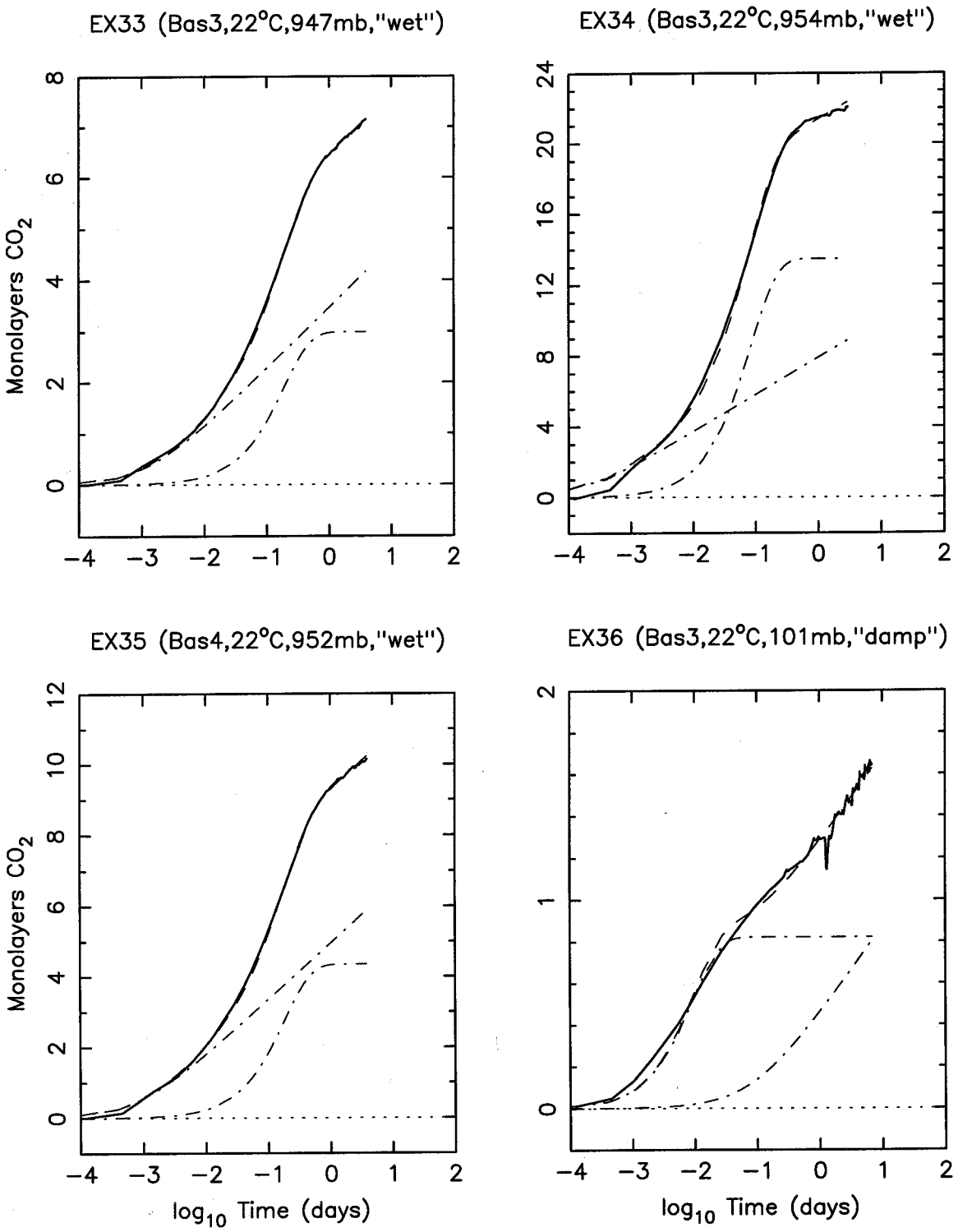

Figure 4-4 Model fits to data, with early times (continued)
(c) **GROUP 3** [Bas/warm]

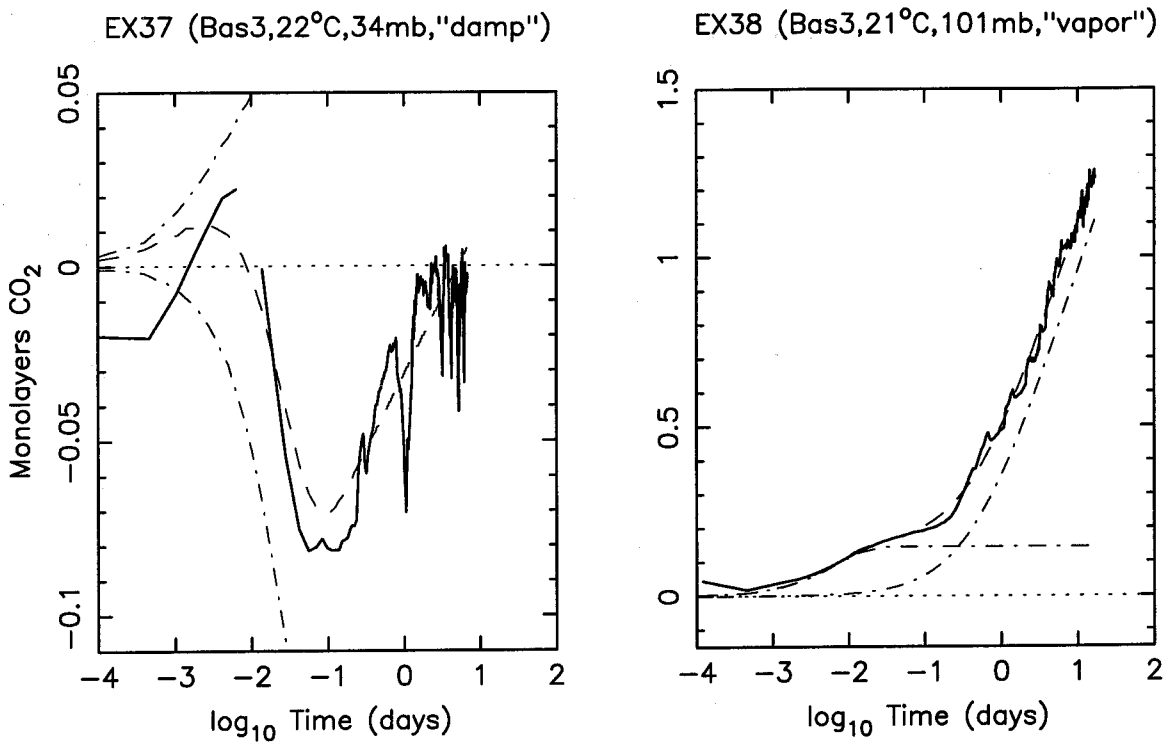

Figure 4-4 Model fits to data, with early times (continued)
(c) **GROUP 3** [Bas/warm]

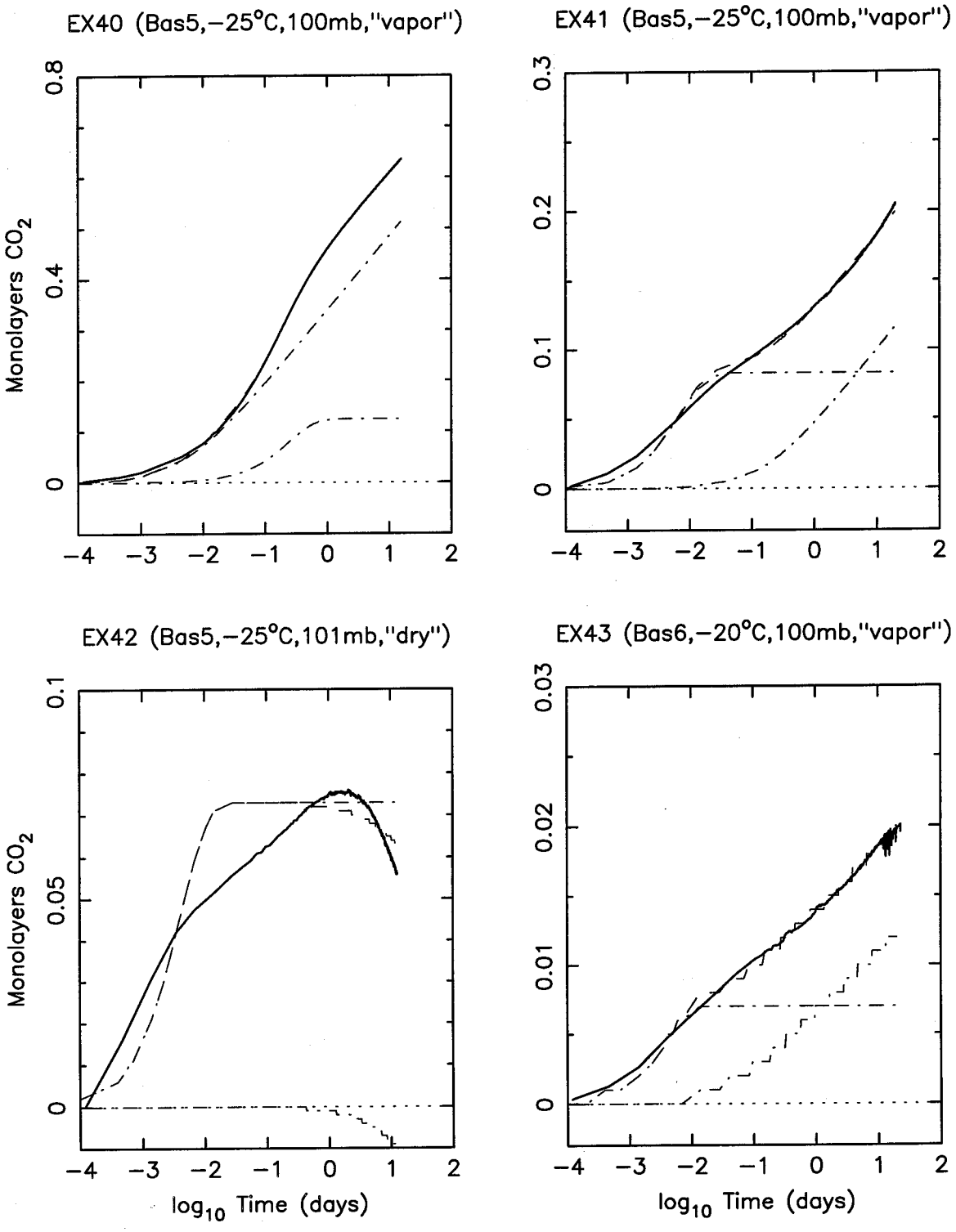

Figure 4-4 Model fits to data, with early times
(d) **GROUP 4** [Bas/cold]

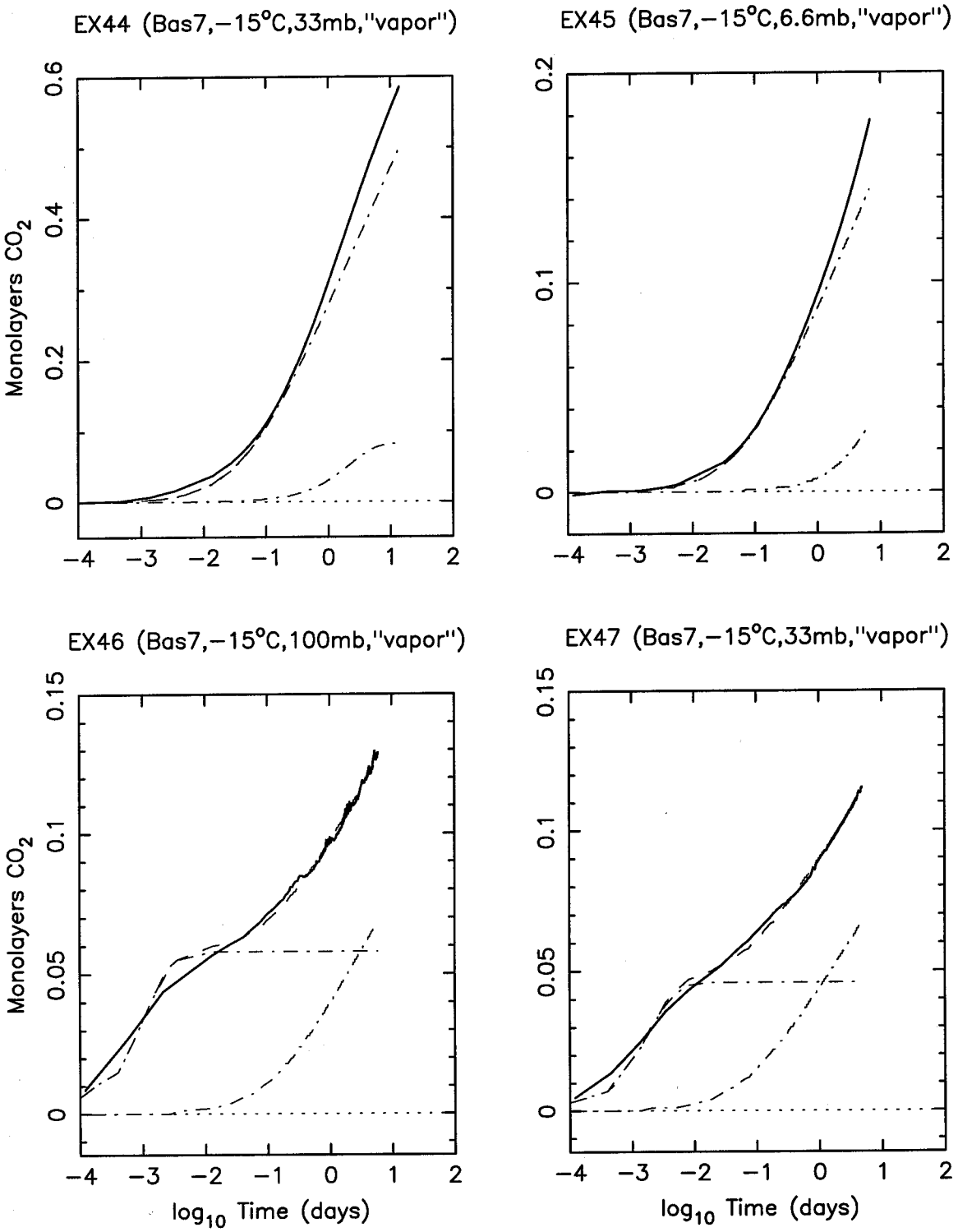

Figure 4-4 Model fits to data, with early times (continued) (d) **GROUP 4** [Bas/cold]

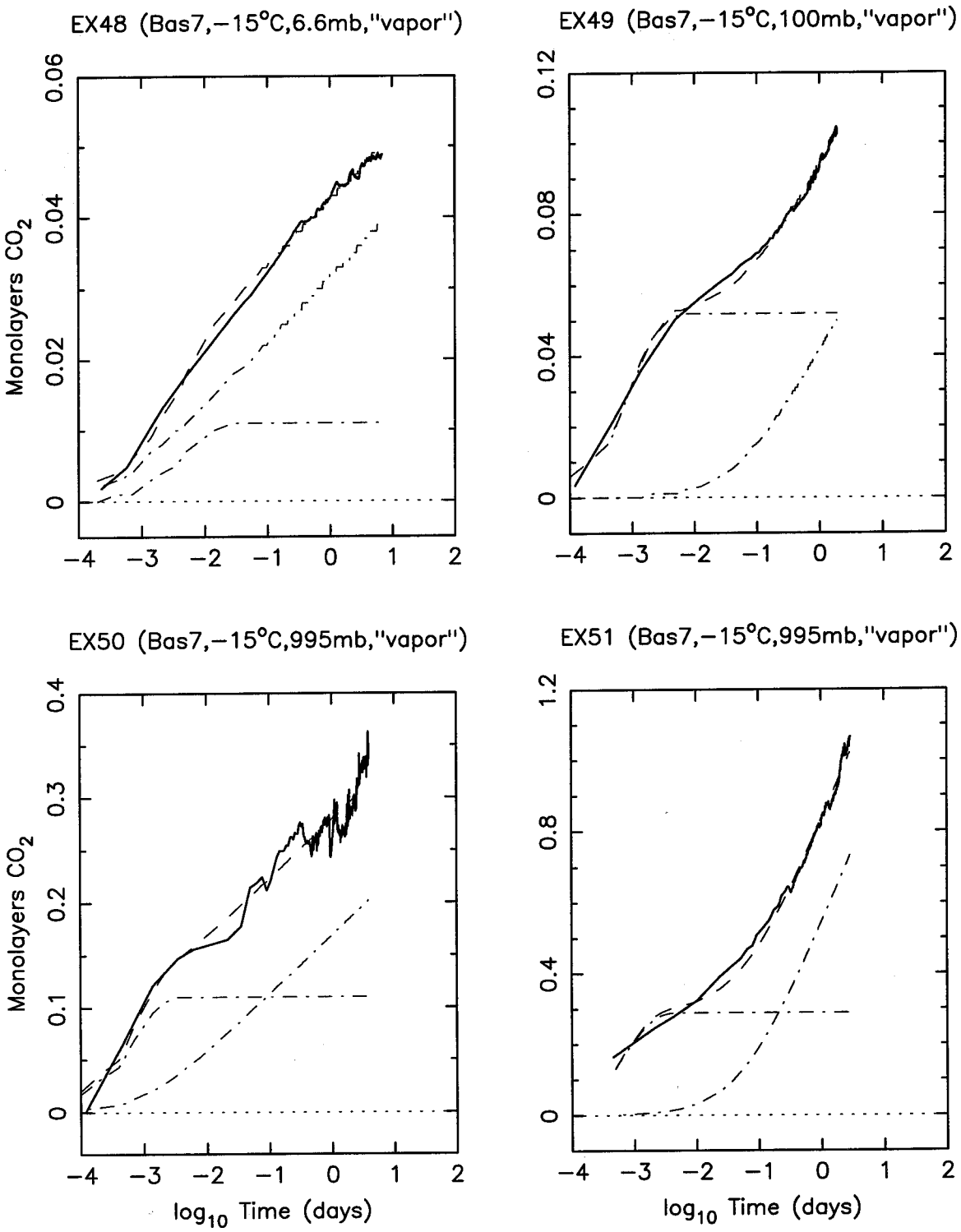

Figure 4-4 Model fits to data, with early times (continued) (d) **GROUP 4** [Bas/cold]

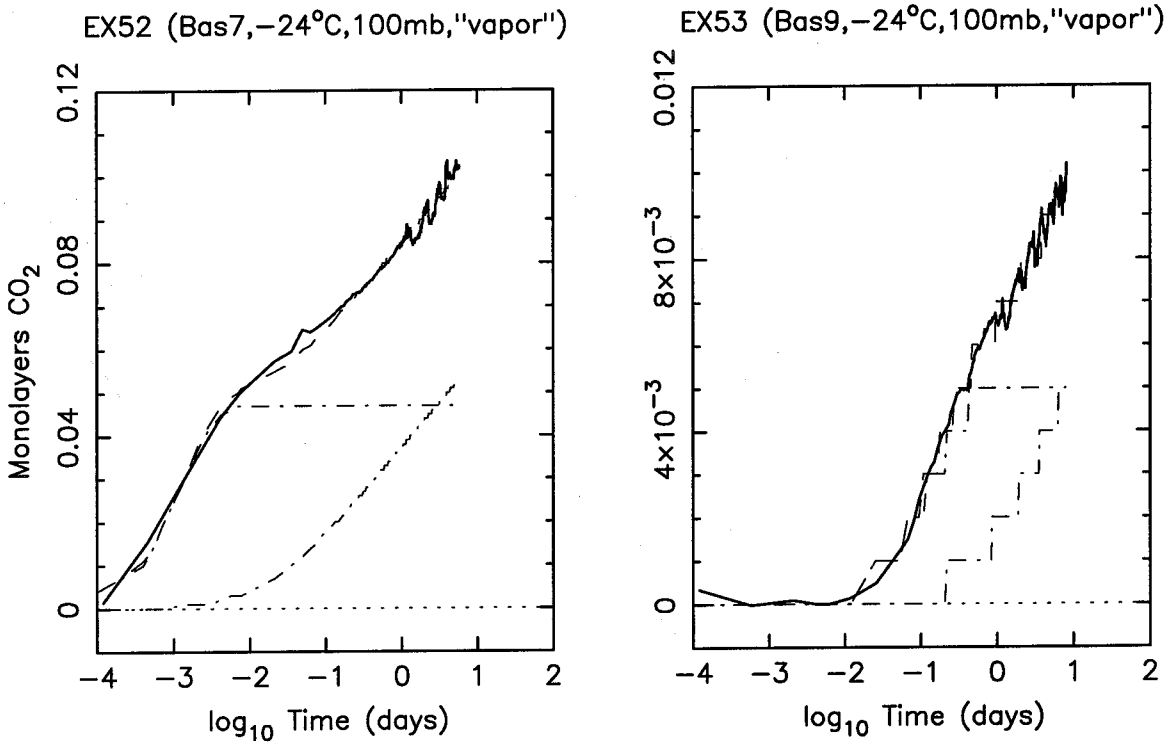

Figure 4-4 Model fits to data, with early times (continued)
(d) **GROUP 4** [Bas/cold]

Table 4-1 Refined model results

	$P=P_o(1-e^{-t/\tau})+D\log_{10}(1+t/t_o)$			
EX #	P_o **[monolayers]**	$\log_{10}\tau$ **[days]**	**D [monolayers/**$\log_{10}$**t]**	$\log_{10}t_o$ **[days]**
GROUP 1 [Di0,Di1]				
6	0.10	-2.5	0.01	-5.2
8	0.23	-2.7	0.06	-1.2
12	0.10	-2.2	0.12	0.1
13	0.13	-1.6	0.29	-0.3
15	0.07	-1.7	0.57	-2.9
16	1.73	-0.4	0.86	-2.6
25	0.11	-0.7	0.55	-3.0
29	0.05	-3.2	0.01	-2.6
30	0.13	-2.7	0.37	-0.5
32	0.16	-2.1	0.62	0.2
GROUP 2 [Di2,Ol1,Qtz,Plag,Ol2,Calc]				
19	0.20	-2.3	1.51	1.3
20	0.11	-0.8	0.26	0.2
21	0.02	-3.6	0.04	>1.0
22	0.01	-3.6	0.13	>1.0
23	-0.01	-0.8	0.06	>1.0
24	0.01	-3.6	0.09	-0.3
39	1.38	-3.3	-0.03	-4.1
GROUP 3 [Bas/warm]				
26	0.82	-3.1	1.34	-2.8
27	0.19	-2.8	0.56	-2.1
28	0.25	-2.7	0.53	-1.6
31	0.08	-2.7	0.22	0.6
33	2.99	-0.7	1.19	-2.9
34	13.48	-1.1	2.11	-3.8
35	4.35	-0.7	1.60	-3.1
36	0.82	-2.0	0.43	-1.1
37	-0.17	-1.6	0.04	-3.1
38	0.15	-2.2	0.71	-0.3
GROUP 4 [Bas/cold]				
40	0.12	-0.6	0.15	-2.3
41	0.08	-2.2	0.06	-0.8
42	0.07	-2.4	-0.03	>1.0
43	0.01	-2.4	0.00	-1.4
44	0.08	0.3	0.20	-1.4
45	0.06	0.9	0.07	-1.2
46	0.06	-2.9	0.04	-1.0
47	0.05	-2.7	0.04	-1.2
48	0.01	-2.3	0.01	-3.5
49	0.05	-3.0	0.03	-1.3
50	0.11	-3.2	0.06	-3.0
51	0.29	-3.1	0.43	-1.3
52	0.05	-2.9	0.02	-1.8
53	0.01	-0.8	0.01	-0.1

best interpreted as timescales for dissolution of CO_2 gas in bulk liquid H_2O (see section 4.2.1).

- An apparent adsorption or dissolution signal——i.e., with a convex-upward inflection, such as an initial ramp or an S-shaped curve——occurs for all but a few experiments (exceptions include EX13,26,44-45,51). For those experiments in which rapid early pressure drops attributable to adsorption were not identified (see Chapter 2)——i.e., EX21-23,37——there is a rise in pressure at very early times seen in Figure 4-4 that may be related to small amounts of adsorbed CO_2. However, interpretation is complicated by the relatively large fluctuations in lab temperature which influence data from these experiments; in addition, results of EX37 are questionable because of the low $P(CO_2)$ introduced over comparable vapor pressure of liquid H_2O (see Chapter 2). Modeled $P_o < 0$ occurs for two of these experiments.
- Two other experiments——EX39,42——show negative longer-term pressure drops ($D < 0$). Results from EX42 were attributed (Chapter 2) to possible desorption of existing H_2O in a nominally "dry" experiment, and EX39 was a unique experiment involving dissolution of pure $CaCO_3$ (Calc) in H_2O (the long-term signal may in fact be positive).

- For those experiments which lack an obvious adsorption signal, model fits nevertheless include an adsorption component. Some give fits that agree reasonably well with data (EX26,44-45), and some do not (EX13,51). The lack of a good fit in the latter---which also occurs for a number of experiments which have easily discernible adsorption signals (e.g., EX30,32)---is probably due to a combination of: (1) overly simplistic modeling of adsorption/dissolution (see section 4.2.1), and (2) a non-logarithmic contribution to the rate of CO_2 uptake (e.g., a parabolic rate). However, the competitive effects of H_2O and CO_2 adsorption, as well as a good fit to logarithmic reaction kinetics in some experiments when adsorption is included, make interpretation difficult.

  If adsorption of CO_2 is adequately modeled by equation [4-9], then results for "dry" and "vapor" experiments suggest that anywhere from ~0.01 to ~0.3 monolayers of CO_2 was adsorbed. Adsorption of <<1 monolayer is consistent with the fact that we were operating with $P(CO_2)$ nowhere near the vapor pressure of CO_2 at experimental temperatures (section 4.2.1). It is only for "damp" and "wet" experiments that P_o exceeds ~0.3 monolayers of CO_2, and in these experiments we are more likely dealing with dissolved CO_2. Therefore, it is not surprising that it is these experiments for which

modeled reaction rates differ most noticeably from those in Chapter 2.

- There is typically a non-zero time, t_o, at which reaction becomes noticeably logarithmic. Since CO_2 uptake continues for times greater than characteristic timescales for adsorption and dissolution, reaction rates inferred for t > 1 day, as calculated in Chapter 2, do not change considerably.

Additional discussion of extended reaction, and correlation of model parameters with environmental conditions, can be found below.

4.4.2 Relation to experimental variables

Modeled parameters for fits to data from pressure-drop experiments with Basalt (**GROUPS 3** and **4**) exposed to various conditions of H_2O content, temperature, and CO_2 pressure are shown in Figure 4-5, (modified from Figure 2-8), incorporating new rates and displaying results for a wide range of H_2O contents in a log-log plot. Part (a) contains points for τ and P_o, the timescale and amount of adsorption (or dissolution) signal, while part (b) plots t_o and D, the timescale and rate for carbonate reaction. It is clear that all three environmental conditions play a role in determining the

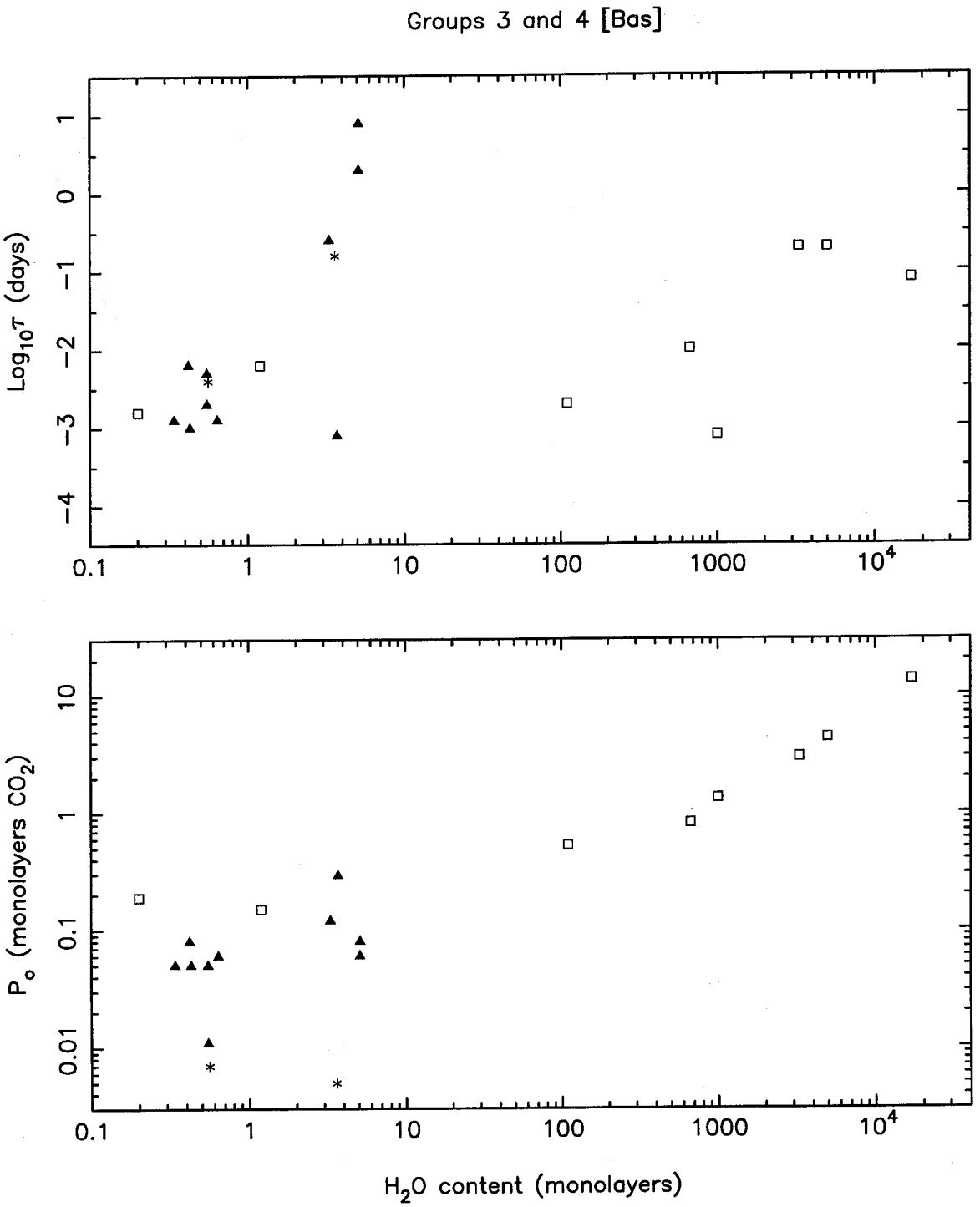

Figure 4-5 Relations between model parameters and experimental variables
(a) Adsorption and dissolution

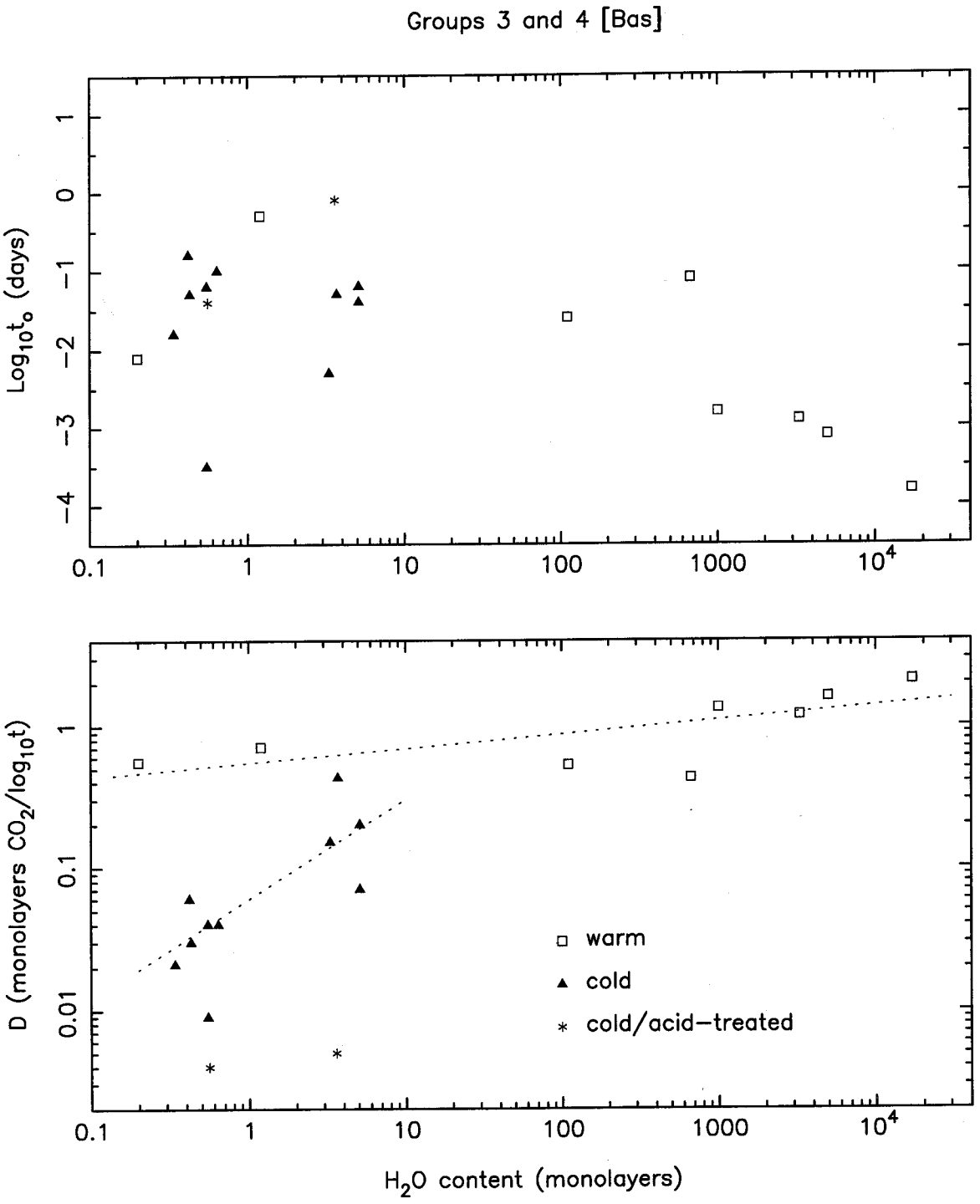

Figure 4-5 Relations between model parameters and experimental variables
(b) Logarithmic reaction

carbonate reaction rate, especially for cold, "vapor" conditions. We focus our discussion on D, the reaction rate.

For warm temperatures (22°C, or 295 K), there is a small effect due to H_2O content, so that experiments with more water tend to give higher rates of CO_2 uptake than those with less. A linear least-squares fit to log-log data for warm Basalt experiments (N = 8; EX31, a dry experiment, is not included, nor is EX37, which is problematic) gives:

$$D \text{ (monolayers } CO_2/\log_{10} t) = 0.55\ H^{0.1} \qquad [4\text{-}10]$$

(see Figure 4-5, part (b)) where H is H_2O content in monolayers, the pre-exponential has a standard error (σ_a) of ~15%, and the exponent has a standard error (σ_b) of ~20%.

The effect of H_2O content is stronger at colder temperatures (-25 to -10°C, or 248 to 263 K). If results for cold Basalt experiments (not including EX43 and EX53, which involved acid-treated powder; EX42, a dry experiment; and EX50, which gave an unusual pressure-drop curve) are fitted as above, we get:

$$D = 0.05\ H^{0.8} \quad [N = 10,\ \sigma_a \text{ and } \sigma_b \sim 10\%] \qquad [4\text{-}11]$$

However, observing that the two triangles plotted in the lower right of cold Basalt data are for 6.6 mb (EX45,48), and that the uppermost triangle is for 995 mb (EX51), it is

possible to be more specific. Thus, for experiments at moderate CO_2 pressure (33-101 mb):

$$D = 0.06\ H^{0.7} \quad [N = 7,\ \sigma_a \text{ and } \sigma_b \sim 10\%] \qquad [4\text{-}12]$$

For a similar range of H_2O content (0.2-5 monolayers), warm experiments give pre-exponentials sufficiently greater than in cold experiments to counter the effect of having smaller exponents. The fits described by equations [4-10] and [4-12] are plotted in Figure 4-5, part (b).

These observations also reinforce the conclusion, first made in Chapter 2, that CO_2 pressure directly influences carbonate formation. Although most cold Basalt experiments were conducted with ~100 mb of CO_2, the few experiments performed with CO_2 pressure an order of magnitude higher or lower give noticeably different results, corresponding to changes in (the pre-exponential of) D of as much as half an order of magnitude.

Acid-treatment of Basalt powders leads to cold results which are about 1-1/2 orders of magnitude lower than for other cold experiments.

Although not plotted here, data from experiments in **GROUP 1**, with monominerallic diopside, Di1, give similar results for the effects of temperature, pressure, and H_2O content. For eight experiments (EX12 and EX29 are not included since they were "dry"), least-squares fits gave:

$$D = 0.5\ H^{0.04} \quad [\text{warm, } N = 5,\ \sigma_a \sim 15\%,\ \sigma_b \sim 70\%] \quad [4\text{-}13]$$

$$D = 0.2\ H^{0.5} \quad [\text{cold, } N = 3,\ \sigma_a \sim 20\%,\ \sigma_b \sim 10\%] \quad [4\text{-}14]$$

Relationships are qualitatively the same as those for Basalt, and would plot in similar locations. The cold diopside results——all for 1 bar CO_2 pressure——are consistent with the one cold Basalt result for 1 bar.

The following conclusion is also consistent with experimental observations: Water need not be consumed in carbonate-forming reactions (unless we have produced hydrous carbonates in our experiments). The only water that need be present is that which, as a polar liquid, provides the chemical pathways for breaking bonds, and which serves as a route for the diffusion of resulting ions——i.e., liquid solution, or a thin film of adsorbed water. However, we really do not know the explanation for the H_2O dependences that we observed.

From Table 4-1, we see that D ~ 0.01-0.2 for "dry" experiments (EX12,29,22,31, not including EX42), possibly due to incomplete removal of H_2O by heat-treatment before experiments. Thus, no lower limit can be put on H_2O required for reaction.

Finally, it cannot be concluded from these experiments that crushed basalt glass is more reactive than monomineralic crystals of diopside.

4.4.3 Possible effect of a rind

In previous work (Stephens and Stevenson, 1990, 1992), we examined the limiting effect of diffusion through a product rind on the rate of carbonate formation in Mars-like environments. In the tarnishing reaction, from the metal corrosion literature (e.g., Booth, 1948; Crank, 1975), the thickness, ℓ, of product formed on a solid by reaction with a gas is given instantaneously by $\ell^2 \sim (Dt)^{1/2}$, assuming a constant diffusivity, D. However, the case of Mars was modeled by an atmosphere with limited CO_2, and by interdependences among temperature, diffusivity, rind thickness, and pressure: $T = T(P)$, $D = D_o e^{-\Delta E/RT}$, and $\ell \sim P_o - P$ (D_o and ΔE are diffusivity pre-exponential and activation energy, and P_o is initial atmospheric CO_2 pressure).

This resulted in an equation for diffusion-limited reaction rate that can be iterated forward in time:

$$dP/dt \sim -D[T(P)] \times P / [T(P) \times \ell(P)] \qquad [4\text{-}15]$$

For a global regolith 1 km deep composed of particles with radius 20 μm, using a greenhouse T(P) relation similar to that used by Pollack et al. (1987), and with the constraints of $P_o \sim 2$ bars and today's pressure ~ 7 mb, we calculated the history of CO_2 pressure on Mars for D_o and ΔE consistent with present-day constraints on diffusivity (from Bhatia and

Perlmutter, 1983; see Stephens and Stevenson, 1990). The resulting pressure decayed very rapidly in the first few 100 m.y., as a result of higher temperatures and therefore higher diffusivities. More recently than ~2 b.y. ago, the pressure declined gradually—roughly exponentially with a timescale of ~1-2 b.y.

In light of present experimental results, in which a diffusive signal ($P(t) \sim t^{1/2}$) is not obviously present, it is necessary to qualify these earlier conclusions. A diffusion-limited regime presumably only arises when carbonate buildup exceeds a few monolayers on particle surfaces. From the amount of modeled reaction at the end ($t = \Delta t_{eff}$) of our experiments (see Figure 4-4), we see that the total CO_2 uptake, assumed identical to thickness of carbonate formed, is ~0.005-1.5 monolayers in "dry" and "vapor" experiments, and ~0.01-10 monolayers in "damp" and "wet" experiments. So, diffusion may play a role, and we cannot rule it out as a contributor to CO_2 uptake in our experiments.

A parabolic contribution to reaction rate will be important on long timescales if the coefficient in front of $t^{1/2}$ is small but finite. An inspection of our fits in the previous section (see Figure 4-4) reveals residuals of as much as ~0.05 monolayers of CO_2 at ~10 days. This occurs for "vapor" experiments such as EX30 and EX51 that gave power-law fits with $dP/dt \sim t^{-0.5}$ in Chapter 2, as well as wetter experiments such as EX15. It gives us an estimate of

the largest parabolic signal that is consistent with our data, namely $P(t) = (0.05/10^{1/2})t^{1/2} = 0.016\ t^{1/2}$ (t in days). This could easily become important for timescales of more than $\sim 10^2$ years.

Furthermore, the logarithmic reaction kinetics used for carbonate growth are sufficient to limit the amount of carbonate formed over geologic time on Mars. Not only is the process very slow, but it must be physically limited for $t \rightarrow \infty$ (e.g., CO_2 supply runs out), just as it had to be for $t \rightarrow 0$ (with a transition from linear kinetics at $t = t_o$).

4.5 MARS CLIMATE HISTORY

If logarithmic reaction kinetics applies over long timescales, then we can place a finite limit on the total carbonate formed on Mars over geologic time. For "damp" or "wet" conditions, we have (equation [4-7]):

$$P_{reac}(t) = D \log_{10}(1 + t/t_o) \qquad [4\text{-}16]$$

where D ~ 1 monolayer $CO_2/\log_{10}t$ and $t_o \sim 10^{-3}$ days. After ~3-4 b.y. on Mars (10^{12} days), we would have reacted $P(CO_2)$ equivalent to ~15 monolayers per particle. Thus, for each unit of surface area on Mars, the mass of the column of CO_2 atmosphere stored as carbonate, $M_A(CO_2)$, would be given by:

$$M_A(CO_2) = P(CO_2)/g$$
$$= (15 \times A_s \times \rho \times d) \; / \; (A \times N_A \; / \; M) \qquad [4\text{-}17]$$

where $g = 374$ cm/s^2 is the gravitational acceleration at the surface of Mars, $\rho = 2.9$ g/cm^3 is the density of basalt, $A = 20$ Å^2/molecule is the area occupied by a CO_2 molecule (McClellan and Harnsberger, 1967), $N_A = 6 \times 10^{23}$ molecules/mole is Avogadro's number, and $M = 44$ g/mole is the molecular weight of CO_2.

For a global layer of basalt powder, with specific surface area $A_s = 1$ m^2/g (consistent with Viking Lander observations, e.g., Arvidson et al., 1989) and thickness $d = 100$ m, and under conditions of plentiful water, the equivalent CO_2 uptake is therefore:

$$P(CO_2) \sim 60 \text{ mb} \qquad [4\text{-}18]$$

This is roughly an order of magnitude greater than the ~1-10 mb obtained for regolith CO_2 *adsorption* by Fanale and Salvail (1994) using similar parameters.

There are several possible explanations for why the reaction rate observed in the experiments appears to be insufficient for reducing the pressure of the Martian atmosphere by ~1 bar:

(a) We may have underestimated the storage capacity of the regolith. Particles an order of magnitude smaller than those assumed above (i.e., specific surface area larger), a regolith an order of magnitude thicker, or some combination of these two factors, would suffice to increase the total uptake of CO_2 to about the desired value. We have utilized conservative estimates, and do not really know the size distribution or extent of the Martian regolith.

(b) Non-uniform or intermittent wet conditions, as in low-temperature hydrothermal environments (e.g., Romanek et al., 1994), may have led to scattered but large regions of carbonate production.

(c) The undetected but probably finite diffusion-limited reaction through a product rind might dominate at times much longer than experimental timescales. For example, the upper bound of 0.05 monolayer in 10 days (section 4.4.3), if extrapolated according to $t^{1/2}$, as is appropriate for diffusion, will yield a CO_2 uptake of ~1 bar in $<10^6$ years.

(d) Rates of carbonate formation measured in our "vapor" experiments, when applied to models of atmospheric evolution on Mars, may thus be insignificant when compared to other mechanisms (or a combination of mechanisms) of CO_2 loss, such as atmospheric escape or sputtering (Luhmann et al., 1992; Jakosky et al., 1994), impact

erosion (Melosh and Vickery, 1989), or regolith adsorption (Fanale et al., 1982; Fanale and Salvail, 1994).

(e) Mars never had a dense CO_2 atmosphere (Kasting, 1991).

Chapter 5

CONCLUSIONS

5.1 CARBONATE FORMATION ON MARS

The experiments reported in this thesis were motivated by a desire to explain the small present CO_2 pressure in the Martian atmosphere, given the common (although not universally accepted) view that Mars once possessed a much denser CO_2 atmosphere. We adopted the premise that carbonate production on the surfaces of regolith particles, mediated by small amounts of H_2O, might explain the decline in the surface pressure over geologic timescales.

Our experiments suggested that this process does occur, but that it may be insufficient to explain the required amount of carbonate production. The principal difficulty lies in the lack of evidence for the reaction proceeding easily beyond one monolayer of product. Although some experiments displayed evidence for the growth of more than a monolayer, they also showed that this arises in a regime of *logarithmic reaction kinetics*, where CO_2 uptake is limited by a decline in the surface area available for reaction.

Diffusion-limited kinetics was not ruled out for timescales much longer than experimental durations, and models with thicker carbonate growths show that this could account for the storage of the early Martian atmosphere.

Other mechanisms for the loss of CO_2 may also contribute in the transition to the present surface pressure. Or, Mars may simply never have had a dense CO_2 atmosphere, although this requires explanations other than a CO_2 greenhouse for the morphological features used to support the hypothesis of a warm, wet early Mars.

If substantial quantities of carbonate minerals do represent the sink for atmospheric CO_2, the question of their location on the surface still remains since they have not been confirmed spectroscopically. One possible explanation for the lack of identification of carbonates on Mars is that they form in subsurface, hydrothermal environments.

Below we present a concise outline of our principal empirical and theoretical findings, and provide some directions for future research.

5.2 SUMMARY OF RESULTS

Outcomes of pressure-drop experiments on powders and subsequent laboratory analysis are summarized below:

Design and experimental conditions:

- We exposed powders (~1-20 m^2/g) of basalt glass, diopside, olivine, plagioclase, and quartz to conditions simulating the past and present surface of Mars:

  CO_2 pressure: 7 mb to 1 bar

  temperature: -30^oC to $+25^oC$

  H_2O content: "dry" (no added H_2O)

  "vapor" (~1-5 equivalent monolayers)

  "damp" (1 ml H_2O per 5 g powder)

  "wet" (5 ml H_2O per 5 g powder)

  (1 ml H_2O ~ 100-1000 monolayers)

- A sensitive manometer was used to acquire precise measurements of differential pressure over periods of 10^{-4} to 10^2 days. Changes were due to CO_2 uptake by powder. dP/dt exceeded leak rates in all but portions of 2-3 experiments out of 41 conducted. Experiments gave repeatable (within ~15% for P or dP/dt) results.

Pressure-drop results:

- *Reaction:* Continuing pressure drops, P(t), suggested that CO_2 reacted with powders to form carbonate, and occurred in all but a few unusual experiments. Fits to $dP/dt = At^B$ after ~1 day gave $B = -0.85 \pm 0.2$, implying logarithmic reaction kinetics (i.e., reaction rate,

$dP/dt \sim 1/t$). Subsequent fits to $P(t) = P_o\ (1 - e^{-t/\tau}) + D \log_{10}(1 + t/t_o)$ gave *rates* of D = 0.01-2 monolayers CO_2 per $\log_{10}t$, with $t_o \ll 1$ day. Reaction *amounts* totaled ~0.005-10 monolayers. Parabolic kinetics, arising from diffusion through a product layer, probably did not exceed $P(t) \sim 0.02\ t^{1/2}$.

- *Adsorption and dissolution:* Initial pressure drops for all experiments were attributed to adsorption (reversible) or dissolution. Powder surfaces rapidly adsorbed CO_2: ~0.01-0.3 monolayers were typically adsorbed in 10^{-3} to 10^{-2} days for "dry," "vapor," and some "damp" experiments. Dissolution of CO_2 in H_2O was observed for most "damp" and "wet" experiments: ~0.1-15 equivalent monolayers in 10^{-3} to 1 day. Dissolution and adsorption were both well fit by $P(t) = P_o\ (1 - e^{-t/\tau})$.
- *Effects of sample composition and acid-treatment:* Rates varied with sample composition (basalt and diopside > olivine > plagioclase and quartz). Basalt glass was *not* more reactive than diopside; forsteritic olivine appeared less reactive, but only two "damp" experiments were run; calcic plagioclase (surprisingly) and quartz (as expected) gave very slow rates, but only one "damp" run each was performed. Basalt powder pretreated with weak acid displayed rates reduced by over an order of magnitude (although diopside did not),

suggesting something removed by acid contributes to CO_2 uptake.

- *Effects of H_2O content, temperature, and CO_2 pressure:* Rates increased with H_2O content, temperature, and CO_2 pressure. A fit to data for basalt at 295 K gave $D = 0.55\ H^{0.1}$, where H is H_2O content in monolayers; at 248-263 K, the effect of H_2O is stronger: $D = 0.06\ H^{0.7}$. Similar relationships hold for diopside. D ~ 0.01-0.2 for "dry" experiments, possibly due to incomplete heat removal of H_2O. No lower limit was put on H_2O required for reaction.

Infrared spectroscopy:

- Reflectance spectra at mid-infrared wavelengths (2.5-12.5 μm) were obtained for all "dry" and "vapor" experimental powders, and ratioed to starting spectra for maximum sensitivity to added phases. Controls and reference spectra showed that results were repeatable, and that carbonate absorptions were detectable with as little as 0.3 wt% calcite added to diopside.
- Prominent spectral features near 7 μm in basalt and diopside samples coincided with CO_3^{-2} absorptions at 6.9 μm for calcite. Additional absorptions near 6.1 μm in basalt and 4.0 μm in diopside were also consistent with the presence of calcite. Noise due to silicate

absorption in ratioed spectra made it difficult to identify SiO_2 or other reaction byproducts.

- Absorption ratios near 7 μm ranged from ~0.05 (corresponding to perhaps 3 wt% added calcite) to as little as ~0.002, below which we were unable to identify added phases. There was a clear positive correlation between absorption ratios and experimental CO_2 uptakes (and hence H_2O content), which strengthened the conclusion that carbonate——probably calcite but perhaps magnesite or dolomite——formed in pressure-drop experiments.
- Using X-ray photoelectron spectroscopy (XPS) to analyze the surface layers of diopside crystals and chips of basalt glass exposed to conditions similar to those in pressure-drop experiments revealed no carbonate product, although carbonate observed with infrared spectroscopy may occur deep enough that XPS cannot see it at the surface of bulk samples. Moreover, carbonate signatures on bulk samples as well as on powders proved difficult to distinguish from organic carbon.

Additional modeling results and other theoretical conclusions are reviewed below:

- *Modeled experimental processes:* Logarithmic reaction kinetics ($dP/dt \sim 1/t$) resulted when we assumed that only a fraction of product deposits onto a surface that

is the source of cations (i.e., uniform deposition onto active surface *and* onto product that is not constrained to a monolayer). We also incorporated a single-layer adsorption model, $P(t) \sim 1 - e^{-t/\tau}$, which followed from assuming that the rate of depletion of surface area varies with the amount of surface area left.

- *Logarithmic growth applied to Mars:* Using experimentally determined logarithmic reaction rates, a finite limit was placed on total carbonate formed on Mars over geologic time. For a global layer of basalt powder, only high specific surface area (>1 m^2/g), a deep regolith (>100 m), or plentiful H_2O (equivalent to films >5 monolayers thick) allow total CO_2 stored as carbonate to exceed ~10-100 mb. Unless very wet conditions once existed, or unless diffusive transport becomes significant over geologic timescales, carbonate formation probably could not have removed an early, dense CO_2 atmosphere.
- *Diffusion-limited growth:* Experimental results do not preclude a model in which carbonate forms by CO_2 diffusion through a product rind. Consideration of relations among temperature, diffusivity, rind thickness, and pressure led to a diffusion-limited reaction rate, $dP/dt \sim f(P)$, that was iterated forward in time. CO_2 pressure for a warm, wet early Mars would have decayed

rapidly in the first few 100 m.y., and more gradually since ~2 b.y. ago.

5.3 DIRECTIONS FOR FUTURE WORK

Further experimental investigation of carbonate formation under Martian conditions could reveal the following:

- Potential lower limits on water vapor abundance (and CO_2 pressure) necessary to form carbonates. Also, a clearer understanding of differences in reactivity for various rocks and minerals (e.g., different basalts, pyroxenes, olivines, and feldspars), as well as the inhibiting effects of competition with other reactants (e.g., SO_2 or O_2, especially with Fe-bearing minerals).
- Better experimental control of powder surfaces, e.g., by heating to higher temperatures immediately before exposure to experimental atmosphere, perhaps accompanied by more prolonged evacuation closer to vacuum pressure. Also, an explanation for greatly reduced rates of CO_2 uptake in acid-treated basalt samples.
- Precise identification of carbonate products with high-resolution microscopic and spectroscopic techniques. In addition, further infrared spectroscopic analysis could better distinguish among candidate carbonates.

- Better characterization of long-term rates. One way to do this is to use the pressure-drop method described in this thesis, with better control of experimental temperatures. Also, either large samples or fine powders in tightly closed containers—with CO_2 and H_2O at known temperature and pressure—could be unsealed after ~10^2-10^3 days for surface or bulk analysis of products. Many samples could be run simultaneously this way, and perhaps a means could be devised to monitor them (e.g., with infrared spectroscopy) through their containers *during experiments*.
- Additional parameters that are possibly diagnostic of reaction mechanisms. For example, powder pore sizes could be determined from surface area measurements; the pH of powders exposed to H_2O could be measured after, or monitored during, runs; and the amount of H_2O actually present in experimental atmospheres and/or on particle surfaces could be similarly measured or monitored (e.g., by spectroscopic analysis through a suitable window, or perhaps by gas chromatography).

Appendices

A.1 PRELIMINARY PRESSURE-DROP APPARATUS

Shown on the following page, in Figure A.1-1, is the apparatus initially used to perform pressure-drop experiments. Samples were Diopside 0 (not pretreated), heated in a circulating bath (B, a different instrument than the one used for later experiments) with fluid level (water) carefully controlled, and exposed to approximately 1 bar of CO_2. Three experiments were "dry" (no added H_2O vapor), and one involved "vapor" conditions (see below). The general-purpose absolute manometer utilized (P) was later incorporated (as PA) into the apparatus described in Chapter 2. The capacities of the "pre-mixing" volume (G) and other volumes in the apparatus were determined by letting gas expand into different parts of the system, using the known capacity of a calibration volume (C). (Once the capacity of G was determined, it was used for calibration when G was later incorporated into the apparatus described in Chapter 2.) The "combined sample volume"——bounded by valves *a* and *b* and including S and P——had a capacity of 591 cm^3.

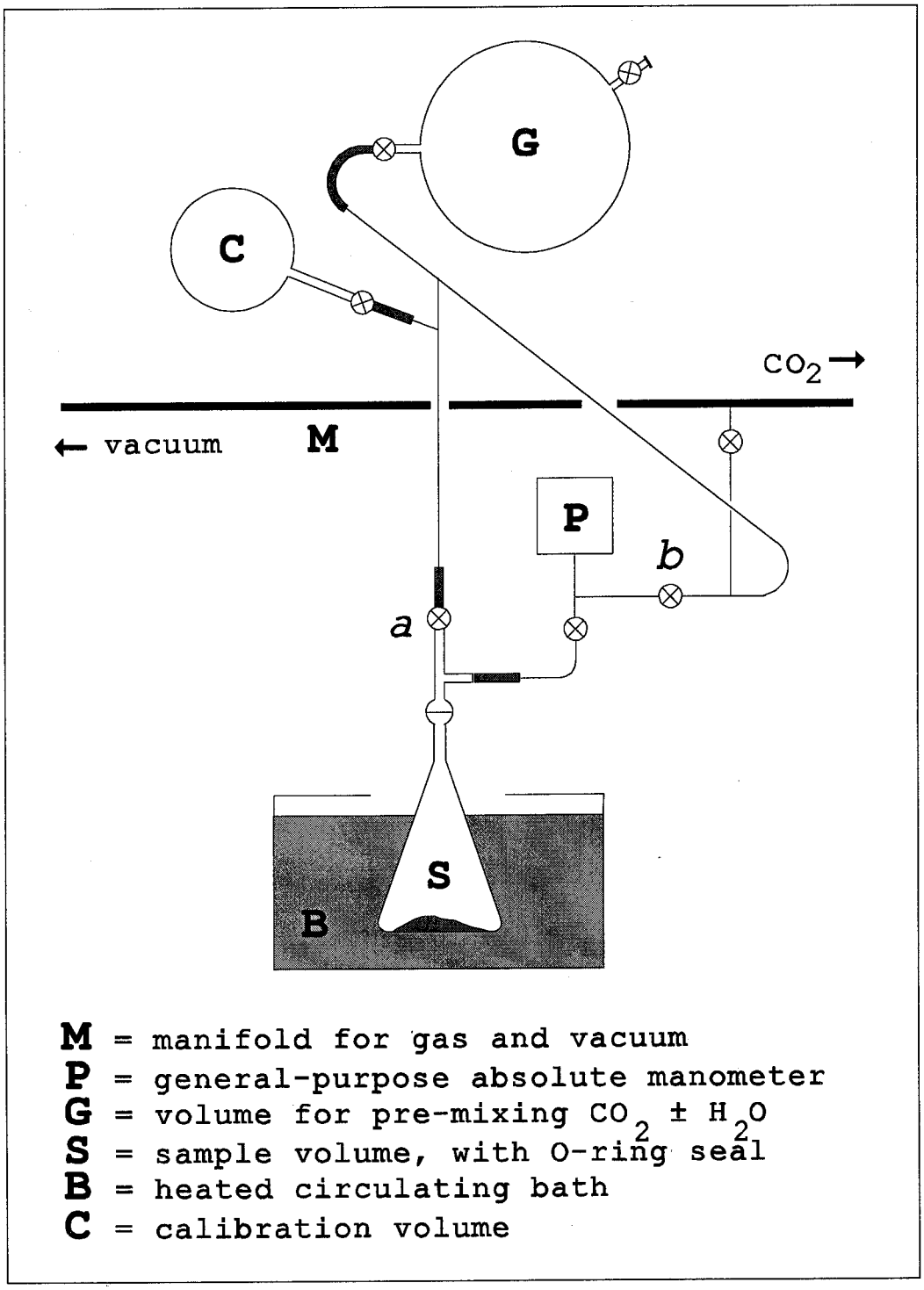

Figure A.1-1 Schematic of preliminary pressure-drop apparatus

Experimental conditions are shown below.

Table A.1-1 Conditions of preliminary experiments (see Table 2-1 for legend)

EX #	Date started	Δt_{tot} [hrs]	Δt_{eff} [hrs]	Mass [g]	T [°C]	$P_o(CO_2)$ [mb]	H_2O content
1	2-8-91	71	3.5	5.5	80	1069	dry
2	2-14	0.5	0.5	5.5	26	1029	dry
3	2-18	45	4.7	28	30	919	vapor
4	2-20	0.5	0.5	28	30	1074	dry

The three "dry" experiments yielded no detectable reaction above noise levels, suggesting the following result: If we were indeed operating in a thermodynamically favorable regime (supported by Gooding, 1978, for the gas-solid reaction), then the lack of a reaction at warm temperatures suggested that a reaction in the 200-300 K regime would be less likely if reaction kinetics dominate. The completely dry scenario was thus excluded at that time (above the limit computed below).

The one "vapor" experiment involved introducing 91 µl of H_2O to G before adding CO_2 and then letting both gases expand into S and P. Thus, approximately (600 ml/5000 ml) $\times$ 9 $\times$ 10^{-3} ml (or 4 $\times$ 10^{-5} moles) of H_2O made it into the "combined sample volume." Since the specific surface area of Di0 was never measured, we used A_s ~ 3 m^2/g (Di0 was

ground under conditions similar to those used for Di1). This gives an H_2O film thickness of <<1 monolayer, assuming uniform deposition:

$$(10\ \text{Å}^2/\text{molecule} \times 6\times10^{23}\ \text{molecules/mole} \times 4\times10^{-5}\ \text{moles}) / (28\ \text{g} \times 3\ \text{m}^2/\text{g/monolayer}) \sim 0.03\ \text{monolayers} \qquad [A.1\text{-}1]$$

This "vapor" experiment also yielded no signal above noise levels. Detectability limits for these preliminary experiments are computed below.

For the "vapor" experiment, EX3, the total run-time was ~2 days (the circulator was turned off after Δt_{eff} = 4.7 hrs, and then turned on again the next morning and the following morning, so that Δt_{tot} = 45 hrs). No pressure signal was detected by visually monitoring the readout of manometer PA——beyond fluctuations of about ±0.1 torr (due to lab temperature variations, since the top of the bath was open, and possibly also due to the limiting displayed resolution of the manometer). Thus, the largest reaction signal that could have gone undetected was:

$$(1.3\times10^2\ \text{dynes/cm}^2 \times 600\ \text{cm}^3) / (8\times10^7\ \text{ergs/mole/K} \times 300\ \text{K} \times 28\ \text{g} \times 2\ \text{days}) \sim 0.06\ \mu\text{moles/g/day} \qquad [A.1\text{-}2]$$

where 1 μmole of CO_2 per g of silicate ~ 0.1 monolayer of CO_2.

In the case of the three "dry" experiments, similar upper limits could be calculated. EX1 is the only one with a larger pressure fluctuation (±0.5 torr--the circulator had greater difficulty maintaining 80°C); using this (along with mass = 5.5 g and Δt_{tot} ~ 3 days) gives ~1 μmole/g/day. EX2 (±0.1 torr, 5.5 g, 0.5 hrs) gives ~30 μmoles/g/day, and EX4 (±0.1 torr, 28 g, 0.5 hrs) gives ~6 μmoles/g/day.

(An initial pressure drop of up to 2-3 torr occurred for all four experiments. However, in each case this occurred within the first 5 minutes and could not be separated from adsorption or other transient behavior.)

Booth (1980) measured CO_2-uptake rates of ~1 μmole of CO_2 per g of silicate in tens of hours. We detected no reaction above this level in one "dry," warm (80°C) experiment, but this is not surprising given that carbonate may not have been a thermodynamically favored reaction product at that temperature (see Appendix A.3, and Gooding, 1978). Our limits for "dry" experiments performed nearer to room temperature are less useful, since we did not run them long enough to impose meaningful limits. More useful information about "dry" carbonate formation was obtained from our later experiments (Chapter 2). Finally, the "vapor" experiment conducted at 30°C gives a "negative" result which is consistent with Booth's findings (and with ours--see

Chapter 2), since the ~0.03 monolayers of water used may not have been enough for significant reaction.

A.2 VAPOR PRESSURE TABLES FOR H_2O AND CO_2

Shown below are tables of vapor pressure for H_2O and CO_2, taken from the *CRC Handbook of Chemistry and Physics*, 58th edition (Weast, 1977). Pressure are in torr (1 torr = 1 mm Hg = 1.33 mb), are rounded off from handbook values, and are shown for intervals of 5 or 10°C (except 20-26°C).

Table A.2-1 Pressure of H_2O vapor

(a) over water:

T (°C)	P (torr)	T (°C)	P (torr)
-15	1.44	24	22.38
-10	2.15	25	23.76
-5	3.16	26	25.21
0	4.58	30	31.82
5	6.54	40	55.32
10	9.21	50	92.51
15	12.79	60	149.38
20	17.54	70	233.7
21	18.65	80	355.1
22	19.83	90	525.76
23	21.07	100	760.00

(b) over ice:

T (°C)	P (torr)
-50	0.03
-40	0.10
-30	0.29
-25	0.48
-20	0.78
-15	1.24
-10	1.95
-5	3.01
0	4.58

Table A.2-2 Pressure of CO_2 over liquid

T (°C)	P (torr)	T (°C)	P (torr)
-50	5128	0	26,142
-40	7545	10	33,763
-30	10,718	20	42,959
-20	14,781	30	54,086
-10	19,872		

A.3 P-T STABILITY DIAGRAMS FOR CARBONATES

Gooding (1978) performed thermodynamic calculations to define boundaries for gas-solid reactions in partial pressure stability diagrams. Reactions are of the type:

$$aS_1 + bG_1 + cG_2 + \ldots \rightleftharpoons iS_2 + jS_3 + \ldots + xG_n + yG_{n+1} + \ldots \qquad [A.3\text{-}1]$$

in which a single solid mineral, S_1, reacts with atmospheric gases, G_1, G_2, ..., to form solid decomposition products, S_2, S_3, ..., and residual gases, G_n, G_{n+1}, ... The activities of the solid phases are taken to be one, and for the low-pressure atmospheres of both Earth and Mars, the equilibrium constant for this reaction reduces to:

$$K = [\ (P_{Gn})^x \times (P_{Gn+1})^y \times \cdots\ ] \ / \ [\ (P_{G1})^b \times (P_{G2})^c \times \cdots\ ] \qquad [A.3\text{-}2]$$

P is partial pressure of gaseous components. K is found from expressions involving changes in Gibbs free energy, ΔG:

$$K = \exp(-\Delta G/RT) \qquad [A.3\text{-}3]$$

where values for Gibbs free energy are taken from the literature or scaled to values for analogous compounds.

These last two equations taken together give straight-line boundaries for stability fields of reactions in a diagram of log $P(H_2O)$ versus log $P(CO_2)$. For example, Figure A.3-1 depicts gas-solid reactions involving diopside:

$$CaMgSi_2O_6 + 2\ CO_2 \rightleftharpoons CaMg(CO_3)_2 + 2\ SiO_2 \qquad [A.3\text{-}4]$$

$$CaMgSi_2O_6 + 2\ CO_2 \rightleftharpoons CaCO_3 + MgCO_3 + 2\ SiO_2 \qquad [A.3\text{-}5]$$

$$CaMgSi_2O_6 + 3\ CO_2 + H_2O \rightleftharpoons Mg_3Si_4O_{10}(OH)_2 + 3\ CaCO_3 + SiO_2 \qquad [A.3\text{-}6]$$

$$Mg_3Si_4O_{10}(OH)_2 + 3\ CO_2 + 3\ CaCO_3 \rightleftharpoons 3\ CaMg(CO_3)_2 + 4\ SiO_2 + H_2O \qquad [A.3\text{-}7]$$

$$Mg_3Si_4O_{10}(OH)_2 + 3\ CO_2 \rightleftharpoons 3\ MgCO_3 + 4\ SiO_2 + H_2O \qquad [A.3\text{-}8]$$

$Log_{10}K$ at -33°C [and at 25°C] for each of these reactions is 16.7 [10.1], 14.2 [8.07], 34.2 [21.1], 16.4 [9.61], and

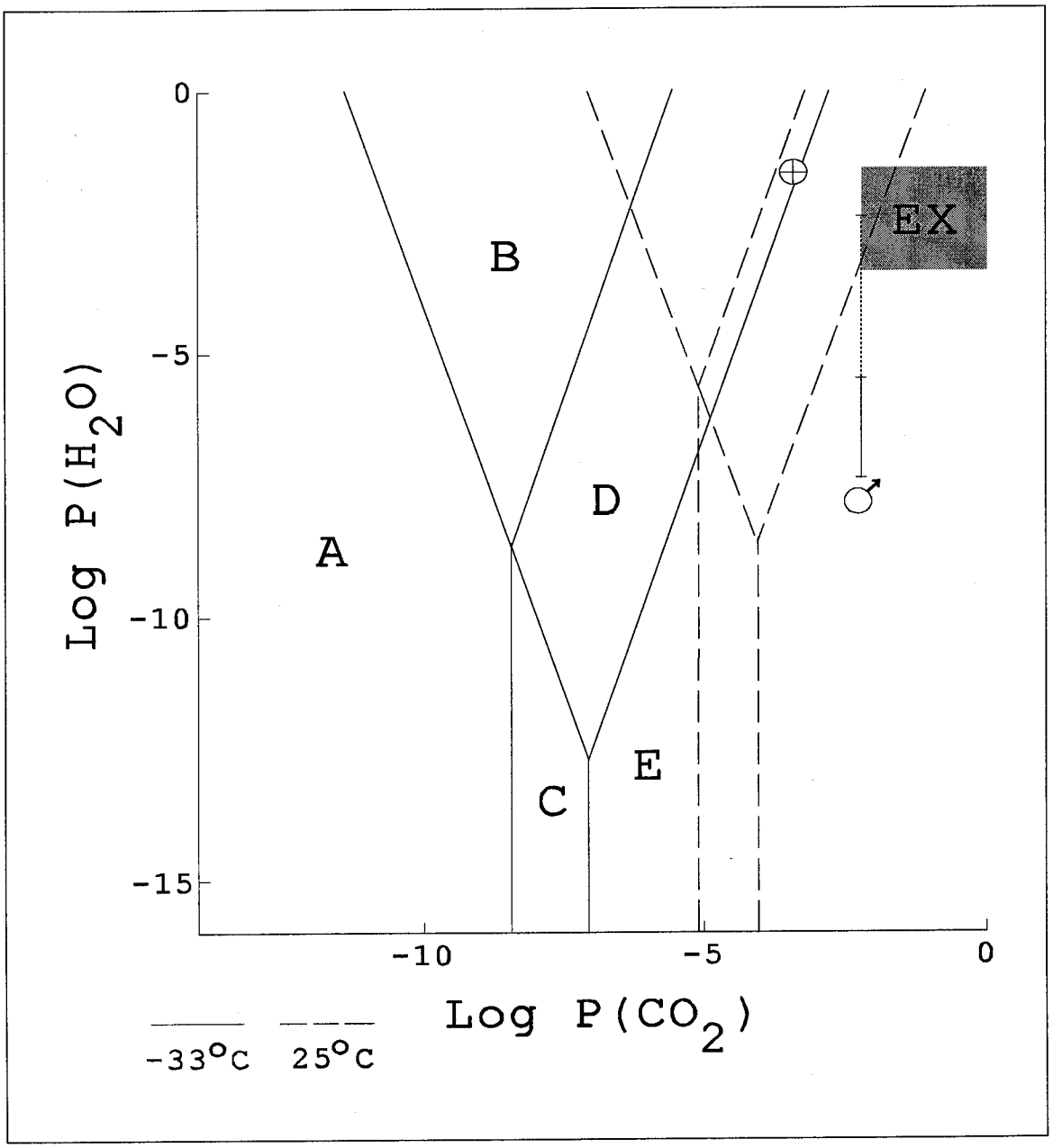

Figure A.3-1 Stability fields of diopside and its decomposition products in equilibrium with gaseous H_2O and CO_2 (after Gooding, 1978)

A = $CaMgSi_2O_6$
B = $Mg_3Si_4O_{10}(OH)_2$ [talc] + $CaCO_3$
C = $CaMg(CO_3)_2$ + SiO_2
D = $Mg_3Si_4O_{10}(OH)_2$ + $CaMg(CO_3)2$
E = $MgCO_3$ + $CaCO_3$ + $CaMg(CO_3)_2$ + SiO_2

P is in bars. Reference points are shown for the Earth, Mars, and experimental conditions (see text).

8.33 [3.15]. Five stability fields are depicted for each temperature. The reference point for the Earth (circle with cross) is for a relative humidity of 50% at 25°C. The observed range of water vapor abundance in the Martian atmosphere (bars joined by solid line, labeled by circle with arrow), equivalent to 1-80 precipitable μm of H_2O, and its probable maximum limit, the vapor pressure of ice at 0°C (bar at top of dotted line), are shown. So far, all of Figure A.3-1 is taken from Gooding (1978).

The shaded box (labeled EX) in Figure A.3-1 represents conditions of experiments performed for this thesis——$P(CO_2)$ from 7 to 1000 mb, and $P(H_2O)$ equivalent to the vapor pressure of water from -30 to 25°C. The $P(H_2O)$ boundaries of the box represent upper limits on the pressure of water vapor in our experiments, since the atmosphere for "vapor" experiments was not always saturated with water vapor, and because some experiments were meant to be "dry."

Thus, in one sense, we have succeeded in simulating Martian conditions in our experiments. Although temperatures below -30°C were not explored, the effects of dry, low-$P(CO_2)$ conditions representative of the present Martian climate *were* investigated.

Also, both experimental and Martian conditions of P and T are within the boundaries of thermodynamic equilibrium for carbonate formation from diopside. Although not shown here, Gooding's calculations for olivine (both the forsterite and

fayalite end-members, Mg_2SiO_4 and Fe_2SiO_4) and plagioclase (the anorthite end-member, $CaAl_2Si_2O_8$, but not the albite end-member, $NaAlSi_3O_8$) also place both Mars and our experiments on the carbonate-production side of P-T stability diagrams.

A.4 DETAILS OF BET TECHNIQUE AND RESULTS

Brunauer, Emmett, and Teller (1938) are responsible for a theory of multimolecular adsorption which explains the shapes of adsorption isotherms (volume of gas adsorbed as a function of pressure) for many gases at temperatures near their condensation points. Their derivation of the multimolecular isotherm equation is a generalization of unimolecular theory. They show that the forces responsible for the binding energy of multimolecular adsorption are the same as those that produce condensation; the polarization of the second layer of adsorbed gas by the first layer (i.e., due to attraction of dipoles induced into a non-polar gas like argon) is insufficient to constitute a major portion of the binding energy between adsorbed layers.

The adsorption isotherm equation in BET theory is:

$$V = V_m c\ P/P_o\ /\ (1 - P/P_o) \times [1 + (c-1)\ P/P_o] \qquad [A.4\text{-}1]$$

where V, the volume of gas adsorbed, is in terms of P/P_o, the pressure relative to the saturation vapor pressure of the adsorbing gas; V_m is the volume of gas in an adsorbed monolayer; and c is a constant for a given temperature. This equation gives an S-shaped isotherm when V is plotted against P/P_o for a given mass of adsorbing solid; these isotherms occur for most solids when adsorption is performed at low temperature with inert gases (for an elaboration on the practical application of BET theory, see Orr, 1977a, 1977b, in addition to Brunauer et al., 1938).

For purposes of obtaining a specific surface area (i.e., area occupied by a monolayer of adsorbed gas), the reduced form of the above equation is used:

$$P / V (P_o - P) = 1/V_m c + [(c-1) / V_m c] P/P_o \qquad [A.4\text{-}2]$$

When $P/V(P_o-P)$ is plotted against P/P_o, this gives a straight line having intercept $1/V_m c$ and slope $(c-1)/V_m c$. Specific surface area, A_S, in m^2/g, is therefore:

$$A_S = 10^{-20} \times V_m \, A \, N_A / M \qquad [A.4\text{-}3]$$

where A is the surface area occupied by a molecule in its liquid form (see below), in $Å^2$/molecule; N_A is Avogadro's number, 6.023×10^{23} molecules/mole; M is the molar volume of gas at STP, 22.4×10^3 cm^3/mole; and V_m is simply the

inverse of slope plus intercept (see above), in cm^3/g. In practice, the plots are nearly linear for values of P/P_o between 0.05 and 0.35.

Using the apparatus shown in Figure A.4-1, we introduced incremental volumes of inert gas from a calibration volume (C) into a sample volume (S), which was evacuated beforehand and contained a known mass of solid powder. The sample volume was kept at the temperature of liquid nitrogen (carefully monitored with a vapor pressure thermometer), so that P_o was equal to the saturation vapor pressure of the inert gas used, at approximately 78 K. Comparison of the pressure in C (before opening the valve to S) with the pressure in C plus S (after opening the valve) gives the incremental adsorbed volume of gas at the second pressure. Other quantities that must be measured include room temperature, which enters the calculation of incremental adsorbed volume just described, and the capacity (not taken up by solid sample) of the sample volume, accomplished beforehand by expanding helium in incremental amounts into the sample volume (He is not appreciably adsorbed). Finally, a correction was made in the case of some gases for non-ideal behavior at low temperature.

We used nitrogen, argon, and krypton as adsorbate gases (N_2 has a saturation vapor pressure of 760 torr at liquid nitrogen temperature, and a molecular surface area of 16.2 $Å^2$/molecule; Ar has P_o = 197 torr, and

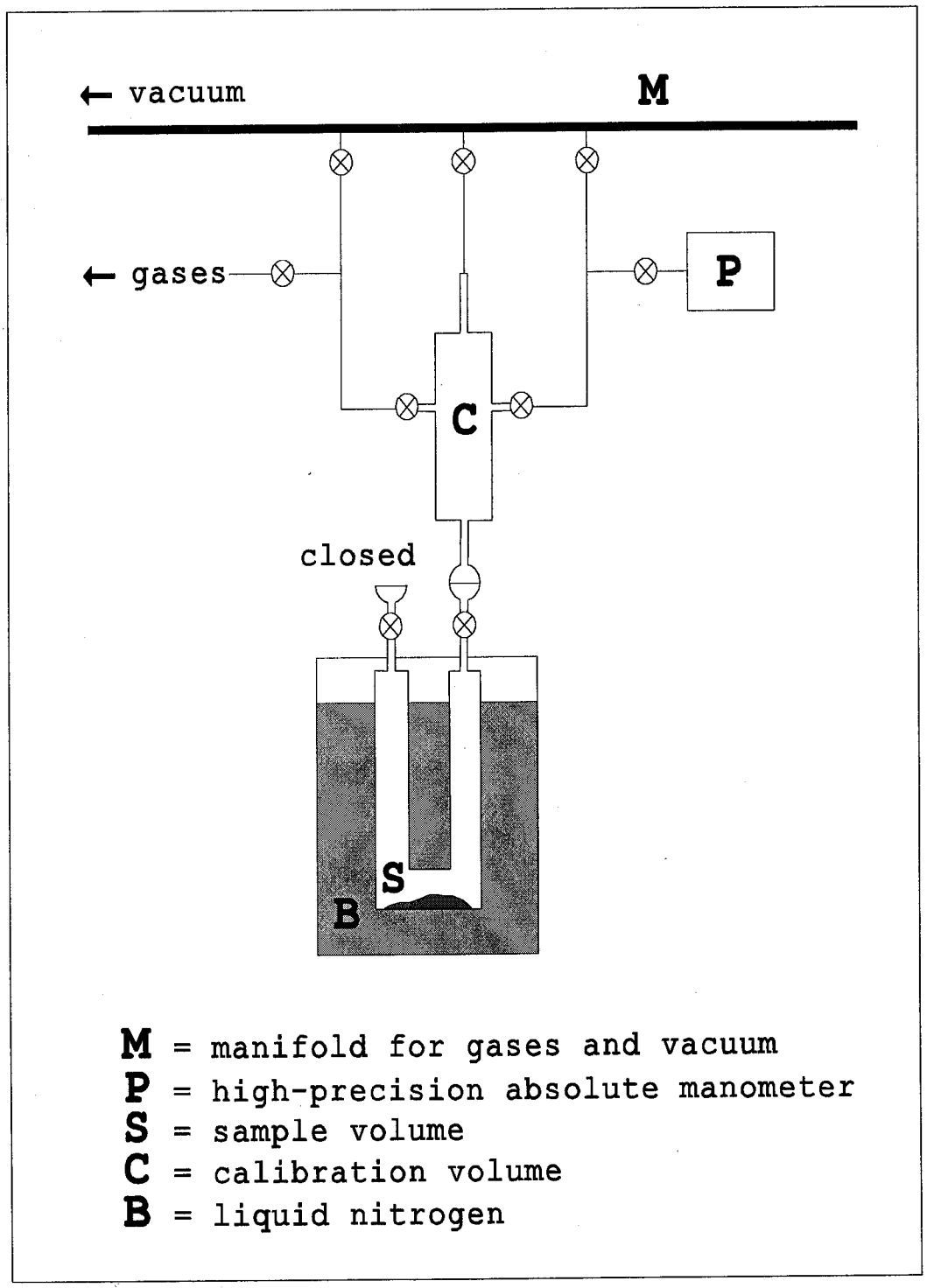

Figure A.4-1 Schematic of inert-gas adsorption apparatus used for measurement of BET specific surface area

A = 18.0 $Å^2$/molecule; and Kr has P_o = 1.7 torr, and A = 20.2 $Å^2$/molecule, both for the solid phase of Kr, which applies at 78 K). Results for measurements of all experimental samples (except Di0, which was not measured) are shown below:

Table A.4-1 BET specific surface area measurements

Sample	Date of measurement	Gas used	Mass (g)	Measured A_s (m^2/g)	Result with uncertainty
Di1	11-22-91	N_2	1.15	-	2.7 ± 0.3
	11-22-91	Ar	1.15	2.7	
Di2	9-3-93	Ar	1.18	10.3	10 ± 0.4
	10-7-93	N_2	1.18	9.6	
Ol1	10-7-93	Ar	1.08	21	21 ± 1.4
Qtz	10-15-93	Ar	0.133	3.0	2.3 ± 1
	11-29-93	Kr	0.133	1.6	
Plag	10-7-93	Ar	1.21	6.1	6.1 ± 0.6
Ol2	10-7-93	Ar	0.665	21	21 ± 2.5
Calc	12-3-93	N_2	1.07	1.5	1.5 ± 1
Bas1	8-19-93	Ar	1.30	0.62	0.65 ± 0.02
	8-19-93	Kr	1.30	0.65	
Bas2	6-13-94	Ar	0.89	1.51	1.5 ± 0.1
Bas3	6-13-94	Ar	1.015	1.01	1.0 ± 0.1
Bas4	5-5-94	Ar	1.01	0.72	0.66 ± 0.05
	5-5-94	N_2	1.01	0.61	
Bas5	12-1-93	Ar	0.855	1.73	2.0 ± 0.2
	12-3-93	N_2	0.855	2.20	
Bas6	4-22-94	Ar	0.53	12	12 ± 1
Bas7	4-22-94	Ar	1.00	0.79	0.79 ± 0.02
	5-5-94	N_2	1.00	2.5	
	5-6-94	Ar	0.96	0.78	
	5-6-94	N_2	0.96	-	
Bas8	6-13-94	Ar	0.865	1.39	1.4 ± 0.1
Bas9	6-13-94	Ar	0.74	3.9	3.9 ± 0.4

Uncertainties were estimated as follows. A visual fit to $P/V(P_o-P)$ versus P/P_o was performed, for values of P/P_o from 0.05 to 0.35 (recorded roughly every 0.02), and the slope and intercept were used to calculate specific surface area. The uncertainty tabulated above was determined from the estimated error in this fitting process, and from the degree to which more than one result agreed. Aside from one sample, all measurements were for portions of powders on which experiments were not performed. In the case of Bas3, no powder remained after pressure-drop experiments, and so the EX31 sample was used (after a "dry" experiment).

A.5 CONTROL EXPERIMENTS AND DESORPTION LEGS

Results for control experiments (**GROUP 0**), and for those portions of experiments conducted after $t = \Delta t_{eff}$ (including desorption legs) are shown in Figure A.5-1, parts (a) and (b) respectively, pages 226-229 and 230-233.

In plots for experiments prior to EX8, individual manually recorded data points are shown as open circles, and dashed lines are interpolated between them. For experiments in which pressure or temperature changes occurred following $t = \Delta t_{eff}$, abrupt changes in differential pressure often result. Desorption legs are displayed for EX8,12,13,42 (see Table 2-1 in Chapter 2); they begin at or near zero

differential pressure, and are negative because pressure is increasing in our sample volume relative to the reference volume.

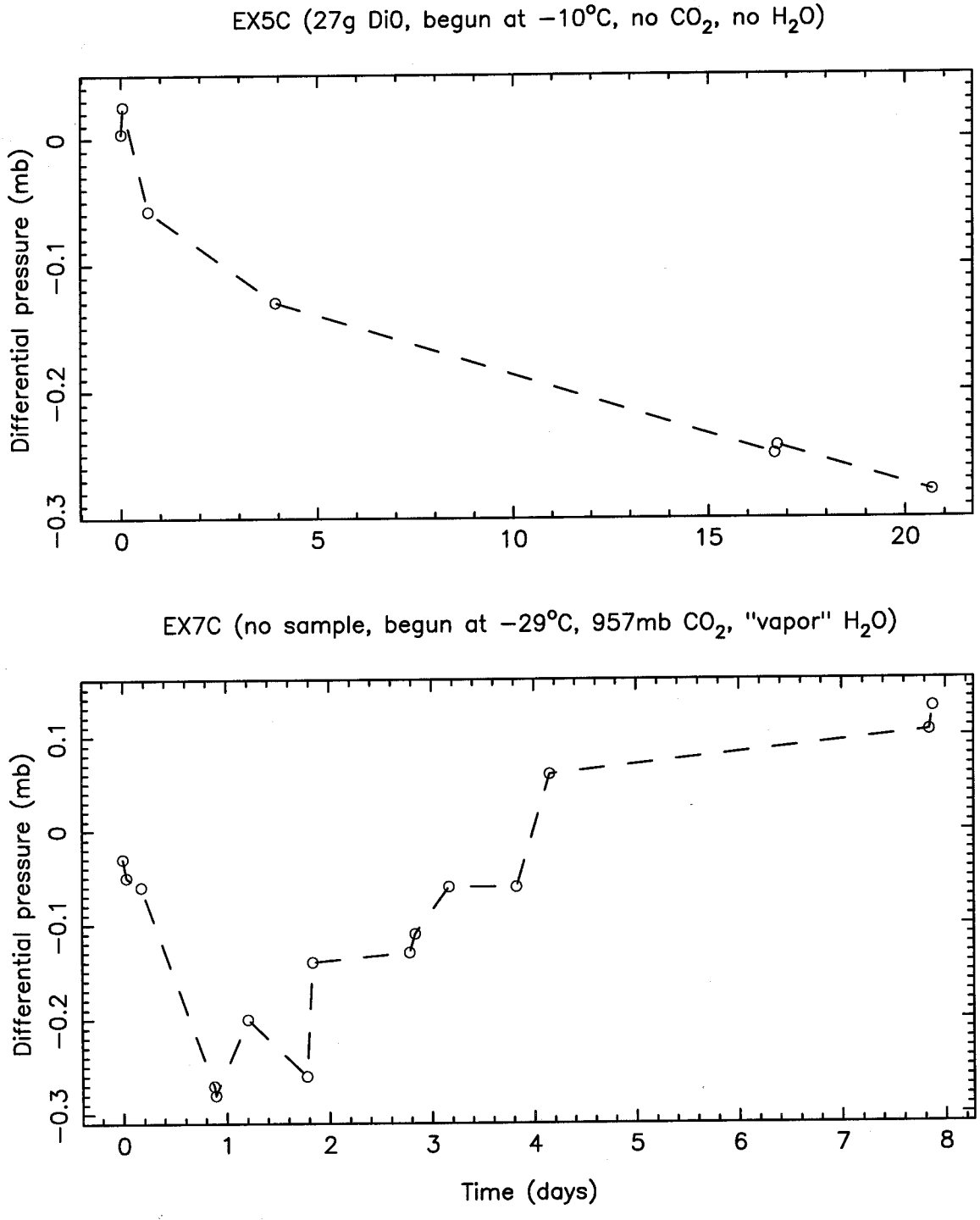

Figure A.5-1 Additional plots of raw P(t) data
(a) **GROUP O** [control experiments]

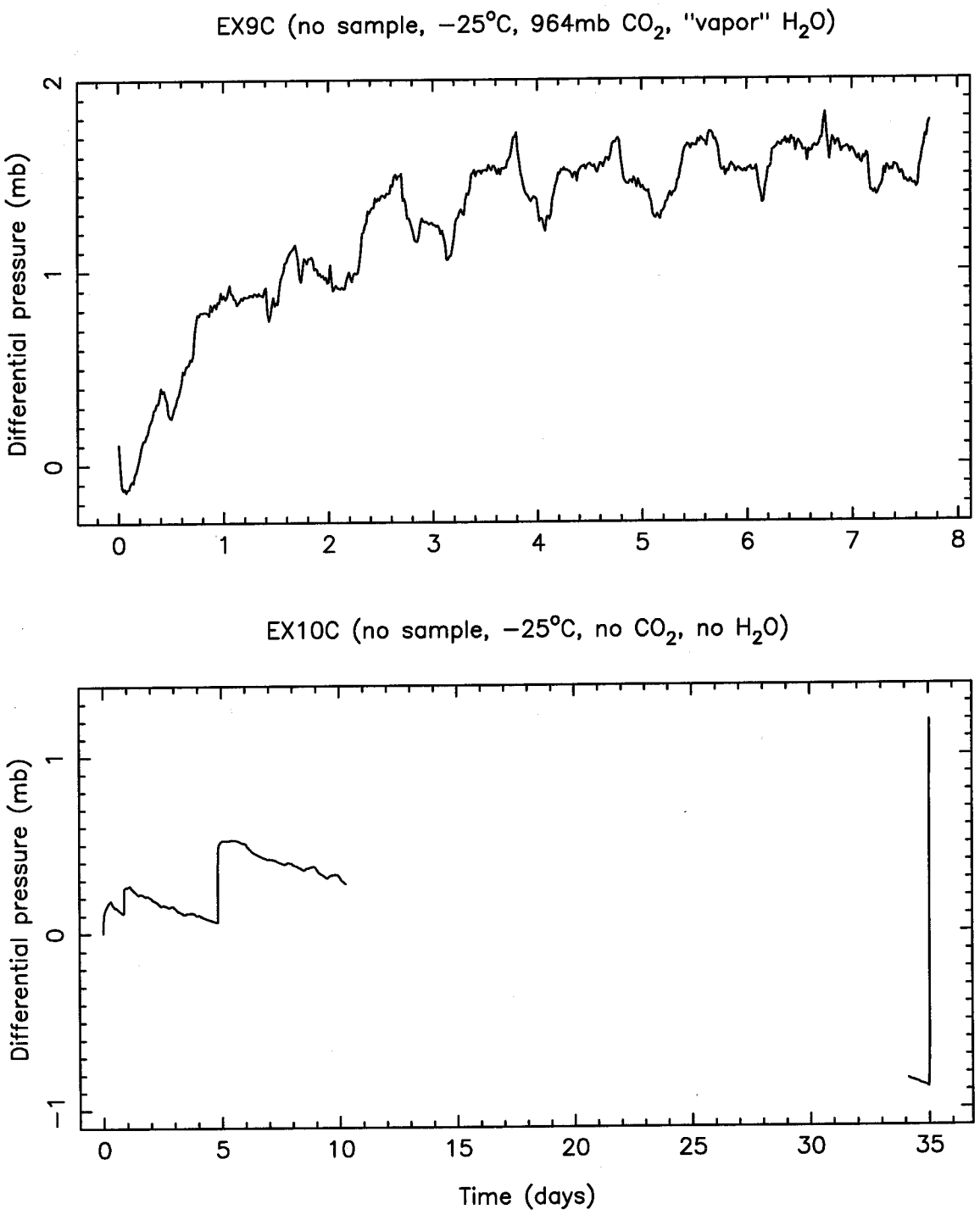

Figure A.5-1 Additional plots of raw P(t) data (continued)
(a) **GROUP 0** [control experiments]

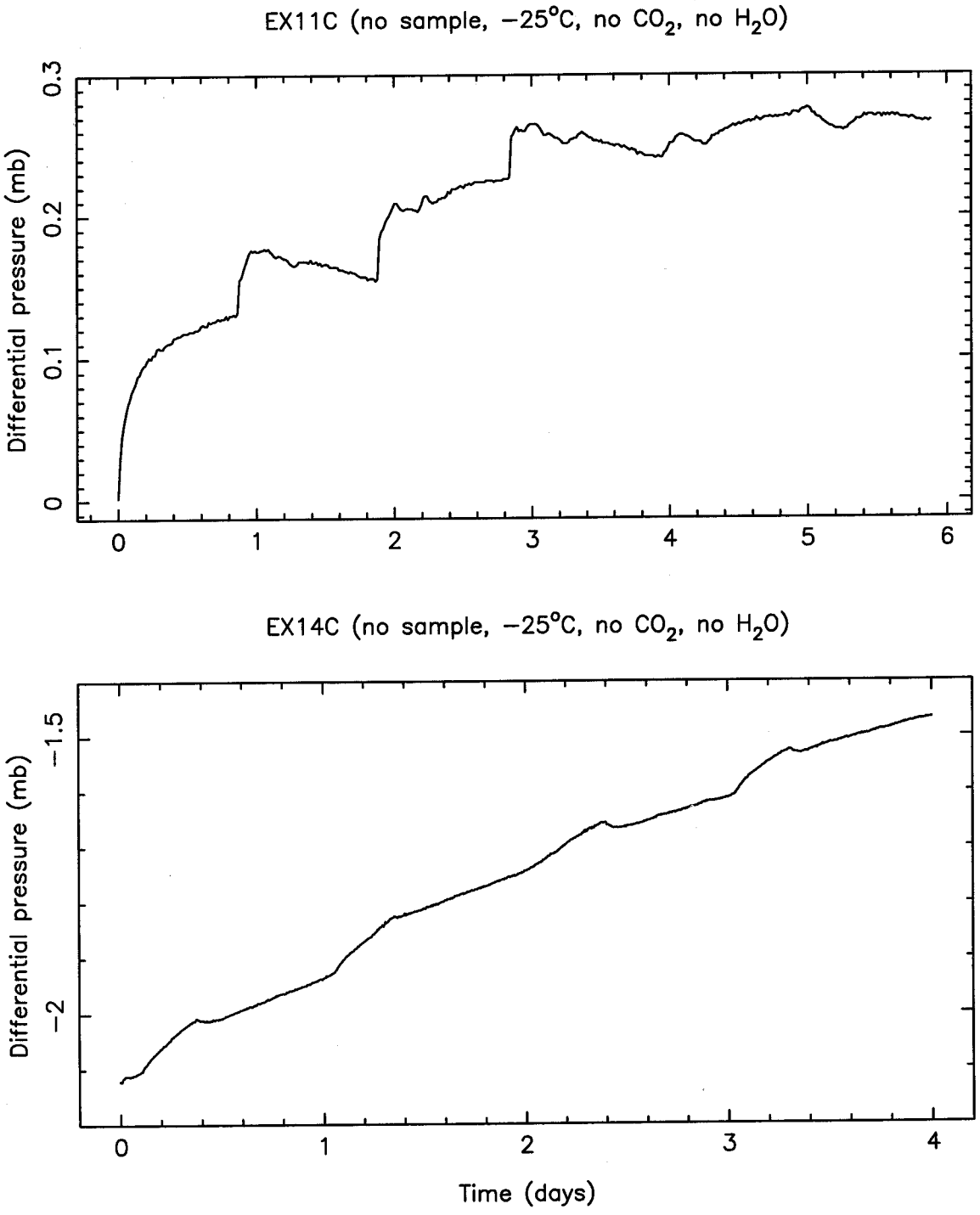

Figure A.5-1 Additional plots of raw P(t) data (continued)
(a) **GROUP 0** [control experiments]

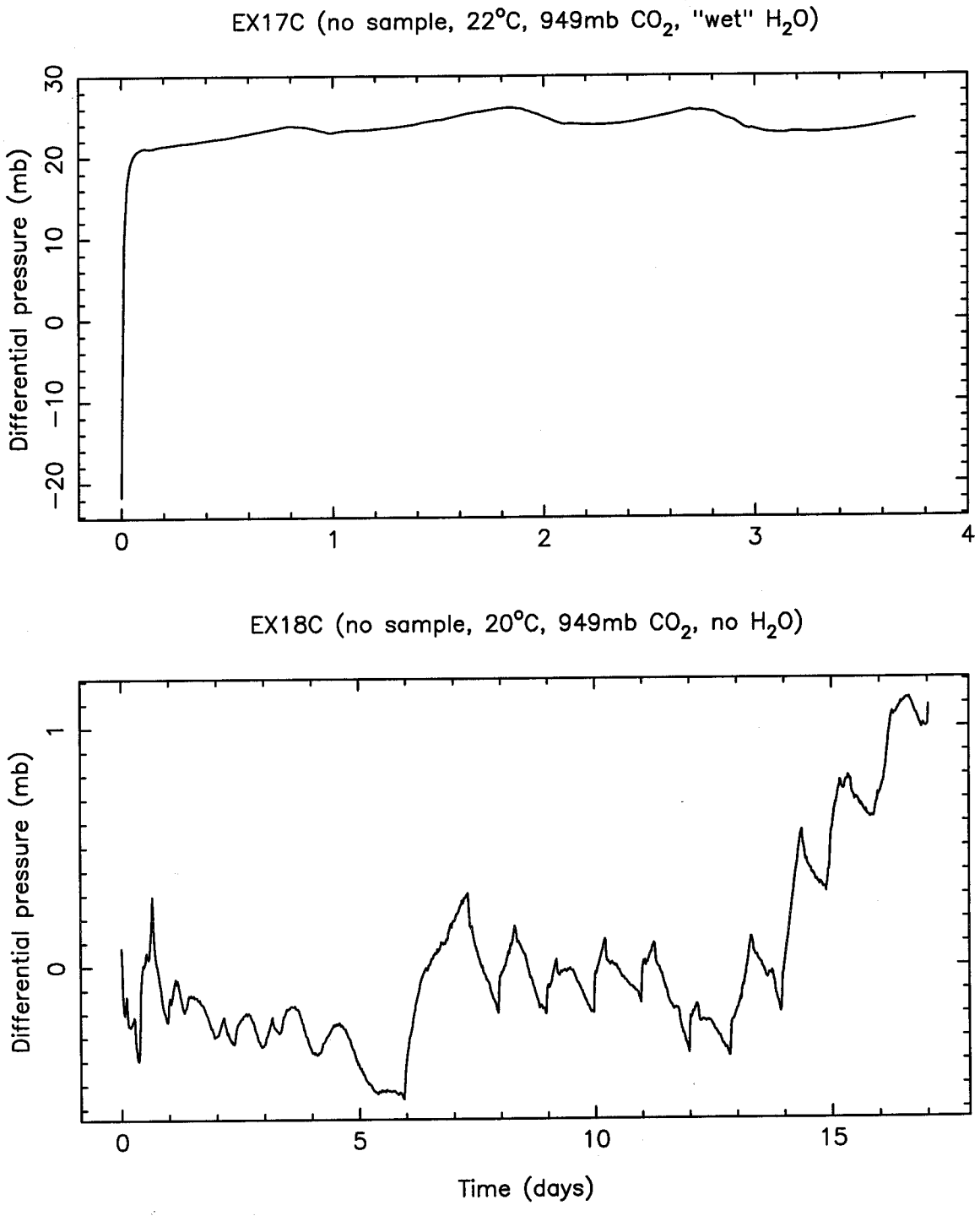

Figure A.5-1 Additional plots of raw P(t) data (continued)
(a) **GROUP 0** [control experiments]

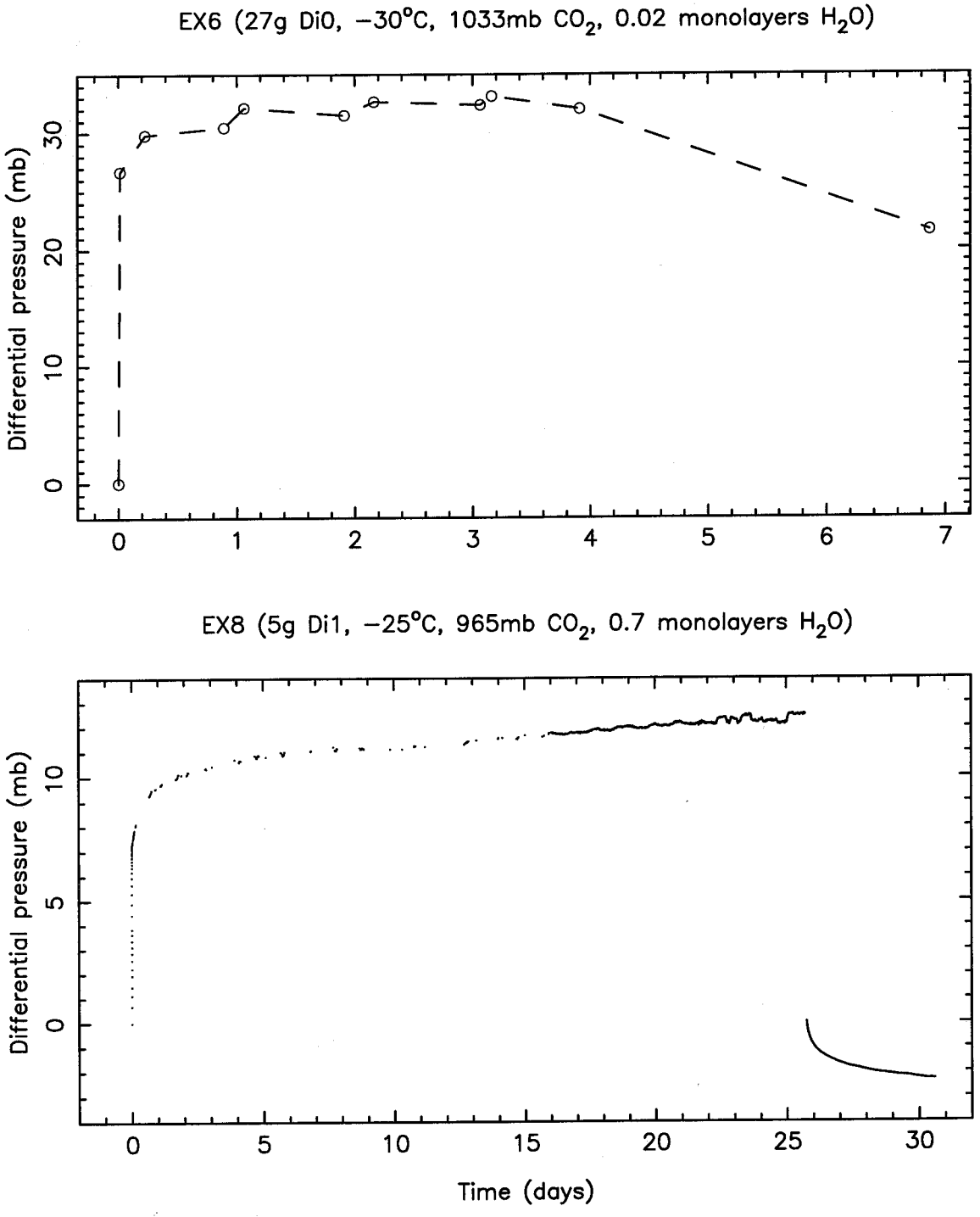

Figure A.5-1 Additional plots of raw P(t) data
(b) Including times after t = Δt_{eff}

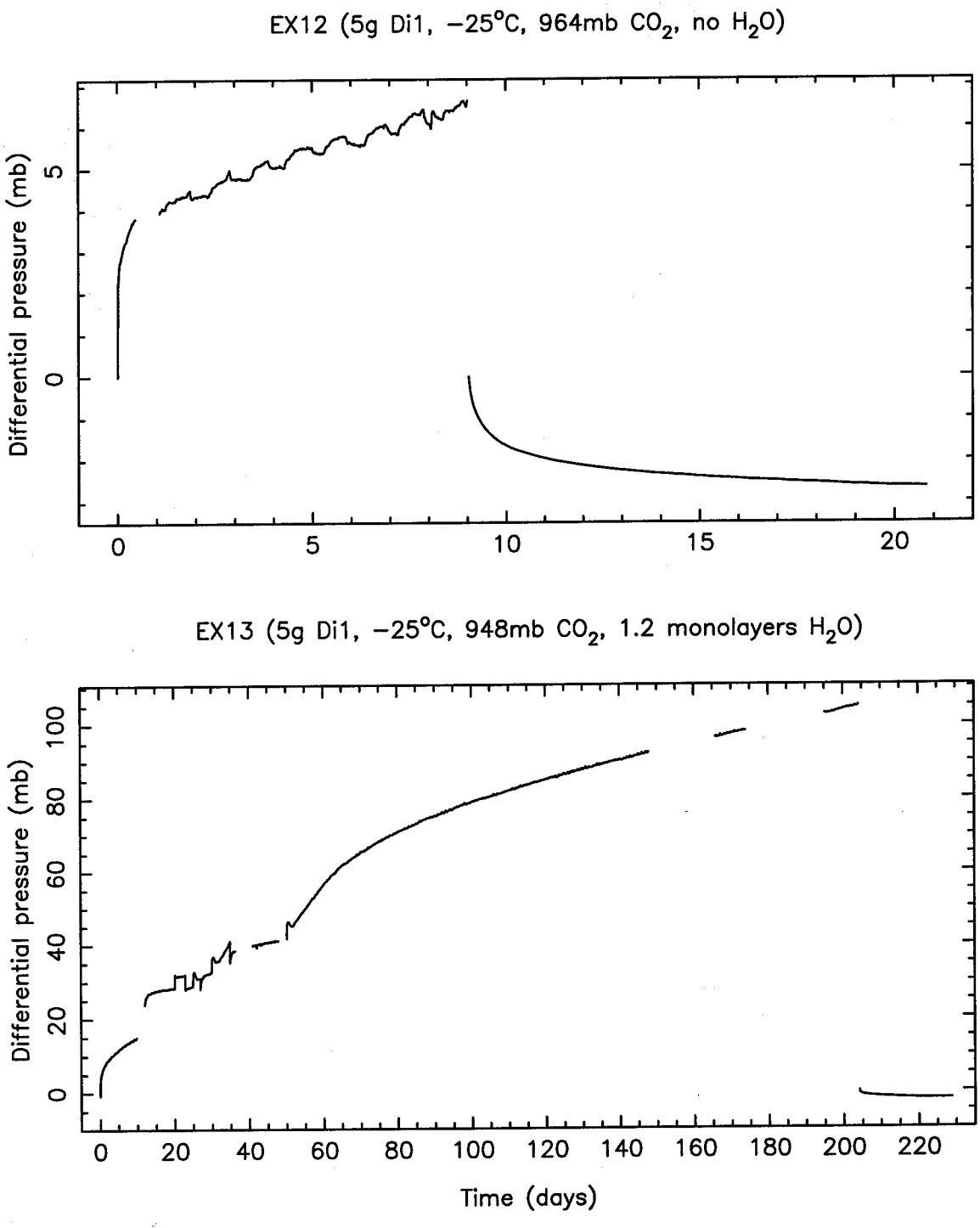

Figure A.5-1 Additional plots of raw P(t) data (continued)
(b) Including times after t = Δt_{eff}

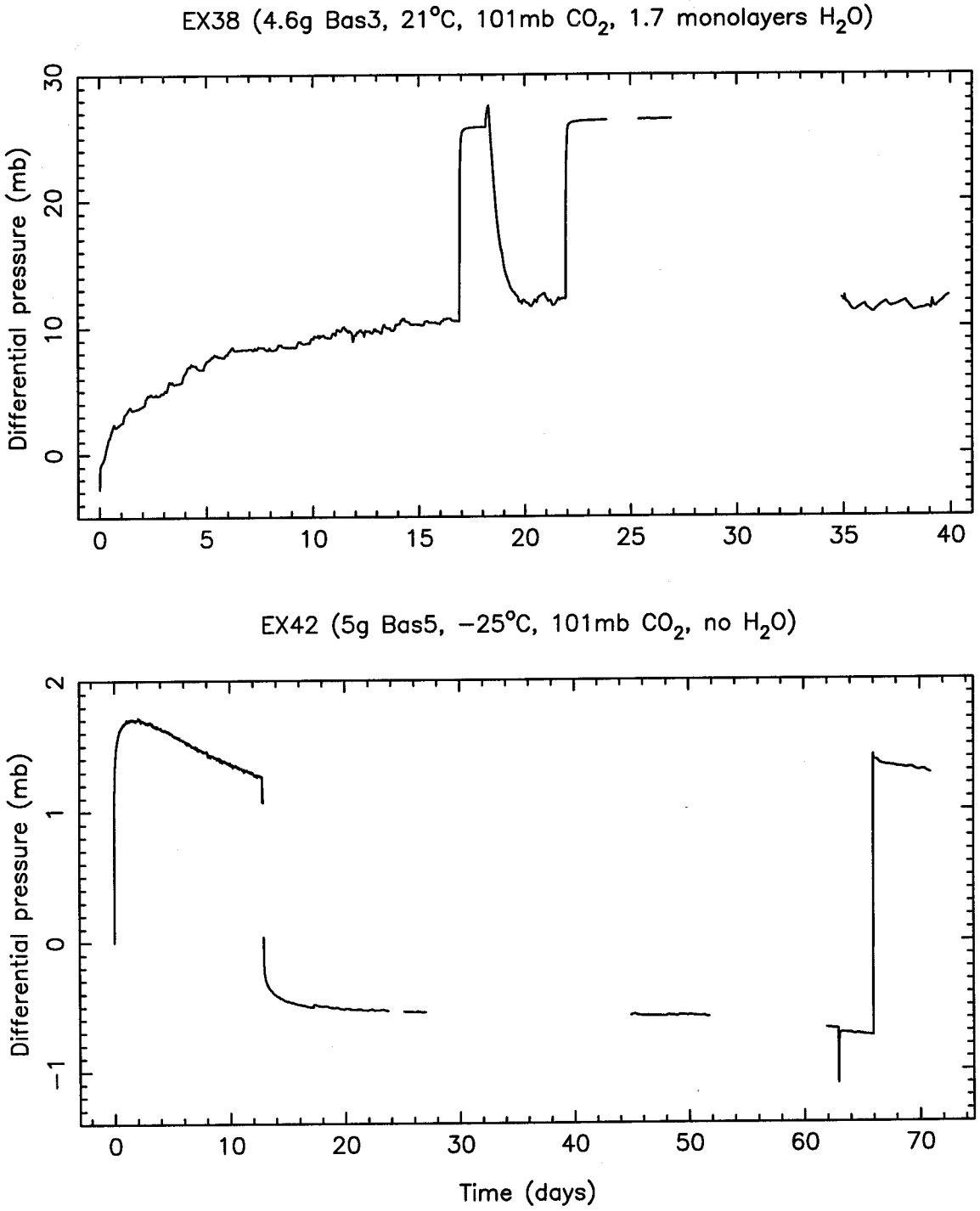

Figure A.5-1 Additional plots of raw P(t) data (continued)
(b) Including times after t = Δt_{eff}

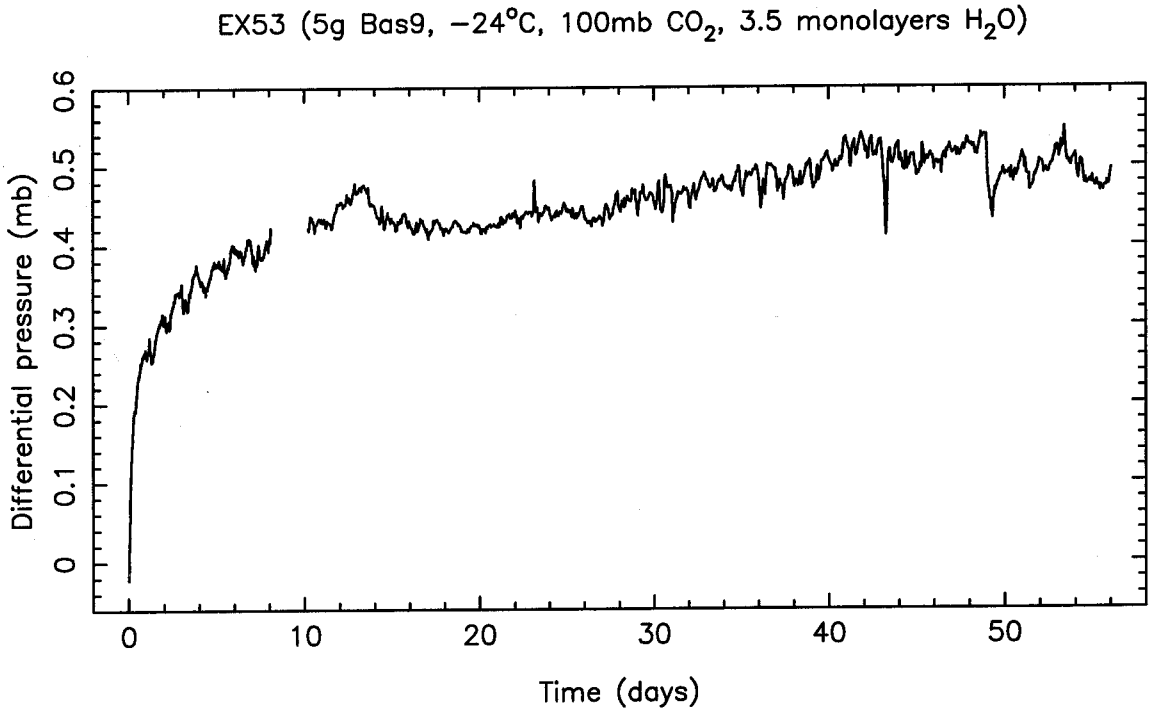

Figure A.5-1 Additional plots of raw P(t) data (continued)
(b) Including times after t = Δt_{eff}

References

Adamson, A.W. (1990). *Physical Chemistry of Surfaces*, 5th ed. John Wiley and Sons, New York, 777 pp.

Allen, C.C., J.L. Gooding, M. Jercinovic, and K. Keil (1981). Altered basaltic glass: A terrestrial analog to the soil of Mars. *Icarus, 45*, 347-369.

Anderson, D.M., M.J. Schwarz, and A.R. Tice (1978). Water vapor adsorption by sodium montmorillonite at -5°C. *Icarus, 34*, 638-644.

Arvidson, R.E., J.L. Gooding, and H.J. Moore (1989). The Martian surface as imaged, sampled, and analyzed by the Viking landers. *Rev. Geophys., 27*, 39-60.

Baird, A., P. Toulmin, III, B.C. Clark, H. Rose, Jr., K. Keil, R.P. Christian, and J.L. Gooding (1976). Mineralogic and petrologic implications of Viking geochemical results from Mars: Interim results. *Science, 194*, 1288-1293.

Baker, V.R., R.G. Strom, V.C. Gulick, J.S. Kargel, G. Komatsu, and V.S. Kale (1991). Ancient oceans, ice sheets and the hydrological cycle on Mars. *Nature, 352*, 589-594.

Ballou, E.V., P.C. Wood, T. Wydeven, M.E. Lehwalt, and R.E. Mack (1978). Chemical interpretation of Viking Lander 1 life detection experiment. *Nature, 271,* 644-645.

Berner, R.A., A.C. Lasaga, and R.M. Garrels (1983). The carbonate-silicate geochemical cycle and its effect on atmospheric carbon dioxide over the past 100 million years. *Am. J. Sci., 283,* 641-683.

Bhatia, S.K. and D.D. Perlmutter (1983). Effect of the product layer on the kinetics of the CO_2-lime reaction. *Am. Inst. Chem. Eng. J., 29,* 79-86.

Blaney, D.L. and T.B. McCord (1989). An observational search for carbonates on Mars. *J. Geophys. Res., 94,* 10,159-10,166.

Blasius, K.R., J.A. Cutts, J.E. Guest, and H. Masursky (1977). Geology of the Valles Marineris: First analysis of imaging from the Viking 1 orbiter primary mission. *J. Geophys. Res., 82,* 4067-4091.

Bogard, D.D. and P. Johnson (1983). Martian gases in an Antarctic meteorite? *Science, 221,* 651-654.

Booth, F. (1948). A note on the theory of surface diffusion reactions. *Trans. Faraday Soc., 44,* 796-801.

Booth, M.C. (1980). *Carbonate Formation on Mars.* Ph.D. thesis, University of California at Los Angeles, 144 pp.

Booth, M.C. and H.H. Kieffer (1978). Carbonate formation in Marslike environments. *J. Geophys. Res., 83,* 1809-1815.

Brady, P.V. (1991). The effect of silicate weathering on global temperature and atmospheric CO_2. *J. Geophys. Res., 96,* 18,101-18,106.

Brunauer, S., P.H. Emmett, and E. Teller (1938). Adsorption of gases in multimolecular layers. *J. Am. Chem. Soc., 60,* 309-319.

Burns, R.G. (1993). Rates and mechanisms of chemical weathering of ferromagnesian silicate minerals on Mars. *Geochim. Cosmochim. Acta, 57,* 4555-4574.

Burns, R.G. and D.S. Fisher (1993). Rates of oxidative weathering on the surface of Mars. *J. Geophys. Res., 98,* 3365-3372.

Cabrera, N. and N.F. Mott (1949). Theory of the oxidation of metals. *Rep. Progr. Phys., 12,* 163-184.

Carr, M.H. (1986). Mars: A water-rich planet? *Icarus, 68,* 187-216.

Carr, M.H. (1987). Water on Mars. *Nature, 326,* 30-35.

Carr, M.H. (1989). Recharge of the early atmosphere of Mars by impact-induced release of CO_2. *Icarus, 79,* 311-327.

Carr, M.H. and G.D. Clow (1981). Martian channels and valleys: Their characteristics, distribution, and age. *Icarus, 48,* 91-117.

Carr, M.H. and G.G. Schaber (1977). Martian permafrost features. *J. Geophys. Res.*, *82*, 4039-4054.

Carr, M.H. and H. Wanke (1992). Earth and Mars: Water inventories as clues to accretional histories. *Icarus*, *98*, 61-71.

Carr, M.H., L.S. Crumpler, J.A. Cutts, R. Greeley, J.E. Guest, and H. Masursky (1977). Martian impact craters and emplacement of ejecta by surface flow. *J. Geophys. Res.*, *82*, 4055-4065.

Christensen, P.R. (1982). Martian dust mantling and surface composition: Interpretation of thermophysical properties. *J. Geophys. Res.*, *87*, 9985-9998.

Christensen, P.R. (1983). Eolian intracrater deposits on Mars: Physical properties and global distribution. *Icarus*, *56*, 496-518.

Christensen, P.R. (1986a). Regional dust deposits on Mars: Physical properties, age, and history. *J. Geophys. Res.*, *91*, 3533-3545.

Christensen, P.R. (1986b). The spatial distribution of rocks on Mars. *Icarus*, *68*, 217-238.

Clark, B.C. (1978). Implications of abundant hygroscopic minerals in the Martian regolith. *Icarus*, *34*, 645-665.

Clark, B.C. (1987). Comets, volcanism, the salt-rich regolith, and cycling of volatiles on Mars. *Icarus*, *71*, 250-256.

Clark, B.C. (1993). Geochemical components in Martian soil. *Geochim. Cosmochim. Acta, 57*, 4575-4581.

Clark, B.C. and D.C. Van Hart (1981). The salts of Mars. *Icarus, 45*, 370-378.

Clark, B.C., A.K. Baird, R.J. Weldon, D.M. Tsusaki, L. Schnabel, and M.P. Candelaria (1982). Chemical composition of Martian fines. *J. Geophys. Res., 87*, 10,059-10,067.

Clifford, S.M. (1991). The role of thermal vapor diffusion in the subsurface hydrologic evolution of Mars. *Geophys. Res. Let., 18*, 2055-2058.

Clifford, S.M. (1993). A model for the hydrologic and climatic behavior of water on Mars. *J. Geophys. Res., 98*, 10,973-11,016.

Clifford, S.M. and D. Hillel (1983). The stability of ground ice in the equatorial region of Mars. *J. Geophys. Res., 88*, 2456-2474.

Clifford, S.M. and D. Hillel (1986). Knudsen diffusion: The effect of small pore size and low gas pressure on gaseous transport in soil. *Soil Sci., 141*, 289-297.

Crank, J. (1975). *The Mathematics of Diffusion*, 2nd ed. Clarendon Press, Oxford, 414 pp.

Davies, G.F. and R.E. Arvidson (1981). Martian thermal history, core segregation, and tectonics. *Icarus, 45*, 339-346.

Dean, J.A., ed. (1985). *Lange's Handbook of Chemistry*, 13th ed. McGraw-Hill, New York, 1856 pp.

Dreibus, G. and H. Wanke (1987). Volatiles on Earth and Mars: A comparison. *Icarus*, *71*, 225-240.

Eggleston, C.M., M.F. Hochella, Jr., and G.A. Parks (1989). Sample preparation and aging effects on the dissolution rate and surface composition of diopside. *Geochim. Cosmochim. Acta*, *53*, 797-804.

Evans, U.R. (1982). *An Introduction to Metallic Corrosion*, 3rd ed. Edward Arnold and American Society for Metals, Metals Park, Ohio, 301 pp.

Fanale, F.P. (1976). Martian volatiles: Their degassing history and geochemical fate. *Icarus*, *28*, 179-202.

Fanale, F.P. and W.A. Cannon (1974). Exchange of adsorbed H_2O and CO_2 between the regolith and atmosphere of Mars caused by changes in surface insolation. *J. Geophys. Res.*, *79*, 3397-3402.

Fanale, F.P. and W.A. Cannon (1978). Mars: The role of the regolith in determining atmospheric pressure and the atmosphere's response to insolation changes. *J. Geophys. Res.*, *83*, 2321-2325.

Fanale, F.P. and J.R. Salvail (1994). Quasi-periodic atmosphere-regolith-cap CO_2 redistribution in the Martian past. *Icarus*, *111*, 305-316.

Fanale, F.P., J.R. Salvail, W.B. Banerdt, and R.S. Saunders (1982). Mars: The regolith-atmosphere-cap system and climate change. *Icarus, 50,* 381-407.

Fanale, F.P., J.R. Salvail, A.P. Zent, and S.E. Postawko (1986). Global distribution and migration of subsurface ice on Mars. *Icarus, 67,* 1-18.

Farmer, C.B. (1976). Liquid water on Mars. *Icarus, 28,* 279-289.

Farmer, C.B. and P.E. Doms (1979). Global seasonal variation of water vapor on Mars and the implications for permafrost. *J. Geophys. Res., 84,* 2881-2888.

Farmer, C.B., D.W. Davies, and D.D. La Porte (1976). Mars: Northern summer ice cap-water vapor observations from Viking 2. *Science, 194,* 1339-1341.

Fegley, B., Jr. (1988). Thermochemical kinetics of SO_2 reactions with possible Venus crustal minerals: First data for calcite (abstract). *Lunar Planet. Sci. Abs. XIX,* 315-316.

Fegley, B., Jr., and R.G. Prinn (1989). Estimation of the rate of volcanism on Venus from reaction rate measurements. *Nature, 337,* 55-58.

Fegley, B., Jr., and A.H. Treiman (1992). Chemistry of atmosphere-surface interactions on Venus and Mars. In: *Venus and Mars: Atmospheres, Ionospheres, and Solar Wind Interactions* (J.G. Luhmann, M. Tatrallyay, and

R.O. Pepin, eds.). Am. Geophys. Union Monograph 66, Am. Geophys. Union, Washington, D.C., 7-71.

Fegley, B., Jr., A.H. Treiman, and V.L. Sharpton (1992). Venus surface mineralogy: Observational and theoretical constraints. *Proc. Lunar Planet. Sci., 22*, 3-19.

Flasar, F.M. and R.M. Goody (1976). Diurnal behaviour of water on Mars. *Planet. Space Sci., 24*, 161-181.

Gooding, J.L. (1978). Chemical weathering on Mars: Thermodynamic stabilities of primary minerals (and their alteration products) from mafic igneous rocks. *Icarus, 33*, 483-513.

Gooding, J.L. (1986). Planetary surface weathering. In: *The Solar System: Observations and Interpretations* (M.G. Kivelson, ed.), Rubey vol. IV. Prentice-Hall, Englewood Cliffs, N.J., 207-229.

Gooding, J.L. and K. Keil (1978). Alteration of glass as a possible source of clay minerals on Mars. *Geophys. Res. Let., 5*, 727-730.

Gooding, J.L., S.J. Wentworth, and M.E. Zolensky (1988). Calcium carbonate and sulfate of possible extraterrestrial origin in the EETA 79001 meteorite. *Geochim. Cosmochim. Acta, 52*, 909-915.

Gooding, J.L., S.J. Wentworth, and M.E. Zolensky (1991). Aqueous alteration of the Nakhla meteorite. *Meteoritics, 26*, 135-143.

Greeley, R. and B.D. Schneid (1991). Magma generation on Mars: Amounts, rates, and comparisons with Earth, Moon, and Venus. *Science, 254*, 996-998.

Gregg, S.J. and K.S.W. Sing (1982). *Adsorption, Surface Area, and Porosity*, 2nd ed. Academic Press, London, 303 pp.

Haberle, R.M., D. Tyler, C.P. McKay, and W.L. Davis (1994). A model for the evolution of CO_2 on Mars. *Icarus, 109*, 102-120.

Huguenin, R.L. (1976). Mars: Chemical weathering as a massive volatile sink. *Icarus, 28*, 203-212.

Huguenin, R.L. (1982). Chemical weathering and the Viking biology experiments on Mars. *J. Geophys. Res., 87*, 10,069-10,082.

Ingersoll, A.P. (1970). Mars: Occurrence of liquid water. *Science, 168*, 972-973.

Ingersoll, A.P. (1974). Mars: The case against permanent CO_2 frost caps. *J. Geophys. Res., 79*, 3403-3410.

Jakosky, B.M. (1983). The role of seasonal reservoirs in the Mars water cycle: II. Coupled models of the regolith, the polar caps, and atmospheric transport. *Icarus, 55*, 19-39.

Jakosky, B.M. and P.R. Christensen (1986). Global duricrust on Mars: Analysis of remote-sensing data. *J. Geophys. Res., 91*, 3547-3559.

Jakosky, B.M. and C.B. Farmer (1982). The seasonal and global behavior of water vapor in the Mars atmosphere: Complete global results of the Viking atmospheric water detector experiment. *J. Geophys. Res., 87*, 2999-3019.

Jakosky, B.M., R.O. Pepin, R.E. Johnson, and J.L. Fox (1994). Mars atmospheric loss by solar-wind-induced sputtering and photochemical escape. *Icarus, 111*, 271-288.

Jones, G.C. and B. Jackson (1993). *Infrared Transmission Spectra of Carbonate Minerals*. Chapman and Hall, London.

Kahn, R. (1985). The evolution of CO_2 on Mars. *Icarus, 62*, 175-190.

Kargel, J.S., R.L. Kirk, B. Fegley, Jr., and A.H. Treiman (1994). Carbonate-sulfate volcanism on Venus? *Icarus, 112*, 219-252.

Karlsson, H.R., R.N. Clayton, E.K. Gibson, Jr., and T.K. Mayeda (1992). *Science, 255*, 1409-1411.

Kasting, J.F. (1991). CO_2 condensation and the climate of early Mars. *Icarus, 94*, 1-13.

Kasting, J.F. and O.B. Toon (1989). Climate evolution on the terrestrial planets. In: *Origin and Evolution of Planetary and Satellite Atmospheres* (S.K. Atreya, J.B. Pollack, and M.S. Matthews, eds.). University of Arizona Press, Tucson, 423-449.

Kieffer, H.H., S.C. Chase, T.Z. Martin, E.D. Miner, and F.D. Palluconi (1976). Martian north pole summer temperatures: Dirty water ice. *Science, 194*, 1341-1344.

Kieffer, H.H., T.Z. Martin, A.R. Peterfreund, B.M. Jakosky, E.D. Miner, and F.D. Palluconi (1977). Thermal and albedo mapping of Mars during the Viking Primary Mission. *J. Geophys. Res., 82*, 4249-4291.

Klein, H.P. (1978). The Viking biological experiments on Mars. *Icarus, 34*, 666-674.

Kliore, A., D.L. Cain, G.S. Levy, V.R. Eshleman, G. Fjeldbo, and F.D. Drake (1965). Occultation experiment: Results of the first direct measurement of Mars's atmosphere and ionosphere. *Science, 149*, 1243-1248.

Kliore, A., G. Fjeldbo, B.L. Seidel, and S.I. Rasool (1969). Mariners 6 and 7: Radio occultation measurements of the atmosphere of Mars. *Science, 166*, 1393-1397.

Kubaschewski, O. and B.E. Hopkins (1962). *Oxidation of Metals and Alloys*, 2nd ed. Academic Press, New York, 319 pp.

Kuiper, G.P., ed. (1952). *The Atmospheres of the Earth and Planets*, 2nd ed. University of Chicago Press, 434 pp.

Landsberg, P.T. (1955). On the logarithmic rate law in chemisorption and oxidation. *J. Chem. Phys., 23*, 1079-1087.

Lasaga, A.C. (1984). Chemical kinetics of water-rock interactions. *J. Geophys. Res., 89*, 4009-4025.

Leighton, R.B. and B.C. Murray (1966). Behavior of carbon dioxide and other volatiles on Mars. *Science, 153,* 136-144.

Lucchitta, B.K. (1981). Mars and Earth: Comparison of cold-climate features. *Icarus, 45,* 264-303.

Lucchitta, B.K. (1982). Ice sculpture in the Martian outflow channels. *J. Geophys. Res., 87,* 9951-9973.

Luhmann, J.G., R.E. Johnson, and M.H.G. Zhang (1992). Evolutionary impact of sputtering of the Martian atmosphere by O^+ pickup ions. *Geophys. Res. Let., 19,* 2151-2154.

Martin, T.Z. (1981). Mean thermal and albedo behavior of the Mars surface and atmosphere over a Martian year. *Icarus, 45,* 427-446.

McClellan, A.L. and H.F. Harnsberger (1967). Cross-sectional areas of molecules adsorbed on solid surfaces. *J. Colloid Interface Sci., 23,* 577-599.

McKay, C.P. and W.L. Davis (1991). Duration of liquid water habitats on early Mars. *Icarus, 90,* 214-221.

McKay, C.P. and S.S. Nedell (1988). Are there carbonate deposits in the Valles Marineris, Mars? *Icarus, 73,* 142-148.

McKay, C.P., G.D. Clow, R.A. Wharton, Jr., and S.W. Squyres (1985). Thickness of ice on perennially frozen lakes. *Nature, 313,* 561-562.

McSween, H.Y., Jr., and R.P. Harvey (1993). Outgassed water on Mars: Constraints from melt inclusions in SNC meteorites. *Science, 259*, 1890-1892.

Melosh, H.J. and A.M. Vickery (1989). Impact erosion of the primordial atmosphere of Mars. *Nature, 338*, 487-489.

Mitchell, J.F.B. (1989). The "greenhouse" effect and climate change. *Rev. Geophys., 27*, 115-139.

Mittlefehldt, D.W. (1994). ALH84001, a cumulate orthopyroxenite member of the Martian meteorite clan. *Meteoritics, 29*, 214-221.

Mogk, D.W. (1990). Application of Auger electron spectroscopy to studies of chemical weathering. *Rev. Geophys., 28*, 337-356.

Moore, H.J. and B.M. Jakosky (1989). Viking landing sites, remote-sensing observations, and physical properties of Martian surface materials. *Icarus, 81*, 164-184.

Muhleman, D.O., B.J. Butler, A.W. Grossman, and M.A. Slade (1991). Radar images of Mars. *Science, 253*, 1508-1513.

Nedell, S.S., S.W. Squyres, and D.W. Andersen (1987). Origin and evolution of the layered deposits in the Valles Marineris, Mars. *Icarus, 70*, 409-441.

Neugebauer, G., G. Munch, H.H. Kieffer, S.C. Chase, Jr., and E.D. Miner (1971). Mariner 1969 infrared radiometer results: Temperatures and thermal properties of the Martian surface. *Astron. J., 76*, 719-749.

Orr, C. (1977a). Pore size and volume measurement. In: *Treatise on Analytical Chemistry*, 1st ed. (I.M. Kolthoff, P.J. Elving, and F.H. Stross, eds.), part III, vol. 4. John Wiley and Sons, New York, 359-402.

Orr, C. (1977b). Surface area measurement. In: *Treatise on Analytical Chemistry*, 1st ed. (I.M. Kolthoff, P.J. Elving, and F.H. Stross, eds.), part III, vol. 4. John Wiley and Sons, New York, 321-358.

Owen, T. and H.P. Mason (1969). Mars: Water vapor in its atmosphere. *Science, 165*, 893-895.

Parker, T.J., R.S. Saunders, and D.M. Schneeberger (1989). Transitional morphology in west Deuteronilus Mensae, Mars: Implications for modification of the lowland/upland boundary. *Icarus, 82*, 111-145.

Parker, T.J., D.S. Gorsline, R.S. Saunders, D.C. Pieri, and D.M. Schneeberger (1993). Coastal geomorphology of the Martian northern plains. *J. Geophys. Res., 98*, 11,061-11,078.

Pepin, R.O. (1994). Evolution of the Martian atmosphere. *Icarus, 111*, 289-304.

Pieri, D. (1976). Distribution of small channels on the Martian surface. *Icarus, 27*, 25-50.

Pieri, D.C. (1980). Martian valleys: Morphology, distribution, age, and origin. *Science, 210*, 895-897.

Plescia, J.B. (1993). An assessment of volatile release from recent volcanism in Elysium, Mars. *Icarus, 104,* 20-32.

Pollack, J.B. (1979). Climatic change on the terrestrial planets. *Icarus, 37,* 479-553.

Pollack, J.B. and D.C. Black (1982). Noble gases in planetary atmospheres: Implications for the origin and evolution of atmospheres. *Icarus, 51,* 169-198.

Pollack, J.B. and Y.L. Yung (1980). Origin and evolution of planetary atmospheres. *Ann. Rev. Earth Planet. Sci., 8,* 425-487.

Pollack, J.B., J.F. Kasting, S.M. Richardson, and K. Poliakoff (1987). The case for a wet, warm climate on early Mars. *Icarus, 71,* 203-224.

Pollack, J.B., T. Roush, F. Witteborn, J. Bregman, D. Wooden, C. Stoker, and O.B. Toon (1990). Thermal emission spectra of Mars (5.4-10.5 μm): Evidence for sulfates, carbonates, and hydrates. *J. Geophys. Res., 95,* 14,595-14,627.

Romanek, C.S., M.M. Grady, I.P. Wright, D.W. Mittlefehldt, R.A. Socki, C.T. Pillinger, and E.K. Gibson, Jr. (1994). Record of fluid-rock interactions on Mars from the meteorite ALH84001. *Nature, 372,* 655-657.

Salisbury, J.W., L.S. Walter, N. Vergo, and D.M. D'Aria (1991). *Infrared (2.1-25 μm) Spectra of Minerals.* Johns Hopkins University Press, Baltimore, 267 pp.

Schaefer, M.W. (1990). Geochemical evolution of the northern plains of Mars: Early hydrosphere, carbonate development, and present morphology. *J. Geophys. Res., 95*, 14,291-14,300.

Schaefer, M.W. (1993a). Aqueous geochemistry on early Mars. *Geochim. Cosmochim. Acta, 57*, 4619-4625.

Schaefer, M.W. (1993b). Volcanic recycling of carbonates on Mars. *Geophys. Res. Let., 20*, 827-830.

Schubert, G., D.L. Turcotte, S.C. Solomon, and N.H. Sleep (1989). Coupled evolution of the atmospheres and interiors of planets and satellites. In: *Origin and Evolution of Planetary and Satellite Atmospheres* (S.K. Atreya, J.B. Pollack, and M.S. Matthews, eds.). University of Arizona Press, Tucson, 450-483.

Schultz, P.H. (1985). The Martian atmosphere before and after the Argyre impact. In: *MECA Workshop on the Evolution of the Martian Atmosphere*. Lunar and Planetary Institute, Houston, 22-23.

Sharp, R.P. (1973). Mars: Fretted and chaotic terrain. *J. Geophys. Res., 78*, 4073-4083.

Shorthill, R.W., H.J. Moore, II, R.F. Scott, R.E. Hutton, S. Liebes, Jr., and C.R. Spitzer (1976). The "soil" of Mars (Viking 1). *Science, 194*, 91-97.

Sidorov, Yu.I. and M.Yu. Zolotov (1986). Weathering of Martian surface rocks. In: *Chemistry and Physics of*

Terrestrial Planets (S.K. Saxena, ed.). Springer-Verlag, Amsterdam, 191-223.

Smoluchowski, R. (1968). Mars: Retention of ice. *Science, 159*, 1348-1350.

Soderblom, L.A. (1992). The composition and mineralogy of the Martian surface from spectroscopic observations. In: *Mars* (H.H. Kieffer, B.M. Jakosky, C.W. Snyder, and M.S. Matthews, eds.). University of Arizona Press, Tucson, 557-593.

Soderblom, L.A., T.J. Kreidler, and H. Masursky (1973). Latitudinal distribution of a debris mantle on the Martian surface. *J. Geophys. Res., 78*, 4117-4122.

Spohn, T. (1991). Mantle differentiation and thermal evolution of Mars, Mercury, and Venus. *Icarus, 90*, 222-236.

Squyres, S.W. and M.H. Carr (1986). Geomorphic evidence for the distribution of ground ice on Mars. *Science, 231*, 249-252.

Stephens, S.K. and D.J. Stevenson (1990). Dry carbonate formation on Mars: A plausible sink for a CO_2 atmosphere? (abstract). *Lunar Planet. Sci. Abs. XXI*, 1198-1199.

Stephens, S.K. and D.J. Stevenson (1992). Carbonate formation on Mars: History of the CO_2 atmosphere from models of diffusion-limited growth in non-aqueous environments (abstract). In: *Workshop on the Martian*

Surface and Atmosphere Through Time (R.M. Haberle and B.M. Jakosky, eds.). LPI Tech. Rpt. 92-02, Lunar and Planetary Institute, Houston, 136-137.

Stephens, S.K., D.J. Stevenson, G.R. Rossman, and L.F. Keyser (1993). Carbonate Formation on Mars: Latest Experiments (abstract). In: *Mars: Past, Present, and Future--Results from the MSATT Program* (R.M. Haberle, ed.). LPI Tech. Rpt. 93-06, Part 1, Lunar and Planetary Institute, Houston, 46-48.

Stephens, S.K., D.J. Stevenson, and L.F. Keyser (1994). Carbonate Formation on Mars: Latest Experiments and Models (abstract). *Lunar Planet. Sci. Abs. XXV*, 1343-1344.

Stevenson, D.J., T. Spohn, and G. Schubert (1983). Magnetism and thermal evolution of the terrestrial planets. *Icarus*, *54*, 466-489.

Stumm, W. and J.J. Morgan (1981). *Aquatic Chemistry: An Introduction Emphasizing Chemical Equilibria in Natural Waters*, 2nd ed. John Wiley and Sons, New York, 780 pp.

Tingle, T.N., M.F. Hochella, Jr., C.H. Becker, and R. Malhotra (1990). Organic compounds on crack surfaces in olivine from San Carlos, Arizona, and Hualalai Volcano, Hawaii. *Geochim. Cosmochim. Acta*, *54*, 477-485.

Toon, O.B., J.B. Pollack, W. Ward, J.A. Burns, and K. Bilski (1980). The astronomical theory of climatic change on Mars. *Icarus*, *44*, 552-607.

Toulmin, P., III., A.K. Baird, B.C. Clark, K. Keil, H.J. Rose, Jr., R.P. Christian, P.H. Evans, and W.C. Kelliher (1977). Geochemical and mineralogical interpretation of the Viking inorganic chemical results. *J. Geophys. Res.*, *82*, 4625-4634.

Treiman, A.H., R.A. Barrett, and J.L. Gooding (1993). Preterrestrial aqueous alteration of the Lafayette (SNC) meteorite. *Meteoritics*, *28*, 86-97.

Walker, J.C.G. (1978). Atmospheric evolution of the inner planets. In: *Comparative Planetology* (C. Ponnamperuma, ed.). Academic Press, New York, 141-163.

Walker, J.C.G., P.B. Hays, and J.F. Kasting (1981). A negative feedback mechanism for the long-term stabilization of Earth's surface temperature. *J. Geophys. Res.*, *86*, 9776-9782.

Watson, L.L., I.D. Hutcheon, S. Epstein, and E.M. Stolper (1994). Water on Mars: Clues from deuterium/hydrogen and water contents of hydrous phases in SNC meteorites. *Science*, *265*, 86-90.

Weast, R.C., ed. (1977). *CRC Handbook of Chemistry and Physics*, 58th ed. CRC Press, Cleveland.

Wechsler, A.E. and P.E. Glaser (1965). Pressure effects on postulated lunar materials. *Icarus*, *4*, 335-352.

White, A.F. and M.F. Hochella, Jr. (1992). Surface chemistry associated with the cooling and subaerial weathering of recent basalt flows. *Geochim. Cosmochim. Acta, 56*, 3711-3721.

White, W.B. (1974). The carbonate minerals. In: *The Infrared Spectra of Minerals* (V.C. Farmer, ed.). Mineralogical Society, London, 227-284.

Zent, A.P. and C.P. McKay (1994). The chemical reactivity of the Martian soil and implications for future missions. *Icarus, 108*, 146-157.

Zent, A.P., F.P. Fanale, and S.E. Postawko (1987). Carbon dioxide: Adsorption on palagonite and partitioning in the Martian regolith. *Icarus, 71*, 241-249.